CHALLENGES AND OPPORTUNITIES OF TARGETING MUSCLE FOR THERAPY

EDITED BY: Carlo Rinaldi, Helen Cristina Miranda and Yoshitsugu Aoki

PUBLISHED IN: Frontiers in Physiology and Frontiers in Pharmacology

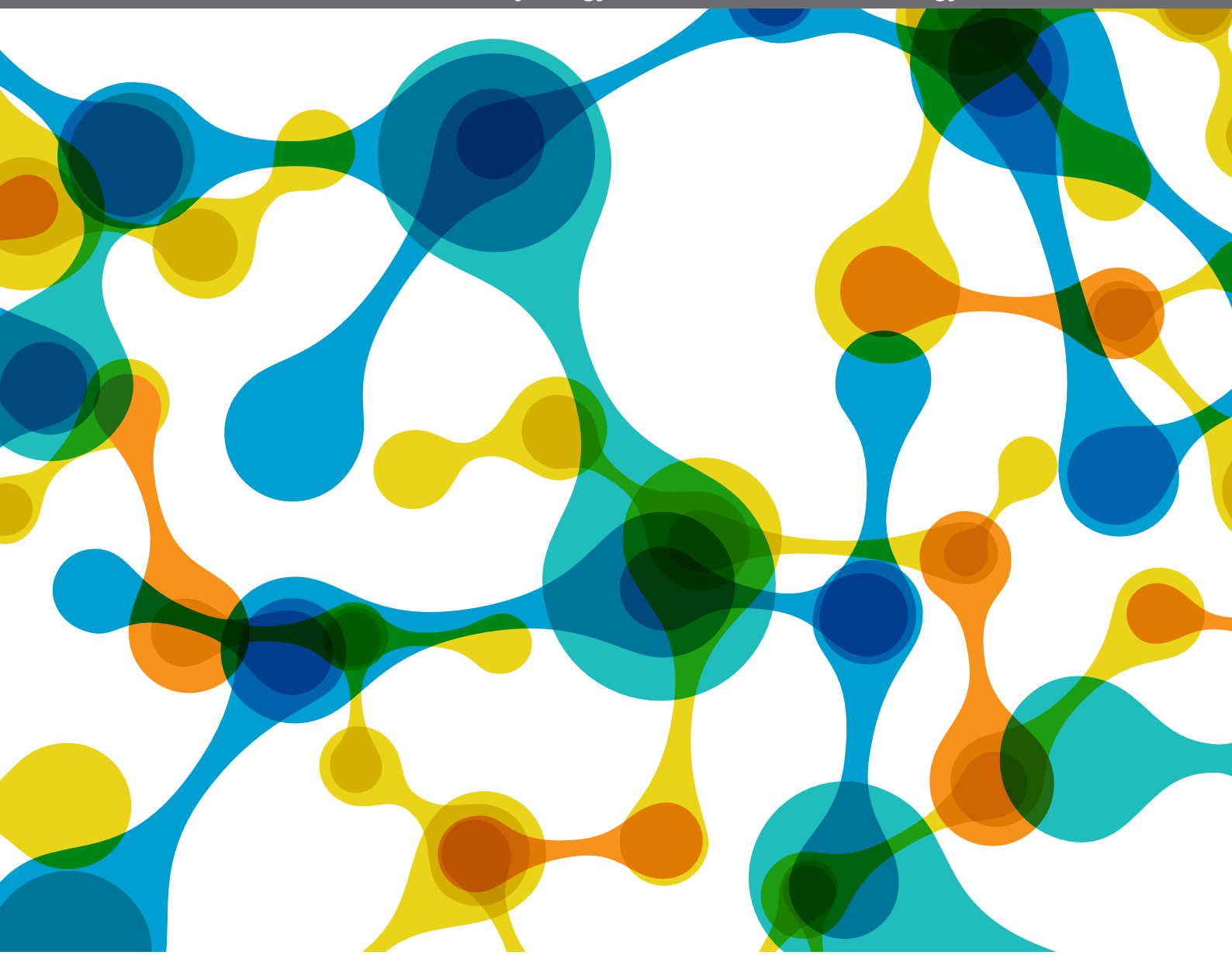

frontiers Research Topics

ISSN 1664-8714
ISBN 978-2-88974-784-9
DOI 10.3389/978-2-88974-784-9

About Frontiers

Frontiers is more than just an open-access publisher of scholarly articles: it is a pioneering approach to the world of academia, radically improving the way scholarly research is managed. The grand vision of Frontiers is a world where all people have an equal opportunity to seek, share and generate knowledge. Frontiers provides immediate and permanent online open access to all its publications, but this alone is not enough to realize our grand goals.

Frontiers Journal Series

The Frontiers Journal Series is a multi-tier and interdisciplinary set of open-access, online journals, promising a paradigm shift from the current review, selection and dissemination processes in academic publishing. All Frontiers journals are driven by researchers for researchers; therefore, they constitute a service to the scholarly community. At the same time, the Frontiers Journal Series operates on a revolutionary invention, the tiered publishing system, initially addressing specific communities of scholars, and gradually climbing up to broader public understanding, thus serving the interests of the lay society, too.

Dedication to Quality

Each Frontiers article is a landmark of the highest quality, thanks to genuinely collaborative interactions between authors and review editors, who include some of the world's best academicians. Research must be certified by peers before entering a stream of knowledge that may eventually reach the public - and shape society; therefore, Frontiers only applies the most rigorous and unbiased reviews.
Frontiers revolutionizes research publishing by freely delivering the most outstanding research, evaluated with no bias from both the academic and social point of view. By applying the most advanced information technologies, Frontiers is catapulting scholarly publishing into a new generation.

What are Frontiers Research Topics?

Frontiers Research Topics are very popular trademarks of the Frontiers Journals Series: they are collections of at least ten articles, all centered on a particular subject. With their unique mix of varied contributions from Original Research to Review Articles, Frontiers Research Topics unify the most influential researchers, the latest key findings and historical advances in a hot research area! Find out more on how to host your own Frontiers Research Topic or contribute to one as an author by contacting the Frontiers Editorial Office: frontiersin.org/about/contact

CHALLENGES AND OPPORTUNITIES OF TARGETING MUSCLE FOR THERAPY

Topic Editors:
Carlo Rinaldi, University of Oxford, United Kingdom
Helen Cristina Miranda, Case Western Reserve University, United States
Yoshitsugu Aoki, National Center of Neurology and Psychiatry (Japan), Japan

Citation: Rinaldi, C., Miranda, H. C., Aoki, Y., eds. (2022). Challenges and Opportunities of Targeting Muscle for Therapy. Lausanne: Frontiers Media SA. doi: 10.3389/978-2-88974-784-9

Table of Contents

frontiers in Physiology

EDITORIAL
published: 07 March 2022
doi: 10.3389/fphys.2022.848220

Editorial: Challenges and Opportunities for Neuromuscular Disease Modelling Using Urine-derived Stem Cells

*Chaitra Sathyaprakash, Katsuhiko Kunitake and Yoshitsugu Aoki**

Department of Molecular Therapy, National Institute of Neuroscience, National Center of Neurology and Psychiatry, Kodaira, Japan

Keywords: urine-derived stem cells, human disease models, skeletal myotubes, muscle, transdifferentiation

Editorial on the Research Topic

Challenges and Opportunities for Neuromuscular Disease Modelling Using Urine-derived Stem Cells

Restoration of dystrophin function in muscle via exon-skipping antisense oligonucleotides (ASO) has been long heralded as a promising therapeutic strategy to treat Duchenne muscular dystrophy (DMD). The existence of over 1,800 *DMD* mutations in the form of deletions and duplications has made this disease very challenging to generate models and perform screening studies to identify the most efficient exon-skipping therapies for clinical trials. However, increasing discoveries of several other cellular disease mechanisms associated with DMD have increased the scope for targeted treatment and the need for patient-specific DMD myogenic models to screen. Recent studies in *Frontiers of Physiology* identify several secondary cellular phenotypes in murine models of muscular dystrophy (Dong et al.; Valentine et al.), which may serve as essential targets in combinatorial therapies in DMD patients. While these mouse models are applicable as surrogates for human diseases, human-specific pre-clinical studies are crucial to examine the effects on individual patients.

In recent years multiple studies have suggested urine-derived stem cell (USC) cultures as a solution to overcome the challenge of obtaining somatic cells from human patients. A screening study using RNA sequencing and protein profiling via immunofluorescence and immunoblotting demonstrated that USCs readily express 571 genes that have been implicated in 16 neuromuscular diseases (NMD) (Falzarano et al., 2021). To confirm whether USCs model relevant cell lineages, changes in gene expression was examined in USCs and MyoD-induced myogenic cells from 3 non-disease individuals. Differential expression analysis of the mRNAs expressed in these cells, following bulk RNA transcriptomics, showed that 154 genes associated with NMDs were enriched in the myogenic cells compared to USCs. Conversely, 127 genes were enriched in USCs compared with the myogenic cells. Furthermore, 165 genes associated with NMDs were not expressed in the myogenic cells. A number of genes not expressed in USCs were switched on followed MyoD-induction, though their expression at the protein level was not tested. These included *DES, SGCD, SGCA, DTNA, MYL1* and *STAC3* (**Figure 1**). Similarly, a number of genes not usually expressed in the myogenic cells were downregulated following MyoD-induction from USCs, including *COL6A*. Significantly, the *DMD* gene was not expressed in either USCs or the induced myogenic cells, despite the authors previously demonstrating dystrophin protein's presence in similar cultures (Falzarano et al., 2016). Therefore, further optimisation for the time of analysis after this conversion is desired prior to establishing USC-myotubes as a model for NMDs. Alternative protocols using retroviral transduction of lineage determining transcription factor, MyoD1 combined with a histone methyltransferase inhibitor, 3- deazaneplanocin A hydrochloride (DZNep) in primary USC cultures also generates pure myotube cultures, expressing myogenin,

OPEN ACCESS

Edited and reviewed by:
Peter J. Reiser,
The Ohio State University,
United States

****Correspondence:***
Yoshitsugu Aoki
tsugu56@ncnp.go.jp

Specialty section:
This article was submitted to Striated Muscle Physiology, a section of the journal Frontiers in Physiology

Received: *04 January 2022*
Accepted: *28 January 2022*
Published: *07 March 2022*

Citation:
Sathyaprakash C, Kunitake K and Aoki Y (2022) Editorial: Challenges and Opportunities for Neuromuscular Disease Modelling Using Urine-derived Stem Cells. Front. Physiol. 13:848220. doi: 10.3389/fphys.2022.848220

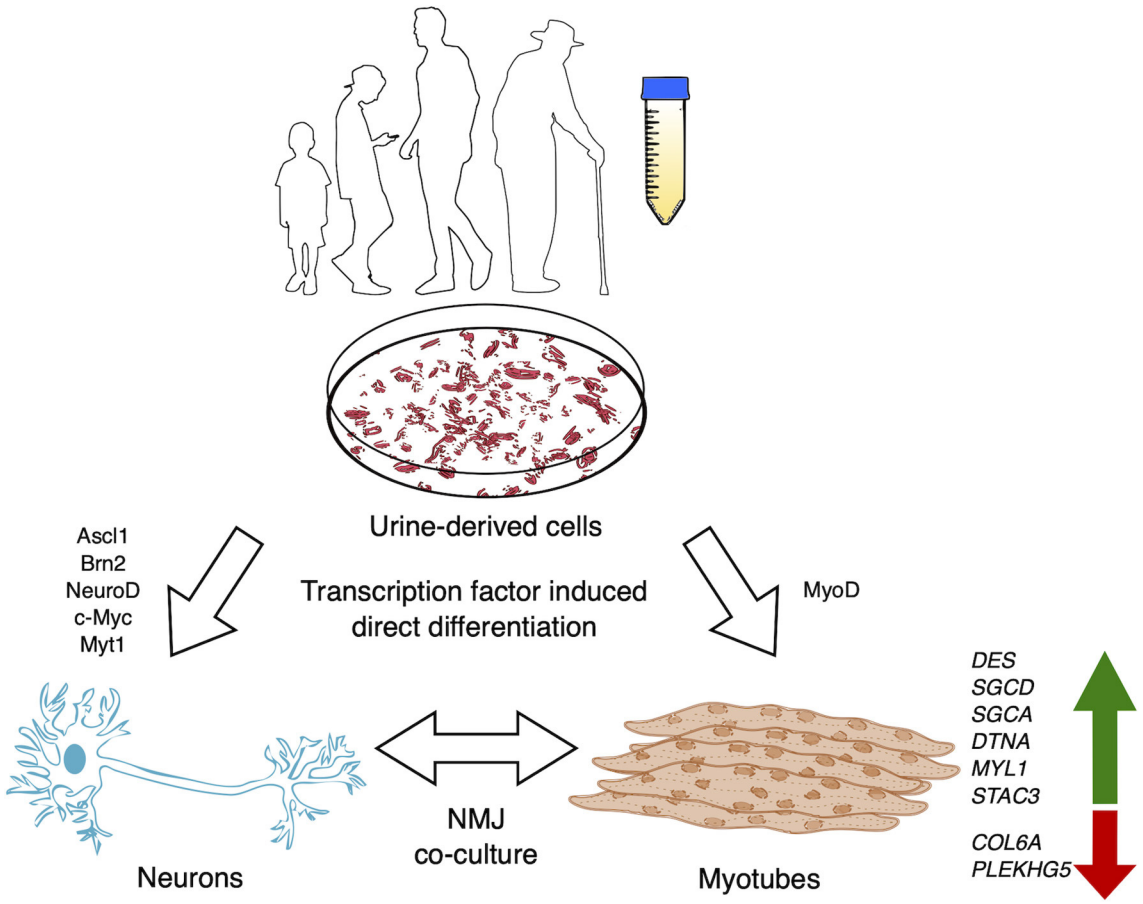

FIGURE 1 | USCs may be isolated from the voided urine of patients with neurodegenerative or neuromuscular disease and non-disease individuals of any age or debilitating condition. USCs may be utilized in a myriad of ways, including the potential to derive directly induced cellular models (myotubes, motor neurons or co-cultures). Zhang et al. (2016) performed direct conversion of USCs into neuronal cells via exogenous expression of Ascl1, Brn2, NeuroD, c-Myc, and Myt1l, while myotubes may be *myodifferentiated* via MyoD expression. Genes implicated in NMDs are upregulated in USC-myotubes, making them a promising model for human neuromuscular diseases.

followed by increasing levels of myosin heavy chain-2 and dystrophin (Takizawa et al., 2019). Furthermore, using this model Takizawa et al. (2020) demonstrated highly successful exon 23-skipping in myotubes derived from DMD patient USCs using ASO transfection, showing restored levels of dystrophin mRNA and protein. Overall, using the method of DMD patient-derived USC-myotube direct differentiation largely increases the efficiency of obtaining human cellular models of any DMD mutation and provides a robust screening platform for exon-skipping therapies, which are likely to benefit pre-clinical trials for DMD, and indeed any neuromuscular or neurodegenerative diseases.

Increasing research establishing USCs as a faster, cheaper, rapidly proliferating, and contaminant-free source of cells has opened the doors for the opportunity to generate human cell models from the voided urine of the most vulnerable individuals, including DMD pediatric cases or late-stage amyotrophic lateral sclerosis patients. Protocols to transdifferentiate USCs into neuronal cells has been demonstrated, though high yield and expression of specific markers for neuronal subtypes has yet to be achieved (Zhang et al., 2016; Xu et al., 2019; Liu et al., 2020) (**Figure 1**). Meanwhile, fibroblasts can be directly converted to motor neurons with a yield of 66.4% $ISL1^+$/$Hoechst^+$ and >90% $ISL1^+$/$TUJ1^+$ (Tang et al., 2017). Regulating epigenetic states of USCs via additional compounds, like DZNep promotion of USC-*myodifferentiation*, to modulate *neurodifferentiation* for direct reprogramming should significantly benefit the study of adult-onset diseases in addition to DMD.

DMD patients will likely require the therapeutic intervention of secondary pathways altered in disease to restore full muscle integrity and function. For example, prior analysis of post-mortem human samples from DMD patients exhibited altered levels of specific fatty acids and phosphatidylcholine (PC) in the muscle cell membrane. Recent lipidomics data from dystrophic *mdx* mice revealed similarly altered ratios of PC 34:1 and 34:2, including some differences absent in humans (Valentine et al.). Due to such differences between the species, patient-derived USC-myotubes cultures revealing the cellular mechanisms that

lead to alterations in human tissue may be crucial. This includes patient- specific differences in onset, progression and severity in lipid membrane composition and screening for therapies to restore non-disease lipid levels. Similarly, USC-myotubes may be used to examine the efficacy of metformin treatment on muscle function by examining sarcolemma integrity across large cohorts of patient-derived USC-myotube cultures, which was shown to improve muscle strength in mice (Dong et al.).

USCs may be robustly harvested from individuals of any age or debilitating condition, significantly broadening the cohort of patients accessible to study. In the case of neuromuscular diseases like DMD, the potential for these cells to be used for pre-clinical therapeutic screening, modeling understudied cognitive disease mechanisms and regenerative therapies, is highly optimistic. However, another significant challenge in the field lies in the efficiency of exon-skipping ASOs to be targeted to muscle tissue *in vivo*. At present, this remains outside the scope that USC-derived cultures may provide. Nevertheless, the authors feel that USCs are likely to become increasingly used as a model to study neuromuscular and neurodegenerative diseases, with several promising uses.

AUTHOR CONTRIBUTIONS

CS: writing—original draft. KK and YA: writing—review and editing. All authors contributed to the article and approved the submitted version.

ACKNOWLEDGMENTS

We thank C. Rinaldi and H. Miranda for giving us the opportunity to publish an editorial.

REFERENCES

Falzarano, M. S., D'Amario, D., Siracusano, A., Massetti, M., Amodeo, A., La Neve, F., et al. (2016). Duchenne muscular dystrophy myogenic cells from urine-derived stem cells recapitulate the dystrophin genotype and phenotype. *Hum. Gene Ther.* 27, 772–783. doi: 10.1089/hum.2016.079

Falzarano, M. S., Rossi, R., Grilli, A., Fang, M., Osman, H., Sabatelli, P., et al. (2021). Urine-derived stem cells express 571 neuromuscular disorders causing genes, making them a potential in vitro model for rare genetic diseases. *Front. Physiol.* 12, 1–10. doi: 10.3389/fphys.2021.716471

Liu, D., Rychkov, G., Al-Hawwas, M., Manaph, N. P. A., Zhou, F., Bobrovskaya, L., et al. (2020). Conversion of human urine-derived cells into neuron-like cells by small molecules. *Mol. Biol. Rep.* 47, 2713–2722. doi: 10.1007/s11033-020-05370-1

Takizawa, H., Hara, Y., Mizobe, Y., Ohno, T., Suzuki, S., Inoue, K., et al. (2019). Modelling Duchenne muscular dystrophy in MYOD1-converted urine-derived cells treated with 3-deazaneplanocin A hydrochloride. *Sci. Rep.* 9, 3807. doi: 10.1038/s41598-019-40421-z

Takizawa, H., Sato, M., and Aoki, Y. (2020). Exon skipping in directly reprogrammed myotubes obtained from human urine-derived cells. *J. Vis. Exp.* 2020, 3–11. doi: 10.3791/60840

Tang, Y., Liu, M. L., Zang, T., and Zhang, C. L. (2017). Direct reprogramming rather than iPSC-based reprogramming maintains aging hallmarks in human motor neurons. *Front. Mol. Neurosci.* 10, 359. doi: 10.3389/fnmol.2017.00359

Xu, G., Wu, F., Gu, X., Zhang, J., You, K., Chen, Y., et al. (2019). Direct Conversion of Human Urine Cells to Neurons by Small Molecules. *Sci. Rep.* 9, 16707. doi: 10.1038/s41598-019-53007-6

Zhang, S.-Z., Ma, L.-X., Qian, W.-J., Li, H.-F., Wang, Z.-F., Wang, H.-X., et al. (2016). Modeling neurological disease by rapid conversion of human urine cells into functional neurons. *Stem Cells Int.* 2016, 2452985. doi: 10.1155/2016/2452985

Conflict of Interest: The authors declare that the research was conducted in the absence of any commercial or financial relationships that could be construed as a potential conflict of interest.

frontiers in Physiology

ORIGINAL RESEARCH
published: 03 December 2020
doi: 10.3389/fphys.2020.580223

Ficus carica L. Attenuates Denervated Skeletal Muscle Atrophy via PPARα/NF-κB Pathway

Junxi Dai[1,2,3], Yaoxian Xiang[1,2,3], Da Fu[4], Lei Xu[1,2,3], Junjian Jiang[1,2,3] and Jianguang Xu[1,2,3,5]**

[1] Department of Hand Surgery, Huashan Hospital, Fudan University, Shanghai, China, [2] Key Laboratory of Hand Reconstruction, Ministry of Health, Shanghai, China, [3] Shanghai Key Laboratory of Peripheral Nerve and Microsurgery, Shanghai, China, [4] Central Laboratory, Shanghai Tenth People's Hospital, Shanghai, China, [5] School of Rehabilitation Science, Shanghai University of Traditional Chinese Medicine, Shanghai, China

Treatment options for denervated skeletal muscle atrophy are limited, in part because the underlying molecular mechanisms are not well understood. Unlike previous transcriptomics studies conducted in rodent models of peripheral nerve injury, in the present study, we performed high-throughput sequencing with denervated atrophic biceps muscle and normal (non-denervated) sternocleidomastoid muscle samples obtained from four brachial plexus injury (BPI) patients. We also investigated whether *Ficus carica* L. (FCL.) extract can suppress denervated muscle atrophy in a mouse model, along with the mechanism of action. We identified 1471 genes that were differentially expressed between clinical specimens of atrophic and normal muscle, including 771 that were downregulated and 700 that were upregulated. Gene Ontology (GO) and Kyoto Encyclopedia of Genes and Genomes (KEGG) pathway analyses revealed that the differentially expressed genes were mainly enriched in the GO terms "structural constituent of muscle," "Z disc," "M band," and "striated muscle contraction," as well as "Cell adhesion molecules," "Glycolysis/Gluconeogenesis," "Peroxisome proliferator-activated receptor alpha (PPARα) signaling pathway," and "P53 signaling pathway." In experiments using mice, the reduction in wet weight and myofiber diameter in denervated muscle was improved by FCL. extract compared to saline administration, which was accompanied by downregulation of the proinflammatory cytokines interleukin (IL)-1β and IL-6. Moreover, although both denervated groups showed increased nuclear factor (NF)-κB activation and PPARα expression, the degree of NF-κB activation was lower while PPARα and inhibitor of NF-κB IκBα expression was higher in FCL. extract-treated mice. Thus, FCL. extract suppresses denervation-induced inflammation and attenuates muscle atrophy by enhancing PPARα expression and inhibiting NF-κB activation. These findings suggest that FCL. extract has therapeutic potential for preventing denervation-induced muscle atrophy caused by peripheral nerve injury or disease.

Keywords: denervated muscle atrophy, *Ficus carica*, NF-κß, PPAR, muscle atrophy, peripheral nerve injury

OPEN ACCESS

Edited by:
Helen Cristina Miranda, Case Western Reserve University, United States

Reviewed by:
Juan C. Saez, Pontificia Universidad Católica de chile, Chile
Fei Ding, Nantong University, China

****Correspondence:***
Junjian Jiang
jjjdoctor@126.com
Jianguang Xu
xjg@shutcm.edu.cn

Specialty section:
This article was submitted to Striated Muscle Physiology, a section of the journal Frontiers in Physiology

Received: *05 July 2020*
Accepted: *13 October 2020*
Published: *03 December 2020*

Citation:
Dai JX, Xiang YX, Fu D, Xu L, Jiang JJ and Xu JG (2020) Ficus carica L. Attenuates Denervated Skeletal Muscle Atrophy via PPARα/NF-κB Pathway. Front. Physiol. 11:580223. doi: 10.3389/fphys.2020.580223

INTRODUCTION

Peripheral nerve injury often leads to skeletal muscle atrophy, which seriously affects normal limb function and the quality of life of patients (Burns et al., 2012; Ehmsen and Höke, 2020). At present, there are limited clinically effective treatments for reversing or delaying the process of muscle atrophy; however, clarifying the underlying mechanisms can lead to the development of effective therapeutic strategies.

Denervation causes a series of biochemical and physiologic alterations in muscle, resulting from changes in gene expression (Shen et al., 2019). The gene expression profile associated with denervated muscle atrophy has been examined by microarray analysis or high-throughput RNA sequencing (RNA-seq) (Kunkel et al., 2011; Ebert et al., 2012; Jian et al., 2018), which has identified numerous genes such as muscle RING finger 1 (Furlow et al., 2013), high-mobility group box-1 (Yang et al., 2018), and microRNAs including miR-206 (Huang et al., 2016), miR-21 (Soares et al., 2014), and miR29b (Li et al., 2017) that mediate muscle degeneration. It is worth noting that these previous studies were mostly carried out using rodent models of muscle atrophy induced by sciatic nerve transection. Other than investigations on amyotrophic lateral sclerosis and spinal muscular atrophy, there have been no published microarray or RNA-seq studies to date using denervated atrophic muscle from humans (Birger et al., 2019; Onodera et al., 2020).

Oxidative stress plays an important role in the process of muscle atrophy (Scalabrin et al., 2019; Shen et al., 2019; Odeh et al., 2020). Increased production of reactive oxygen species (ROS) in atrophic muscle can lead to oxidative stress along with mitochondrial dysfunction and cellular damage (Muller et al., 2007; Pollock et al., 2017; Scalabrin et al., 2019), and can activate or inactivate transcription factors, metabolic enzymes, and membrane channels (Winterbourn and Hampton, 2008). Inflammation also contributes to the physiologic adaptation of skeletal muscle to denervation (Ma et al., 2018; Shen et al., 2019; Wu et al., 2019). Atrophic muscles have elevated levels of proinflammatory cytokines such as tumor necrosis factor (TNF)-α, interleukin (IL)-1, and IL-6 (Cea et al., 2013; Ma et al., 2019; Wu et al., 2019). Local infusion of recombinant murine IL-6 was shown to induce muscle atrophy in rats (Wu et al., 2019), and inhibition of IL-6 signaling alleviated the severity of muscle atrophy (Cánoves et al., 2013). Thus, drugs with anti-inflammatory and antioxidant effects can potentially prevent muscle atrophy.

Ficus carica L. (FCL.) is a flowering plant that contains flavonoids, psoralen, and bergapten and has antioxidant, anti-inflammatory, and antiapoptotic properties (Ali et al., 2012; Badgujar et al., 2014; Melisa et al., 2014; Zhang et al., 2019). FCL. was shown to enhance the levels of the antioxidant enzymes superoxide dismutase and glutathione peroxidase in the serum and liver of diabetic mice and block apoptosis in pancreatic β-cells (Zhang et al., 2019). However, the effect of FCL. on denervated muscle is unknown.

To address this point, in this study, we carried out high-throughput transcriptome sequencing of human muscle samples obtained from four patients with brachial plexus injury (BPI) in order to identify critical pathways and genes related to the atrophy of denervated muscle, and thus gain insight into the molecular basis of this process. As a secondary aim, we examined whether FCL. extract can reverse or delay muscle atrophy in a mouse model along with the mechanism of action.

MATERIALS AND METHODS

Human Muscle Tissue Sample Collection

All experiments of this study were performed in accordance with the guidelines of the Ethics Committee on Human and Animal Experiments (Huashan Hospital, Fudan University). Human atrophic and normal muscles were obtained from four donors diagnosed with BPI, including two with total BPI, one with upper and middle trunk BPI, and one with upper trunk BPI. Inclusion criteria were as follows: (1) total BPI or upper back injury diagnosed by preoperative physical examination and electromyography; (2) uninjured accessory nerve and second to fourth cervical nerve; (3) 18–50 years old; (4) no other diseases; and (5) willing to participate in this study. For the characteristics of these patients, see **Supplementary Table 1**. Pieces of denervated biceps muscle and normal (non-denervated) sternocleidomastoid muscle about 2 cm in length and 1 cm in diameter were resected from each patient during surgery, and preserved in tissue stage solution (Miltenyi Biotec, Gladbach, Germany) until use.

RNA-Seq

Total RNA was extracted from muscle tissue samples using the miRNA Isolation Kit (mirVana; Thermo Fisher Scientific, Waltham, MA, United States; AM1561) according to the manufacturer's protocol. RNA integrity was evaluated using the Agilent 2100 Bioanalyzer (Agilent Technologies, Santa Clara, CA, United States), and samples with RNA integrity number $\geq$ 7 were retained for analysis. Libraries were constructed using the TruSeq Stranded mRNA LTSample Prep Kit (Illumina, San Diego, CA, United States) according to the manufacturer's instructions, and were sequenced on the Illumina HiSeq X Ten platform, generating 125/150-bp paired-end reads. Index-coded sample clustering was performed using the TruSeqPE Cluster Kit v3-cBot-HS (Illumina) on a cBot Cluster Generation System according to the manufacturer's protocol. The Illumina HiSeq X platform was used to sequence the library preparations; 125/150-bp paired-end reads and 50-bp single-end reads were generated.

Bioinformatic Analysis

Quality Control and Mapping

Raw data (raw reads) were processed using Trimmomatic (Bolger et al., 2014). Reads containing poly-N and those of low quality were removed to obtain clean reads, which were mapped to the reference genome using hisat2 (Kim et al., 2015).

Identification of Differentially Expressed Genes (DEGs) and Gene Ontology (GO) and Kyoto Encyclopedia of Genes and Genomes (KEGG) Pathway Enrichment Analyses

The fragments per kilobase of transcript per million mapped reads value (Roberts et al., 2011) of each gene was calculated using cufflinks (Trapnell et al., 2010), and the read counts of each gene were obtained with htseq-count (Anders et al., 2015). Differentially expressed genes (DEGs) were identified using the DESeq package of R software with the estimateSize Factors and nbinomTest functions. A P-value < 0.05 and fold change > 2 or < 0.5 were set as the thresholds for significantly different expression. Hierarchical cluster analysis of DEGs was performed to explore gene expression patterns. Gene Ontology (GO) enrichment and Kyoto Encyclopedia of Genes and Genomes (KEGG) pathway enrichment analysis of DEGs were performed using R based on the hypergeometric distribution (Minoru et al., 2008).

Animal Procedures

Male C57 BL/6 mice aged 6–8 weeks and weighing 22–25 g ($N = 24$) were purchased from the laboratory animal center of Charles River Laboratories (Beijing, China). Mice were housed in standard cages in a room at 23°C and 50% relative humidity on a 12:12-h light/dark cycle. The mice were randomly assigned to three groups: the mice that received a sham operation (Control group), the denervated mice that were administered with saline (Den-saline group), and the denervated mice that were infused with FCL. (Den-FCL. group). Mice in both denervated groups were subjected to unilateral sciatic nerve transection under anesthesia as previously described (Wu et al., 2019). Briefly, after deep anesthetization, a 0.5-cm-long portion of the sciatic nerve in the right hind leg of the mouse was resected; the two nerve ends were buried in muscle, and the incision was closed using 4-0 absorbable sutures. After sciatic nerve transection, mice in the FCL. group were treated daily with FCL. extract dissolved in 9% saline (0.15 g/ml saline) by intragastric administration (10 ml/kg). Mice in the saline group received the same amount of saline daily.

Wet Weight

After 21 days, mice were anesthetized and the gastrocnemius muscles of both left and right hind legs were removed and after saline wash then weighed. The wet weight ratio was defined as the muscle weight of the nerve injury side divided by the weight of the contralateral side. Then these muscle samples were stored in 4% paraformaldehyde and at −80°C until use.

Hematoxylin–Eosin (HE) and Masson's Trichrome Staining

Biceps and sternocleidomastoid tissue samples from patients and gastrocnemius muscle samples from mice were fixed in 4% paraformaldehyde and embedded in paraffin. The samples were cut at a thickness of 5 μm and the sections were stained with hematoxylin–eosin (HE) (Beyotime, Shanghai, China) and Masson's trichrome (Beyotime) to evaluate histopathologic changes. The mean diameter of myofibers was determined by blinded analysis using ImageJ software (National Institutes of Health, Bethesda, MD, United States) from five randomly captured images per mouse in each experimental condition.

Immunohistochemistry

Expression of the proinflammation factors IL-1β and IL-6 in gastrocnemius muscle was detected by immunohistochemistry. The sections were deparaffinized with xylene and rehydrated with ethanol, and antigen retrieval was performed in 0.01 M citrate buffer (pH 6.0) in a pressure cooker, followed by natural cooling to room temperature. The sections were incubated in 0.3% hydrogen peroxide at room temperature for 10 min; goat serum was used to block the sections for 15 min at room temperature, which were then incubated overnight at 4°C with a rabbit polyclonal anti-IL-1 antibody (1:200 dilution) and IL-6 antibody (1:200 dilution) (both from Abcam, Cambridge, United Kingdom) followed by horseradish peroxidase-conjugated goat anti-rabbit IgG antibody (ABclonal, Wuhan, China) for 30 min at room temperature. Immunodetection was performed using diaminobenzidine solution according to the manufacturer's instructions. After washing, the sections were counterstained, dehydrated, and then coverslipped using neutral gum sealant.

Quantitative Real-Time PCR (qPCR)

The RNeasy kit (Qiagen, Valencia, CA, United States) was used to extract total RNA from gastrocnemius muscle. cDNA was synthesized using a first-strand cDNA synthesis kit with oligo dT primers (Invitrogen, Carlsbad, CA, United States) and used for quantitative real-time PCR (qPCR) (MJ Research, Waltham, MA, United States). The thermal cycling conditions were as follows: 94°C for 5 min; 35 cycles at 94°C for 30 s, 55°C for 45 s, and 72°C for 1 min; and 72°C for 5 min. Relative expression level of the target gene was calculated using the cycle threshold (Ct) value corrected with that of the β-actin gene (*ACTB*) (relative expression = $2[Ct_{sample} - Ct_{ACTB}]$). The primers used to amplify the mouse peroxisome proliferator-activated receptor alpha (*PPARα*) gene were as follows: forward, GTGTGACATCCCGACAGAC and reverse, CTCACTTCCAGAAACACGA.

Western Blot Analysis

Frozen gastrocnemius muscle samples were homogenized in radioimmunoprecipitation assay buffer containing 1 mM phenylmethylsulfonyl fluoride and Protease Inhibitor Cocktail (Roche Applied Science). Lysates were centrifuged for 20 min at 12,000 × g (4°C) and the protein level in the supernatant was quantified with a bicinchoninic acid assay kit (Beyotime). Proteins were separated by SDS–PAGE (Beyotime) and transferred to a polyvinylidene difluoride membrane (Beyotime) that was blocked with 5% non-fat dry milk in Tris-buffered saline at room temperature, followed by incubation with primary antibodies: rabbit anti-PPARα (1:1000; Affinity Biosciences, United States), rabbit anti-NF-κß P65 (1:5000; Abcam, United Kingdom) and anti-phospho-NF-κß P65 (1:5000; Abcam, United Kingdom), and rabbit anti-IκBα antibodies

(1:1000; Affinity Biosciences, United States). After three washes, the membrane was incubated with appropriate secondary antibody (Abcam) at room temperature for 1 h. Enhanced chemiluminescence detection reagent and X-ray film were used for protein visualization.

Enzyme-Linked Immunosorbent Assay (ELISA)

Expression levels of IL-1β and IL-6 in the gastrocnemius muscle of mice were determined with ELISA kits (Multisciences Biotech, Hangzhou, China) according to the manufacturer's instructions. After measuring optical density at 450 nm, the expression level was calculated from standard curves.

Statistical Analysis

All data are presented as mean ± SD. One-way ANOVA was studied to analysis and compare data from three groups. Statistical analyses were performed using SPSS v17.0 software (SPSS Inc., Chicago, IL, United States). *P*-values < 0.05 were considered statistically significant.

RESULTS

Human Muscle Atrophy

Hematoxylin–eosin staining of sternocleidomastoid muscle tissue sections showed that the myocytes had a regular arrangement with an intact membrane. In contrast, myocytes in denervated biceps muscle had a disordered arrangement and contained numerous vacuoles; Masson's trichrome staining revealed that the intercellular matrix was covered with collagen fibers, with a much larger stained area than in the sternocleidomastoid muscle (**Figure 1**).

DEGs in Denervated Human Muscle

We identified 1471 DEGs by RNA-seq analysis of atrophic biceps muscle and normal (non-denervated) sternocleidomastoid muscle from patients with BPI, including 771 downregulated and 700 upregulated genes; these are presented as a heatmap (**Figure 2A**) and in a volcano plot (**Figure 2B**).

GO and KEGG Pathways of DEGs

A total of 288 enriched GO terms and 28 KEGG pathways were associated with the identified DEGs. The top 30 enriched GO terms according to the threshold *P*-value ($P < 0.05$) included: (1) molecular function, such as "structural constituent of muscle," "muscle alpha-actinin binding," and "actin binding"; (2) cellular component, such as "Z disc," "M band," and "MHC class II protein complex"; and (3) biological process, such as "striated muscle contraction," "glycogen metabolic process," and "cardiac muscle contraction" (**Figure 2C**).

The top 20 enriched KEGG pathways of the DEGs included "Cell adhesion molecules," "Glycolysis/Gluconeogenesis," "PPAR signaling pathway," "p53 signaling pathway," "Dilated cardiomyopathy," "Insulin signaling pathway," "MAPK signaling

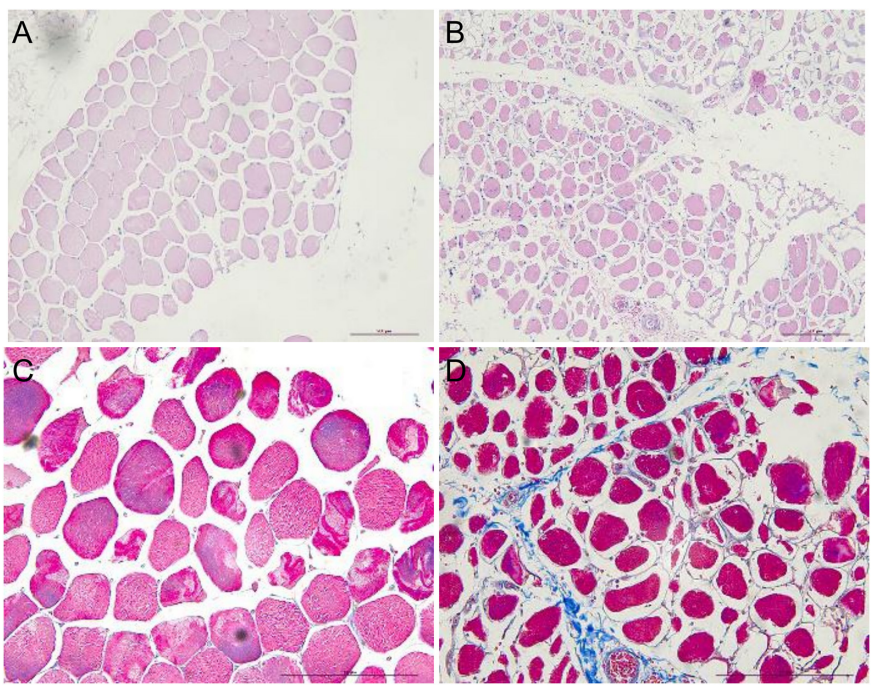

FIGURE 1 | HE and Masson's trichrome staining showing atrophy of human sternocleidomastoid muscle (left figures) and biceps muscle (right figures). **(A,B)** HE staining showing the irregular arrangement of myocytes in denervated muscle and a smaller stained area compared to normal (non-denervated) sternocleidomastoid muscle. **(C,D)** Masson's trichrome staining showing the intercellular matrix of denervated muscle covered with blue collagen fiber. Scale bar, 200 μm.

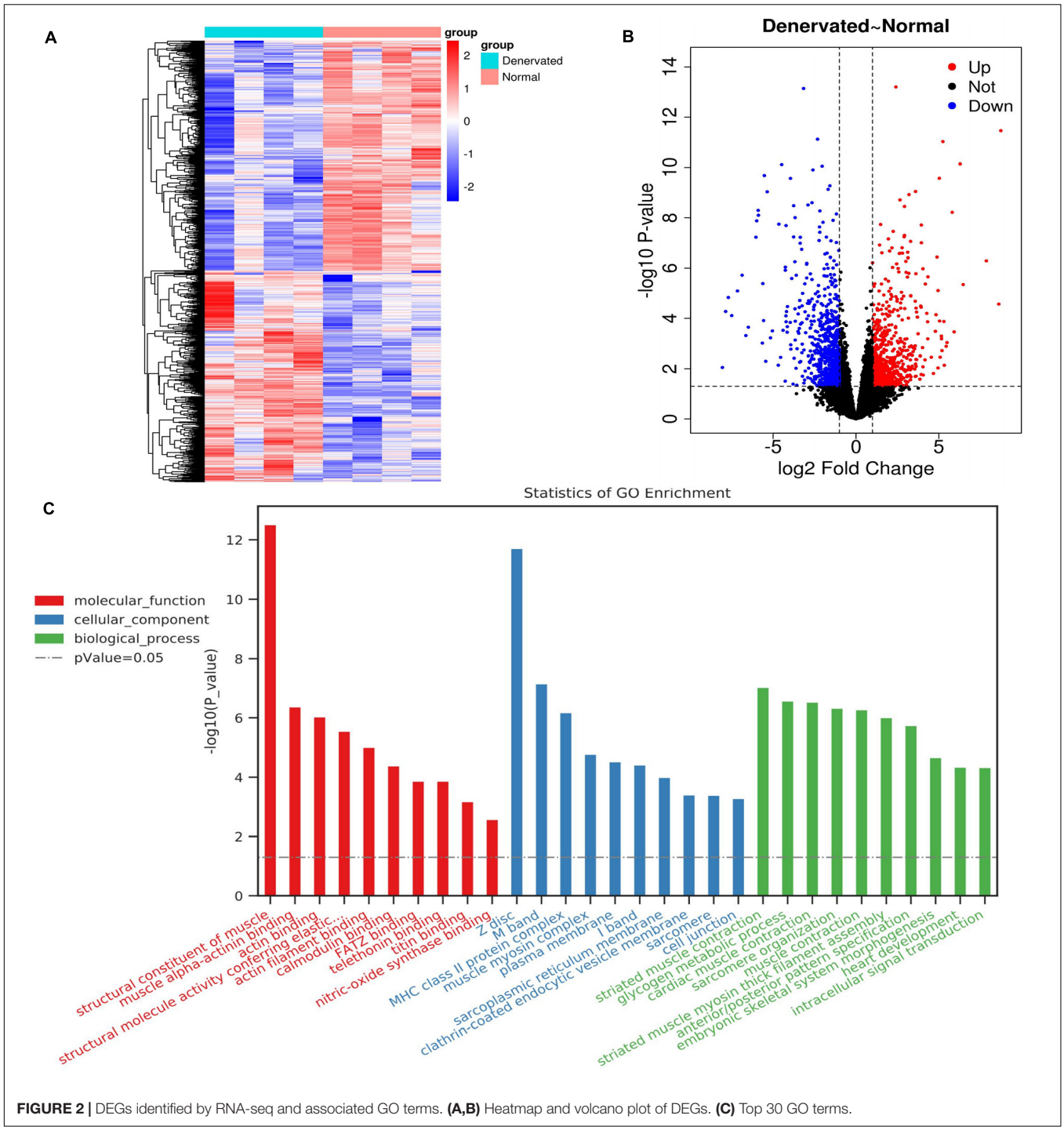

FIGURE 2 | DEGs identified by RNA-seq and associated GO terms. **(A,B)** Heatmap and volcano plot of DEGs. **(C)** Top 30 GO terms.

pathway," and so on (**Figure 3A**). For the gene network of the top four KEGG pathways, see **Figure 3B**.

FCL. Attenuates Skeletal Muscle Atrophy

After 21 days of FCL. infusion, the denervation-induced loss of muscle wet weight was significantly attenuated, and the mean fibro-diameter of gastrocnemius muscle was larger than in saline-infused mice (**Figure 4**).

FCL. Inhibits IL-1β and IL-6 Production in Atrophic Muscles

To determine whether FCL. extract treatment affects the inflammatory response in muscles after denervation, we assessed the expression levels of the proinflammatory cytokines IL-1β and IL-6 in the denervated muscles of mice treated with FCL. extract or saline. Immunohistochemical analysis revealed that IL-1β and IL-6 were upregulated in the denervated muscle of both

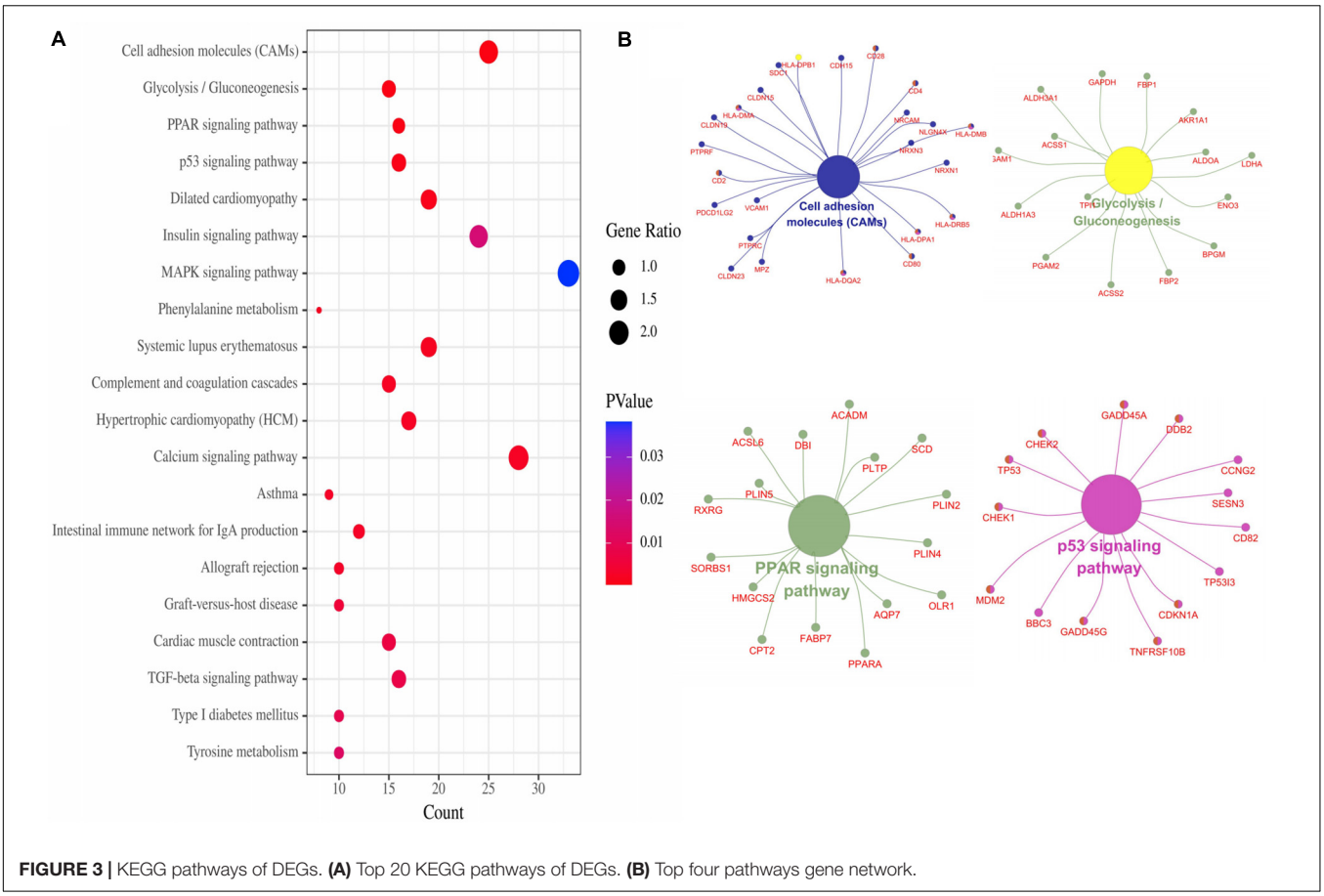

FIGURE 3 | KEGG pathways of DEGs. **(A)** Top 20 KEGG pathways of DEGs. **(B)** Top four pathways gene network.

treatment groups compared to the control group. However, IL-1β and IL-6 positive-expression was lower in the atrophic muscle of mice treated with FCL. extract compared to those treated with saline (**Figure 4**).

We also examined IL-6 and IL-1β levels in mouse gastrocnemius muscle by ELISA. Consistent with the immunohistochemistry results, we found that the levels of both cytokines were elevated in atrophic muscle, and were lower in mice treated with FCL. (**Figure 5**) extract than in those treated with saline. These data suggest that FCL. extract attenuates denervation-induced muscle atrophy by inhibiting the inflammatory response in muscle.

FCL. Attenuates Skeletal Muscle Atrophy by Stimulating PPARα Expression

The RNA-seq results showed that the PPAR signaling pathway is involved in the process of denervated muscle atrophy. To determine whether FCL. extract acts by modulating PPAR signaling, PPARA mRNA and protein expression was evaluated by qPCR and western blotting, respectively (**Figure 6**). *PPARA* mRNA and PPARα protein levels were upregulated in denervated muscle, with higher levels in mice treated with FCL. extract than in those treated with saline, suggesting that FCL. extract attenuates skeletal muscle atrophy by promoting PPARα expression.

FCL. Suppresses Inflammation in Atrophic Muscle by Inhibiting Nuclear Factor (NF)-κB Activation

Previous studies have shown that the anti-inflammatory activity of PPARα involves the inactivation of P65-nuclear factor (NF)-κB through the upregulation of inhibitor of NF-κB (IκBα) (Korbecki et al., 2019). To determine whether FCL. extract attenuates denervated muscle atrophy via this mechanism, we evaluated the activation of NF-κB and expression of IκBα (**Figure 6**). P65-NF-κB activation was increased in denervated muscle; however, this effect was abrogated by FCL. compared to saline infusion. Meanwhile, IκBα expression was higher in Den-FCL. group mice than in Den-saline group. Thus, FCL. attenuates skeletal muscle atrophy by promoting the activation of PPARα and thereby inhibiting NF-κB activity.

DISCUSSION

A long period of denervation in patients with peripheral nerve injury or disease can lead to skeletal muscle atrophy (Xiong et al., 2012; Ehmsen and Höke, 2020). However, the mechanisms underlying denervated muscle atrophy are not fully understood. Microarray and RNA-seq studies have identified key genes and singling pathways involved in this process (Jian et al., 2018;

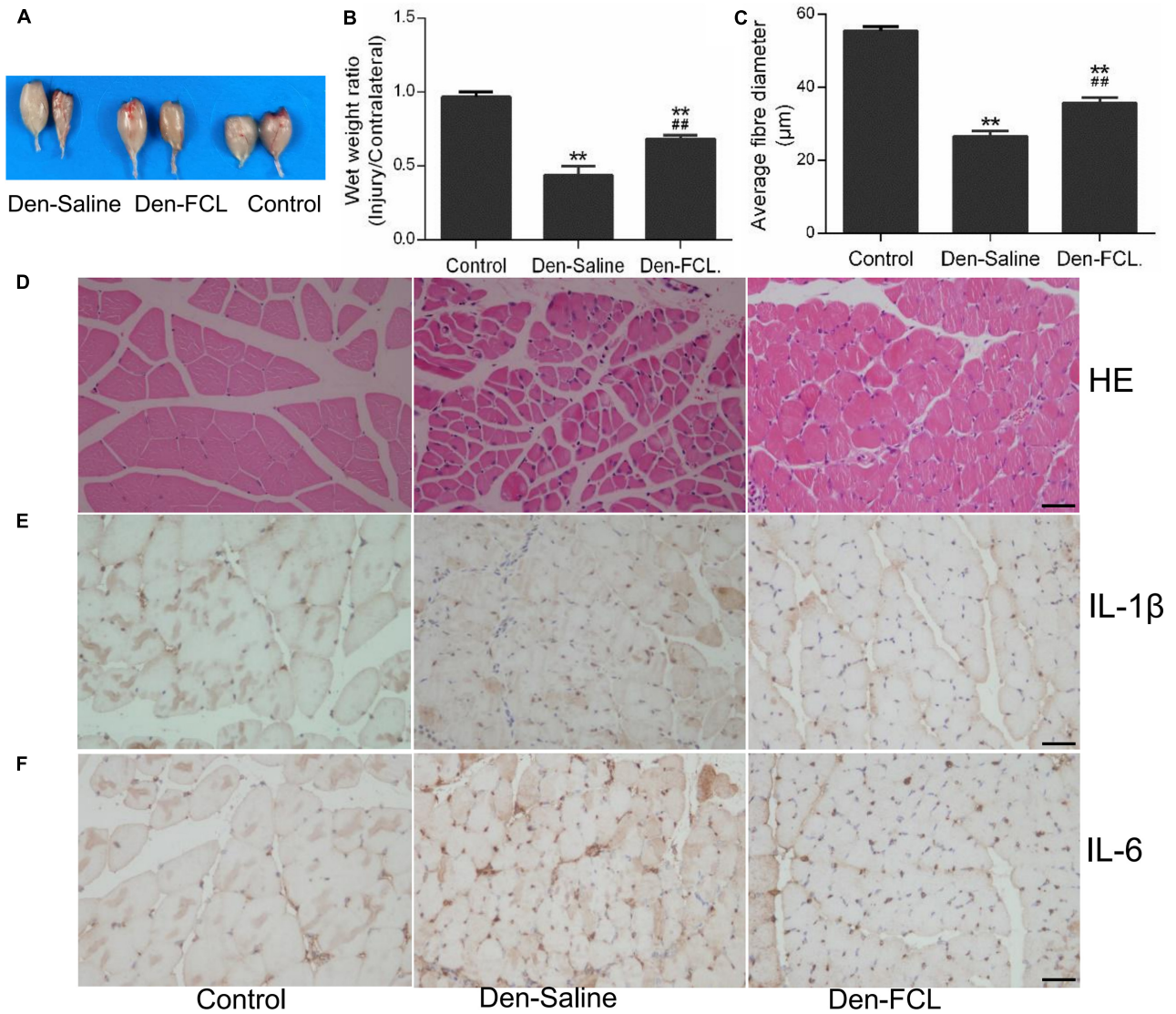

FIGURE 4 | FCL. extract attenuates skeletal muscle atrophy and inhibits IL-1β and IL-6 production in denervated muscle (n = 4 mice in each group). **(A,B)** The wet weight ratio of gastrocnemius at 21 days post-denervation. **(C,D)** HE staining of muscle tissue and means ± SEM of fibro-diameter showing muscle atrophy that was reduced by FCL. extract treatment. **(E,F)** Compared to control group muscle, IL-1β and IL-6 positive-expression was increased in the denervated muscle of Den-saline group mice; the levels of both cytokines were lower in the Den-FCL. mice. Scale bar, 50 μm. $^{**}p < 0.01$ versus Control. $\#\#p < 0.01$ versus Den-Saline.

Shen et al., 2019), but most of the data were from rodent models of peripheral nerve injury and not from human studies.

In the present work, we used high-throughput sequencing to compare gene expression profiles of atrophic biceps muscle and normal sternocleidomastoid muscle from four patients with BPI. Biceps muscle denervation in these patients was confirmed by preoperative physical examination and electromyography. We used the sternocleidomastoid muscle as a control because of the ethical constraint associated with the resection of biceps muscle from the contralateral healthy upper arm of the patient or from a healthy human subject. The sternocleidomastoid muscle was exposed during the surgical process and innervation was confirmed to be intact; we therefore resected this muscle along with the biceps muscle from the same patient in order to reduce heterogeneity across our sample set. We identified 1471 DEGs between denervated and non-denervated muscles, including 700 upregulated and 771 downregulated genes. Most of the enriched GO terms were directly associated with skeletal muscle molecular function and cellular component, such as "structural constituent of muscle," "Z disc," "M band," and "striated muscle contraction"; additionally, other GO terms also included some terms related to the metabolic process, such as "glycogen metabolic process," "glycogen catabolic process," and "canonical glycolysis."

The KEGG pathway analysis showed that the DEGs were mainly enriched in "Cell adhesion molecules," "Glycolysis/Gluconeogenesis," "PPAR signaling pathway," and

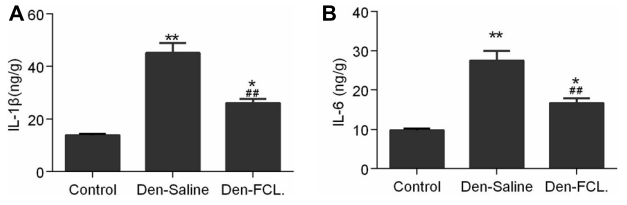

FIGURE 5 | Expression levels of IL-1β and IL-6 in gastrocnemius were detected using ELISA kits. Both IL-1β and IL-6 expressions were increased in the denervated mice muscle, and the elevated level of both cytokines was lower in the Den-FCL. mice (n = 4 mice in each group). **(A)** IL-1β expression was determined. **(B)** IL-6 expression was determined. $^{**}p < 0.01$ and $^{*}p < 0.05$ versus Control. $\#\#p < 0.01$ versus Den-Saline.

"p53 signaling pathway." Cell adhesion is one cell's autonomous capability of adhering to pluricellular organisms at the basis of the formation of tissues and organs, and cell adhesive processes have be considered as key features of skeletal muscle morphogenesis (Cifuentes et al., 1994; Zhou et al., 2015; Bauer et al., 2019). Kobayashi et al. (1992) have demonstrated that compared with adult mice, the number of neural cell adhesion molecule-positive nerve fibers in motor nerve of sternomastoid was increased in old mice, which show neuromuscular remodeling, indicates that cell adhesion molecules may play a role in regulating the instability of motor nerve terminals. The skeletal muscle accounts for a significant amount of glucose uptake and storage, in pathological conditions, this metabolic regulation ability of skeletal muscle will be perturbed (Deshmukh, 2016; Josep et al., 2016). Thus, lots of pathways related to energy metabolism were enriched in our study, such as "Glycolysis/Gluconeogenesis," "Insulin signaling pathway," "Phenylalanine metabolism," "Type I diabetes mellitus," and "Tyrosine metabolism." These findings highlight that the dysfunctional energy metabolism following denervation contribute to muscle atrophy.

The PPAR family comprises three transcription factors—namely, PPARα, PPARβ/δ, and PPARγ—that regulate inflammation and glucose and lipid metabolism by binding to PPAR response elements in the promoter region of target genes (Aleshin and Reiser, 2013; Di et al., 2014; Antonopoulos et al., 2016; Zhong et al., 2017). Recent studies have shown that PPARα encoded by the *PPARA* gene regulates the expression of genes related to inflammation, oxidative stress response, energy metabolism, and mitochondrion and peroxisome function (Sander, 2014; Mitchell et al., 2017; Luo et al., 2020). P53 family members (e.g., tumor protein [TP]53, TP73, and TP63) modulate the expression of Tripartite motif-containing (TRIM)63, which regulates the proteasomal degradation of structural muscle proteins, particularly myofibril components (Ehmsen and Höke, 2020).

Muscle homeostasis depends on the stability of the muscle microenvironment, which is composed of muscle cells (stem cells and interstitial cells), motoneurons, and secreted cytokines (Madaro et al., 2018; Wu et al., 2019). Oxidative stress induces changes in the muscle microenvironment. The release of H_2O_2 and ROS from muscle cell mitochondria is increased following denervation (Pollock et al., 2017), which can lead to oxidative stress and consequently, mitochondrial dysfunction, protein degradation, and cellular damage (Qiu et al., 2018; Scalabrin et al., 2019). Inflammation plays an important role in the process of muscle atrophy (Cánoves et al., 2013; Shen et al., 2019; Wu et al., 2019); the enhanced production of proinflammatory cytokines such as IL-1β and IL-6 in atrophic muscle increases ubiquitin expression and the accumulation of ubiquitinated proteins, which promotes protein degradation (Cánoves et al., 2013; Cea et al., 2013; Ma et al., 2019; Ehmsen and Höke, 2020). In our study, IL-1β and IL-6 production was increased in the atrophic muscle of mice at 21 days post-denervation. Given these observations, drugs that can suppress inflammation and oxidative stress may be effective in attenuating and preventing muscle atrophy. FCL. was shown to improve diabetes and inhibit tumor cell proliferation (Umar et al., 2013; Soltana et al., 2019; Zhang et al., 2019) and has known antioxidant, anti-inflammatory, and antiapoptotic effects (Ali et al., 2012; Umar et al., 2013; Melisa et al., 2014; Zhang et al., 2019). We found here that FCL. extract alleviated the severity of denervation-induced muscle atrophy in mice, which was associated with lower levels of IL-1β and IL-6 compared to Den-saline group mice. These results imply that FCL. attenuates muscle atrophy by inhibiting inflammation in denervated muscle.

We observed that p65-NF-κB activity was increased in the denervated muscle of mice. NF-κB is activated during the inflammatory response, which stimulates prostaglandin synthesis (Senf et al., 2008; Korbecki et al., 2019). The regulation of these pathways involves positive feedback but also upregulation of PPARα which prevents the pro-infammatory response from being excessively activated (Delerive et al., 1999; Kono et al., 2009; Korbecki et al., 2019). Meanwhile, according to our RNA-seq findings, PPAR pathway was one of major signaling pathways and the pathway network revealed that PPARA mRNA is only one of three PPAR family genes existing in the DEGs enriched PPAR pathway. To determine whether the attenuation of inflammation in denervated muscle by FCL. extract involves PPARα, we examined *PPARA* transcript and PPARα protein expression and found that both were significantly increased in Den-FCL. group mice compared to Den-saline group mice, suggesting that FCL. extract suppresses the inflammation associated with muscle denervation by promoting of PPARα expression. It is worth noting that PPAR level was increased in denervated muscle regardless of the treatment, possibly reflecting a positive feedback mechanism that counters inflammation induced by denervation (**Figure 6**).

The anti-inflammatory activity of PPARα involves inactivation of NF-κB, which may involve direct binding of the p65 subunit or enhanced ubiquitination and proteolytic degradation of p65 (Delerive et al., 1999; Korbecki et al., 2019). PPARα has been shown to induce IκBα expression, which blocks the nuclear translocation of NF-κB (Delerive et al., 2000). We observed that IκBα expression was higher while NF-κB activity was lower in FCL. extract-treated mice than in those which were administered saline. Thus, FCL. extract may suppress inflammation by enhancing PPARα expression, which inactivates NF-κB through the upregulation of IκBα.

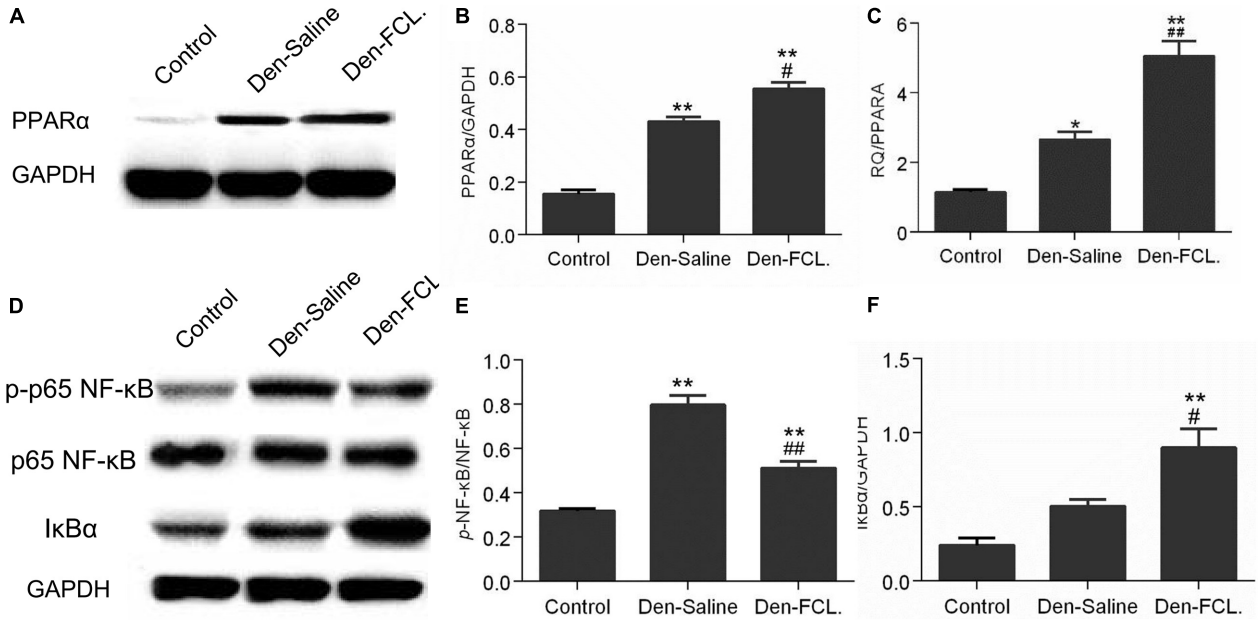

FIGURE 6 | FCL. attenuates skeletal muscle atrophy via PPARα/NF-κB signaling. **(A,B)** Elevated expression of PPARα in both denervated group mice were determined by western blotting. PPARα elevation level of Den-FCL group mice was much higher than the Den-saline group. **(C)** *PPARA* mRNA levels determined by qPCR showed a trend similar to that of the protein. **(D–F)** p65-NF-κB activity was increased after muscle denervation, but was reduced by FCL. extract as compared to saline treatment. Meanwhile, the Den-FCL. group mice showed higher IκBα expression level than other groups (n = 4 mice in each group). $^{**}p < 0.01$ and $^{*}p < 0.05$ versus Control. $^{\#\#}p < 0.01$ and $^{\#}p < 0.05$ versus Den-Saline.

There are some limitations in our study including: (1) the effects of chemical compositions of FCL remain unclear, which are needed to be confirmed to facilitate reproducibility; (2) the number of human samples is limited; it is necessary for detecting dynamic numbers of DEGs over time-denervation to collect more human denervated samples at various nerve injury timings; and (3) we only determined the effect of FCL. extract at 21 days after denervation in mice, which does not allow for a fine-tuning of the molecular events along the process, and the effect of FCL. extract at other time points is still unknown.

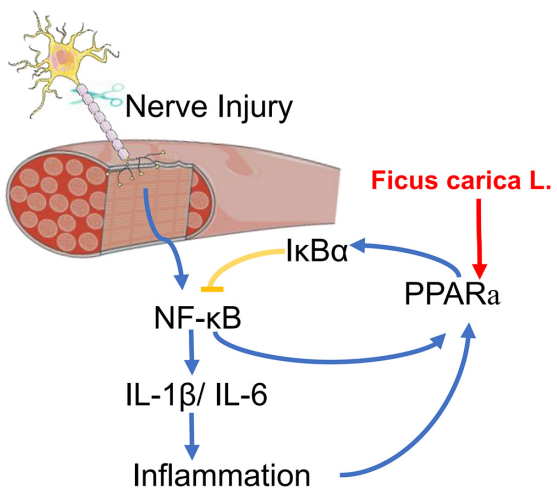

FIGURE 7 | A scheme for FCL. extract attenuating denervated muscle atrophy by inhibiting the inflammation response through PPARα/NF-κB signaling pathways.

CONCLUSION

In summary, this is the first study to apply transcriptome sequencing to the investigation of denervation-induced muscle atrophy using clinical specimens from patients with BPI. The results presented here provide insight into the molecular basis of denervated muscle atrophy. We also showed that treatment with FCL. extract can delay the atrophy of denervated muscle in mice, which may involve suppression of the inflammatory response via regulation of PPARα and NF-κB signaling (**Figure 7**). Although additional studies are needed to identify the specific compound(s) in FCL. extract responsible for its protective effects, our findings provide evidence for the therapeutic potential of FCL. extract to delay or prevent denervation-induced muscle atrophy caused by peripheral nerve injury or disease.

DATA AVAILABILITY STATEMENT

This article contains previously unpublished data. The gene expression dataset is available on NCBI SRA (https://www.ncbi.nlm.nih.gov/sra/PRJNA644778) and the accession number is PRJNA644778.

ETHICS STATEMENT

The studies involving human participants were reviewed and approved by the Ethical Committee, Huashan hospital, Fudan University. The patients/participants provided their written informed consent to participate in this study. The animal study was reviewed and approved by the Institutional Animal Care and Use Committee of Huashan hospital, Fudan University.

AUTHOR CONTRIBUTIONS

JJ and JX designed the study. JD, YX, DF, and LX performed the experiments. JD and YX analyzed the data. JD wrote the manuscript. YX made the figures. All authors contributed to the article and approved the submitted version.

FUNDING

This study was supported by Shanghai Municipal Key Clinical specialty (shslczdzk05601).

SUPPLEMENTARY MATERIAL

The Supplementary Material for this article can be found online at: https://www.frontiersin.org/articles/10.3389/fphys.2020.580223/full#supplementary-material

Supplementary Table 1 | The characteristic data of four donors.

REFERENCES

Aleshin, S., and Reiser, G. (2013). Role of the peroxisome proliferator-activated receptors (PPAR)-α, β/δ and γ triad in regulation of reactive oxygen species signaling in brain. *Biol. Chem.* 394, 1553–1570. doi: 10.1515/hsz-2013-0215

Ali, B., Mujeeb, M., Aeri, V., Mir, S. R., Faiyazuddin, M., and Shakeel, F. (2012). Anti-inflammatory and antioxidant activity of Ficus carica Linn. leaves. *Nat. Prod. Res.* 26, 460–465. doi: 10.1080/14786419.2010.488236

Anders, S., Pyl, P. T., and Huber, W. (2015). HTSeq–a Python framework to work with high-throughput sequencing data. *Bioinformatics* 31, 166–169. doi: 10.1093/bioinformatics/btu638

Antonopoulos, A. S., Margaritis, M., Verheule, S., Recalde, A., and Antoniades, C. (2016). Mutual regulation of epicardial adipose tissue and myocardial redox state by PPAR-γ/adiponectin signalling. *Circ. Res.* 118, 842–855. doi: 10.1161/CIRCRESAHA.115.307856

Badgujar, S. B., Patel, V. V., Bandivdekar, A. H., and Mahajan, R. T. (2014). Traditional uses, phytochemistry and pharmacology of Ficus carica: a review. *Pharm. Biol.* 52, 1487–1503. doi: 10.3109/13880209.2014.892515

Bauer, M. S., Baumann, F., Daday, C., Redondo, P., Durner, E., Jobst, M. A., et al. (2019). Structural and mechanistic insights into mechanoactivation of focal adhesion kinase. *Proc. Natl. Acad. Sci. U. S. A.* 116, 6766–6774. doi: 10.1073/pnas.1820567116

Birger, A., Ben-Dor, I., Ottolenghi, M., Turetsky, T., Gil, Y., Sweetat, S., et al. (2019). Human iPSC-derived astrocytes from ALS patients with mutated C9ORF72 show increased oxidative stress and neurotoxicity. *EBioMedicine* 50, 274–289. doi: 10.1016/j.ebiom.2019.11.026

Bolger, A. M., Lohse, M., and Usadel, B.(2014). Trimmomatic: a flexible trimmer for Illumina sequence data. *Bioinformatics*. 30, 2114–2120. doi: 10.1093/bioinformatics/btu170

Burns, T. M., Graham, C. D., Rose, M. R., and Simmons, Z. (2012). Quality of life and measures of quality of life in patients with neuromuscular disorders. *Muscle Nerve* 46, 9–25. doi: 10.1002/mus.23245

Cánoves, P. M., Scheele, C., Pedersen, B. K., and Serrano, A. L. (2013). Interleukin-6 myokine signaling in skeletal muscle: a double-edged sword? *FEBS J.* 280, 4131–4148. doi: 10.1111/febs.12338

Cea, L. A., Cisterna, B. A., Puebla, C., Frank, M., Figueroa, X. F., Cardozo, C., et al. (2013). De novo expression of connexin hemichannels in denervated fast skeletal muscles leads to atrophy. *Proc. Natl. Acad. Sci. U. S. A.* 110, 16229–16234. doi: 10.1073/pnas.1312331110

Cifuentes, D. C., Nicolet, M., and Mège, R. M. (1994). Cell adhesion and development of skeletal muscle. *C. R. Seances Soc. Biol. Fil.* 188, 505–525.

Delerive, P., De, B. K., Besnard, S., Vanden, B. W., Peters, J. M., Gonzalez, F. J., et al. (1999). Peroxisome proliferator-activated receptor alpha negatively regulates the vascular inflammatory gene response by negative cross-talk with transcription factors NF-kappaB and AP-1. *J. Biol. Chem.* 274, 32048–32054. doi: 10.1074/jbc.274.45.32048

Delerive, P., Gervois, P., Fruchart, J. C., and Staels, B. (2000). Induction of IkappaBalpha expression as a mechanism contributing to the antiinflammatory activities of peroxisome proliferator-activated receptor-alpha activators. *J. Biol. Chem.* 275, 36703–36707. doi: 10.1074/jbc.M004045200

Deshmukh, A. S. (2016). Insulin-stimulated glucose uptake in healthy and insulin-resistant skeletal muscle. *Horm. Mol. Biol. Clin. Investig.* 26, 13–24. doi: 10.1515/hmbci-2015-0041

Di, B. B., Li, H. W., Li, W. P., Shen, X. H., Sun, Z. J., and Wu, X. (2014). Pioglitazone inhibits high glucose-induced expression of receptor for advanced glycation end products in coronary artery smooth muscle cells. *Mol. Med. Rep.* 11, 2601–2607. doi: 10.3892/mmr.2014.3113

Ebert, S. M., Dyle, M. C., Kunkel, S. D., Bullard, S. A., Bongers, K. S., Fox, D. K., et al. (2012). Stress-induced skeletal muscle Gadd45a expression reprograms myonuclei and causes muscle atrophy. *J. Biol. Chem.* 287, 27290–27301. doi: 10.1074/jbc.M112.374777

Ehmsen, J. T., and Höke, A. (2020). Cellular and molecular features of neurogenic skeletal muscle atrophy. *Exp. Neurol.* 331:113379. doi: 10.1016/j.expneurol.2020.113379

Furlow, J. D., Watson, M. L., Waddell, D. S., Neff, E. S., Baehr, L. M., Ross, A. P., et al. (2013). Altered gene expression patterns in muscle ring finger 1 null mice during denervation- and dexamethasone-induced muscle atrophy. *Physiol. Genom.* 45, 1168–1185. doi: 10.1152/physiolgenomics.00022.2013

Huang, Q. K., Qiao, H. Y., Fu, M. H., Li, G., Li, W. B., Chen, Z., et al. (2016). MiR-206 attenuates denervation-induced skeletal muscle atrophy in rats through regulation of satellite cell differentiation via TGF-β1, Smad3, and HDAC4 signaling. *Med. Sci. Monit.* 22, 1161–1170. doi: 10.12659/msm.897909

Jian, W., Zhang, P., Yin, X., and Jiang, B. (2018). The whole transcriptome involved in denervated muscle atrophy following peripheral nerve injury. *Front. Mol. Neurosci.* 7:69. doi: 10.3389/fnmol.2018.00069

Josep, M. A., Campos, N., José, M. L., Rueda, R., and Leocadio, R. M. (2016). Skeletal muscle regulates metabolism via interorgan crosstalk: roles in health and disease. *J. Ame. Med. Dir. Assoc.* 17, 789–796. doi: 10.1016/j.jamda.2016.04.019

Kim, D., Langmead, B., and Salzberg, S. L. (2015). HISAT: a fast spliced aligner with low memory requirements. *Nat. Methods* 12, 357–360. doi: 10.1038/nmeth.3317

Kobayashi, H., Robbins, N., and Rutishauser, U. (1992). Neural cell adhesion molecule in aged mouse muscle. *Neuroscience* 48, 237–248. doi: 10.1016/0306-4522(92)90352-3

Kono, K., Kamijo, Y., Hora, K., Takahashi, K., Higuchi, M., and Kiyosawa, K. (2009). PPAR{alpha} attenuates the proinfammatory response in activated mesangial cells. *Am. J. Physiol. Ren. Physiol.* 296, F328–F336. doi: 10.1152/ajprenal.00484.2007

Korbecki, J., Bobiński, R., and Dutka, M. (2019). Self-regulation of the inflammatory response by peroxisome proliferator-activated receptors. *Inflamm. Res.* 68, 443–458. doi: 10.1007/s00011-019-01231-1

Kunkel, S. D., Suneja, M., Ebert, S. M., Bongers, K. S., Fox, D. K., Malmberg, S. E., et al. (2011). mRNA expression signatures of human skeletal muscle atrophy identify a natural compound that increases muscle mass. *Cell Metab.* 13, 627–638. doi: 10.1016/j.cmet.2011.03.020

Li, J., Chan, M. C., Yu, Y., Bei, Y., Chen, P., Zhou, Q., et al. (2017). miR-29b contributes to multiple types of muscle atrophy. *Nat. Commun.* 25:15201. doi: 10.1038/ncomms15201

Luo, R., Su, L. Y., Li, G., Yang, J., Liu, Q., Yang, L. X., et al. (2020). Activation of PPARA-mediated autophagy reduces Alzheimer disease-like pathology and cognitive decline in a murine model. *Autophagy* 16, 52–69. doi: 10.1080/15548627.2019.1596488

Ma, W., Xu, T., Wang, Y., Wu, C., Wang, L., Yang, X., et al. (2018). The role of inflammatory factors in skeletal muscle injury. *Biotarget* 2018:7. doi: 10.21037/biotarget.2018.04.01

Ma, W. J., Zhang, R., Huang, Z. W., Zhang, Q. Y., Xie, X. Y., Yang, X. M., et al. (2019). PQQ ameliorates skeletal muscle atrophy, mitophagy and fiber type transition induced by denervation via inhibition of the inflammatory signaling pathways. *Ann. Transl. Med.* 7:440. doi: 10.21037/atm.2019.08.101

Madaro, L., Passafaro, M., Sala, D., Etxaniz, U., Lugarini, F., Proietti, D., et al. (2018). Denervation-activated STAT3-IL-6 signalling in fibro-adipogenic progenitors promotes myofibres atrophy and fibrosis. *Nat. Cell Biol.* 20, 917–927. doi: 10.1038/s41556-018-0151-y

Melisa, B., Nathalie, R. M., and Silvia, N. L. (2014). Ficus carica L. (Moraceae): an ancient source of food and health. *Food Chem.* 164, 119–127. doi: 10.1016/j.foodchem.2014.04.112

Minoru, K., Michihiro, A., Susumu, G., Masahiro, H., Mika, H., Masumi, I., et al. (2008). KEGG for linking genomes to life and the environment. *Nucleic Acids Res.* 36, D480–D484. doi: 10.1093/nar/gkm882

Mitchell, B. R., Kaberi, P. D., John, R., Barbara, A., Christopher, L., and Corton, J. C. (2017). PPARα-independent transcriptional targets of perfluoroalkyl acids revealed by transcript profiling. *Toxicology* 387, 95–107. doi: 10.1016/j.tox.2017.05.013

Muller, F. L., Song, W., Jang, Y. C., Liu, Y. H., Sabia, M., Richardson, A., et al. (2007). Denervation-induced skeletal muscle atrophy is associated with increased mitochondrial ROS production. *Am. J. Physiol. Regul. Integr. Comp. Physiol.* 293, R1159–R1168. doi: 10.1152/ajpregu.00767.2006

Odeh, M., Livne, Y. T., Haas, T., and Bengal, E. (2020). P38α MAPK coordinates the activities of several metabolic pathways that together induce atrophy of denervated muscles. *FEBS J.* 287, 73–93. doi: 10.1111/febs.15070

Onodera, K., Shimojo, D., Ishihara, Y., Yano, M., Miya, F., Banno, H., et al. (2020). Unveiling synapse pathology in spinal bulbar muscular atrophy by genome-wide transcriptome analysis of purified motor neurons derived from disease specific iPSCs. *Mol. Brain* 13:18. doi: 10.1186/s13041-020-0561-1

Pollock, N., Staunton, C. A., Vasilaki, A., McArdle, A., and Jackson, M. J. (2017). Denervated muscle fibers induce mitochondrial peroxide generation in neighboring innervated fibers: role in muscle aging. *Free Radic. Biol. Med.* 112, 84–92. doi: 10.1016/j.freeradbiomed.2017.07.017

Qiu, J., Fang, Q., Xu, T., Wu, C., Lai, X., Wang, L., et al. (2018). Mechanistic role of reactive oxygen species and therapeutic potential of antioxidants in denervation- or fasting-induced skeletal muscle atrophy. *Front. Physiol.* 14:215. doi: 10.3389/fphys.2018.00215

Roberts, A., Trapnell, C., Donaghey, J., Rinn, J. L., and Pachter, L. (2011). Improving RNA-Seq expression estimates by correcting for fragment bias. *Genome Biol.* 12:R22. doi: 10.1186/gb-2011-12-3-r22

Sander, K. (2014). Integrated physiology and systems biology of PPARα. *Mol. Metab.* 3, 354–371. doi: 10.1016/j.molmet.2014.02.002

Scalabrin, M., Pollock, N., Staunton, C. A., Brooks, S. V., McArdle, A., Jackson, M. J., et al. (2019). Redox responses in skeletal muscle following denervation. *Redox Biol.* 26:101294. doi: 10.1016/j.redox.2019.101294

Senf, S. M., Dodd, L. S., Mcclung, J. M., and Judge, A. R. (2008). Hsp70 overexpression inhibits NF-kappaB and Foxo3a transcriptional activities and prevents skeletal muscle atrophy. *FASEB J.* 22, 3836–3845. doi: 10.1096/fj.08-110163

Shen, Y., Zhang, R., Xu, L., Wan, Q., and Sun, H. (2019). Microarray analysis of gene expression provides new insights into denervation-induced skeletal muscle atrophy. *Front. Physiol.* 11:1298. doi: 10.3389/fphys.2019.01298

Soares, R. J., Cagnin, S., Chemello, F., Silvestrin, M., Musaro, A., De Pitta, C., et al. (2014). Involvement of microRNAs in the regulation of muscle wasting during catabolic conditions. *J. Biol. Chem.* 289, 21909–21925. doi: 10.1074/jbc.M114.561845

Soltana, H., Pinon, A., Limami, Y., Zaid, Y., and Hammami, M. (2019). Antitumoral activity of Ficus carica L. on colorectal cancer cell lines. *Cell. Mol. Biol.* 65, 6–11. doi: 10.14715/cmb/2019.65.6.2

Trapnell, C., Williams, B. A., Pertea, G., Mortazavi, A., Kwan, G., Van Baren, M. J., et al. (2010). Transcript assembly and quantification by RNA-Seq reveals unannotated transcripts and isoform switching during cell differentiation. *Nat. Biotechnol.* 28, 511–515. doi: 10.1038/nbt.1621

Umar, Z. U., Moh'D, A., and Tanko, Y. (2013). Effects of ethanol leaf extract of ficus glumosa on fasting blood glucose and serum lipid profile in diabetic rats. *Niger. J. Physiol. Sci.* 28, 99–104.

Winterbourn, C. C., and Hampton, M. B. (2008). Thiol chemistry and specificity in redox signaling. *Free Radic. Biol. Med.* 45, 549–561. doi: 10.1016/j.freeradbiomed.2008.05.004

Wu, C., Tang, L., Ni, X., Xu, T., Fang, Q., Xu, L., et al. (2019). Salidroside attenuates denervation-induced skeletal muscle atrophy through negative regulation of pro-inflammatory cytokine. *Front. Physiol.* 10:665. doi: 10.3389/fphys.2019.00665

Xiong, W.-M., Huang, J.-H., Xie, L., Qiao, Y., Lu, X.-M., Peng, J.-C., et al. (2012). Overexpression of MyoD attenuates denervated rat skeletal muscle atrophy and dysfunction. *Neurosci. Med.* 3, 387–393. doi: 10.4236/nm.2012.34048

Yang, X. F., Xue, P. P., Liu, X., Xu, X., and Chen, Z. B. (2018). HMGB1/autophagy pathway mediates the atrophic effect of TGF-β1 in denervated skeletal muscle. *Cell Commun. Signal.* 16:97. doi: 10.1186/s12964-018-0310-6

Zhang, Y., Li, Y., Ma, P., Chen, J., and Xie, W. (2019). Ficus carica leaves extract inhibited pancreatic β-cell apoptosis by inhibiting AMPK/JNK/caspase-3 signaling pathway and antioxidation. *Biomed. Pharmacother.* 122:109689. doi: 10.1016/j.biopha.2019.109689

Zhong, C. B., Xi, C., Zhou, X. Y., and Wang, X. B. (2017). The role of peroxisome proliferator-activated receptor γ in mediating cardioprotection against ischemia/reperfusion injury. *J. Cardiovasc. Pharmacol. Ther.* 23, 46–56. doi: 10.1177/1074248417707049

Zhou, J., Aponte-Santamaría, C., Sturm, S., Bullerjahn, J. T., Bronowska, A., and Gräter, F. (2015). Mechanism of focal adhesion kinase mechanosensing. *PLoS Comput. Biol.* 11:e1004593. doi: 10.1371/journal.pcbi.1004593

Conflict of Interest: The authors declare that the research was conducted in the absence of any commercial or financial relationships that could be construed as a potential conflict of interest.

frontiers in Pharmacology

REVIEW
published: 12 March 2021
doi: 10.3389/fphar.2021.642858

Genetic Approaches for the Treatment of Facioscapulohumeral Muscular Dystrophy

Kenji Rowel Q. Lim[1] *and Toshifumi Yokota*[1,2]*

[1]Department of Medical Genetics, Faculty of Medicine and Dentistry, University of Alberta, Edmonton, AB, Canada, [2]The Friends of Garrett Cumming Research and Muscular Dystrophy Canada, HM Toupin Neurological Science Research Chair, Edmonton, AB, Canada

Facioscapulohumeral muscular dystrophy (FSHD) is an autosomal dominant disorder characterized by progressive, asymmetric muscle weakness at the face, shoulders, and upper limbs, which spreads to the lower body with age. It is the third most common inherited muscular disorder worldwide. Around 20% of patients are wheelchair-bound, and some present with extramuscular manifestations. FSHD is caused by aberrant expression of the *double homeobox protein 4* (*DUX4*) gene in muscle. *DUX4* codes for a transcription factor which, in skeletal muscle, dysregulates numerous signaling activities that culminate in cytotoxicity. Potential treatments for FSHD therefore aim to reduce the expression of *DUX4* or the activity of its toxic protein product. In this article, we review how genetic approaches such as those based on oligonucleotide and genome editing technologies have been developed to achieve these goals. We also outline the challenges these therapies are facing on the road to translation, and discuss possible solutions and future directions

Keywords: facioscapulohumeral muscular dystrophy, DUX4, antisense oligonucleotides, RNAi, DNA decoys, DNA aptamers, CRISPR, gene modulation

OPEN ACCESS

Edited by:
Carlo Rinaldi,
University of Oxford, United Kingdom

Reviewed by:
Qing Lyu,
Chongqing Institute of Green and Intelligent Technology, China
Judit Balog,
Leiden University Medical Center, Netherlands

***Correspondence:**
Toshifumi Yokota
toshifumi.yokota@ualberta.ca

Specialty section:
This article was submitted to Translational Pharmacology, a section of the journal Frontiers in Pharmacology

Received: *16 December 2020*
Accepted: *01 February 2021*
Published: *12 March 2021*

Citation:
Lim KRQ and Yokota T (2021) Genetic Approaches for the Treatment of Facioscapulohumeral Muscular Dystrophy. Front. Pharmacol. 12:642858. doi: 10.3389/fphar.2021.642858

INTRODUCTION

Facioscapulohumeral muscular dystrophy (FSHD) is an autosomal dominant disorder that affects 1 in 8,000–22,000 people in the world and is the third most common inherited muscular dystrophy (Wang and Tawil, 2016). It presents as a progressive, distinctively asymmetric weakening of muscles in the face, shoulders, and upper limbs. Muscles in other regions may become affected with age; around 20% of patients become wheelchair-bound (Richards et al., 2012). Extramuscular symptoms are uncommon, with a few patients experiencing restrictive lung disease, cardiac conduction abnormalities, hearing loss, or retinal vasculopathy (Fitzsimons et al., 1987; Padberg et al., 1995; Laforêt et al., 1998; Lutz et al., 2013; Scully et al., 2014; Lim et al., 2020c). Age of onset and disease severity are both widely variable in FSHD (Tawil et al., 2014; Wang and Tawil, 2016). Intriguingly though, 4–21% of patients who manifest symptoms before the age of five almost all follow a more severe and rapid course of the disease (Klinge et al., 2006; Goselink et al., 2017). There is no available cure for FSHD. Patients are currently managed for their symptoms at best.

While the genetic mechanisms leading to FSHD are diverse and complex, these all result in aberrant expression of the *double homeobox protein 4* (*DUX4*) gene in skeletal muscle. *DUX4* has roles in early embryonic development, where it appears to be essential for zygotic gene activation (De Iaco et al., 2017; Hendrickson et al., 2017). Under healthy conditions, *DUX4* is epigenetically silenced

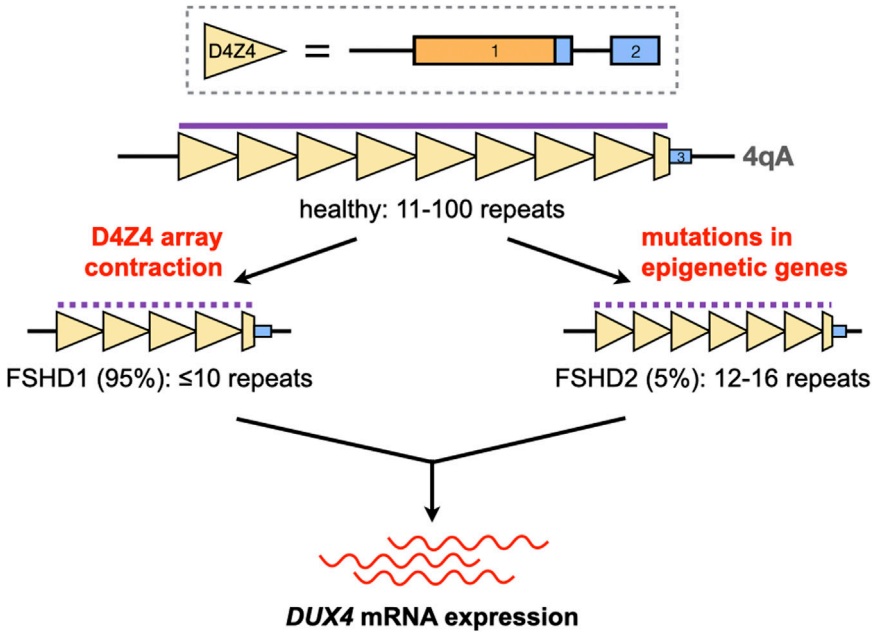

FIGURE 1 | Activation of *DUX4* expression in FSHD. The *DUX4* gene is located in the D4Z4 macrosatellite repeat array at chromosome 4q35. Each D4Z4 repeat (yellow triangles) contains *DUX4* exons 1 and 2 (solid boxes; orange, open reading frame); exon three is found downstream of the last repeat in the array. The D4Z4 array is normally 11–100 repeats long and hypermethylated (purple line) in healthy individuals. Contractions of this array or mutations in genes coding for epigenetic regulators, in the 4qA haplotype, disrupt the silencing of *DUX4* (dotted purple line) and lead to its aberrant expression in skeletal muscle.

after the 4-cell stage in humans and kept as such in all developed tissues but the testis (Snider et al., 2010) and thymus (Das and Chadwick, 2016). This repression is compromised in patients with FSHD, allowing for the synthesis of the DUX4 transcription factor whose activities in skeletal muscle induce potent cytotoxicity by dysregulating pathways involved in cell death, oxidative stress, and muscle development, among others (Dixit et al., 2007; Lim et al., 2020c).

Various approaches are being explored to treat FSHD. Pharmacological treatments have been evaluated mostly with the aim of improving muscular symptoms, and include the use of prednisone, β2 receptor agonists, myostatin inhibitors, and antioxidants, among others. Unfortunately, these generally offered little to no therapeutic benefit based on results from clinical trials (Hamel and Tawil, 2018; Le Gall et al., 2020). Intramuscular transplantation of myoblasts or mesoangioblasts (perivascular myogenic stem cells) from unaffected muscles of FSHD patients into immunodeficient mice revealed that these could integrate with recipient muscle fibers fairly well (Vilquin et al., 2005; Morosetti et al., 2011). However, follow-up studies examining the benefits of such cell-based therapies on FSHD muscle pathology or function are currently unavailable and so their potential for treating FSHD remains uncertain.

In response to developing a more targeted form of treatment, reducing muscle-specific *DUX4* expression and DUX4-mediated toxicity have become attractive goals for FSHD therapy (Bao et al., 2016; Bouwman et al., 2020; Cohen et al., 2020). Indeed, a number of genetic methods have been employed to achieve one or both of these, including oligonucleotide-based strategies to knockdown *DUX4* transcript levels or reduce DUX4 protein activity, and genome editing to correct FSHD-associated mutations. The pre-clinical development of these strategies and others has shown much promise, and identifies possible candidates for clinical trials. Compared to pharmaceutical and cell-based interventions, genetic treatments target the root cause of the disease (i.e., *DUX4*) and are thus expected to lead to more effective or far-reaching therapeutic effects. In this article, we review the various genetic approaches that have been developed for FSHD therapy, discuss the challenges they may be facing on their way to the clinic, and offer some potential solutions as well as directions for future research.

DUX4 EXPRESSION AND FSHD

Much of the complexity associated with FSHD genetics comes from the curious location of *DUX4* in the genome. The *DUX4* gene is part of the D4Z4 macrosatellite repeat array at chromosome 4q35, which is typically 11–100 repeats long in healthy individuals (Gabriëls et al., 1999; Lemmers et al., 2010). There is a homologous D4Z4 repeat array at chromosome 10q26, but mutations in this region have not been linked to FSHD (Bakker et al., 1995; Deidda et al., 1995; Lemmers et al., 2010). Each D4Z4 repeat contains the first two exons of *DUX4*, with the entire open reading frame of the gene in exon 1 (Gabriëls et al., 1999) (**Figure 1**). *DUX4* has other exons downstream of the array; the full-length isoform that contributes to FSHD pathology ends at exon 3 (Snider et al., 2010; Himeda and Jones, 2019). Only

exons from the last D4Z4 repeat contribute to the *DUX4* mRNA, and a polyadenylation signal (PAS) at exon 3 is required to stabilize the pathogenic *DUX4* transcript, a feature that is only present in the disease-permissive 4qA haplotype (Lemmers et al., 2002; Lemmers et al., 2004; Lemmers et al., 2010). Finally, the 4q35 D4Z4 repeat array is normally hypermethylated, which keeps the *DUX4* gene repressed in most adult tissues (Hewitt et al., 1994). Two mechanisms activate *DUX4* expression in FSHD: D4Z4 repeat array contraction, and mutations in genes coding for epigenetic regulators **(Figure 1)**. These cause approximately 95% (FSHD1) and 5% (FSHD2) of cases, respectively (Wang and Tawil, 2016). Despite vast differences in their underlying genetics, FSHD1 and FSHD2 are clinically indistinguishable, implying that aberrant *DUX4* expression is the key genetic event leading to FSHD pathogenesis.

In FSHD1, contraction of the 4qA D4Z4 array to ≤10 repeats activates *DUX4* expression by increasing chromatin accessibility and promoting DNA hypomethylation in the region (van Overveld et al., 2003; Hewitt, 2015). It was previously thought that individuals with ≤10 D4Z4 repeats in one 4qA chromosome form a homogeneous FSHD1 population, but it is now known that this is not the case. Clinical variability is high in individuals with 7–10 D4Z4 repeats, with most cases ranging from mild to asymptomatic (Ricci et al., 2013; Lemmers et al., 2015). This spread of phenotypes is attributed to inter-individual differences in D4Z4 methylation, indicating that factors other than array contraction may be more important in determining disease penetrance within this repeat range (Van Overveld et al., 2005; Lemmers et al., 2015). Conversely, penetrance is more complete in individuals with 1-6 D4Z4 repeats. Disease severity is also roughly inversely correlated with repeat count in these patients, e.g. those with the severe early-onset form of FSHD typically have 1-3 D4Z4 repeats (Lunt et al., 1995; Ricci et al., 2013; Nikolic et al., 2016). Considering the 1–10 D4Z4 repeat range, it appears that the lower the number of repeats present, the less contribution factors other than contraction size have in influencing the FSHD1 phenotype.

Unlike in FSHD1, moderately-sized D4Z4 arrays are observed in FSHD2. On average, FSHD2 patients have 12–16 D4Z4 repeat units on at least one 4qA chromosome, which is at the shorter end of the range that characterizes the general population (de Greef et al., 2010; Himeda and Jones, 2019). However, at our current level of understanding, D4Z4 array size has little to do with FSHD2 development. Instead, the majority of FSHD2 patients (~80%) carry mutations in *SMCHD1*, which codes for a protein involved in maintaining repressive chromatin architecture (Lemmers et al., 2012); others have mutations in *DNMT3B* or *LRIF1*, which code for a DNA methyltransferase or an interactor of SMCHD1, respectively (van den Boogaard et al., 2016; Hamanaka et al., 2020). These mutations lead to D4Z4 hypomethylation independent of D4Z4 array size, creating a permissive environment for *DUX4* expression on the 4qA chromosome. One study showed that the extent of D4Z4 hypomethylation correlated with disease severity in FSHD2, at least for *SMCHD1* mutation carriers (Lemmers et al., 2015). Because of their role in D4Z4 methylation, *SMCHD1* and *DNMT3B* are also genetic modifiers for FSHD1, leading to cases with characteristics of both FSHD1 and FSHD2 (Sacconi et al., 2013; van den Boogaard et al., 2016; de Greef et al., 2018; Sacconi et al., 2019).

GENETIC THERAPIES FOR FSHD

Figure 2 summarizes the genetic therapies that have been developed for FSHD, which are covered in the following sections. Briefly, we have potential genetic therapies targeting DUX4 at the DNA, RNA, and protein levels. There are also therapies that focus on inhibiting the effects of DUX4-mediated toxicity, thereby modifying the disease phenotype.

Oligonucleotide Therapies

Depending on their structure and chemistry, oligonucleotides can inhibit *DUX4* expression in a variety of ways. One of the most extensively tested for FSHD are antisense oligonucleotides (AOs), single-stranded nucleic acid analogues that can bind target mRNA sequences by Watson-Crick base-pairing. There are two kinds of AOs. The first are those that reduce gene expression by interfering with mRNA splicing and processing (Lim and Yokota, 2018). These AOs act as steric blockers, preventing factors from accessing critical sequences in the mRNA such as splice sites, and are usually phosphorodiamidate morpholino oligomers (PMOs) or phosphorothioated 2′-O-methyl RNAs (2′-OMePS). The second are those that reduce gene expression by inducing target mRNA degradation (Lim and Yokota, 2020). The AOs in this group are gapmers, fully phosphorothioated oligonucleotides that have a central DNA stretch flanked by bases of modified chemistry, e.g. locked nucleic acids (LNA) or 2′-O-methoxyethyl RNAs (2′-MOE). When a gapmer binds its target mRNA, a DNA/RNA hybrid is created in the middle of the AO that is recognized by ribonuclease H, which proceeds to bind the hybrid and cleave its RNA portion.

AOs of both kinds have successfully inhibited *DUX4* expression in patient-derived cells and FSHD mouse models **(Table 1)**. PMOs and 2′-OMePS AOs targeting splice acceptor sites for *DUX4* exons 2 and 3 **(Figure 3)** gave 30–90% *DUX4* mRNA knockdown (at 10 and 50 nM tested doses) in myotubes from treated primary patient myoblasts (Vanderplanck et al., 2011; Ansseau et al., 2017). Corresponding reductions in DUX4 downstream target gene expression and DUX4-positive nuclei, as well as improvements in muscle cell morphology, were observed. AOs targeting the exon 3 splice acceptor site were particularly more effective, one of which was tested in mice as a vivo-PMO (Ansseau et al., 2017; Derenne et al., 2020). Vivo-PMOs are PMOs that have been covalently linked to an octaguanidine dendrimer for improving uptake in tissues (Morcos et al., 2008). Mice transduced with *DUX4* constructs at the tibialis anterior (TA) were intramuscularly (i.m.) injected at the same muscle with 10 μg of the vivo-PMO, which led to 30-fold lower *DUX4* expression than the control vivo-PMO-treated leg by semi-quantitative RT-PCR, 10 days after treatment (Ansseau et al., 2017). Histopathological improvements were observed in another study using the same AO (Derenne et al., 2020). PMOs have also

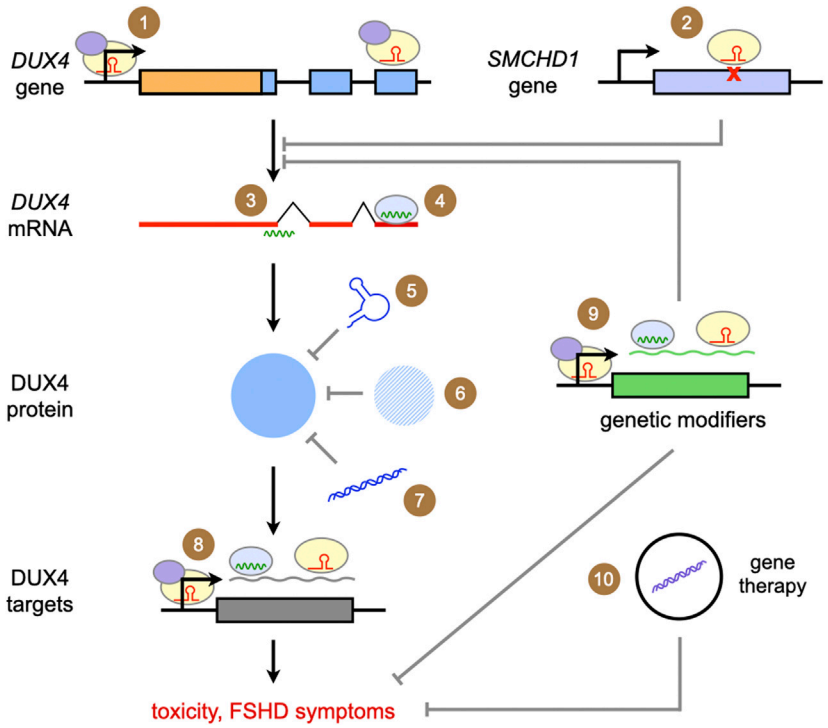

FIGURE 2 | Summary of genetic approaches for the treatment of FSHD. The approaches covered in this review are depicted above. Ultimately, all focus on reducing *DUX4* expression, DUX4 protein activity, or the effects of DUX4-mediated toxicity. (1) Targeted gene repression with CRISPR/dCas9-KRAB; (2) correction of a *SMCHD1* mutation with CRISPR/Cas9; (3) gene knockdown with antisense oligonucleotides; (4) gene knockdown/silencing with RNA interference; competing with DUX4 activity through (5) DNA aptamers, (6) introduction of proteins homologous or similar to DUX4, and (7) DNA decoys; (8) gene knockdown/silencing of DUX4 downstream targets; (9) gene knockdown/silencing of genetic modifiers of *DUX4* expression or DUX4-mediated toxicity (10) delivery of genes coding for proteins that ameliorate DUX4-mediated toxicity or secondary features of FSHD pathology.

been used to target the PAS in exon 3 **(Figure 3)**, which knocked down *DUX4* transcript expression in immortalized patient-derived myotubes by 25–52% at a 50 nM dose (Marsollier et al., 2016) and in a xenograft FSHD mouse model by nearly 100% with a 20-μg injection (Chen et al., 2016a). Reduced expression of DUX4 downstream target genes, transcriptomic-level restoration, and loss of DUX4-positive nuclei were observed *in vitro*; treatment showed no significant improvements in muscle cell fusion, however.

Our group has recently published on the efficacy of using gapmers for inhibiting *DUX4* mRNA expression. We designed LNA gapmers to target sites at *DUX4* exons 1 and 3 (Lim et al., 2020b), as well as 2′-MOE gapmers to target only sites at exon 3 (Lim et al., 2020a) **(Figure 3)**. The LNA and 2′-MOE gapmers targeted overlapping sequences at exon 3, upstream of the PAS. All gapmers knocked down *DUX4* mRNA levels almost completely (~99%) at 100 nM and by more than 50% at 10 nM regardless of chemistry in immortalized patient-derived myotubes. This demonstrates an increased potency of gapmers compared to steric-blocking AOs, perhaps due to the direct nature of transcript degradation induced by the gapmers. More sustained knockdown of DUX4 downstream target genes was observed for LNA than 2′-MOE gapmers at 10 nM. LNA gapmer treatment also restored more FSHD signature genes upon RNA sequencing analysis, hinting that LNA gapmers may be the more potent of the two in terms of *DUX4* knockdown. Focusing on exon 3-targeting gapmers, we saw improvements in muscle cell fusion and size, as well as minimal to no effects on potential off-target genes *in vitro*. A separate study also found that treatment with one of the 2′-MOE gapmers increased membrane repair in immortalized patient myoblasts (Bittel et al., 2020). One gapmer from each chemistry was also tested in the *FLExDUX4* model, which carry a stably integrated, Cre-inducible *DUX4* transgene (Jones and Jones, 2018). Non-induced *FLExDUX4* mice exhibit low levels of *DUX4* expression mimicking what is seen in patient muscle cells, and was used for preliminary studies. Significant *DUX4* knockdown was induced in these mice following three 20-μg i.m. TA injections, at 70–84% for the LNA gapmer and 65% for the 2′-MOE gapmer, on average.

Another class of oligonucleotide therapy is RNA interference (RNAi), which makes use of small interfering RNAs (siRNAs) or microRNAs (miRNAs) **(Table 2)**. Unlike AOs, siRNAs and miRNAs require association with effector proteins to reduce target gene expression. siRNAs targeting *DUX4* promoter elements or exons **(Figure 3)** knocked down *DUX4* transcript levels by 50–90% *in vitro*, with corresponding restorative effects on DUX4 downstream targets (Vanderplanck et al., 2011; Lim et al., 2015). Interestingly, siRNAs against the promoter likely inhibited *DUX4* expression through epigenetic silencing at the

TABLE 1 | Summary of results from pre-clinical studies on antisense oligonucleotides for *DUX4* knockdown.

Study	Chemistry	*DUX4* target	Model	*DUX4* knockdown (dose)	Other results
Vanderplanck et al. (2011)	2′-OMePS	Ex2 SA, Ex3 SA	Primary FSHD myoblasts, differentiated post-treatment	30% (ex2 SA, 50 nM), 50% (ex3 SA, 10 nM)	Reduced TP53 levels, *TRIM43* expression
Marsollier et al. (2016)	PMO	Ex3 PAS, downstream elements	Immortalized FSHD myotubes	25–52% (50 nM)	Reduced DUX4 downstream gene expression; fusion not affected
Chen et al. (2016a)	PMO	Ex2 SA, Ex3 PAS	Primary FSHD myotubes	Not assessed	Reduced DUX4^{+} nuclei, DUX4 downstream gene expression (only for PAS PMOs); transcriptomic improvements
		Ex3 PAS	FSHD xenograft mice, 1x e.p. into xenograft, evaluated 2 weeks post-treatment	~100% (20 μg)	Reduced DUX4 downstream gene expression
Ansseau et al. (2017)	2′-OMePS	Ex2 SA, Ex3 SA	Primary aFSHD and dFSHD myoblasts, differentiated post-treatment	~90% (ex2 SA, 50 nM; ex3 SA, 10 nM)	Reduced DUX4^{+} nuclei; saw improvements in size (in aFSHD but not dFSHD myotubes)
	Vivo-PMO	Ex3 SA	AAV-DUX4 mice, 1x i.m. TA, evaluated 10 days post-treatment	30-Fold lower than control vivo-PMO	None
Derenne et al. (2020)	Vivo-PMO	Ex3 SA	DUX4 IMEP mice, 1x i.p., evaluated 1 week post-treatment	Not assessed	2.5-fold decrease in histological lesion compared to non-treated
Lim et al. (2020b)	LNA gapmer	Ex1, Ex3	Immortalized FSHD myotubes	~100% (100 nM)	Reduced DUX4 downstream gene expression; partial transcriptomic restoration; improved muscle cell fusion/size
		Ex3	*FLExDUX4* mice, 3x i.m., evaluated 1 or 7 days post-treatment	84% (1 day, 20 μg/i.m.), 70% (7 days, 20 μg/i.m.)	Gapmer uptake observed in and between muscle fibers
Lim et al. (2020a)	2′-MOE gapmer	Ex3	Immortalized FSHD myotubes	~100% (100 nM)	Reduced DUX4 downstream gene expression; partial transcriptomic restoration; improved muscle cell fusion/size
		Ex3	*FLExDUX4* mice, 3x i.m., evaluated 1 day post-treatment	~65% (20 μg/i.m.)	None

2′-OMePS, phosphorothioated 2′-O-methyl RNAs; PMO, phosphorodiamidate morpholino oligomer; LNA, locked nucleic acid; 2′-MOE, 2′-O-methoxyethyl; Ex, exon; SA, splice acceptor; PAS, polyadenylation signal; e.p., electroporation; i.m., intramuscular injection; i.p., intraperitoneal injection; TA, tibialis anterior; AAV, adeno-associated virus; IMEP, intramuscular injection and electroporation of naked plasmid DNA; aFSHD, atrophic FSHD myotubes; dFSHD, disorganized FSHD myotubes.

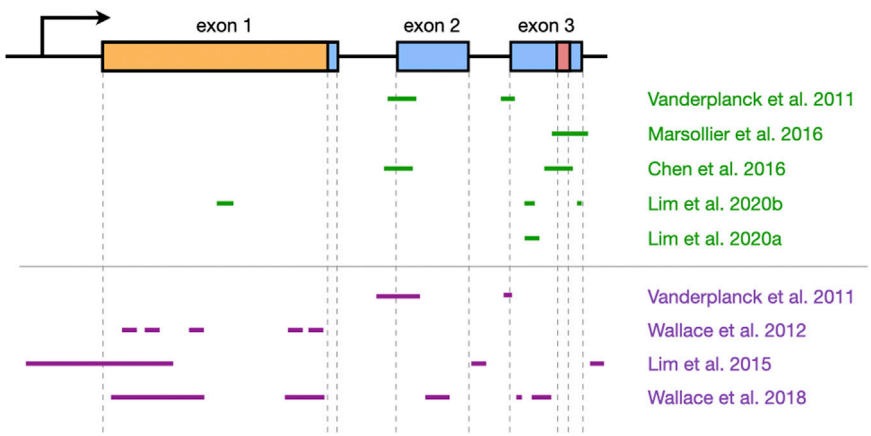

FIGURE 3 | Overview of *DUX4* regions that have been targeted by oligonucleotide therapies. The structure of the *DUX4* gene is shown at the top (arrow indicates promoter region; boxes, exons; lines, introns; orange, open reading frame; red, polyadenylation signal), and the regions that have been targeted by antisense oligonucleotides (green) or RNA interference (purple) are shown at the bottom. Approximate locations are shown, and the figure is not to scale. Note that Ansseau et al. (2017) used the same oligonucleotides as Vanderplanck et al. (2011). *DUX4* structure was based on information from Ensembl, transcript ID ENST00000569241.5.

DNA level, since 2′-MOE gapmers against the same region did not affect *DUX4* transcript levels (Holoch and Moazed, 2015; Lim et al., 2015). Meanwhile, one group screened a large number of miRNAs **(Figure 3)** and found two targeting exon 1 (mi1155, mi405) to knock down *DUX4* expression the best at >75% in *DUX4*-luciferase reporter cells (Wallace et al., 2012; Wallace et al., 2018). Treatment of *DUX4*-transduced mice (i.m., TA) with 3×10^{10} adeno-associated viruses (AAVs) carrying mi405 constructs

TABLE 2 | Summary of results from pre-clinical studies on RNA interference for *DUX4* knockdown.

Study	Approach	*DUX4* target	Model	*DUX4* knockdown (dose)	Other results
Vanderplanck et al. (2011)	siRNA	Ex2 SA, Ex3 SA	Primary FSHD myoblasts, differentiated post-treatment	80% (ex3 SA, 10 nM)	Reduced DUX4, Atrogin1, TP53, protein levels, and MuRF1$^+$ nuclei; improved muscle size
Wallace et al. (2012)	miRNA	Ex1	DUX4-luciferase reporter HEK293 cells	>50% (dose not given)	Reduced DUX4 protein levels
		Ex1	AAV-DUX4 mice, 1x i.m. TA, evaluated 2–4 weeks post-treatment	64% (3×10^{10} particles)	Reduced DUX4 protein levels (90%); improved histopathology; lack of caspase-3$^+$ myofibers; improved grip strength
Lim et al. (2015)	siRNA	Promoter, Ex1, In2, downstream elements	Primary FSHD myoblasts, differentiated post-treatment	Up to ~50–90% (100 pmol)	Reduced DUX4$^+$ nuclei, *ZSCAN4* expression
Wallace et al. (2018)	miRNA	Ex1, Ex2, Ex3	DUX4-luciferase reporter HEK293 cells	Up to >75% (dose not given)	Reduced DUX4 protein levels (up to >75%)
		Ex1	AAV-DUX4 mice, 1x i.m. TA/isolated limb perfusion, evaluated at various timepoints post-treatment	Not assessed	One miRNA was more toxic than the other upon histological evaluation

siRNA, small interfering RNA; miRNA, microRNA; Ex, exon; In, intron; SA, splice acceptor; i.m., intramuscular injection; TA, tibialis anterior; AAV, adeno-associated virus.

reduced *DUX4* mRNA expression by 64%, and DUX4 protein levels by 90% (Wallace et al., 2012). Histopathology was improved with this miRNA, but not with mi1155 that instead showed signs of overt toxicity (Wallace et al., 2018).

Oligonucleotides can also be designed to target the DUX4 protein. Double-stranded DNA decoys containing the DUX4 binding motif have recently been developed to sequester and prevent DUX4 from activating its downstream targets (Mariot et al., 2020). Indeed, the expression levels of DUX4 downstream targets *ZSCAN4* and *TRIM43* were knocked down by 39–91% in primary patient myotubes upon treatment with these decoys. The DNA decoys were also tested in AAV-DUX4 mice, where administration either by intramuscular electroporation or AAV delivery led to decreased expression of *Tm7sf4*, another DUX4 downstream target. On a related note, single-stranded DNA aptamers have recently been developed with high, preferential affinity to the DUX4 DNA-binding domain (Klingler et al., 2020). However, these aptamers have yet to be tested for their therapeutic potential. Developing oligonucleotides for targets other than *DUX4* may be useful as well. For instance, *PITX1* is a direct transcriptional target of DUX4 whose overexpression induces an FSHD-like dystrophic phenotype in mice (Dixit et al., 2007; Pandey et al., 2012). Intravenous injection of AOs against *Pitx1* in *Pitx1*-transgenic mice improved grip strength and decreased muscle pathology (Pandey et al., 2014). *FRG1* is another direct transcriptional target of *DUX4*, whose knockdown by RNAi reversed dystrophic histopathology and improved treadmill performance in *FRG1*-overexpressing mice (Bortolanza et al., 2011; Ferri et al., 2015). It would be interesting to see if similar effects could be observed if these strategies were used to treat *DUX4*-overexpressing mouse models such as *FLExDUX4* (Jones and Jones, 2018), the doxycycline-inducible iDUX4pA (Bosnakovski et al., 2017a; Bosnakovski et al., 2020), or the tamoxifen-inducible TIC-DUX4 (Giesige et al., 2018).

CRISPR

The bacterial defense system based on clustered regularly interspaced short palindromic repeats (CRISPR) has been adapted and developed to become perhaps one of the most revolutionary tools for targeted genome editing to date. In its most common configuration, CRISPR has two basic components: an endonuclease for cleaving DNA (the CRISPR-associated or Cas protein), and an RNA molecule that associates with this enzyme and tells it where in the genome to cut (the guide RNA or gRNA) (Jinek et al., 2012; Jiang and Doudna, 2017). The gRNA is designed complementary to the target DNA site, which additionally has to have a protospacer-adjacent motif sequence nearby to facilitate Cas binding (Mojica et al., 2009; O'Connell et al., 2014). Upon binding of the gRNA-Cas complex, a double-stranded break is introduced into the target DNA. This break is subsequently resolved by non-homologous end joining or homology-directed repair, which create random insertions/deletions or precise edits at the site, respectively, and form the basis of CRISPR-based genome editing.

CRISPR has been previously used to correct an FSHD2-associated *SMCHD1* mutation, a missense variant in intron 34 that introduced an out-of-frame 53-bp pseudoexon in the final transcript (Goossens et al., 2019). CRISPR/Cas9 with gRNAs against the intronic sequences flanking this pseudoexon restored the *SMCHD1* reading frame and increased wild-type *SMCHD1* expression in primary and immortalized patient myotubes, resulting in reduced *DUX4* mRNA expression. It has been suggested that CRISPR be used to edit the permissive 4qA to the restrictive 4qB haplotype (Cohen et al., 2020), but attempts on realizing this approach have not yet been reported in the literature. In addition to genome editing, CRISPR can also be used for the targeted modulation of gene expression. Using a catalytically-deficient version of Cas9 (dCas9) fused to a KRAB transcriptional repressor, together with gRNAs against the *DUX4* promoter or exon 1, one group achieved ~45% *DUX4* knockdown in myotubes differentiated from treated primary patient myoblasts (Himeda et al., 2016). A trend toward increased chromatin repression of the *DUX4* gene at the contracted locus was observed. When dCas9-KRAB was used with gRNAs solely targeting *DUX4* exon 3 or various regions within/upstream of the D4Z4 repeat sequence, no significant *DUX4* knockdown

was observed. The same group used dCas9-KRAB to inhibit the expression of other genes—*BRD2*, *BAZ1A*, *KDM4C*, and *SMARCA5*—which led to about 40–60% *DUX4* knockdown in primary patient myotubes (Himeda et al., 2018). These genes code for epigenetic regulators, and were previously identified from an RNAi screen as candidates whose knockdown lowered *DUX4* transcript levels without negatively impacting the expression of genes involved in muscle development or homeostasis. On a related note, CRISPR/Cas9 has itself been employed for a genome-wide knockout screen to search for genes whose loss-of-function was protective against DUX4 cytotoxicity (Lek et al., 2020). Hypoxia signaling pathway members were identified as the most promising candidates, in accordance with the role of oxidative stress in DUX4-mediated pathogenesis (Dmitriev et al., 2016; Denny and Heather, 2017; Lim et al., 2020c).

Other Approaches

Preliminary findings from basic research studies are providing solid foundations for the development of more strategies for FSHD therapy. One interesting approach is to use other proteins to compete with DUX4 activity. DUX4-s is a short isoform of DUX4 that contains only the first 159 N-terminal amino acids of the protein, spanning both homeodomains (Mitsuhashi et al., 2018). It is non-pathogenic, and its expression has been detected in both healthy and FSHD skeletal muscle (Snider et al., 2010; Geng et al., 2011; Mitsuhashi et al., 2018). Since DUX4-s shares the exact same homeodomains as full-length DUX4, it is thought that overexpression of the former will prevent the latter from binding its usual genomic targets. Indeed, co-injection of *DUX4-s* and full-length *DUX4* mRNA at a 20:1 ratio into fertilized zebrafish eggs decreased embryo mortality rates to ~10%, improved musculature, and led to 70% of embryos having an overall normal phenotype (Mitsuhashi et al., 2013). In contrast, eggs injected with only full-length *DUX4* mRNA had an embryo mortality rate of ~40%, and less than 20% of resulting embryos were phenotypically wild-type. As the physiological functions of DUX4-s are unknown, more research into this area may help further develop this approach as an FSHD therapy. The DUX4 homeodomains are also highly similar and functionally interchangeable with those of PAX7 (Bosnakovski et al., 2017b). Overexpression of *Pax7* or its homolog *Pax3* considerably improved viability in *DUX4*-inducible C2C12 cells (Bosnakovski et al., 2008). This rescue was diminished in a dose-dependent manner when *DUX4* expression was induced at higher levels, indicating that Pax7 or Pax3 may be exerting their effects via competition with the DUX4 protein. Although promising, pre-clinical testing of DUX4-s and PAX7/3 in FSHD mouse models have yet to be performed.

Research into understanding FSHD biology or *DUX4*-mediated cytotoxicity has also uncovered more potential targets for therapy. These include genes involved in apoptosis (*CDKN1A*, *MYC*), immune response activation (*RNASEL*, *EIF2AK2*), and epigenetic regulation (*H3.X*, *H3.Y*), to name a few (Lim et al., 2020c). As previously mentioned, RNAi and CRISPR screens have been instrumental in adding to this list by identifying genetic modifiers of *DUX4* expression (Himeda et al., 2018; Lek et al., 2020). Modulating the expression of these genes, either by oligonucleotide- or CRISPR-based approaches, may be therapeutic avenues worth investigating. Developing treatments to alleviate FSHD symptoms may be beneficial as well. For instance, AAV delivery of a follistatin gene construct into TIC-DUX4 FSHD model mice (i.m.) increased mass and improved strength in injected muscles (Giesige et al., 2018). Follistatin is an inhibitor of myostatin, which in turn is a known inhibitor of muscle growth (Rodino-Klapac et al., 2009). It is important to note though that follistatin did not reverse DUX4-induced histopathology in treated mice, suggesting that treatments directed at secondary pathological features of FSHD are probably not curative and may be more useful when administered in conjunction with *DUX4*-targeting genetic therapies.

CHALLENGES FOR FSHD GENETIC THERAPIES

The development of genetic therapies for FSHD is at a relatively young phase, with most pre-clinical work limited to *in vitro* models. Only a handful of these experimental therapies have moved on to *in vivo* testing **(Table 1)**, of which only one was evaluated for its efficacy in ameliorating FSHD symptoms (Wallace et al., 2012; Wallace et al., 2018). This may be explained by the lack of appropriate FSHD animal models at the time, an effort that was largely hindered by the lethal effects of DUX4 (DeSimone et al., 2020). Various groups have since capitalized on using conditional methods to overexpress *DUX4* in mice, allowing for more refined control of DUX4 toxicity and ushering in the production of FSHD animal models amenable to pre-clinical study (Bosnakovski et al., 2017a; Bosnakovski et al., 2020; Giesige et al., 2018; Jones and Jones, 2018). With the impending progression of FSHD genetic therapies into *in vivo* testing, certain challenges will have to be considered and overcome to ensure treatment success not only in animal models but also and ultimately in patients. We consider challenges relevant to oligonucleotide- and CRISPR-based therapies, as these have advanced the most in pre-clinical development.

Delivery is perhaps one of the largest hurdles these therapies have to face *in vivo*. In order for genetic therapies to work, they will have to reach their target DNA/RNA sequences in the nuclei of their target cells. Preliminary work using AOs for instance have shown that levels of *DUX4* knockdown *in vivo* are not usually as high as those observed *in vitro* (Wallace et al., 2012; Ansseau et al., 2017; Lim et al., 2020a; Lim et al., 2020b). The same divide *in vitro* and *in vivo* efficacy has been observed for similar genetic approaches in other muscular disorders, such as Duchenne muscular dystrophy (DMD) (Echigoya et al., 2017; Lim et al., 2019; Nguyen and Yokota, 2019). For oligonucleotide therapies, much of the challenge will be to get them into muscle cells and, once inside, to have them successfully escape from endosomes and reach the nucleus (Juliano, 2016). This is especially problematic for charge-neutral chemistries such as PMOs (Summerton and Weller, 1997), which are not readily recognized by cell surface receptors nor are they particularly disruptive toward cell membranes. Conjugation of cell-penetrating entities to oligonucleotides in order to enhance cellular

uptake and endosomal escape are actively being investigated, as are the use of non-viral delivery vehicles like lipid nanoparticles, polymeric nanocarriers, and exosomes (Dominska and Dykxhoorn, 2010; Juliano, 2016; Tong et al., 2019). Chemically modifying the oligonucleotides themselves to appear more recognizable to muscle cell surface receptors is currently being looked into as well (Dominska and Dykxhoorn, 2010; Juliano, 2016; Tong et al., 2019). Viral vectors may be applicable for RNAi strategies using miRNAs or shRNAs, but their immunogenicity will have to be carefully considered when delivered *in vivo*.

CRISPR components, on the other hand, have mostly been delivered using viral vectors. This has mostly been effective, except for two major concerns: the packaging limit into viruses and immunogenicity. The SpCas9 (the most used Cas variant) gene construct is ~4.2 kb long, which is quite near the packaging capacity of AAVs at ~4.4–4.7 kb (Wu et al., 2010; Tong et al., 2019; Wilbie et al., 2019). Use of a two-vector delivery system has been necessary at times, one for Cas9 and another for the gRNA/s. How this division exactly affects CRISPR efficacy is still poorly understood, but could be unfavorable when considering that we have to maximize the likelihood of all CRISPR components being present in the same nuclei—a challenge that is perhaps made more difficult by the syncytial nature of mature muscle cells and the fact that only a very few nuclei actually express *DUX4* (Tassin et al., 2013). Lentiviral and retroviral vectors have larger capacities at 7–10 kb, but are prone to inducing unwanted integration of their cargo into the host genome (Tong et al., 2019). Adenoviral vectors have even larger capacities at about 36 kb, and are emerging as effective vehicles for CRISPR delivery (Ehrke-Schulz et al., 2017; Tong et al., 2019; Ricobaraza et al., 2020). The discovery of smaller Cas variants such as CjCas9 (2.95 kb gene size) is also helping overcome this packaging limit (Kim et al., 2017). However, due to their immunogenicity, there is always the risk of complications and so the use of immunosuppressive agents remain important, especially since responses may still be activated at high doses of virus, and individual reactions to viral agents are difficult to predict (Tong et al., 2019; Xu et al., 2019; Shirley et al., 2020). Non-viral delivery approaches, similar to those described for oligonucleotide therapies, are also being developed for CRISPR to overcome both issues of packaging and immunogenicity (Lino et al., 2018; Wilbie et al., 2019).

Safety is another concern. Oligonucleotide and CRISPR therapies can be toxic through hybridization-dependent or -independent means (Frazier, 2015). One aspect of hybridization-dependent toxicity is off-target gene knockdown/knockout/editing, resulting from the recognition of non-target sequences that share imperfect complementarity with a given oligonucleotide or gRNA. Only a few studies on *DUX4*-targeting therapies have examined off-target effects—dose-dependent knockdown was found in some non-target genes, whereas no effect was observed in others (Lim et al., 2020a; Lim et al., 2020b). A more thorough analysis of off-target effects is recommended for future studies, perhaps using genome- or transcriptome-wide approaches (Kim et al., 2015; Tsai et al., 2015; Yoshida et al., 2019). Fortunately, the specificity of these genetic therapies is constantly being improved through chemical modification or by performing *in silico* screens to predict the off-targeting potential of certain oligonucleotide sequences prior and in addition to *in vitro* testing (Kamola et al., 2015; Tycko et al., 2016; Hendling and Barišić, 2019; Wang et al., 2019). In the case of CRISPR, splitting the Cas enzyme into two interdependent halves and limiting the duration of Cas activity via self-restricting mechanisms have emerged as possible approaches to reduce the chance of off-target effects (Ran et al., 2013; Shen et al., 2014; Moore et al., 2015; Chen et al., 2016b).

Hybridization-dependent toxicity can also come from on-target effects. This is not much of an issue for the FSHD-associated *DUX4* isoform, since it is not supposed to be expressed in the first place, and its expression appears to be muscle-specific (Himeda et al., 2014). Non-pathogenic *DUX4* isoforms are, however, expressed in healthy tissues (Snider et al., 2010; Himeda and Jones, 2019). As the physiological functions of these isoforms are currently unknown, it would be hard to predict the consequences of their reduced expression. Regardless, as a form of caution, genetic therapies should be designed to preferentially target skeletal muscle or regions specific to the pathogenic *DUX4* isoform. Use of viruses with muscle-specific tropism or ligand-directed oligonucleotides/non-viral delivery vehicles can help ensure tissue-specific treatment (Juliano, 2016). As for target sequence design, exon 3 is the region most specific to the pathogenic, full-length *DUX4* isoform. Most oligonucleotide therapies target this exon and so are not particularly concerning; however, therapies targeting other exons, the *DUX4* promoter region, or D4Z4 sequences on other tissues will have to be closely monitored for potential adverse effects. Another on-target effect is the potential integration of genetic material from viral delivery vectors—however, this threat can be minimized by using AAVs or non-viral delivery methods.

On the other hand, hybridization-independent toxicity refers to effects caused by the therapies themselves that are not attributed to their intended sequence-dependent genetic activities. Certain secondary structures on oligonucleotides and gRNAs can be recognized by pattern recognition receptors and lead to an innate immune response (Agrawal and Kandimalla, 2004; Kim et al., 2004; Lee and Yokota, 2013; Kim et al., 2018; Wienert et al., 2018; Wilbie et al., 2019). The formation of such structures therefore has to be considered during the sequence design process for these modalities. Pre-existing adaptive immunity against Cas proteins is also common in the population (Chew, 2018; Crudele and Chamberlain, 2018; Wagner et al., 2019). Whereas Cas proteins are now being engineered to become less immunogenic (Ferdosi et al., 2019; Mehta and Merkel, 2020), efforts to reduce the persistence of Cas activity as described previously are also potential solutions. Aside from immune response activation, hepatotoxicity and nephrotoxicity have been previously linked to phosphorothioated AOs (Frazier, 2015). This toxicity has been partially attributed to the propensity of AOs to bind cellular proteins (Brown et al., 1994; Liang et al., 2015; Kakiuchi-Kiyota et al., 2016; Shen et al., 2018). Accordingly in one study, chemical modifications that reduced the overall protein-binding affinity of gapmers prevented hepatotoxicity in mice, without sacrificing therapeutic efficacy (Shen et al., 2019). Certain sequence patterns have also been found to correlate with the hepatotoxic potential of oligonucleotides (Hagedorn et al., 2013; Burdick et al., 2014). The development of predictive *in silico* tools may help prevent the integration of such sequences during oligonucleotide design (Hagedorn et al., 2013); use of *in vitro* screening for potential

AO toxicity prior to therapeutic evaluation would be recommended (Dieckmann et al., 2018; Shen et al., 2019).

Another challenge to consider is that *DUX4* expression is very rare in skeletal muscle, only detected in 1/1000 or 1/200 nuclei in FSHD myoblasts and myotubes, respectively (Snider et al., 2010; Tassin et al., 2013). This poses an issue when evaluating the efficacy of *DUX4*-targeting therapies, by preventing a robust read-out of *DUX4* knockdown. This explains why some studies have instead opted to use *DUX4*-transfected models, which may create an overly toxic, non-representative environment compared to what is seen in patients. Fortunately, we now have robust protocols that enable reliable detection of endogenous *DUX4* mRNA levels, based on real-time quantitative reverse transcription PCR or RNA *in situ* hybridization (Lim et al., 2020b, Lim et al., 2015; Amini Chermahini et al., 2019). Induction of endogenous *DUX4* expression using media supplements such as KOSR has been likewise helpful (Pandey et al., 2015). DUX4 protein detection has shown some success, owing to the development of good antibodies (Dixit et al., 2007; Snider et al., 2010; Geng et al., 2011), but may remain a challenge in certain conditions when considering the potentially short half-life of the DUX4 protein (Geng et al., 2011; Rickard et al., 2015) or the proposed stochastic model of *DUX4* expression in muscle cells (Snider et al., 2010; Rickard et al., 2015). Of course, evaluating effects on DUX4 downstream transcriptional targets or FSHD biomarkers as proxies for *DUX4* knockdown remain options for therapeutic evaluation.

Finally, one has to recognize the unique clinical presentation of FSHD when translating these genetic therapies into patients. One of the most distinctive features of FSHD is its asymmetric phenotype (Wang and Tawil, 2016). We are far from understanding how this occurs—what determines which parts of the muscle get affected first, why certain muscle groups are spared more than others, why the pattern of muscle weakness differs between patients, and so on. The best strategy at the moment would probably be to develop an approach that equally benefits all muscle groups. This requires that therapeutic efficacy be evaluated in representative muscles across the body during *in vivo* testing, and not only on commonly assessed muscles such as the TA. If anything, therapeutic effects on muscles in the upper parts of the body have to be prioritized, given their early involvement in FSHD (Wang and Tawil, 2016). Another approach would be to administer genetic therapies locally, injecting only the affected muscles. While this takes advantage of the patchy nature of FSHD pathology, this method requires a way to reliably locate affected muscle areas and may not be practical if too many muscles have become involved; it will also not improve the state of any extramuscular symptoms. Needless to say, developing therapies that would address the unique characteristics of FSHD would require the use of animal models that resemble the disease fairly well. As previously mentioned, recent advancements in the conditional control of *DUX4* expression have helped us get closer to generating such models, resulting in mice with dystrophic histopathology, impaired muscle strength, and asymmetric muscle degeneration similar to those seen in patients (DeSimone et al., 2020). Due to the inducible nature of *DUX4* expression in these models, the severity of resulting phenotypes is also tunable, allowing for therapeutic testing in a variety of disease states. This is a rather helpful aspect, considering the wide variability in disease presentation seen in patients with FSHD.

CONCLUSION

The discovery of *DUX4* as the genetic cause of FSHD has greatly accelerated efforts not only to understand the disorder but also to treat it. As we have seen, *DUX4* has proven itself to be a useful target for genetic therapy. Oligonucleotide- and CRISPR-based approaches have demonstrated the feasibility of *DUX4* knockdown in reversing muscle-specific FSHD pathology, with promising preliminary results *in vitro* and *in vivo*. However, there is much to be done before these therapies can reach the patients they are meant for. Challenges in delivery, efficacy, safety, and in dealing with the unique pathology of FSHD all have to be taken into consideration *in vivo*. The field can use the lessons learned from the application of these therapies in other muscular disorders to help overcome such hurdles. Development of alternative genetic approaches for FSHD therapy should also be encouraged. For instance, strategies to interfere with DUX4 transcription factor activity or to modulate the expression of genes that impart protection against the cytotoxicity of DUX4 appear to have therapeutic potential. The ongoing identification of genes involved in FSHD pathogenesis by basic research and transcriptomic studies are providing new targets for genetic therapies as well. Finally, although FSHD is predominantly a skeletal muscle disease, it will be necessary to create therapies that address its extramuscular symptoms, especially since these tend to manifest in the more severe cases of the disease. Further investigations into both the pathological and physiological roles of *DUX4* in other tissues are steps toward achieving this goal. Such studies should also help us better assess the possible effects of *DUX4*-targeting genetic therapies in non-muscle tissues. Appreciating all the work that has been accomplished thus far, we have certainly come a long way in the development of genetic therapies for FSHD. With continued efforts from both basic and translational research teams in the FSHD community, it may only be a matter of time until we see these therapies making their way into clinical trials.

AUTHOR CONTRIBUTIONS

KL performed a literature review and wrote the manuscript draft. KL and TY edited the manuscript. TY supervised the work and acquired funding.

FUNDING

This work was funded by the Friends of Garrett Cumming Research Chair Fund, HM Toupin Neurological Science Research Chair Fund, Muscular Dystrophy Canada, Canadian Institutes of Health Research (CIHR) FDN 143251, Alberta Innovates, the University of Alberta Faculty of Medicine and Dentistry, University Hospital Foundation, and the Women and Children's Health Research Institute (WCHRI) IG 3279. Muscular Dystrophy Association 629268, FSHD Canada Foundation 30004574-01, FSHD Society 30003892-17-01.

REFERENCES

Agrawal, S., and Kandimalla, E. R. (2004). Antisense and siRNA as agonists of Toll-like receptors. *Nat. Biotechnol.* 22, 1533–1537. doi:10.1038/nbt1042

Amini Chermahini, G., Rashnonejad, A., and Harper, S. Q. (2019). RNAscope *in situ* hybridization-based method for detecting DUX4 RNA expression *in vitro*. *RNA* 25, 1211–1217. doi:10.1261/rna.070177.118

Ansseau, E., Vanderplanck, C., Wauters, A., Harper, S. Q., Coppée, F., and Belayew, A. (2017). Antisense oligonucleotides used to target the DUX4 mRNA as therapeutic approaches in FaciosScapuloHumeral muscular dystrophy (FSHD). *Genes* 8, 93. doi:10.3390/genes8030093

Bakker, E., Wijmenga, C., Vossen, R. H., Padberg, G. W., Hewitt, J., van der Wielen, M., et al. (1995). The FSHD-linked locus D4F104S1 (p13E-11) on 4q35 has a homologue on 10qter. *Muscle Nerve Suppl.* 2, S39–S44. doi:10.1002/mus.880181309

Bao, B., Maruyama, R., and Yokota, T. (2016). Targeting mRNA for the treatment of facioscapulohumeral muscular dystrophy. *Intractable Rare Dis. Res.* 5, 168–176. doi:10.5582/irdr.2016.01056

Bittel, A. J., Sreetama, S. C., Bittel, D. C., Horn, A., Novak, J. S., Yokota, T., et al. (2020). Membrane repair deficit in facioscapulohumeral muscular dystrophy. *Int. J. Mol. Sci.* 21, 5575. doi:10.3390/ijms21155575

Bortolanza, S., Nonis, A., Sanvito, F., Maciotta, S., Sitia, G., Wei, J., et al. (2011). AAV6-mediated systemic shRNA delivery reverses disease in a mouse model of facioscapulohumeral muscular dystrophy. *Mol. Ther.* 19, 2055–2064. doi:10.1038/mt.2011.153

Bosnakovski, D., Chan, S. S. K., Recht, O. O., Hartweck, L. M., Gustafson, C. J., Athman, L. L., et al. (2017a). Muscle pathology from stochastic low level DUX4 expression in an FSHD mouse model. *Nat. Commun.* 8, 550. doi:10.1038/s41467-017-00730-1

Bosnakovski, D., Toso, E. A., Hartweck, L. M., Magli, A., Lee, H. A., Thompson, E. R., et al. (2017b). The DUX4 homeodomains mediate inhibition of myogenesis and are functionally exchangeable with the Pax7 homeodomain. *J. Cel Sci.* 130, 3685–3697. doi:10.1242/jcs.205427

Bosnakovski, D., Shams, A. S., Yuan, C., da Silva, M. T., Ener, E. T., Baumann, C. W., et al. (2020). Transcriptional and cytopathological hallmarks of FSHD in chronic DUX4-expressing mice. *J. Clin. Invest.* 130, 2465–2477. doi:10.1172/JCI133303

Bosnakovski, D., Xu, Z., Gang, E. J., Galindo, C. L., Liu, M., Simsek, T., et al. (2008). An isogenetic myoblast expression screen identifies DUX4-mediated FSHD-associated molecular pathologies. *EMBO J.* 27, 2766–2779. doi:10.1038/emboj.2008.201

Bouwman, L. F., van der Maarel, S. M., and de Greef, J. C. (2020). The prospects of targeting DUX4 in facioscapulohumeral muscular dystrophy. *Curr. Opin. Neurol.* 33, 635–640. doi:10.1097/WCO.0000000000000849

Brown, D. A., Kang, S. H., Gryaznov, S. M., DeDionisio, L., Heidenreich, O., Sullivan, S., et al. (1994). Effect of phosphorothioate modification of oligodeoxynucleotides on specific protein binding. *J. Biol. Chem.* 269, 26801–26805. doi:10.1016/S0021-9258(18)47090-1

Burdick, A. D., Sciabola, S., Mantena, S. R., Hollingshead, B. D., Stanton, R., Warneke, J. A., et al. (2014). Sequence motifs associated with hepatotoxicity of locked nucleic acid--modified antisense oligonucleotides. *Nucleic Acids Res.* 42, 4882–4891. doi:10.1093/nar/gku142

Chen, J. C., King, O. D., Zhang, Y., Clayton, N. P., Spencer, C., Wentworth, B. M., et al. (2016a). Morpholino-mediated knockdown of DUX4 toward facioscapulohumeral muscular dystrophy therapeutics. *Mol. Ther.* 24, 1405–1411. doi:10.1038/mt.2016.111

Chen, Y., Liu, X., Zhang, Y., Wang, H., Ying, H., Liu, M., et al. (2016b). A self-restricted CRISPR system to reduce off-target effects. *Mol. Ther.* 24, 1508–1510. doi:10.1038/mt.2016.172

Chew, W. L. (2018). Immunity to CRISPR Cas9 and Cas12a therapeutics. *Wiley Interdiscip. Rev. Syst. Biol. Med.* 10 (1). doi:10.1002/wsbm.1408

Cohen, J., DeSimone, A., Lek, M., and Lek, A. (2020). Therapeutic approaches in facioscapulohumeral muscular dystrophy. *Trends Mol. Med.* 27, 123–137. doi:10.1016/j.molmed.2020.09.008

Crudele, J. M., and Chamberlain, J. S. (2018). Cas9 immunity creates challenges for CRISPR gene editing therapies. *Nat. Commun.* 9, 3497. doi:10.1038/s41467-018-05843-9

Das, S., and Chadwick, B. P. (2016). Influence of repressive histone and DNA methylation upon D4Z4 transcription in non-myogenic cells. *PLoS One* 11, e0160022, doi:10.1371/journal.pone.0160022

de Greef, J. C., Krom, Y. D., den Hamer, B., Snider, L., Hiramuki, Y., van den Akker, R. F. P., et al. (2018). Smchd1 haploinsufficiency exacerbates the phenotype of a transgenic FSHD1 mouse model. *Hum. Mol. Genet.* 27, 716–731. doi:10.1093/hmg/ddx437

de Greef, J. C., Lemmers, R. J., Camaño, P., Day, J. W., Sacconi, S., Dunand, M., et al. (2010). Clinical features of facioscapulohumeral muscular dystrophy 2. *Neurology* 75, 1548–1554. doi:10.1212/WNL.0b013e3181f96175

De Iaco, A., Planet, E., Coluccio, A., Verp, S., Duc, J., and Trono, D. (2017). DUX-family transcription factors regulate zygotic genome activation in placental mammals. *Nat. Genet.* 49, 941–945. doi:10.1038/ng.3858

Deidda, G., Cacurri, S., Grisanti, P., Vigneti, E., Piazzo, N., and Felicetti, L. (1995). Physical mapping evidence for a duplicated region on chromosome 10qter showing high homology with the facioscapulohumeral muscular dystrophy locus on chromosome 4qter. *Eur. J. Hum. Genet.* 3, 155–167. doi:10.1159/000472291

Denny, A. P., and Heather, A. K. (2017). Are antioxidants a potential therapy for FSHD? A review of the literature. *Oxid. Med. Cel. Longev.* 2017, 7020295. doi:10.1155/2017/7020295

Derenne, A., Tassin, A., Nguyen, T. H., De Roeck, E., Jenart, V., Ansseau, E., et al. (2020). Induction of a local muscular dystrophy using electroporation *in vivo*: an easy tool for screening therapeutics. *Sci. Rep.* 10, 11301. doi:10.1038/s41598-020-68135-7

DeSimone, A. M., Cohen, J., Lek, M., and Lek, A. (2020). Cellular and animal models for facioscapulohumeral muscular dystrophy. *Dis. Model. Mech.* 13, dmm046904. doi:10.1242/dmm.046904

Dieckmann, A., Hagedorn, P. H., Burki, Y., Brügmann, C., Berrera, M., Ebeling, M., et al. (2018). A sensitive in vitro approach to assess the hybridization-dependent toxic potential of high affinity gapmer oligonucleotides. *Mol. Ther. Nucleic Acids* 10, 45–54. doi:10.1016/j.omtn.2017.11.004

Dixit, M., Ansseau, E., Tassin, A., Winokur, S., Shi, R., Qian, H., et al. (2007). DUX4, a candidate gene of facioscapulohumeral muscular dystrophy, encodes a transcriptional activator of PITX1. *Proc. Natl. Acad. Sci. USA* 104, 18157–18162. doi:10.1073/pnas.0708659104

Dmitriev, P., Bou Saada, Y., Dib, C., Ansseau, E., Barat, A., Hamade, A., et al. (2016). DUX4-induced constitutive DNA damage and oxidative stress contribute to aberrant differentiation of myoblasts from FSHD patients. *Free Radic. Biol. Med.* 99, 244–258. doi:10.1016/j.freeradbiomed.2016.08.007

Dominska, M., and Dykxhoorn, D. M. (2010). Breaking down the barriers: siRNA delivery and endosome escape. *J. Cel Sci.* 123, 1183–1189. doi:10.1242/jcs.066399

Echigoya, Y., Lim, K. R. Q., Trieu, N., Bao, B., Miskew Nichols, B., Vila, M. C., et al. (2017). Quantitative antisense screening and optimization for exon 51 skipping in Duchenne muscular dystrophy. *Mol. Ther.* 25, 2561. doi:10.1016/j.ymthe.2017.07.014

Ehrke-Schulz, E., Schiwon, M., Leitner, T., Dávid, S., Bergmann, T., Liu, J., et al. (2017). CRISPR/Cas9 delivery with one single adenoviral vector devoid of all viral genes. *Sci. Rep.* 7, 17113. doi:10.1038/s41598-017-17180-w

Ferdosi, S. R., Ewaisha, R., Moghadam, F., Krishna, S., Park, J. G., Ebrahimkhani, M. R., et al. (2019). Multifunctional CRISPR-Cas9 with engineered immunosilenced human T cell epitopes. *Nat. Commun.* 10, 1842. doi:10.1038/s41467-019-09693-x

Ferri, G., Huichalaf, C. H., Caccia, R., and Gabellini, D. (2015). Direct interplay between two candidate genes in FSHD muscular dystrophy. *Hum. Mol. Genet.* 24, 1256–1266. doi:10.1093/hmg/ddu536

Fitzsimons, R. B., Gurwin, E. B., and Bird, A. C. (1987). Retinal vascular abnormalities in facioscapulohumeral muscular dystrophy. A general association with genetic and therapeutic implications. *Brain* 110 (Pt 3), 631–648. doi:10.1093/brain/110.3.631

Frazier, K. S. (2015). Antisense oligonucleotide therapies: the promise and the challenges from a toxicologic pathologist's perspective. *Toxicol. Pathol.* 43, 78–89. doi:10.1177/0192623314551840

Gabriëls, J., Beckers, M. C., Ding, H., De Vriese, A., Plaisance, S., van der Maarel, S. M., et al. (1999). Nucleotide sequence of the partially deleted D4Z4 locus in a patient with FSHD identifies a putative gene within each 3.3 kb element. *Gene* 236, 25–32. doi:10.1016/s0378-1119(99)00267-x

Geng, L. N., Tyler, A. E., and Tapscott, S. J. (2011). Immunodetection of human double homeobox 4. *Hybridoma* 30, 125–130. doi:10.1089/hyb.2010.0094

Giesige, C. R., Wallace, L. M., Heller, K. N., Eidahl, J. O., Saad, N. Y., Fowler, A. M., et al. (2018). AAV-mediated follistatin gene therapy improves functional

outcomes in the TIC-DUX4 mouse model of FSHD. *JCI Insight* 3, e123538. doi:10.1172/jci.insight.123538

Goossens, R., van den Boogaard, M. L., Lemmers, R. J. L. F., Balog, J., van der Vliet, P. J., Willemsen, I. M., et al. (2019). Intronic SMCHD1 variants in FSHD: testing the potential for CRISPR-Cas9 genome editing. *J. Med. Genet.* 56, 828–837. doi:10.1136/jmedgenet-2019-106402

Goselink, R. J. M., Voermans, N. C., Okkersen, K., Brouwer, O. F., Padberg, G. W., Nikolic, A., et al. (2017). Early onset facioscapulohumeral dystrophy—a systematic review using individual patient data. *Neuromuscul. Disord.* 27, 1077–1083. doi:10.1016/j.nmd.2017.09.007

Hagedorn, P. H., Yakimov, V., Ottosen, S., Kammler, S., Nielsen, N. F., Høg, A. M., et al. (2013). Hepatotoxic potential of therapeutic oligonucleotides can Be predicted from their sequence and modification pattern. *Nucleic Acid Ther.* 23, 302–310. doi:10.1089/nat.2013.0436

Hamanaka, K., Šikrová, D., Mitsuhashi, S., Masuda, H., Sekiguchi, Y., Sugiyama, A., et al. (2020). Homozygous nonsense variant in LRIF1 associated with facioscapulohumeral muscular dystrophy. *Neurology* 94, e2441–e2447. doi:10.1212/WNL.0000000000009617

Hamel, J., and Tawil, R. (2018). Facioscapulohumeral muscular dystrophy: update on pathogenesis and future treatments. *Neurotherapeutics* 15, 863–871. doi:10.1007/s13311-018-00675-3

Hendling, M., and Barišić, I. (2019). In-silico design of DNA oligonucleotides: challenges and approaches. *Comput. Struct. Biotechnol. J.* 17, 1056–1065. doi:10.1016/j.csbj.2019.07.008

Hendrickson, P. G., Doráis, J. A., Grow, E. J., Whiddon, J. L., Lim, J. W., Wike, C. L., et al. (2017). Conserved roles of mouse DUX and human DUX4 in activating cleavage-stage genes and MERVL/HERVL retrotransposons. *Nat. Genet.* 49, 925–934. doi:10.1038/ng.3844

Hewitt, J. E. (2015). Loss of epigenetic silencing of the DUX4 transcription factor gene in facioscapulohumeral muscular dystrophy. *Hum. Mol. Genet.* 24, R17–R23. doi:10.1093/hmg/ddv237

Hewitt, J. E., Lyle, R., Clark, L. N., Valleley, E. M., Wright, T. J., Wijmenga, C., et al. (1994). Analysis of the tandem repeat locus D4Z4 associated with facioscapulohumeral muscular dystrophy. *Hum. Mol. Genet.* 3, 1287–1295. doi:10.1093/hmg/3.8.1287

Himeda, C. L., Debarnot, C., Homma, S., Beermann, M. L., Miller, J. B., Jones, P. L., et al. (2014). Myogenic enhancers regulate expression of the facioscapulohumeral muscular dystrophy-associated DUX4 gene. *Mol. Cel. Biol.* 34, 1942–1955. doi:10.1128/MCB.00149-14

Himeda, C. L., and Jones, P. L. (2019). The genetics and epigenetics of facioscapulohumeral muscular dystrophy. *Annu. Rev. Genomics Hum. Genet.* 20, 265–291. doi:10.1146/annurev-genom-083118-014933

Himeda, C. L., Jones, T. I., and Jones, P. L. (2016). CRISPR/dCas9-mediated transcriptional inhibition ameliorates the epigenetic dysregulation at D4Z4 and represses DUX4-fl in FSH muscular dystrophy. *Mol. Ther.* 24, 527–535. doi:10.1038/mt.2015.200

Himeda, C. L., Jones, T. I., Virbasius, C. M., Zhu, L. J., Green, M. R., and Jones, P. L. (2018). Identification of epigenetic regulators of DUX4-fl for targeted therapy of facioscapulohumeral muscular dystrophy. *Mol. Ther.* 26, 1797–1807. doi:10.1016/j.ymthe.2018.04.019

Holoch, D., and Moazed, D. (2015). RNA-mediated epigenetic regulation of gene expression. *Nat. Rev. Genet.* 16, 71–84. doi:10.1038/nrg3863

Jiang, F., and Doudna, J. A. (2017). CRISPR-Cas9 structures and mechanisms. *Annu. Rev. Biophys.* 46, 505–529. doi:10.1146/annurev-biophys-062215-010822

Jinek, M., Chylinski, K., Fonfara, I., Hauer, M., Doudna, J. A., and Charpentier, E. (2012). A programmable dual-RNA-guided DNA endonuclease in adaptive bacterial immunity. *Science* 337, 816–821. doi:10.1126/science.1225829

Jones, T., and Jones, P. L. (2018). A cre-inducible DUX4 transgenic mouse model for investigating facioscapulohumeral muscular dystrophy. *PLoS One* 13, e0192657. doi:10.1371/journal.pone.0192657

Juliano, R. L. (2016). The delivery of therapeutic oligonucleotides. *Nucleic Acids Res.* 44, 6518–6548. doi:10.1093/nar/gkw236

Kakiuchi-Kiyota, S., Whiteley, L. O., Ryan, A. M., and Mathialagan, N. (2016). Development of a method for profiling protein interactions with LNA-modified antisense oligonucleotides using protein microarrays. *Nucleic Acid Ther.* 26, 93–101. doi:10.1089/nat.2015.0576

Kamola, P. J., Kitson, J. D., Turner, G., Maratou, K., Eriksson, S., Panjwani, A., et al. (2015). In silico and *in vitro* evaluation of exonic and intronic off-target effects form a critical element of therapeutic ASO gapmer optimization. *Nucleic Acids Res.* 43, 8638–8650. doi:10.1093/nar/gkv857

Kim, D., Bae, S., Park, J., Kim, E., Kim, S., Yu, H. R., et al. (2015). Digenome-seq: genome-wide profiling of CRISPR-Cas9 off-target effects in human cells. *Nat. Methods* 12, 237–243. doi:10.1038/nmeth.3284

Kim, D. H., Longo, M., Han, Y., Lundberg, P., Cantin, E., and Rossi, J. J. (2004). Interferon induction by siRNAs and ssRNAs synthesized by phage polymerase. *Nat. Biotechnol.* 22, 321–325. doi:10.1038/nbt940

Kim, E., Koo, T., Park, S. W., Kim, D., Kim, K., Cho, H. Y., et al. (2017). *In vivo* genome editing with a small Cas9 orthologue derived from *Campylobacter* jejuni. *Nat. Commun.* 8, 14500. doi:10.1038/ncomms14500

Kim, S., Koo, T., Jee, H.-G., Cho, H.-Y., Lee, G., Lim, D.-G., et al. (2018). CRISPR RNAs trigger innate immune responses in human cells. *Genome Res.* 28, 367–373. doi:10.1101/gr.231936.117

Klinge, L., Eagle, M., Haggerty, I. D., Roberts, C. E., Straub, V., and Bushby, K. M. (2006). Severe phenotype in infantile facioscapulohumeral muscular dystrophy. *Neuromuscul. Disord.* 16, 553–558. doi:10.1016/j.nmd.2006.06.008

Klingler, C., Ashley, J., Shi, K., Stiefvater, A., Kyba, M., Sinnreich, M., et al. (2020). DNA aptamers against the DUX4 protein reveal novel therapeutic implications for FSHD. *FASEB J.* 34, 4573–4590. doi:10.1096/fj.201902696

Laforêt, P., de Toma, C., Eymard, B., Becane, H. M., Jeanpierre, M., Fardeau, M., et al. (1998). Cardiac involvement in genetically confirmed facioscapulohumeral muscular dystrophy. *Neurology* 51, 1454–1456. doi:10.1212/wnl.51.5.1454

Le Gall, L., Sidlauskaite, E., Mariot, V., and Dumonceaux, J. (2020). Therapeutic strategies targeting DUX4 in FSHD. *J. Clin. Med.* 9, 2886. doi:10.3390/jcm9092886

Lee, J. J., and Yokota, T. (2013). Antisense therapy in neurology. *J. Pers. Med.* 3, 144–176. doi: doi:10.3390/jpm3030144

Lek, A., Zhang, Y., Woodman, K. G., Huang, S., DeSimone, A. M., Cohen, J., et al. (2020). Applying genome-wide CRISPR-Cas9 screens for therapeutic discovery in facioscapulohumeral muscular dystrophy. *Sci. Transl. Med.* 12, eaay0271. doi:10.1126/scitranslmed.aay0271

Lemmers, R. J., de Kievit, P., Sandkuijl, L., Padberg, G. W., van Ommen, G. J., Frants, R. R., et al. (2002). Facioscapulohumeral muscular dystrophy is uniquely associated with one of the two variants of the 4q subtelomere. *Nat. Genet.* 32, 235–236. doi:10.1038/ng999

Lemmers, R. J., Goeman, J. J., van der Vliet, P. J., van Nieuwenhuizen, M. P., Balog, J., Vos-Versteeg, M., et al. (2015). Inter-individual differences in CpG methylation at D4Z4 correlate with clinical variability in FSHD1 and FSHD2. *Hum. Mol. Genet.* 24, 659–669. doi:10.1093/hmg/ddu486

Lemmers, R. J., Tawil, R., Petek, L. M., Balog, J., Block, G. J., Santen, G. W., et al. (2012). Digenic inheritance of an SMCHD1 mutation and an FSHD-permissive D4Z4 allele causes facioscapulohumeral muscular dystrophy type 2. *Nat. Genet.* 44, 1370–1374. doi:10.1038/ng.2454

Lemmers, R. J., van der Vliet, P. J., Klooster, R., Sacconi, S., Camaño, P., Dauwerse, J. G., et al. (2010). A unifying genetic model for facioscapulohumeral muscular dystrophy. *Science* 329, 1650–1653. doi:10.1126/science.1189044

Lemmers, R. J., Wohlgemuth, M., Frants, R. R., Padberg, G. W., Morava, E., and van der Maarel, S. M. (2004). Contractions of D4Z4 on 4qB subtelomeres do not cause facioscapulohumeral muscular dystrophy. *Am. J. Hum. Genet.* 75, 1124–1130. doi:10.1086/426035

Liang, X., Sun, H., Shen, W., and Crooke, S. T. (2015). Identification and characterization of intracellular proteins that bind oligonucleotides with phosphorothioate linkages. *Nucleic Acids Res.* 43, 2927–2945. doi:10.1093/nar/gkv143

Lim, J. W., Snider, L., Yao, Z., Tawil, R., Van Der Maarel, S. M., Rigo, F., et al. (2015). DICER/AGO-dependent epigenetic silencing of D4Z4 repeats enhanced by exogenous siRNA suggests mechanisms and therapies for FSHD. *Hum. Mol. Genet.* 24, 4817–4828. doi:10.1093/hmg/ddv206

Lim, K. R. Q., Bittel, A., Maruyama, R., Echigoya, Y., Nguyen, Q., Huang, Y., et al. (2020a). DUX4 transcript knockdown with antisense 2′-O-methoxyethyl gapmers for the treatment of facioscapulohumeral muscular dystrophy. *Mol. Ther.* 29, 848–858. doi:10.1016/j.ymthe.2020.10.010

Lim, K. R. Q., Maruyama, R., Echigoya, Y., Nguyen, Q., Zhang, A., Khawaja, H., et al. (2020b). Inhibition of DUX4 expression with antisense LNA gapmers as a therapy for facioscapulohumeral muscular dystrophy. *Proc. Natl. Acad. Sci. U S A.* 117, 16509–16515. doi:10.1073/pnas.1909649117

Lim, K. R. Q., Nguyen, Q., and Yokota, T. (2020c). DUX4 signalling in the pathogenesis of facioscapulohumeral muscular dystrophy. *Int. J. Mol. Sci.* 21, 729. doi:10.3390/ijms21030729

Lim, K. R. Q., Echigoya, Y., Nagata, T., Kuraoka, M., Kobayashi, M., Aoki, Y., et al. (2019). Efficacy of multi-exon skipping treatment in Duchenne muscular dystrophy dog model neonates. *Mol. Ther.* 27. doi:10.1016/j.ymthe.2018.10.011

Lim, K. R. Q., and Yokota, T. (2018). "Invention and early history of exon skipping and splice modulation," in *Exon skipping and inclusion therapies: methods and protocols*. Editors T. Yokota and R. Maruyama (New York, NY: Springer), 3–30.

Lim, K. R. Q., and Yokota, T. (2020). Invention and early history of gapmers. *Methods Mol. Biol.* 2176, 3–19. doi:10.1007/978-1-0716-0771-8_1

Lino, C. A., Harper, J. C., Carney, J. P., and Timlin, J. A. (2018). Delivering CRISPR: a review of the challenges and approaches. *Drug Deliv.* 25, 1234–1257. doi:10.1080/10717544.2018.1474964

Lunt, P. W., Jardine, P. E., Koch, M. C., Maynard, J., Osborn, M., Williams, M., et al. (1995). Correlation between fragment size at D4F104S1 and age at onset or at wheelchair use, with a possible generational effect, accounts for much phenotypic variation in 4q35-facioscapulohumeral muscular dystrophy (FSHD). *Hum. Mol. Genet.* 4, 951–958. doi:10.1093/hmg/4.5.951

Lutz, K. L., Holte, L., Kliethermes, S. A., Stephan, C., and Mathews, K. D. (2013). Clinical and genetic features of hearing loss in facioscapulohumeral muscular dystrophy. *Neurology* 81, 1374–1377. doi:10.1212/WNL.0b013e3182a84140

Mariot, V., Joubert, R., Marsollier, A.-C., Hourdé, C., Voit, T., and Dumonceaux, J. (2020). A deoxyribonucleic acid decoy trapping DUX4 for the treatment of facioscapulohumeral muscular dystrophy. *Mol. Ther. Nucleic Acids*. doi:10.1016/j.omtn.2020.10.028

Marsollier, A. C., Ciszewski, L., Mariot, V., Popplewell, L., Voit, T., Dickson, G., et al. (2016). Antisense targeting of 3' end elements involved in DUX4 mRNA processing is an efficient therapeutic strategy for facioscapulohumeral dystrophy: a new gene-silencing approach. *Hum. Mol. Genet.* 25, 1468–1478. doi:10.1093/hmg/ddw015

Mehta, A., and Merkel, O. M. (2020). Immunogenicity of Cas9 protein. *J. Pharm. Sci.* 109, 62–67. doi:10.1016/j.xphs.2019.10.003

Mitsuhashi, H., Ishimaru, S., Homma, S., Yu, B., Honma, Y., Beermann, M. L., et al. (2018). Functional domains of the FSHD-associated DUX4 protein. *Biol. Open* 7, bio033977. doi:10.1242/bio.033977

Mitsuhashi, H., Mitsuhashi, S., Lynn-Jones, T., Kawahara, G., and Kunkel, L. M. (2013). Expression of DUX4 in zebrafish development recapitulates facioscapulohumeral muscular dystrophy. *Hum. Mol. Genet.* 22, 568–577. doi:10.1093/hmg/dds467

Mojica, F. J., Díez-Villaseñor, C., García-Martínez, J., and Almendros, C. (2009). Short motif sequences determine the targets of the prokaryotic CRISPR defence system. *Microbiology* 155, 733–740. doi:10.1099/mic.0.023960-0

Moore, R., Spinhirne, A., Lai, M. J., Preisser, S., Li, Y., Kang, T., et al. (2015). CRISPR-based self-cleaving mechanism for controllable gene delivery in human cells. *Nucleic Acids Res.* 43, 1297–1303. doi:10.1093/nar/gku1326

Morcos, P. A., Li, Y., and Jiang, S. (2008). Vivo-Morpholinos: a non-peptide transporter delivers Morpholinos into a wide array of mouse tissues. *Biotechniques* 45, 613–passim. doi:10.2144/000113005

Morosetti, R., Gidaro, T., Broccolini, A., Gliubizzi, C., Sancricca, C., Tonali, P. A., et al. (2011). Mesoangioblasts from facioscapulohumeral muscular dystrophy display *in Vivo* a variable myogenic ability predictable by their *in Vitro* behavior. *Cell Transplant.* 20, 1299–1313. doi:10.3727/096368910X546571

Nguyen, Q., and Yokota, T. (2019). Antisense oligonucleotides for the treatment of cardiomyopathy in Duchenne muscular dystrophy. *Am. J. Transl. Res.* 11, 1202–1218.

Nikolic, A., Ricci, G., Sera, F., Bucci, E., Govi, M., Mele, F., et al. (2016). Clinical expression of facioscapulohumeral muscular dystrophy in carriers of 1-3 D4Z4 reduced alleles: experience of the FSHD Italian national registry. *BMJ Open* 6, e007798. doi:10.1136/bmjopen-2015-007798

O'Connell, M. R., Oakes, B. L., Sternberg, S. H., East-Seletsky, A., Kaplan, M., and Doudna, J. A. (2014). Programmable RNA recognition and cleavage by CRISPR/Cas9. *Nature* 516, 263–266. doi:10.1038/nature13769

Padberg, G. W., Brouwer, O. F., de Keizer, R. J., Dijkman, G., Wijmenga, C., Grote, J. J., et al. (1995). On the significance of retinal vascular disease and hearing loss in facioscapulohumeral muscular dystrophy. *Muscle Nerve Suppl.* 2, S73–S80. doi:10.1002/mus.880181314

Pandey, S. N., Cabotage, J., Shi, R., Dixit, M., Sutherland, M., Liu, J., et al. (2012). Conditional over-expression of PITX1 causes skeletal muscle dystrophy in mice. *Biol. Open* 1, 629–639. doi:10.1242/bio.20121305

Pandey, S. N., Khawaja, H., and Chen, Y. W. (2015). Culture conditions affect expression of DUX4 in FSHD myoblasts. *Molecules* 20, 8304–8315. doi:10.3390/molecules20058304

Pandey, S. N., Lee, Y. C., Yokota, T., and Chen, Y. W. (2014). Morpholino treatment improves muscle function and pathology of Pitx1 transgenic mice. *Mol. Ther.* 22, 390–396. doi:10.1038/mt.2013.263

Ran, F. A., Hsu, P. D., Lin, C. Y., Gootenberg, J. S., Konermann, S., Trevino, A. E., et al. (2013). Double nicking by RNA-guided CRISPR Cas9 for enhanced genome editing specificity. *Cell* 154, 1380–1389. doi:10.1016/j.cell.2013.08.021

Ricci, G., Scionti, I., Sera, F., Govi, M., D'Amico, R., Frambolli, I., et al. (2013). Large scale genotype-phenotype analyses indicate that novel prognostic tools are required for families with facioscapulohumeral muscular dystrophy. *Brain* 136, 3408–3417. doi:10.1093/brain/awt226

Richards, M., Coppée, F., Thomas, N., Belayew, A., and Upadhyaya, M. (2012). Facioscapulohumeral muscular dystrophy (FSHD): an enigma unravelled?. *Hum. Genet.* 131, 325–340. doi:10.1007/s00439-011-1100-z

Rickard, A. M., Petek, L. M., and Miller, D. G. (2015). Endogenous DUX4 expression in FSHD myotubes is sufficient to cause cell death and disrupts RNA splicing and cell migration pathways. *Hum. Mol. Genet.* 24, 5901–5914. doi:10.1093/hmg/ddv315

Ricobaraza, A., Gonzalez-Aparicio, M., Mora-Jimenez, L., Lumbreras, S., and Hernandez-Alcoceba, R. (2020). High-capacity adenoviral vectors: expanding the scope of gene therapy. *Int. J. Mol. Sci.* 21, 3643. doi:10.3390/ijms21103643

Rodino-Klapac, L. R., Haidet, A. M., Kota, J., Handy, C., Kaspar, B. K., and Mendell, J. R. (2009). Inhibition of myostatin with emphasis on follistatin as a therapy for muscle disease. *Muscle Nerve* 39, 283–296. doi:10.1002/mus.21244

Sacconi, S., Briand-Suleau, A., Gros, M., Baudoin, C., Lemmers, R. J. L. F., Rondeau, S., et al. (2019). FSHD1 and FSHD2 form a disease continuum. *Neurology* 92, e2273–e2285. doi:10.1212/WNL.0000000000007456

Sacconi, S., Lemmers, R. J., Balog, J., van der Vliet, P. J., Lahaut, P., van Nieuwenhuizen, M. P., et al. (2013). The FSHD2 gene SMCHD1 is a modifier of disease severity in families affected by FSHD1. *Am. J. Hum. Genet.* 93, 744–751. doi:10.1016/j.ajhg.2013.08.004

Scully, M. A., Eichinger, K. J., Donlin-Smith, C. M., Tawil, R., and Statland, J. M. (2014). Restrictive lung involvement in facioscapulohumeral muscular dystrophy. *Muscle Nerve* 50, 739–743. doi:10.1002/mus.24218

Shen, B., Zhang, W., Zhang, J., Zhou, J., Wang, J., Chen, L., et al. (2014). Efficient genome modification by CRISPR-Cas9 nickase with minimal off-target effects. *Nat. Methods* 11, 399–402. doi:10.1038/nmeth.2857

Shen, W., De Hoyos, C. L., Sun, H., Vickers, T. A., Liang, X., and Crooke, S. T. (2018). Acute hepatotoxicity of 2' fluoro-modified 5-10-5 gapmer phosphorothioate oligonucleotides in mice correlates with intracellular protein binding and the loss of DBHS proteins. *Nucleic Acids Res.* 46, 2204–2217. doi:10.1093/nar/gky060

Shen, W., De Hoyos, C. L., Migawa, M. T., Vickers, T. A., Sun, H., Low, A., et al. (2019). Chemical modification of PS-ASO therapeutics reduces cellular protein-binding and improves the therapeutic index. *Nat. Biotechnol.* 37, 640–650. doi:10.1038/s41587-019-0106-2

Shirley, J. L., de Jong, Y. P., Terhorst, C., and Herzog, R. W. (2020). Immune responses to viral gene therapy vectors. *Mol. Ther.* 28, 709–722. doi:10.1016/j.ymthe.2020.01.001

Snider, L., Geng, L. N., Lemmers, R. J., Kyba, M., Ware, C. B., Nelson, A. M., et al. (2010). Facioscapulohumeral dystrophy: incomplete suppression of a retrotransposed gene. *Plos Genet.* 6, e1001181. doi:10.1371/journal.pgen.1001181

Summerton, J., and Weller, D. (1997). Morpholino antisense oligomers: design, preparation, and properties. *Antisense Nucleic Acid Drug Dev.* 7, 187–195. doi:10.1089/oli.1.1997.7.187

Tassin, A., Laoudj-Chenivesse, D., Vanderplanck, C., Barro, M., Charron, S., Ansseau, E., et al. (2013). DUX4 expression in FSHD muscle cells: how could such a rare protein cause a myopathy?. *J. Cel. Mol. Med.* 17, 76–89. doi:10.1111/j.1582-4934.2012.01647.x

Tawil, R., van der Maarel, S. M., and Tapscott, S. J. (2014). Facioscapulohumeral dystrophy: the path to consensus on pathophysiology. *Skelet. Muscle* 4, 12. doi:10.1186/2044-5040-4-12

Tong, S., Moyo, B., Lee, C. M., Leong, K., and Bao, G. (2019). Engineered materials for *in vivo* delivery of genome-editing machinery. *Nat. Rev. Mater.* 4, 726–737. doi:10.1038/s41578-019-0145-9

Tsai, S. Q., Zheng, Z., Nguyen, N. T., Liebers, M., Topkar, V. V., Thapar, V., et al. (2015). GUIDE-seq enables genome-wide profiling of off-target cleavage by CRISPR-Cas nucleases. *Nat. Biotechnol.* 33, 187–197. doi:10.1038/nbt.3117

Tycko, J., Myer, V. E., and Hsu, P. D. (2016). Methods for optimizing CRISPR-cas9 genome editing specificity. *Mol. Cell* 63, 355–370. doi:10.1016/j.molcel.2016.07.004

van den Boogaard, M. L., Lemmers, R. J. L. F., Balog, J., Wohlgemuth, M., Auranen, M., Mitsuhashi, S., et al. (2016). Mutations in DNMT3B modify epigenetic repression of the D4Z4 repeat and the penetrance of facioscapulohumeral dystrophy. *Am. J. Hum. Genet.* 98, 1020–1029. doi:10.1016/j.ajhg.2016.03.013

Van Overveld, P. G., Enthoven, L., Ricci, E., Rossi, M., Felicetti, L., Jeanpierre, M., et al. (2005). Variable hypomethylation of D4Z4 in facioscapulohumeral muscular dystrophy. *Ann. Neurol.* 58, 569–576. doi:10.1002/ana.20625

van Overveld, P. G., Lemmers, R. J., Sandkuijl, L. A., Enthoven, L., Winokur, S. T., Bakels, F., et al. (2003). Hypomethylation of D4Z4 in 4q-linked and non-4q-linked facioscapulohumeral muscular dystrophy. *Nat. Genet.* 35, 315–317. doi:10.1038/ng1262

Vanderplanck, C., Ansseau, E., Charron, S., Stricwant, N., Tassin, A., Laoudj-Chenivesse, D., et al. (2011). The FSHD atrophic myotube phenotype is caused by DUX4 expression. *PLoS One* 6, e26820. doi:10.1371/journal.pone.0026820

Vilquin, J. T., Marolleau, J. P., Sacconi, S., Garcin, I., Lacassagne, M. N., Robert, I., et al. (2005). Normal growth and regenerating ability of myoblasts from unaffected muscles of facioscapulohumeral muscular dystrophy patients. *Gene Ther.* 12, 1651–1662. doi:10.1038/sj.gt.3302565

Wagner, D. L., Amini, L., Wendering, D. J., Burkhardt, L. M., Akyüz, L., Reinke, P., et al. (2019). High prevalence of *Streptococcus* pyogenes Cas9-reactive T cells within the adult human population. *Nat. Med.* 25, 242–248. doi:10.1038/s41591-018-0204-6

Wallace, L. M., Liu, J., Domire, J. S., Garwick-Coppens, S. E., Guckes, S. M., Mendell, J. R., et al. (2012). RNA interference inhibits DUX4-induced muscle toxicity in vivo: implications for a targeted FSHD therapy. *Mol. Ther.* 20, 1417–1423. doi:10.1038/mt.2012.68

Wallace, L. M., Saad, N. Y., Pyne, N. K., Fowler, A. M., Eidahl, J. O., Domire, J. S., et al. (2018). Pre-clinical safety and off-target studies to support translation of AAV-mediated RNAi therapy for FSHD. *Mol. Ther. Methods Clin. Dev.* 8, 121–130. doi:10.1016/j.omtm.2017.12.005

Wang, D., Zhang, C., Wang, B., Li, B., Wang, Q., Liu, D., et al. (2019). Optimized CRISPR guide RNA design for two high-fidelity Cas9 variants by deep learning. *Nat. Commun.* 10, 4284. doi:10.1038/s41467-019-12281-8

Wang, L. H., and Tawil, R. (2016). Facioscapulohumeral dystrophy. *Curr. Neurol. Neurosci. Rep.* 16, 66. doi:10.1007/s11910-016-0667-0

Wienert, B., Shin, J., Zelin, E., Pestal, K., and Corn, J. E. (2018). In vitro-transcribed guide RNAs trigger an innate immune response via the RIG-I pathway. *PLoS Biol.* 16, e2005840. doi:10.1371/journal.pbio.2005840

Wilbie, D., Walther, J., and Mastrobattista, E. (2019). Delivery aspects of CRISPR/Cas for *in Vivo* genome editing. *Acc. Chem. Res.* 52, 1555–1564. doi:10.1021/acs.accounts.9b00106

Wu, Z., Yang, H., and Colosi, P. (2010). Effect of genome size on AAV vector packaging. *Mol. Ther.* 18, 80–86. doi:10.1038/mt.2009.255

Xu, C. L., Ruan, M. Z. C., Mahajan, V. B., and Tsang, S. H. (2019). Viral delivery systems for CRISPR. *Viruses* 11, 28. doi:10.3390/v11010028

Yoshida, T., Naito, Y., Yasuhara, H., Sasaki, K., Kawaji, H., Kawai, J., et al. (2019). Evaluation of off-target effects of gapmer antisense oligonucleotides using human cells. *Genes Cells* 24, 827–835. doi:10.1111/gtc.12730

Conflict of Interest: TY is a co-founder and shareholder of OligomicsTx Inc., which aims to commercialize antisense technology.

The remaining author declares that the research was conducted in the absence of any commercial or financial relationships that could be construed as a potential conflict of interest.

frontiers in Physiology

REVIEW
published: 09 April 2021
doi: 10.3389/fphys.2021.647010

Abnormal Calcium Handling in Duchenne Muscular Dystrophy: Mechanisms and Potential Therapies

Satvik Mareedu[1], *Emily D. Million*[2], *Dongsheng Duan*[2,3] *and Gopal J. Babu*[1]*

[1] Department of Cell Biology and Molecular Medicine, New Jersey Medical School, Rutgers University, Newark, NJ, United States, [2] Department of Molecular Microbiology and Immunology, The University of Missouri, Columbia, MO, United States, [3] Department of Biomedical, Biological & Chemical Engineering, The University of Missouri, Columbia, MO, United States

Duchenne muscular dystrophy (DMD) is an X-linked muscle-wasting disease caused by the loss of dystrophin. DMD is associated with muscle degeneration, necrosis, inflammation, fatty replacement, and fibrosis, resulting in muscle weakness, respiratory and cardiac failure, and premature death. There is no curative treatment. Investigations on disease-causing mechanisms offer an opportunity to identify new therapeutic targets to treat DMD. An abnormal elevation of the intracellular calcium (Ca_i^{2+}) concentration in the dystrophin-deficient muscle is a major secondary event, which contributes to disease progression in DMD. Emerging studies have suggested that targeting Ca^{2+}-handling proteins and/or mechanisms could be a promising therapeutic strategy for DMD. Here, we provide an updated overview of the mechanistic roles the sarcolemma, sarcoplasmic/endoplasmic reticulum, and mitochondria play in the abnormal and sustained elevation of Ca_i^{2+} levels and their involvement in DMD pathogenesis. We also discuss current approaches aimed at restoring Ca^{2+} homeostasis as potential therapies for DMD.

Keywords: Duchenne muscular dystrophy, calcium, sarco(endo)plasmic reticulum calcium ATPase, sarcolipin, ryanodine receptor, sarcolemma, dystrophin, mitochondria

OPEN ACCESS

Edited by:
Helen Cristina Miranda, Case Western Reserve University, United States

Reviewed by:
Stewart Ian Head, Western Sydney University, Australia
George G. Rodney, Baylor College of Medicine, United States

***Correspondence:**
Gopal J. Babu
babugo@njms.rutgers.edu

Specialty section:
This article was submitted to Striated Muscle Physiology, a section of the journal Frontiers in Physiology

Received: *28 December 2020*
Accepted: *02 March 2021*
Published: *09 April 2021*

Citation:
Mareedu S, Million ED, Duan D and Babu GJ (2021) Abnormal Calcium Handling in Duchenne Muscular Dystrophy: Mechanisms and Potential Therapies. Front. Physiol. 12:647010. doi: 10.3389/fphys.2021.647010

INTRODUCTION

Duchenne muscular dystrophy (DMD) is X-linked and is the most common form of muscle wasting disease. It affects 1 in 3,500 to 5,000 male births (Mendell and Lloyd-Puryear, 2013). DMD is caused by mutations in the dystrophin gene, which leads to the loss of a functional dystrophin protein (Monaco et al., 1986). DMD is characterized by progressive loss of muscle mass and function due to muscle degeneration, necrosis, and fatty fibrosis, resulting in wheelchair dependence (Ervasti and Campbell, 1993; Bushby et al., 2010; Connolly et al., 2013; Aartsma-Rus et al., 2016; Duan et al., 2021). Eventually, patients die of respiratory failure and/or cardiomyopathy (Finsterer, 2006). There is currently no curative treatment for DMD. Restoring dystrophin function via gene replacement or repair therapy is attractive and promising. Although there is a favorable outcome in preclinical studies, the immunogenicity of the newly expressed dystrophin protein remains a concern. In addition, the complexity of thousands of disease-causing mutations in the dystrophin gene creates challenges for gene repair therapy. Alternatively, targeting major disease-causing mechanisms offers an opportunity to treat all DMD patients without the complications of dystrophin replacement or repair therapies.

Dystrophin is a rod-shaped cytoskeletal protein, primarily expressed in muscles. Dystrophin links the intracellular cytoskeleton network to the transmembrane components of the dystrophin–glycoprotein complex (Gao and McNally, 2015; Allen et al., 2016). Growing evidence suggests dystrophin in addition to maintaining the structural integrity of the sarcolemma plays a key role in regulating signaling pathways. This includes the nitric oxide pathway, Ca^{2+} entry, and the production of reactive oxygen species (ROS). In the absence of dystrophin, these pathways are damaged and contribute to muscle pathology. For details on these pathways and their clinical implications in DMD, refer to a recent review by Allen et al. (2016).

Among the various disease-causing mechanisms, changes in intracellular calcium (Ca_i^{2+}) levels in dystrophin-deficient muscle fibers have been studied for many years. An increase in both Ca^{2+} influx and cytosolic Ca^{2+} concentration has been reported in *mdx* myofibers (Turner et al., 1988; Hopf et al., 1996). Although many studies have shown higher levels of Ca^{2+} content in the muscle fibers from *mdx* mice, others have reported no significant rise in Ca^{2+} concentration (Gillis, 1996, 1999; Gailly, 2002; Whitehead et al., 2006). Dystrophin is indispensable for maintaining the structural integrity of the striated muscle cell (Petrof et al., 1993). Thus, lack of dystrophin destabilizes sarcolemma integrity, making the sarcolemma more susceptible to contraction-induced damage. This leads to myonecrosis (necrosis of myofibers), which in turn stimulates fiber regeneration. In *mdx* mice, the onset of myonecrosis starts at 2 weeks of age. Myonecrosis peaks between 3 and 4 weeks of age and is significantly decreased and stabilized by 6 to 8 weeks of age. Eventually, ∼80% of myofibers in adult *mdx* mice are regenerated fibers (Grounds et al., 2008). A sharp increase in total Ca^{2+} content has been shown at the peak of myonecrosis. The total Ca^{2+} content returns to normal level in later stages (Reeve et al., 1997). Studies from Head's laboratory suggest that regenerated fibers display branched morphology. It has been hypothesized that myofiber branching rather than dystrophin deficiency increases muscle susceptibility to damage (Head, 2010; Chan and Head, 2011). These studies further suggest that the branching of fibers resulted in altered ion channel function and excessive Ca^{2+} influx, which further exacerbates muscle damage. Muscle damage and degeneration are therefore suggested to play an important role in stress-induced membrane tears and dysfunction of sarcolemmal ion channels that lead to abnormal Ca^{2+} influx from the extracellular matrix (ECM) to the cytosol (Turner et al., 1988, 1991; Moens et al., 1993; Alderton and Steinhardt, 2000; Burr and Molkentin, 2015). In addition, there is a defect in Ca^{2+} cycling between the cytosol and the sarcoplasmic reticulum (SR)/endoplasmic reticulum (ER), a major internal Ca^{2+} store in striated muscles. These changes result in a chronic accumulation of Ca^{2+} in the cytoplasm. Thus, the lack of dystrophin results in muscle degeneration and improper regeneration, which may contribute to abnormal Ca_i^{2+} handling.

Several lines of evidence suggest that sustained elevation of cytosolic Ca^{2+} levels underlies muscle pathology and dysfunction in DMD. First, increased cytosolic Ca^{2+} levels enhance the expression and activity of calpains, the Ca^{2+} dependent proteases in dystrophic muscles (Spencer et al., 1995; Hussain et al., 2000; Shanmuga Sundaram et al., 2006; Voit et al., 2017). Calpain activation results in proteolytic damage to cellular proteins and the myofibrillar network (Dayton et al., 1976; MacLennan et al., 1991; Bartoli and Richard, 2005). In support of this notion, treatment with BN 82270, a membrane-permeable calpain inhibitor, improves muscle function in *mdx* mice (Burdi et al., 2006). Studies from our laboratory have shown normalization of Ca_i^{2+} cycling by improving SR Ca^{2+} ATPase (SERCA) activity decreases calpain activity and improves muscle function in dystrophin and utrophin double-mutant (*mdx:utr*$^{-/-}$) mice (Voit et al., 2017). In addition to calpains, increased cytosolic Ca^{2+} levels also activate phospholipase A, which digests cellular membranes such as the sarcolemma (Lindahl et al., 1995). Second, the sustained elevation of Ca_i^{2+} concentration activates apoptotic and necrotic cell death pathways in DMD (Tidball et al., 1995; Morgan et al., 2018). Third, abnormal Ca_i^{2+} concentration may influence muscle differentiation and compromise muscle regeneration. In this regard, we have recently demonstrated improving Ca_i^{2+} cycling in dystrophic myoblasts improves myoblast fusion and differentiation (Niranjan et al., 2019). Fourth, rapid change in free Ca^{2+} levels in the cytoplasm is essential for proper initiation of muscle contraction and relaxation (Calderon et al., 2014). Thus, chronic accumulation of Ca^{2+} in the cytosol can affect muscle function in DMD. Fifth, cytoplasmic Ca^{2+} levels influence mitochondrial Ca^{2+} uptake, which in turn leads to altered metabolism and increased production of ROS. The failure to mitigate supraphysiological levels of oxygen radicals results in the loss of membrane potential and cell death (Feno et al., 2019). Collectively, abnormal Ca_i^{2+} cycling plays a pivotal role in DMD pathogenesis, and restoration of Ca_i^{2+} homeostasis may ameliorate muscle disease and cardiomyopathy in DMD. A better understanding of the molecular mechanisms underlying abnormal Ca_i^{2+} cycling will aid in identifying novel therapeutic targets for DMD. Below, we review Ca^{2+} handling in normal muscle and how changes at the sarcolemma, SR, and mitochondria cause Ca^{2+} dysregulation in DMD. We also highlight the current studies on improving SERCA function as a strategy to mitigate skeletal muscle disease and cardiomyopathy in DMD.

CALCIUM HANDLING IN NORMAL MUSCLE

Contraction and relaxation cycles are controlled voluntarily in skeletal muscle and involuntarily in cardiac muscle and are tied with Ca^{2+} cycling between the SR and cytoplasm. Ca^{2+} cycling in normal muscle is depicted in **Figure 1**. In muscles, extracellular Ca^{2+} concentrations are ∼2–4 mM, and resting cytosolic concentrations are ∼50–250 nM. SR Ca^{2+} concentrations are ∼0.4–0.5 mM (MacLennan and Kranias, 2003; Gehlert et al., 2015; Kuo and Ehrlich, 2015). In the heart, the resting diastolic Ca^{2+} levels are ∼100 nM and during systole, cytosolic Ca^{2+} levels increase to ∼1 μM (MacLennan and Kranias, 2003). Excitation and contraction (EC) coupling in skeletal and cardiac muscles

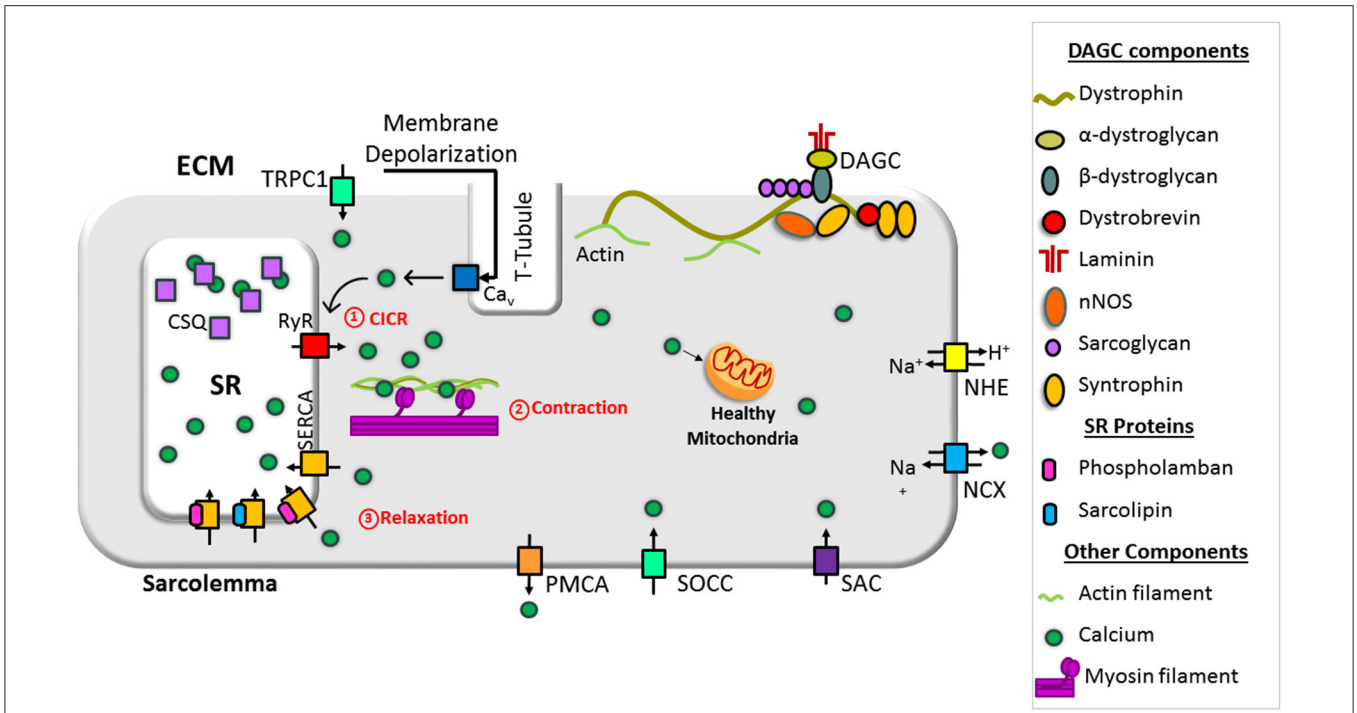

FIGURE 1 | Schematic representation of intracellular Ca^{2+} cycling in a normal muscle cell. Dystrophin stabilizes muscle cells by linking the cytoskeleton (F-actin, intermediate filaments, microtubule) to the extracellular matrix via the dystrophin-associated glycoprotein complex (DAGC). Ca^{2+}-induced Ca^{2+} release (CICR) occurs through activation of voltage-gated, L-type Ca^{2+} channels (Ca_v) and the release of Ca^{2+} from the sarcoplasmic/endoplasmic reticulum (SR) via ryanodine receptor (RyR). CICR activates muscle contraction. Resequestration of Ca^{2+} back into the SR by SR Ca^{2+} ATPase (SERCA) initiates muscle relaxation. The physiological intracellular Ca^{2+} level regulates mitochondrial Ca^{2+} content and function and maintains cellular energetics. DG, dystroglycan; NCX, sodium–calcium exchanger; NHE, sodium–proton exchanger; PMCA, plasma membrane Ca^{2+} ATPase; SAC, stretch-activated channels; SOCC, store-operated Ca^{2+} channel; TRPC1, transient receptor potential channel 1.

shares many similarities. In both muscles, the action potential activates voltage-gated, L-type Ca^{2+} channels ($Ca_v1.1$ in skeletal muscles and $Ca_v1.2$ in cardiac muscle) in the sarcolemma, which promotes Ca^{2+} release from the SR via the ryanodine receptor (RyR1 in skeletal muscles and RyR2 in cardiac muscle). This process is known as Ca^{2+}-induced Ca^{2+} release (CICR) (MacLennan and Kranias, 2003; Rios, 2018). Although CICR was first discovered in skeletal muscle, it does not play a major role in skeletal muscle contraction (Lamb, 2000; Endo, 2009; Rios, 2018). In cardiac muscle, the interaction between $Ca_v1.2$ and RyR2 depends on CICR, whereas in skeletal muscle, $Ca_v1.1$ and RyR1 physically interact. This interaction is independent of the Ca^{2+} influx via $Ca_v1.1$ (Protasi, 2002; Franzini-Armstrong, 2018). It also activates the opening of RyR1 in response to $Ca_v1.1$ voltage sensor activation, a process known as Ca^{2+}-independent, depolarization-induced Ca^{2+} release (also called voltage-induced Ca^{2+} release) (Rios, 2018). The mechanism by which these two channels interact is not fully understood. A recent study shows junctophilins (protein localized in junctional SR) enable the $Ca_v1.1$ to efficiently couple with RyRs through protein–protein interaction. This mechanism is considered crucial for efficient EC coupling in adult skeletal muscles (Nakada et al., 2018). Studies have also shown the importance of store-operated Ca^{2+} entry independent of $Ca_v1.1$ in the regulation of skeletal muscle contraction (Avila-Medina et al., 2018). Store-operated Ca^{2+} entry machinery located in the triad of skeletal muscle contains many proteins including stromal interaction molecule 1 (STIM1), Orai, transient receptor potential canonical (TRPC) channel, and RyRs. These proteins are involved in Ca^{2+} store restoration during the intense work of skeletal muscles (Pan et al., 2014; Avila-Medina et al., 2018).

Both in skeletal and cardiac muscles, Ca^{2+} released from the SR binds to troponin C, a thin filament sarcomeric protein, and initiates muscle contraction. Muscle relaxation is initiated by Ca^{2+} removal from the cytoplasm. Approximately 70–90% of Ca^{2+} is removed by SERCA (SERCA1 and SERCA2a in skeletal muscle and SERCA2a in cardiac muscle) and resequestrated into the lumen of the SR. Most of the remaining Ca^{2+} is extruded out of the cell via sarcolemmal Ca^{2+} transport proteins. These include the sodium (Na^+)–Ca^{2+} exchanger (NCX) and plasma membrane Ca^{2+} ATPase. A small amount of Ca^{2+} is taken up by the mitochondria via the mitochondrial uniporter (MCU). Thus, SR Ca^{2+} cycling is not only important for muscle contraction and relaxation cycle but also helps to maintain cytosolic Ca^{2+} levels. For extensive reviews on Ca^{2+} handling in normal skeletal muscle and heart, refer to the recent reviews (Endo, 2009; Lee, 2010; Eisner et al., 2017; Avila et al., 2019).

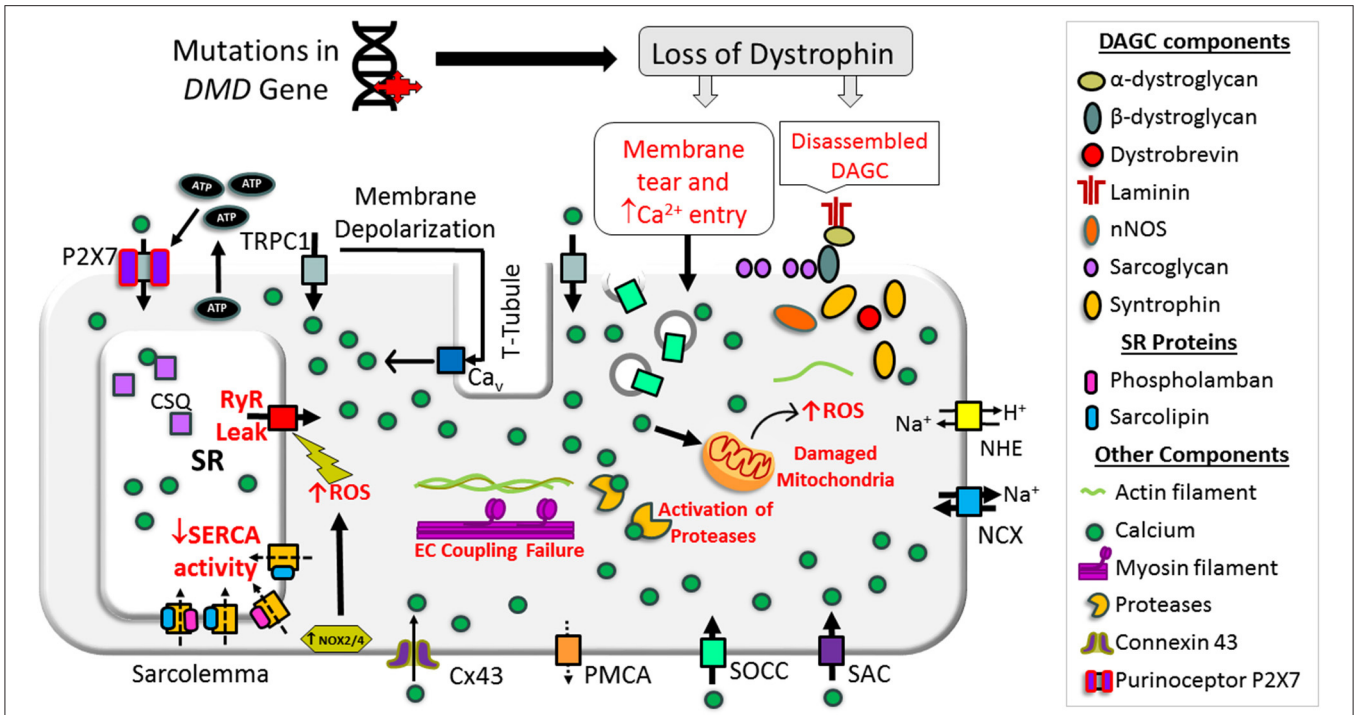

FIGURE 2 | Schematic representation of mechanisms causing Ca_i^{2+} overload in a dystrophin-deficient muscle cell. Loss of dystrophin causes destabilization of dystrophin-associated glycoprotein complex (DAGC), membrane tear, and activation of store-operated calcium channels (SOCCs), resulting in abnormal Ca^{2+} entry. High concentrations of extracellular ATP can activate abnormal Ca^{2+} influx via P2X7. RyR dysfunction causes Ca^{2+} leak from the SR and SERCA dysfunction compromises Ca^{2+} resequestration. NOX activation can also increase RyR Ca^{2+} leak. These changes result in abnormal and chronic elevation of the cytoplasmic Ca^{2+} levels. Supraphysiological level Ca^{2+} activates Ca^{2+}-dependent proteases and phospholipase and causes muscle necrosis and replacement of muscle by fatty and fibrotic tissues. Sustained elevation of cytoplasmic Ca^{2+} levels also affects mitochondrial function and increases reactive oxygen species (ROS). Collectively, these changes lead to muscle wasting and contractile dysfunction. Bold and broken arrows indicate the enhanced and decreased function of the Ca^{2+} channels, respectively. Cx43, connexin 43; NCX, sodium–calcium exchanger; NHE, sodium–proton exchanger; NOX, NADPH oxidases; PMCA, plasma membrane Ca^{2+} ATPase; P2X7, P2X purinoceptor 7; SAC, stretch-activated channels; SOCC, store-operated Ca^{2+} channel; TRPC1, transient receptor potential channel 1.

SARCOLEMMAL CONTRIBUTION TO ABNORMAL Ca_i^{2+} HANDLING IN DYSTROPHIC MUSCLES

In dystrophin-deficient muscle, the function of sarcolemmal Ca^{2+} channels is altered and contributes to the abnormal elevation of cytoplasmic Ca^{2+} concentration. Schematic representation of abnormal Ca^{2+} handling via the sarcolemma in dystrophin-deficient muscle is shown in **Figure 2**.

Ca^{2+} Entry Through Membrane Tearing

A primary function of dystrophin is to link the cytoskeleton with the ECM through direct or indirect interaction with the proteins in the dystrophin-associated glycoprotein complex (DAGC) and direct interaction with actin microfilaments, intermediate filaments, and microtubules (Koenig et al., 1988; Ervasti and Campbell, 1993; Petrof et al., 1993; Chakkalakal et al., 2005; Gao and McNally, 2015). The absence of dystrophin disrupts the DAGC and makes the sarcolemma more susceptible to microtears during mechanical stress (Petrof et al., 1993; Danialou et al., 2001). Increased sarcolemmal membrane permeability is an early feature of patients affected by DMD, allowing cytosolic contents such as creatine kinase to exit skeletal muscle fibers and ions such as Ca^{2+} to enter. On the other hand, in *mdx* mice, blocking NADPH oxidase 2 (NOX2), the main ROS producer, saves muscle from force loss following eccentric contraction (Olthoff et al., 2018). Similarly, *mdx* muscle fibers repair their sarcolemma just as efficiently as wild-type fibers following laser-induced focal damage, suggesting membrane tears of this kind are sealed promptly (Cooper and Head, 2015). Thus, it is now believed that membrane tear is not a primary pathway for Ca^{2+} entry in DMD (Yeung et al., 2005; Allen and Whitehead, 2011; Cooper and Head, 2015; Olthoff et al., 2018).

Ca^{2+} Entry Through Membrane Repair

Calcium signaling plays an important role in sarcolemma repair (Andrews et al., 2014; Cooper and Head, 2015). Increased cytosolic Ca^{2+} levels trigger Ca^{2+}-dependent repair mechanisms in which exocytic vesicles patch sarcolemmal tears. This may result in increased activity of Ca^{2+} leak channels because an antagonist of these channels reduced the higher levels of hydrolysis in dystrophic myotubes to nearly normal levels (Alderton and Steinhardt, 2000). Recent studies have demonstrated the involvement of transient receptor potential

mucolipin 1 (TRPML1), a lysosomal Ca^{2+} release channel needed for lysosomal exocytosis in membrane repair in DMD (Cheng et al., 2014; Yu et al., 2020). In mice, genetic ablation of TRPML1 resulted in DMD-like phenotype with an impairment in the membrane sealing in skeletal muscles (Cheng et al., 2014). On the other hand, transgenic overexpression or pharmacological activation of TRPML1 *in vivo* facilitates sarcolemma repair and alleviates dystrophic phenotypes in both skeletal and cardiac muscles of *mdx* mice (Yu et al., 2020). These studies further show that TRPML1 activation increased lysosomal biogenesis by activating the transcription factor EB and thereby facilitated sarcolemma repair to reduce muscle damage in *mdx* mice (Yu et al., 2020). Therefore, targeting lysosomal Ca^{2+} channels may represent a promising approach to treat DMD and related muscle diseases.

Ca^{2+} Entry Through Store-Operated Calcium Channels

Store-operated calcium channels (SOCCs) are Ca^{2+} channels residing at the sarcolemma that open in response to decreased SR Ca^{2+} concentrations. The activity of SOCCs is enhanced in dystrophic muscle cells, which further contributes to the abnormal elevation of Ca_i^{2+} levels in dystrophic muscles [40]. Two proteins have been identified as necessary players involved in SOCE: STIM, an ER-located Ca^{2+} sensor, and Orai, a highly Ca^{2+} selective ion channel protein in the plasma membrane (Derler et al., 2016). In dystrophin-deficient myoblasts and muscle fibers, the expression of SOCC proteins is increased (Edwards et al., 2010; Andrews et al., 2014). Interestingly, SOCCs can also be activated through a Ca^{2+}-independent pathway. Specifically, Ca^{2+}-independent phospholipase A_2 ($iPLA_2$) acts as an intracellular messenger and triggers Ca^{2+} entry through SOCCs (Smani et al., 2003). An elevation in $iPLA_2$ levels observed in dystrophic muscles (Smani et al., 2003, 2004; Boittin et al., 2010) supports the activation of this pathway.

Ca^{2+} Entry Through the Transient Receptor Potential Canonical Channels

TRPCs are a family of plasma membrane cation channels opened by Ca^{2+} store depletion and/or membrane stretch. In dystrophin-deficient muscles, evidence shows Ca^{2+} enters via eccentric contraction-activated stretch channels (Yeung et al., 2005). Several lines of evidence suggest the opening of TRPCs could be the main contributor of Ca^{2+} entry through the plasma membrane. To start, overexpression of TRPC1, TRPC3, and TRPC6 has been observed in *mdx* muscle (Vandebrouck et al., 2007; Gervasio et al., 2008; Boittin et al., 2010; Matsumura et al., 2011; Miyatake et al., 2016). The most widely studied of these is TRPC1. In the *mdx* muscle, TRPC1 forms a Ca^{2+} influx pathway with tyrosine–protein kinase Src and caveolin-3 (Gervasio et al., 2008). TRPC1 also interacts with dystrophin and α1-syntrophin, a member of the DAGC. In one model for TRPC1 regulation, the DAGC serves as a scaffold for signaling molecules involved in the regulation of channels formed by TRPC1 and other TRPC isoforms (Sabourin et al., 2009). In the absence of dystrophin, this regulation is lost, and SOCE is increased (Vandebrouck et al., 2007). Matsumura et al. (2011) showed that the expression levels of TRPC1 correlated with the severity of muscle disease in *mdx* mice.

In addition to canonical TRPCs, the transient receptor potential vanilloid type 2 (TRPV2) channel may also play a role in increased Ca^{2+} levels. Typically, TRPV2 is localized on intracellular organelles. In dystrophin-deficient muscle, however, it translocates to the plasma membrane (Iwata et al., 2003, 2009).

Contribution of Sodium Regulators in Ca_i^{2+} Levels in DMD

In dystrophic muscle, intracellular Na^+ levels are increased via the opening of voltage-gated Na^+ channels (Nav1.4) (Hirn et al., 2008), Na^+/H^+ exchangers (NHE) type I (Iwata et al., 2007; Burr et al., 2014), and gadolinium sensitive-stretch channels (Yeung et al., 2003). In healthy muscle, the NCX removes excess Ca^{2+} from the cytosol in exchange for Na^+. However, in the presence of excessive cytosolic Na^+ (as in dystrophic muscle), NCX functions in a reverse mode to remove Na^+ from the cell. In doing so, NCX moves Ca^{2+} into the cell. Interestingly, it has been shown that increased SR Ca^{2+} release in dystrophic muscle can also trigger the NCX to work in a reverse mode and thereby increase Ca_i^{2+} concentrations (Deval et al., 2002).

Role of Voltage-Gated, L-Type Ca^{2+} Channels in Ca_i^{2+} Load

The activity of the cardiac L-type Ca^{2+} channel, $Ca_v1.2$, determines Ca^{2+} entry in the plateau phase (phase 2) of the action potential in cardiac myocytes. In *mdx* cardiac myocytes, $Ca_v1.2$ activation is significantly increased (Koenig et al., 2014). This leads to enhanced Ca^{2+} influx via $Ca_v1.2$ during the action potential. It is worth mentioning that enhanced $Ca_v1.2$ activities may disturb cardiac electrophysiology and thereby cause arrhythmias in DMD.

The role of $Ca_v1.1$ activity in abnormal Ca^{2+} entry in dystrophic skeletal muscle is not clear. In delta-sarcoglycan (a component of DAGC)–deficient dystrophic hamsters, the administration of diltiazem, the L-type Ca^{2+} antagonist, reduces muscle Ca^{2+} content (Bhattacharya et al., 1982). This suggests a possible pathological role played by L-type Ca^{2+} channels in dystrophic muscle. In contrast, Friedrich et al. found that $Ca_v1.1$ activity is significantly reduced in the fast-twitch muscles of *mdx* mice (Friedrich et al., 2004). These studies further suggest dystrophin, and the DAGC may regulate the interaction between L-type Ca^{2+} channels and RyR, which is necessary for EC coupling (Friedrich et al., 2004, 2008).

Other Ca^{2+} Entry Mechanisms in Dystrophin-Deficient Muscle

Dystrophic muscle damage triggers the release and elevation of extracellular ATP, which activates specific ionotropic purinoreceptors, P2X7, on immune cells and subsequently contributes to chronic inflammatory and immune responses (Gorecki, 2019). In addition, high concentrations of extracellular ATP have been shown to activate abnormal Ca^{2+} influx into dystrophic muscle cells (Young et al., 2018). This increase in

Ca_i^{2+} is shown to be associated with increased and prolonged activation of P2X7 purinoceptors that increase the sarcolemma permeability in dystrophic muscle cells (Young et al., 2012). Degrading extracellular ATP by apyrase reduced the Ca_i^{2+} levels in *mdx* fibers (Altamirano et al., 2013). Genetic and pharmacological targeting of P2X7 reduced inflammation and increased dystrophic muscle repair (Gorecki, 2019). Thus, targeting purinergic receptors can ameliorate the abnormal Ca^{2+} entry in dystrophic muscles.

Connexins (Cx) are gap junction proteins, which are important for many physiological processes including coordinated depolarization of muscle, and ion movement between muscle cells (Cea et al., 2012). Cx function as gap junction channels and hemichannels, which mediate intercellular and transmembrane signaling, respectively. Hemichannels can act as conduits for Na^+ and Ca^{2+} entry (Cea et al., 2012). In dystrophic muscles, Cx39, Cx43, and Cx45 are found to form functional hemichannels, which are absent in normal muscle fibers (Cea et al., 2016). The *mdx* mice deficient for Cx43/Cx45 expression in skeletal muscle show reduced basal Ca_i^{2+} level and necrotic phenotype (Cea et al., 2016). Cx43 levels are significantly increased and are mislocalized in the lateral sides of cardiomyocytes in mouse models of DMD (Gonzalez et al., 2018). Altered localization of Cx43 predisposed the DMD mice to cardiac arrhythmias (Gonzalez et al., 2018). A recent study shows that hypophosphorylation of Cx43 serine triplet triggers redistribution of Cx43 to the lateral sides of cardiomyocytes and contributes to the dystrophic cardiomyopathy in *mdx* mice (Himelman et al., 2020). The expression of phosphorylation mimic Cx43 in *mdx* cardiomyocytes shows improved Ca_i^{2+} signaling, a reduction of NOX2/ROS production and prevention of arrhythmias (Himelman et al., 2020). Taken together, these studies indicate that Cx overexpression and lateralization contribute to abnormal Ca_i^{2+} homeostasis in dystrophin-deficient cardiac and skeletal muscles.

ROLE OF THE SR IN ABNORMAL Ca_i^{2+} HANDLING IN DYSTROPHIC STRIATED MUSCLES

The SR is the major internal Ca^{2+} store in striated muscles and plays a pivotal role in the regulation of EC coupling by maintaining cytoplasmic Ca^{2+} concentrations during the muscle contraction and relaxation cycle (Santulli et al., 2017). Numerous studies suggest SR Ca^{2+} cycling is compromised in dystrophic muscle (Collet et al., 1999; Woods et al., 2004; Williams and Allen, 2007a; DiFranco et al., 2008; Capote et al., 2010) (**Figure 2**). Below, we review the mechanisms underlying SR Ca^{2+} cycling defects in dystrophin-deficient cardiac and skeletal muscles.

Role of RyR in Abnormal Elevation of Ca_i^{2+} Levels

Ca^{2+} release from the SR occurs via RyR, a macromolecular complex. There are three RyR isoforms reported in mammals. RyR1 is primarily expressed in skeletal muscles, RyR2 is expressed predominantly in the heart, and RyR3 is found in the brain and skeletal muscles (Conti et al., 1996; Lanner et al., 2010).

The role of the SR in cytosolic Ca^{2+} rise has been studied using chemically skinned muscle fibers that have not been mechanically stressed (Divet and Huchet-Cadiou, 2002). Studies on the skinned fibers isolated from extensor digitorum longus (EDL) and soleus muscles show that the SR Ca^{2+} release following exposure to caffeine is significantly slower in *mdx* mice. These studies suggest a more pronounced SR Ca^{2+} leak in EDL and soleus muscle fibers from *mdx* mice. Consistent with these findings, Robin et al. have shown increased passive SR Ca^{2+} leak in isolated intact myofibers prepared from FDB muscles of mdx5cv mice, an alternative dystrophin-deficient mouse model (Robin et al., 2012). On the contrary, Plant and Lynch have shown that the SR Ca^{2+} leak was unaltered in skinned *mdx* fibers (Plant and Lynch, 2003). However, peak caffeine-induced Ca^{2+} release was decreased in *mdx* fibers. In addition, all the above studies show no change in SR Ca^{2+} uptake in skinned fibers from *mdx* mice. The structural and functional defects in both cardiac and skeletal muscle RyRs have been reported in the *mdx* mouse model. Recent studies have shown that the SR Ca^{2+} release mechanism is impaired in both cardiac and skeletal muscles in DMD (Bellinger et al., 2009; Fauconnier et al., 2010). In skeletal muscle, it is believed that progressive S-nitrosylation of RyR1 and depletion of calstabin 1, a critical regulatory subunit of RyR macromolecular complex, are responsible for RyR1 Ca^{2+} leak (Bellinger et al., 2009). Similarly, S-nitrosylation and calstabin 2 depletion cause RyR2 Ca^{2+} leak and contribute to sudden cardiac arrhythmias in *mdx* mice (Fauconnier et al., 2010). In addition, RyR2 phosphorylation and oxidation have been linked to RyR2-mediated Ca^{2+} leak in the *mdx* heart. These studies further show that genetic inhibition of RyR2 phosphorylation at S2808 or S2814 can reduce RyR2 oxidation, suggesting a potential interaction between these posttranslational pathways (Williams and Allen, 2007b; Shannon, 2009; Prosser et al., 2011; Wang et al., 2015).

Role of SERCA and Its Regulators

SERCA plays a key role in resequestering Ca^{2+} into the SR lumen during muscle relaxation. SERCA1 is expressed in fast-twitch skeletal muscles. SERCA2a is predominantly expressed in the heart and also found in slow-twitch muscles. SERCA3 is predominantly expressed in non-muscle tissues (Periasamy and Kalyanasundaram, 2007). In striated muscles, SERCA activity accounts for 70–90% of cytosolic Ca^{2+} removal (Periasamy and Kalyanasundaram, 2007).

It is now clear that the SERCA function is impaired in dystrophic muscles. SERCA activity can be reduced through several mechanisms, including (i) down-regulation of SERCA expression, (ii) posttranslational modification of SERCA protein, and (iii) differential expression and function of SERCA regulators. In the dystrophic myocardium of mouse models and human patients, SERCA2a levels remain unchanged (Voit et al., 2017; Wasala et al., 2020). In the *mdx* mouse, SERCA1a expression is increased in the spared intrinsic laryngeal and toe muscles but is reduced in the EDL muscle (Dowling et al., 2003; Ferretti et al., 2009). In the fast-twitch muscles of *mdx*

and *mdx:utr*$^{-/-}$ mice, SERCA2a expression is significantly increased, likely due to the increased number of slow-twitch fibers (Schneider et al., 2013; Voit et al., 2017). In the extensor carpi ulnaris muscles of the canine DMD model, SERCA2a levels are decreased while SERCA1 expression is unaltered (Voit et al., 2017). These findings suggest differential expression of SERCA isoforms in different dystrophic muscles. Given the different kinetic properties of SERCA1 and SERCA2a, it is likely the muscle- and species-specific changes in SERCA isoform expression represent compensatory alterations in different dystrophic muscles.

Irrespective of SERCA levels, SR Ca^{2+} uptake is significantly reduced in dystrophin-deficient cardiac and skeletal muscles, indicating decreased SERCA function (Schneider et al., 2013; Voit et al., 2017; Wasala et al., 2020; Mareedu et al., 2021). Oxidative posttranslational modification has been shown to play an important role in SERCA activity in non-dystrophic heart diseases (Lancel et al., 2010; Horakova et al., 2013). As dystrophic muscle undergoes oxidative stress (Kim et al., 2013), it is likely that similar posttranslational modifications can also affect SERCA function in DMD.

SERCA function is modulated by several small-molecular-weight membrane proteins including phospholamban (PLN), sarcolipin (SLN), myoregulin (MLN), and dwarf open reading frame (DWORF) (Bhupathy et al., 2007; Anderson et al., 2015; Nelson et al., 2016; Shaikh et al., 2016). PLN, SLN, and MLN are negative regulators, whereas DWORF is a positive regulator of SERCA. PLN is highly expressed in the ventricles (Babu et al., 2007). SLN is expressed in all skeletal muscle tissues in larger mammals; however, its expression is restricted to slow-twitch muscles in rodents (Babu et al., 2007). Whereas, in the hearts of both rodents and large mammals SLN is primarily expressed in atria and expressed at a low level in ventricles (Babu et al., 2007), MLN is primarily expressed in skeletal muscles (Anderson et al., 2015). DWORF is a positive regulator of SERCA and is predominantly expressed in the heart and slow-twitch muscles (Nelson et al., 2016). In addition to these peptides, recent studies suggest that small ubiquitin-like modifier type 1 (SUMO-1) also plays a critical role in cardiac SERCA dysfunction in the setting of heart failure (Kho et al., 2015).

The PLN levels are unaltered in dystrophic skeletal and cardiac muscles, whereas SLN is significantly up-regulated in the skeletal muscles and the ventricles of mouse and dog models and DMD patients (Voit et al., 2017). Little is known about the expression of MLN, DWORF, and SUMO-1 in dystrophin-deficient cardiac and skeletal muscles. It is worth pointing out that complete elimination of PLN exacerbates *mdx* cardiomyopathy (Law et al., 2018), whereas partial or complete elimination of SLN significantly reduces skeletal muscle disease and cardiomyopathy in mouse models of DMD (Voit et al., 2017; Mareedu et al., 2021).

Role of Other SR Ca^{2+} Handling Proteins

The SR luminal resident proteins, including calsequestrin (CSQ), CSQ-like proteins (CLPs), histidine-rich Ca^{2+}-binding protein (HRCBP), calreticulin, and sarcalumenin (SLM), play an important role in buffering luminal Ca^{2+} concentrations and regulating SR Ca^{2+} uptake and release (Beard et al., 2004; Arvanitis et al., 2011; Jiao et al., 2012). Among the various SR luminal proteins, CSQ is the major Ca^{2+}-buffering protein. It is localized within the terminal cisternae of the SR in both cardiac and skeletal muscles. CSQ exists in two isoforms. CSQ1 is mainly expressed in skeletal muscles, whereas CSQ2 is expressed in cardiac and slow-twitch muscle (Murphy et al., 2009).

Increased levels of CSQ and calmodulin (CaM) have been reported in spared extraocular and intrinsic laryngeal muscles of *mdx* mice, whereas these proteins are at low levels in the diaphragm of *mdx* mice (Pertille et al., 2010). The same study also reported that CSQ level was significantly reduced in the soleus and sternomastoid muscles but unaltered in the tibialis anterior (TA) muscles, whereas CaM level decreased only in the TA muscle (Pertille et al., 2010). Collectively, the fiber-type composition of dystrophic and spared muscles in *mdx* mice could contribute to the altered levels of CSQ. There is a discrepancy in the protein levels of cardiac CSQ2 in the dystrophic myocardium. It has been shown that the levels of CSQ2 were drastically reduced in the heart of *mdx* mice (Lohan and Ohlendieck, 2004). However, we and others have shown that CSQ2 levels are unaltered in the hearts of *mdx* and *mdx:utr*$^{-/-}$ mice (Pertille et al., 2010; Voit et al., 2017; Mareedu et al., 2021). Surprisingly, CSQ2 expression is aberrantly increased in the fast-twitch muscles of *mdx* and *mdx:utr*$^{-/-}$ mice (Schneider et al., 2013; Voit et al., 2017). The exact reason for the increase of CSQ2 is not known but may likely be due to the fast- to slow-muscle fiber type switch in mouse models of DMD. The CLPs are significantly reduced in *mdx* skeletal muscle (Culligan et al., 2002). The expression of HRCBP is increased in the *mdx* heart (Lohan and Ohlendieck, 2004). The SLM expression is reduced in both skeletal and cardiac muscles in *mdx* mice (Lohan and Ohlendieck, 2004). Overall, changes in the SR luminal Ca^{2+}-binding proteins support the concept of abnormal Ca_i^{2+} cycling in dystrophic muscles. The differences in the expression levels of these proteins could reflect the severity of the muscle pathology, which varies between disease-free extraocular muscle, slow- and fast-twitch skeletal muscles, and cardiac muscles.

CALCIUM HANDLING IN DYSTROPHIN-DEFICIENT SMOOTH MUSCLES

Although the role of Ca^{2+} dysregulation has been extensively studied in dystrophin-deficient cardiac and skeletal muscle tissues, the implications of dystrophin deficiency in smooth muscles in DMD patients or animal models have not been adequately studied. Studies on the gastric and intestinal smooth muscles of *mdx* mice have shown impaired muscle relaxation, which has been attributed to impairment in Ca_i^{2+} homeostasis (Mule et al., 1999; Mule and Serio, 2001). These studies show that in dystrophic colonic muscle, increased Ca^{2+} influx through L-type voltage-dependent channels is responsible for the sustained mechanical tone. A recent study showed that the enhanced stretch-induced Ca_i^{2+} concentration in the vascular smooth muscle cells of *mdx* mice occurs through the activation of TRPC1, TRPC3, and TRPC6 channels (Lopez et al., 2020). Thus, focusing

on the Ca^{2+} handling in dystrophic smooth muscle cells may have therapeutic implications.

MITOCHONDRIA AND ABNORMAL Ca_i^{2+} HANDLING IN DMD

Mitochondria not only play a vital role in muscle bioenergetics but also contribute to Ca^{2+} homeostasis in striated muscles. Mitochondria store Ca^{2+} transiently (~10 nmol/mg of mitochondrial protein) (Finkel et al., 2015). Ca^{2+} levels in the mitochondria are an important determinant of mitochondrial function and cell survival (Williams et al., 2013; Finkel et al., 2015). When cytoplasmic Ca^{2+} levels are elevated, mitochondrial Ca^{2+} uptake is enhanced (Robert et al., 2001) as a compensatory mechanism to normalize the cytoplasmic Ca^{2+} concentration. Ca^{2+} uptake by mitochondria mainly occurs via the mitochondrial Ca^{2+} uniporter (MCU), whereas Ca^{2+} extrusion occurs through the mitochondrial Na^{+}-Ca^{2+}-Li^{+} exchanger (mtNCLX) (Pathak and Trebak, 2018). During conditions such as mitochondrial Ca^{2+} overload and mitochondrial dysfunction, the mitochondrial permeability transition pore (mPTP), a large channel in the inner mitochondrial membrane, also contributes to Ca^{2+} extrusion (Kwong and Molkentin, 2015). Here, we discuss the interplay between abnormal cytosolic and mitochondrial Ca^{2+} cycling and muscle pathogenesis in DMD (**Figure 3**).

Ca_i^{2+} Overload Contributes to Defective Mitochondrial Dynamics in DMD

Mitochondrial morphology change is a salient feature of dystrophic muscle. Specifically, the mitochondrial size is markedly reduced, the electron density is decreased, and the cristae become more sparse in dystrophic muscle (Pant et al., 2015; Kang et al., 2018; Moore et al., 2020). These changes are caused by increased mitochondrial fission and fusion cycles, referred to as mitochondrial dynamics, in dystrophic skeletal muscles (Pant et al., 2015). In the *mdx* heart, there is substantial structural damage to mitochondria and a significant reduction in ATP production. These changes are associated with decreased mitochondrial autophagy (mitophagy) due to decreased expression of proteins involved in the PINK1/PARKIN mitophagy pathway (Kang et al., 2018). These studies indicate

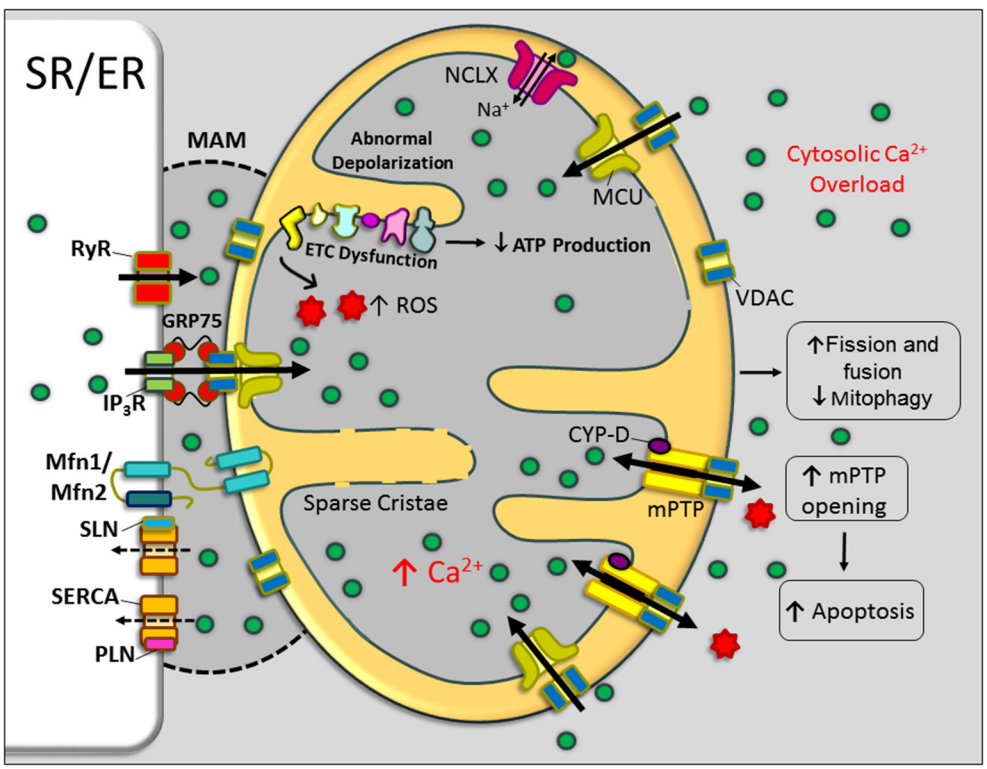

FIGURE 3 | Mitochondrial dysfunction in DMD. Schematic representation of mitochondrial structural and functional alterations in dystrophin-deficient cardiac/skeletal muscle cells. An abnormal elevation of Ca^{2+} in the cytoplasm and mitochondria-associated membrane (MAM) region resulted in increased mitochondrial Ca^{2+} uptake and enhanced activation of mitochondrial permeability transition pore (mPTP) opening. These changes impair mitochondrial function and mitochondrial dynamics and contributing to the metabolic crisis. Currently, there is no experimental evidence for the role of the MAM region and mitochondrial Ca^{2+} uniporter (MCU) in the mitochondrial Ca^{2+} overload in DMD. Bold and broken arrows indicate the enhanced and decreased function of the Ca^{2+} channels, respectively. ER, endoplasmic reticulum; ETC, electron transport chain; GRP75, glucose-regulated protein 75; IP3R, inositol trisphosphate receptor; MFN, mitofusin; NCLX, Na^{+}-Ca^{2+}-Li^{+} exchanger; PLN, phospholamban; ROS, reactive oxygen species; RyR, ryanodine receptor; SERCA, sarcoplasmic/endoplasmic reticulum Ca^{2+} ATPase; SLN, sarcolipin; SR, sarcoplasmic reticulum; VDAC, voltage-dependent anion channel.

that increased mitochondrial dynamics and decreased mitophagy could contribute to mitochondrial dysfunction and disease pathogenesis. It is important to note that mitochondrial abnormalities are reported in the *mdx* heart. These changes are associated with mitochondrial Ca^{2+} load and are preceded by cytosolic Ca^{2+} overload (Jung et al., 2008; Viola et al., 2013; Kyrychenko et al., 2015b). In support of this notion, our recent studies demonstrated that normalizing the Ca_i^{2+} cycling improved the mitochondrial fission and fusion cycles in dystrophic myoblasts (Niranjan et al., 2019).

Abnormal Mitochondrial Ca^{2+} Cycling, Mitochondrial Dysfunction, and Muscle Pathogenesis

Several studies have shown that mitochondria are potential targets of impaired Ca^{2+} homeostasis in muscular dystrophy. Increased mitochondrial Ca^{2+} content, impaired oxidative phosphorylation, increased ROS generation, decreased ATP production, aberrant mPTP opening, and abnormal mitochondrial depolarization have all been reported in cardiac and skeletal muscles of mouse models of DMD (Kuznetsov et al., 1998; Jung et al., 2008; Rybalka et al., 2014; Kyrychenko et al., 2015b; Kang et al., 2018). Similar to animal models, decreased oxidative phosphorylation has been reported in DMD patients (Sperl et al., 1997). Thus, cytosolic Ca^{2+} overload appears to directly contribute to mitochondrial dysfunction. In addition, mitochondrial dysfunction resulted in decreased ATP production, loss of membrane potential, and mPTP opening, which may further aggravate cytosolic Ca^{2+} overload in DMD muscle. In support of this, a recent study using the *Caenorhabditis elegans* as a model system showed that muscle damage in DMD could be a result of mitochondrial dysfunction, leading to cytoplasmic Ca^{2+} overload, which in turn activates various matrix metalloproteinase–mediated collagen degradation (Sudevan et al., 2019). Mitochondrial Ca^{2+} levels are elevated in aged dystrophic cardiomyocytes and are associated with the excessive opening of mPTP and loss of mitochondrial membrane potential (Kyrychenko et al., 2015b). Studies from Molkentin's laboratory have suggested that altered Ca^{2+} handling within the dystrophic muscle cells initiates cell necrosis, in part through the triggering of mPTP opening (Millay et al., 2008). These studies further showed treatment with the cyclophilin inhibitor Debio-025, which inhibits mPTP opening reduced mitochondrial swelling and necrosis in *mdx* mice (Millay et al., 2008). These studies suggest that inhibition of mPTP opening could be beneficial in DMD.

Role of SR–Mitochondria Communication in Ca^{2+} Dysregulation in DMD

Emerging studies have revealed the presence of close contact between the ER and mitochondria called mitochondria-associated membranes (MAMs) (**Figure 3**). MAMs are specialized subdomains of the ER/SR and outer mitochondrial membrane (Garcia-Perez et al., 2011; Patergnani et al., 2011; Csordas et al., 2018). MAMs are critical for correct communication between the ER and mitochondria, particularly, the selective transmission of physiological and pathological Ca^{2+} signals from the ER to mitochondria (Patergnani et al., 2011). MAMs are enriched with voltage-dependent anion channels (VDACs), outer mitochondrial membrane proteins that aid in Ca^{2+} entry close to the junctional SR. In addition to VDAC, glucose-regulated protein 75 (molecular chaperone present on the ER membrane), mitofusin 2 (MFN2), and MFN1 are also involved in the physical interactions between ER/SR and mitochondria (Szabadkai et al., 2006; de Brito and Scorrano, 2008). MAMs also contain proteins involved in ER-associated lipid metabolism, Ca^{2+}-handling proteins, and mitochondrial fission and fusion proteins (Szabadkai et al., 2006; de Brito and Scorrano, 2008; Flis and Daum, 2013; Vance, 2015).

The tight tether between ER/SR and mitochondrial membranes allows Ca^{2+} to be rapidly transferred. This design overcomes the low apparent Ca^{2+} affinity ($K_d \sim 15$–20 M) of the MCU (Rizzuto et al., 1998; Filippin et al., 2003). Many ER/SR-associated Ca^{2+}-handling proteins, such as SERCA, inositol 1,4,5-trisphosphate receptor type 2 (IP3R2), RyR2, SERCA2, CSQ, and PLN, have been found enriched at MAMs, supporting the close correlation between this organellar intersection and Ca^{2+} regulation (Simpson and Russell, 1997; Simpson et al., 1997; Garcia-Perez et al., 2008; Patergnani et al., 2011; Chen et al., 2012; Raturi and Simmen, 2013). A recent study shows that pharmacological blockade or down-regulation of IP3R expression can restore mitochondrial Ca^{2+} levels, mitochondrial membrane potential, mitochondrial dynamics, and mitophagy in *mdx* muscles (Valladares et al., 2018). Another study showed that incubation of Sol8 myotubes expressing mini-dystrophin in cyclosporine A (CsA) normalized IP3R expression levels and aided in better cell survival (Mondin et al., 2009). These studies suggest that IP3R-associated Ca^{2+} dysregulation in the MAM region affects mitochondrial Ca^{2+} content and mitochondrial function in DMD. These findings lead to the speculation that altered expression levels of RyR, IP3R, and SERCA isoforms and their regulators in the MAM region could deeply affect the Ca_i^{2+} signaling in this microdomain and thereby the cell metabolism and cell survival in DMD (**Figure 3**). A more detailed examination of MAM proteins in dystrophic muscle is needed to understand the mechanisms associated with Ca^{2+} mishandling in this microdomain and its contribution to DMD pathogenesis.

In summary, elevated cytoplasmic Ca^{2+} levels including increased Ca^{2+} levels in the MAM region increase mitochondrial Ca^{2+} load, which affects the mitochondrial structure, function, and mPTP opening. This further exacerbates cytosolic Ca^{2+} overload and subsequently contributes to DMD pathogenesis.

Calcium, NOX, and ROS

Increasing evidence suggests functional crosstalk between Ca^{2+} and ROS signaling systems. ROS are generated both in cytosol and mitochondria by NOX and electron complex chain, respectively (Gorlach et al., 2015). ROS produced by NOX5 has been implicated in cardiovascular diseases, renal diseases, and cancer (Touyz et al., 2019). However, studies on the role of NOX isoforms in DMD are limited. In *mdx* mice, NOX2 was shown to be induced in skeletal muscle, whereas NOX4 was induced in the heart (Spurney et al., 2008). Nifedipine treatment,

which reduces resting Ca_i^{2+} concentrations, is associated with reduced expression of gp91phox/p47phox NOX2 subunits (Altamirano et al., 2013). The genetic down-regulation of NOX2 activity reduces Mn^{2+}/Ca^{2+} influx across the dystrophin-deficient sarcolemma and restores autophagy and reduces muscle pathology in *mdx* mice (Pal et al., 2014; Loehr et al., 2016). These studies indicate the involvement of NOX2-driven oxidative stress in increased sarcolemmal Ca^{2+} influx in dystrophic muscles. NOX2-driven oxidative stress was also shown to be involved in dystrophic cardiomyopathy (Shirokova and Niggli, 2013). The expression of NOX2 is increased in the *mdx* heart along with increased superoxide production (Gonzalez et al., 2014). Furthermore, NOX2 inhibition by apocynin restored the Ca^{2+}-handling properties, including the amplitude of Ca^{2+} transient and SR Ca^{2+} content in the dystrophic myocytes. In addition, NOX2 inhibition decreases the SR Ca^{2+} leak in *mdx* myocytes (Gonzalez et al., 2014). On the other hand, genetic inhibition of NOX2 production (by deleting the $p47^{phox}$, a NOX2 regulatory subunit) failed to decrease RyR1 Ca^{2+} leak in *mdx* muscle fibers. These studies further show that NOX4 is activated in the NOX2 ROS-deficient *mdx* muscle and contributes to RyR1 leak (Cully and Rodney, 2020). Based on these findings, the authors proposed ROS-Ca^{2+} crosstalk, in which NOX4-ROS induces RyR1 Ca^{2+} leak and thereby increases the SR/T-tubular junctional Ca^{2+} concentration, which exacerbates NOX2 ROS and contributes to muscle pathology. A recent study shows the down-regulation of miR-448-3p in the *mdx* heart increased *Ncf1* expression, which encodes $p47^{phox}$ (Kyrychenko et al., 2015a). These studies suggest the involvement of NOX2 in oxidative stress and enhanced Ca^{2+} signaling in dystrophic myocardium. In dystrophic myotubes, NOX inhibition abolished iPLA2 activity and reduced Ca^{2+} influx through stretch-activated and store-operated channels (Ismail et al., 2014). In addition, NOX inhibition in *mdx* muscle restored the force loss induced by eccentric contractions and reduced membrane damage (Ismail et al., 2014). Thus, NOX are appealing targets in developing new therapies for muscular dystrophy.

TARGETING Ca^{2+} HANDLING PROTEINS—A THERAPEUTIC VIEW

In light of the significant contribution of Ca^{2+} mishandling in DMD pathogenesis, strategies targeting Ca^{2+} handling may hold great promise to treat DMD. Preclinical studies in animal models have provided compelling evidence supporting these therapeutic modalities (**Table 1**).

Use of Non-specific Ca^{2+}-Channel Blockers for the Treatment of DMD

Calcium accumulation has been demonstrated in skeletal muscle biopsies from fetal human DMD (Farini et al., 2016), suggesting Ca^{2+} abnormalities occur at the early onset of the disease. To determine the optimal time point for Ca^{2+} channel blocking to prevent the pathological onset of the disease, Jorgensen et al. treated *mdx* mice *in utero* with streptomycin, a non-specific Ca^{2+}-channel blocker that inhibits stretch-activated and mechanosensitive ion channels (Jorgensen et al., 2011). Streptomycin treatment delayed the onset of dystrophic symptoms in the limb muscles in young *mdx* mice but did not prevent disease progression. In *mdx* mice, long-term treatment with streptomycin reduced limb-muscle pathology but worsened the diaphragm and cardiac pathology (Jorgensen et al., 2011). These studies argue that blocking Ca^{2+} channels before disease onset is not beneficial. On the other hand, streptomycin treatment after birth reduced creatine kinase activity in the diaphragm and sternomastoid muscles of *mdx* mice (Matsumura et al., 2011). These studies suggest that the differential effects of streptomycin in various dystrophic muscles may be associated with the differential expression of TRPC1 (Matsumura et al., 2011). Thus, care must be taken in the long-term clinical use of non-specific Ca^{2+}-channel blockers in DMD patients.

Blocking Ca^{2+} Entry Through Dystrophin-Deficient Sarcolemma

Membrane leaking has been suggested to contribute to cytosolic Ca^{2+} overload in dystrophic muscle. To address this issue, membrane sealants such as Poloxamer 188 and its derivatives have been developed to stabilize the sarcolemma. Preclinical studies in the murine and canine DMD model suggest that membrane sealants can improve cardiac function (Yasuda et al., 2005; Townsend et al., 2010; Houang et al., 2015; Markham et al., 2015). However, two studies failed to show protection in *mdx* mouse skeletal muscle (Quinlan et al., 2006; Terry et al., 2014). More studies are warranted to validate the therapeutic potency of P188 in preventing Ca^{2+} entry and ameliorating DMD.

Calcium can enter dystrophic muscle cells through the L-type Ca^{2+} channel. L-type Ca^{2+}-channel blockers, such as diltiazem and verapamil, have been shown to reduce serum creatine levels and muscle necrosis in *mdx* mice (Matsumura et al., 2009). Similarly, nifedipine treatment restored cytosolic Ca^{2+} levels and improved muscle function in mouse models of DMD (Altamirano et al., 2013). Although these observations signify the therapeutic benefits of L-type Ca^{2+}-channel blockers in animal models, several clinical trials have revealed no clinical benefit in DMD patients (Spinazzola and Kunkel, 2016). This could be due to many reasons, for example, differences in drug metabolisms and variation in drug dosing. Future studies are warranted to clarify the mechanisms underlying different outcomes in animal models and DMD patients and to develop creative strategies to improve the efficacy in human patients.

Targeting stretch-activated Ca^{2+} channels with streptomycin and spider venom toxin has been shown to attenuate Ca_i^{2+} rise and muscle damage in *mdx* mice (Yeung et al., 2005). Pharmacological inhibition of TRPC1 and TRPC3 channels has been shown to reduce the Ca^{2+} entry into dystrophic skeletal myofibers and also improve their function (Vandebrouck et al., 2002). In *mdx* mice, overexpression of a dominant-negative mutant of the TRPV2 ion channel protects eccentric contraction-induced damage (Zanou et al., 2009). Thus, inhibiting TRP channels is a potential therapeutic strategy to prevent Ca^{2+} entry.

TABLE 1 | Therapies targeting dysregulated Ca^{2+} directly or indirectly.

Drugs	Mechanism of action	Models used	Comments	References
Verapamil, diltiazem, nifedipine	Ca^{2+}-channel blockers	*mdx* mice	Shown benefit in a mouse model but failed to ameliorate the condition in clinical trials.	Matsumura et al., 2009; Altamirano et al., 2013; Spinazzola and Kunkel, 2016
Calpastatin	Calpain blocker	*mdx* mice, Canine model	Initially rescued the dystrophic phenotype in mice but C-101, a leupeptin-based drug was unsuccessful in the canine model	Spencer and Mellgren, 2002; Selsby et al., 2010; Childers et al., 2011
Streptomycin, spider venom	SAC channel blocker	*mdx* mice	Mitigate cytosolic Ca^{2+} rise	Yeung et al., 2005
Enalapril	ACE inhibitor	DMD patients	Improved cardiac function	Kwon et al., 2012
Carvedilol	β-Blocker	DMD patients	Improved cardiac function	Kwon et al., 2012
P-188 NF	Membrane sealant	*mdx* and *mdxutr*$^{-/-}$ mice, canine model	Improved cardiac and respiratory function	Yasuda et al., 2005; Townsend et al., 2010; Houang et al., 2015; Markham et al., 2015
Rycal	RyR-stabilizing compound	*mdx* mice, patient-derived cells	Attenuated SR Ca^{2+} leak and mitigate DMD phenotype	Capogrosso et al., 2018; Barthelemy et al., 2019
AAV.SERCA2a	Overexpression of SERCA2a	*mdx* mice and Canine model	Enhance SR Ca^{2+} uptake and ameliorate DMD	Goonasekera et al., 2011; Duan, 2015; Wasala et al., 2020
AAV.SERCA1	Overexpression of SERCA1	*mdx* mice	Enhance SERCA function and ameliorate DMD phenotype	Morine et al., 2010; Goonasekera et al., 2011; Mazala et al., 2015
AAV.SLN	Reducing the SLN expression levels	*mdx:utr*$^{-/-}$mice	Enhance SERCA function and mitigate DMD	Voit et al., 2017
BGP-15	Inducer of Hsp-72	*mdx* and *mdx:utr*$^{-/-}$mice	Improve muscle function by stabilizing SERCA function	Gehrig et al., 2012
Alisporivir	Cyclophilin D blocker	Zebrafish model	Enhanced mitochondrial function by preventing Ca^{2+} dependent mPTP opening	Schiavone et al., 2017

Targeting Intracellular Ca^{2+} Signaling to Improve Cardiac Function

Angiotensin II or β-receptor–mediated signaling pathways, such as G-protein–coupled receptor pathways, modulate muscle contraction–relaxation via altered Ca_i^{2+} handling. β_2-adrenergic receptor–coupled pathway has been shown to attenuate skeletal muscle degeneration in DMD (Smith et al., 2002; Church et al., 2014; Silva et al., 2014). Treating albuterol, a β_2 agonist, increased muscle strength in animal models but failed to improve muscle function in DMD patients (Skura et al., 2008). On the other hand, treating DMD patients with enalapril, an angiotensin-converting enzyme (ACE) inhibitor, or carvedilol, a β-blocker, improved the left ventricular systolic function without significant adverse effects in one patient study (Kwon et al., 2012).

Preventing SR Ca^{2+} Leak

SR Ca^{2+} leak is a significant contributor to cytosolic Ca^{2+} overload in DMD. Rycal, a RyR-stabilizing compound, was found to attenuate muscle disease in *mdx* mice (Bellinger et al., 2009; Fauconnier et al., 2010; Capogrosso et al., 2018). Rycal is suggested to improve binding of calstabin to RyR and to prevent SR Ca^{2+} leak, thereby restoring Ca_i^{2+} homeostasis (Capogrosso et al., 2018). A recent study showed that Rycal treatment bolsters antisense oligonucleotide-mediated exon skipping in patient-derived myotubes and induced pluripotent stem cell–derived diseased cardiomyocytes (Barthelemy et al., 2019). Although the therapeutic value of Rycal needs to be further validated, these studies suggest that targeting the RyR will boost treatment efficiency in DMD patients.

Enhancing SR Ca^{2+} Uptake

Enhancing cytosolic Ca^{2+} removal is another powerful approach to restore the Ca_i^{2+} homeostasis in dystrophic muscle. This can be achieved by overexpressing SERCA or by targeting its inhibitors to enhance SERCA activity. Several animal studies have shown the beneficial effects of SERCA overexpression in ameliorating muscular dystrophy in mice (Morine et al., 2010; Goonasekera et al., 2011; Shin et al., 2011; Mazala et al., 2015; Wasala et al., 2020). Transgenic overexpression of SERCA1 in skeletal muscles of *mdx* mice has been shown to enhance the EC coupling, improve Ca^{2+} removal from the cytosol, and attenuate dystrophic phenotypes such as fibrosis and increased serum creatine kinase levels (Goonasekera et al., 2011). Similarly, transgenic overexpression of SERCA1 is shown to ameliorate the structural damage and functional impairments of muscles from

mdx:utr$^{-/-}$ *mice* (Mazala et al., 2015). Adeno-associated virus (AAV)-mediated overexpression of SERCA1 in the diaphragm of *mdx* mice increased the proportion of type IIA fibers, reduced the percentage of centrally nucleated fibers, and attenuated the loss of force production following eccentric contractions (Morine et al., 2010). In contrast to SERCA1, SERCA2a is expressed in both skeletal muscle and the heart. We evaluated AAV SERCA2a gene therapy. Delivery to 12-month-old *mdx* mice significantly improved cardiac electrophysiology (Shin et al., 2011). A single intravenous injection in 3-month-old *mdx* mice significantly improves whole-body muscle performance and ameliorates fatal dilated cardiomyopathy in *mdx* mice up to 21 months of age (Wasala et al., 2020). The AAV.SERCA2a vector has been extensively studied in heart failure patients (Zsebo et al., 2014; Lyon et al., 2020). Lessons learned from these studies will help facilitate the translation of AAV.SERCA2a therapy in DMD patients.

Targeting SERCA regulators such as PLN and SLN also has therapeutic implications. Reducing PLN activity is shown to improve Ca^{2+} handling in animal models of heart failure (Kranias and Hajjar, 2012). Surprisingly, genetic PLN knockout worsened cardiac function in *mdx* mice (Law et al., 2018). It is yet unclear whether the partial reduction of PLN activity is beneficial in DMD. Unlike PLN, SLN up-regulation is a common molecular signature in all dystrophin-deficient muscles. Recent studies from our laboratory and others have shown that germline ablation of SLN ameliorates severe muscular dystrophy in a mouse model of DMD (Voit et al., 2017; Tanihata et al., 2018; Mareedu et al., 2019). Most strikingly, the loss of one SLN allele extended the lifespan of *mdx:utr*$^{-/-}$ mice to 20 months. Also, our studies show that the reduction in SLN expression can improve muscle regeneration and prevent fiber-type transition in dystrophic muscles (Voit et al., 2017). Furthermore, AAV-mediated SLN reduction normalized Ca_i^{2+} cycling and improved fusion and differentiation of dystrophin-deficient dog myoblasts (Niranjan et al., 2019). Our recent studies have demonstrated that reducing SLN expression is sufficient to restore cardiac SERCA function and Ca_i^{2+} cycling and to prevent the development of cardiomyopathy in *mdx* mice throughout their lifespan (Mareedu et al., 2021). To translate these findings into a therapeutic strategy, we also knocked down SLN expression in 1-month-old *mdx:utr*$^{-/-}$ mice via AAV-mediated RNA interference (Voit et al., 2017). This AAV treatment markedly reduces SLN expression, attenuates muscle pathology, and improves diaphragm, skeletal muscle, and cardiac function (Voit et al., 2017). In summary, these studies suggest that targeting SLN expression or function is a promising therapeutic strategy to improve SERCA function and ameliorate skeletal muscle disease and cardiomyopathy in DMD.

The therapeutic potential of targeting DWORF has been explored in animal models of heart failure. Cardiac-specific overexpression of DWORF enhances SERCA function, Ca^{2+} cycling, and contractility in mice (Nelson et al., 2016). In addition, overexpression of DWORF in the heart improves Ca^{2+} cycling, prevents pathological remodeling, and improves cardiac function in the muscle-specific LIM protein (MLP) knockout mouse model of dilated cardiomyopathy (Makarewich et al., 2018). A recent study shows that AAV-mediated overexpression of DWORF improved cardiac function in MLP knockout mice, as well as in the myocardial infarction model of heart failure (Makarewich et al., 2020). The expression levels and function of DWORF in dystrophic cardiac and skeletal muscle are yet to be studied. Nevertheless, based on the current findings, DWORF overexpression could be a therapeutic strategy to improve SERCA function and ameliorate muscular dystrophy and cardiomyopathy in DMD.

In addition to these strategies, improving SERCA function through other mechanisms has been shown to ameliorate muscular dystrophy in mice. Transgenic overexpression of heat shock protein 72 (Hsp72) or pharmacological induction of Hsp72 improves several pathological indices in *mdx* and *mdx:utr*$^{-/-}$ mice, partly through the enhancement of SERCA function. These studies show that Hsp72 stabilizes the SERCA pump and increases its activity in dystrophic muscles (Gehrig et al., 2012). A recent study shows that blocking the insulin-like growth factor 2 receptor activates SERCA function and enhances the Ca_i^{2+} removal in muscles of *mdx* mice (Bella et al., 2020).

Reducing Mitochondrial Contribution to Cytosolic Ca^{2+} Overload

Improving mitochondrial function is another attractive therapeutic strategy for DMD. As discussed previously, Ca^{2+}-dependent mitochondrial dysfunction could be due to the opening of mPTP (Briston et al., 2019). Thus, inhibiting cyclophilin, a key regulator of mPTP, could prevent mPTP opening and alleviate mitochondrial dysfunction in DMD. Although CsA treatment failed to improve muscle function in DMD patients (Kirschner et al., 2010), treatment with another cyclophilin inhibitor, Debio 025, which inhibits mPTP opening, has been shown to partially rescue the dystrophic phenotype in *mdx* mice (Reutenauer et al., 2008). Similarly, alisporivir, a derivative of CsA, has been shown to enhance the mitochondrial function in the zebrafish model of DMD (Schiavone et al., 2017). Further exploitation of these compounds and the identification of new compounds that prevent Ca^{2+}-dependent mPTP opening provide an attractive therapeutic strategy to improve mitochondrial function and prevent muscle necrosis in DMD.

Minimizing Downstream Events of Cytosolic Ca^{2+} Overload

Calpain activation leads to proteolytic damage in muscle cells. Overexpression of calpastatin, an endogenous inhibitor of calpain, significantly reduced muscle necrosis in *mdx* mice (Spencer and Mellgren, 2002). On the contrary, the use of C101, a leupeptin-based calpain inhibitor, failed to rescue phenotypes of DMD in animal models (Selsby et al., 2010; Childers et al., 2011). There is no direct study on the PLA_2 inhibition in preventing muscle damage in DMD. However, corticosteroids, in clinical practice, suppress muscle inflammation possibly via PLA_2 inhibition (Hoxha, 2019).

CONCLUSIONS AND FUTURE DIRECTIONS

Over the last several decades, there has been significant growth in our knowledge of the Ca^{2+} mishandling and Ca^{2+} homeostasis dysregulation in DMD. These findings have resulted in several highly promising and novel experimental therapies such as the use of the RyR stabilizer RyCal, SLN silencing, and viral vector–mediated SERCA overexpression. Yet, there are many unanswered questions and conflicting experimental results. Ca_i^{2+} dysregulation is not only implicated in DMD but also involved in other muscular dystrophies, such as limb-girdle muscular dystrophy and laminopathies. Further understanding of the molecular mechanisms involved in Ca^{2+} mishandling may shed light on the secondary disease-causing mechanisms in various forms of muscular dystrophies. This understanding will help identify new therapeutic targets for the treatment of these diseases. Based on current knowledge, future studies may be directed to the following areas for a better understanding of targeting Ca^{2+} dysregulation:

1) *Mitochondria:* Calcium is a key regulator of mitochondrial function. Mounting evidence indicates that mitochondrial dysfunction plays an important role in disease pathogenesis in DMD. Exploring the molecular mechanisms including the MAM region that link the cytoplasmic Ca^{2+} load and mitochondrial Ca^{2+} mishandling may lead to the identification of potential therapeutic targets.
2) *SR Ca^{2+} reuptake:* Based on our recent studies, enhancing SERCA2a expression or activity (through reducing SERCA inhibitors) appears to be a promising strategy to treat both cardiac and skeletal muscle defects in DMD. Therefore, exploring new strategies to improve SERCA function, developing new AAV vectors with improved tropism for both muscle and heart, and identifying small molecules that activate endogenous SERCA pumps will be useful.
3) *The use of large animal models:* Many Ca^{2+}-targeted therapies were performed in mouse models of DMD. These findings need to be verified in large animal models before moving to human trials.
4) *The effects of dystrophin restoration on Ca^{2+} handling:* It is unknown whether partial dystrophin restoration alleviates Ca^{2+}-handling defects in dystrophic muscles. This information is not available and needs to be tested. This will help to design a combination therapy of dystrophin restoration with improved Ca^{2+} handling.

DISCLOSURE

DD is a member of the scientific advisory board for Solid Biosciences and equity holders of Solid Biosciences. The Duan laboratory has received research supports unrelated to this project from Solid Biosciences and Edgewise Therapeutics in the past 3 years. SM, EM, and GB have no conflicts of interest, financial or otherwise. The content of this manuscript is solely the responsibility of the authors and does not necessarily represent the official views of the National Institutes of Health.

AUTHOR CONTRIBUTIONS

All authors discussed, wrote, and commented on the manuscript at all stages.

FUNDING

This work was supported by the National Institute of Arthritis and Musculoskeletal and Skin Diseases, US National Institutes of Health (NIH) grant (Grant #1R01AR069107 to GB, Grant # 1R01AR070517 to DD and GB), Jesse's Journey: The Foundation for Gene and Cell Therapy (to DD and GB), and Jackson Freel DMD Research Fund (to DD). EM was supported by the University of Missouri Life Science Fellowship.

REFERENCES

Aartsma-Rus, A., Ginjaar, I. B., and Bushby, K. (2016). The importance of genetic diagnosis for Duchenne muscular dystrophy. *J. Med. Genet.* 53, 145–151. doi: 10.1136/jmedgenet-2015-103387

Alderton, J. M., and Steinhardt, R. A. (2000). Calcium influx through calcium leak channels is responsible for the elevated levels of calcium-dependent proteolysis in dystrophic myotubes. *J. Biol. Chem.* 275, 9452–9460. doi: 10.1074/jbc.275.13.9452

Allen, D. G., and Whitehead, N. P. (2011). Duchenne muscular dystrophy–what causes the increased membrane permeability in skeletal muscle? *Int. J. Biochem. Cell Biol.* 43, 290–294. doi: 10.1016/j.biocel.2010.11.005

Allen, D. G., Whitehead, N. P., and Froehner, S. C. (2016). Absence of dystrophin disrupts skeletal muscle signaling: roles of Ca^{2+}, reactive oxygen species, and nitric oxide in the development of muscular dystrophy. *Physiol. Rev.* 96, 253–305. doi: 10.1152/physrev.00007.2015

Altamirano, F., Valladares, D., Henriquez-Olguin, C., Casas, M., Lopez, J. R., Allen, P. D., et al. (2013). Nifedipine treatment reduces resting calcium concentration, oxidative and apoptotic gene expression, and improves muscle function in dystrophic mdx mice. *PLoS ONE* 8:e81222. doi: 10.1371/journal.pone.0081222

Anderson, D. M., Anderson, K. M., Chang, C. L., Makarewich, C. A., Nelson, B. R., McAnally, J. R., et al. (2015). A micropeptide encoded by a putative long noncoding RNA regulates muscle performance. *Cell* 160, 595–606. doi: 10.1016/j.cell.2015.01.009

Andrews, N. W., Almeida, P. E., and Corrotte, M. (2014). Damage control: cellular mechanisms of plasma membrane repair. *Trends Cell Biol.* 24, 734–742. doi: 10.1016/j.tcb.2014.07.008

Arvanitis, D. A., Vafiadaki, E., Sanoudou, D., and Kranias, E. G. (2011). Histidine-rich calcium binding protein: the new regulator of sarcoplasmic reticulum calcium cycling. *J. Mol. Cell. Cardiol.* 50, 43–49. doi: 10.1016/j.yjmcc.2010.08.021

Avila, G., de la Rosa, J. A., Monsalvo-Villegas, A., and Montiel-Jaen, M. G. (2019). Ca(2+) channels mediate bidirectional signaling between sarcolemma and sarcoplasmic reticulum in muscle cells. *Cells* 9:55. doi: 10.3390/cells9010055

Avila-Medina, J., Mayoral-Gonzalez, I., Dominguez-Rodriguez, A., Gallardo-Castillo, I., Ribas, J., Ordonez, A., et al. (2018). The complex role of store operated calcium entry pathways and related proteins in the function of cardiac, skeletal and vascular smooth muscle cells. *Front. Physiol.* 9:257. doi: 10.3389/fphys.2018.00257

Babu, G. J., Bhupathy, P., Carnes, C. A., Billman, G. E., and Periasamy, M. (2007). Differential expression of sarcolipin protein during muscle

development and cardiac pathophysiology. *J. Mol. Cell. Cardiol.* 43, 215–222. doi: 10.1016/j.yjmcc.2007.05.009

Barthelemy, F., Wang, R. T., Hsu, C., Douine, E. D., Marcantonio, E. E., Nelson, S. F., et al. (2019). Targeting RyR activity boosts antisense exon 44 and 45 skipping in human DMD skeletal or cardiac muscle culture models. *Mol. Ther. Nucleic Acids* 18, 580–589. doi: 10.1016/j.omtn.2019.09.020

Bartoli, M., and Richard, I. (2005). Calpains in muscle wasting. *Int. J. Biochem. Cell Biol.* 37, 2115–2133. doi: 10.1016/j.biocel.2004.12.012

Beard, N. A., Laver, D. R., and Dulhunty, A. F. (2004). Calsequestrin and the calcium release channel of skeletal and cardiac muscle. *Prog. Biophys. Mol. Biol.* 85, 33–69. doi: 10.1016/j.pbiomolbio.2003.07.001

Bella, P., Farini, A., Banfi, S., Parolini, D., Tonna, N., Meregalli, M., et al. (2020). Blockade of IGF2R improves muscle regeneration and ameliorates Duchenne muscular dystrophy. *EMBO Mol. Med.* 12:e11019. doi: 10.15252/emmm.201911019

Bellinger, A. M., Reiken, S., Carlson, C., Mongillo, M., Liu, X., Rothman, L., et al. (2009). Hypernitrosylated ryanodine receptor calcium release channels are leaky in dystrophic muscle. *Nat. Med.* 15, 325–330. doi: 10.1038/nm.1916

Bhattacharya, S. K., Palmieri, G. M., Bertorini, T. E., and Nutting, D. F. (1982). The effects of diltiazem in dystrophic hamsters. *Muscle Nerve* 5, 73–78. doi: 10.1002/mus.880050114

Bhupathy, P., Babu, G. J., and Periasamy, M. (2007). Sarcolipin and phospholamban as regulators of cardiac sarcoplasmic reticulum Ca^{2+} ATPase. *J. Mol. Cell. Cardiol.* 42, 903–911. doi: 10.1016/j.yjmcc.2007.03.738

Boittin, F. X., Shapovalov, G., Hirn, C., and Ruegg, U. T. (2010). Phospholipase A2-derived lysophosphatidylcholine triggers Ca^{2+} entry in dystrophic skeletal muscle fibers. *Biochem. Biophys. Res. Commun.* 391, 401–406. doi: 10.1016/j.bbrc.2009.11.070

Briston, T., Selwood, D. L., Szabadkai, G., and Duchen, M. R. (2019). Mitochondrial permeability transition: a molecular lesion with multiple drug targets. *Trends Pharmacol. Sci.* 40, 50–70. doi: 10.1016/j.tips.2018.11.004

Burdi, R., Didonna, M. P., Pignol, B., Nico, B., Mangieri, D., Rolland, J. F., et al. (2006). First evaluation of the potential effectiveness in muscular dystrophy of a novel chimeric compound, BN 82270, acting as calpain-inhibitor and anti-oxidant. *Neuromuscul. Disord.* 16, 237–248. doi: 10.1016/j.nmd.2006.01.013

Burr, A. R., Millay, D. P., Goonasekera, S. A., Park, K. H., Sargent, M. A., Collins, J., et al. (2014). Na+ dysregulation coupled with Ca^{2+} entry through NCX1 promotes muscular dystrophy in mice. *Mol. Cell. Biol.* 34, 1991–2002. doi: 10.1128/MCB.00339-14

Burr, A. R., and Molkentin, J. D. (2015). Genetic evidence in the mouse solidifies the calcium hypothesis of myofiber death in muscular dystrophy. *Cell Death Differ.* 22, 1402–1412. doi: 10.1038/cdd.2015.65

Bushby, K., Finkel, R., Birnkrant, D. J., Case, L. E., Clemens, P. R., Cripe, L., et al. (2010). Diagnosis and management of Duchenne muscular dystrophy, part 1: diagnosis, and pharmacological and psychosocial management. *Lancet Neurol.* 9, 77–93. doi: 10.1016/S1474-4422(09)70271-6

Calderon, J. C., Bolanos, P., and Caputo, C. (2014). The excitation-contraction coupling mechanism in skeletal muscle. *Biophys. Rev.* 6, 133–160. doi: 10.1007/s12551-013-0135-x

Capogrosso, R. F., Mantuano, P., Uaesoontrachoon, K., Cozzoli, A., Giustino, A., Dow, T., et al. (2018). Ryanodine channel complex stabilizer compound S48168/ARM210 as a disease modifier in dystrophin-deficient mdx mice: proof-of-concept study and independent validation of efficacy. *FASEB J.* 32, 1025–1043. doi: 10.1096/fj.201700182RRR

Capote, J., DiFranco, M., and Vergara, J. L. (2010). Excitation-contraction coupling alterations in mdx and utrophin/dystrophin double knockout mice: a comparative study. *Am. J. Physiol. Cell Physiol.* 298, C1077–C1086. doi: 10.1152/ajpcell.00428.2009

Cea, L. A., Puebla, C., Cisterna, B. A., Escamilla, R., Vargas, A. A., Frank, M., et al. (2016). Fast skeletal myofibers of mdx mouse, model of Duchenne muscular dystrophy, express connexin hemichannels that lead to apoptosis. *Cell. Mol. Life Sci.* 73, 2583–2599. doi: 10.1007/s00018-016-2132-2

Cea, L. A., Riquelme, M. A., Cisterna, B. A., Puebla, C., Vega, J. L., Rovegno, M., et al. (2012). Connexin- and pannexin-based channels in normal skeletal muscles and their possible role in muscle atrophy. *J. Membr. Biol.* 245, 423–436. doi: 10.1007/s00232-012-9485-8

Chakkalakal, J. V., Thompson, J., Parks, R. J., and Jasmin, B. J. (2005). Molecular, cellular, and pharmacological therapies for Duchenne/Becker muscular dystrophies. *FASEB J.* 19, 880–891. doi: 10.1096/fj.04-1956rev

Chan, S., and Head, S. I. (2011). The role of branched fibres in the pathogenesis of Duchenne muscular dystrophy. *Exp. Physiol.* 96, 564–571. doi: 10.1113/expphysiol.2010.056713

Chen, Y., Csordas, G., Jowdy, C., Schneider, T. G., Csordas, N., Wang, W., et al. (2012). Mitofusin 2-containing mitochondrial-reticular microdomains direct rapid cardiomyocyte bioenergetic responses via interorganelle Ca(2+) crosstalk. *Circ. Res.* 111, 863–875. doi: 10.1161/CIRCRESAHA.112.266585

Cheng, X., Zhang, X., Gao, Q., Ali Samie, M., Azar, M., Tsang, W. L., et al. (2014). The intracellular Ca(2)(+) channel MCOLN1 is required for sarcolemma repair to prevent muscular dystrophy. *Nat. Med.* 20, 1187–1192. doi: 10.1038/nm.3611

Childers, M. K., Bogan, J. R., Bogan, D. J., Greiner, H., Holder, M., Grange, R. W., et al. (2011). Chronic administration of a leupeptin-derived calpain inhibitor fails to ameliorate severe muscle pathology in a canine model of duchenne muscular dystrophy. *Front. Pharmacol.* 2:89. doi: 10.3389/fphar.2011.00089

Church, J. E., Trieu, J., Sheorey, R., Chee, A. Y., Naim, T., Baum, D. M., et al. (2014). Functional beta-adrenoceptors are important for early muscle regeneration in mice through effects on myoblast proliferation and differentiation. *PLoS ONE* 9:e101379. doi: 10.1371/journal.pone.0101379

Collet, C., Allard, B., Tourneur, Y., and Jacquemond, V. (1999). Intracellular calcium signals measured with indo-1 in isolated skeletal muscle fibres from control and mdx mice. *J. Physiol.* 520 (Pt 2), 417–429.

Connolly, A. M., Florence, J. M., Cradock, M. M., Malkus, E. C., Schierbecker, J. R., Siener, C. A., et al. (2013). Motor and cognitive assessment of infants and young boys with Duchenne Muscular Dystrophy: results from the Muscular Dystrophy Association DMD Clinical Research Network. *Neuromuscul. Disord.* 23, 529–539. doi: 10.1016/j.nmd.2013.04.005

Conti, A., Gorza, L., and Sorrentino, V. (1996). Differential distribution of ryanodine receptor type 3 (RyR3) gene product in mammalian skeletal muscles. *Biochem. J.* 316 (Pt 1), 19–23. doi: 10.1042/bj3160019

Cooper, S. T., and Head, S. I. (2015). Membrane injury and repair in the muscular dystrophies. *Neuroscientist* 21, 653–668. doi: 10.1177/1073858414558336

Csordas, G., Weaver, D., and Hajnoczky, G. (2018). Endoplasmic reticulum-mitochondrial contactology: structure and signaling functions. *Trends Cell Biol.* 28, 523–540. doi: 10.1016/j.tcb.2018.02.009

Culligan, K., Banville, N., Dowling, P., and Ohlendieck, K. (2002). Drastic reduction of calsequestrin-like proteins and impaired calcium binding in dystrophic mdx muscle. *J. Appl. Physiol.* 92, 435–445. doi: 10.1152/japplphysiol.00903.2001

Cully, T. R., and Rodney, G. G. (2020). Nox4 - RyR1 - Nox2: regulators of micro-domain signaling in skeletal muscle. *Redox Biol.* 36:101557. doi: 10.1016/j.redox.2020.101557

Danialou, G., Comtois, A. S., Dudley, R., Karpati, G., Vincent, G., Des Rosiers, C., et al. (2001). Dystrophin-deficient cardiomyocytes are abnormally vulnerable to mechanical stress-induced contractile failure and injury. *FASEB J.* 15, 1655–1657. doi: 10.1096/fj.01-0030fje

Dayton, W. R., Reville, W. J., Goll, D. E., and Stromer, M. H. (1976). A Ca^{2+}-activated protease possibly involved in myofibrillar protein turnover. Partial characterization of the purified enzyme. *Biochemistry* 15, 2159–2167.

de Brito, O. M., and Scorrano, L. (2008). Mitofusin 2 tethers endoplasmic reticulum to mitochondria. *Nature* 456, 605–610. doi: 10.1038/nature07534

Derler, I., Jardin, I., and Romanin, C. (2016). Molecular mechanisms of STIM/Orai communication. *Am. J. Physiol. Cell Physiol.* 310, C643–C662. doi: 10.1152/ajpcell.00007.2016

Deval, E., Levitsky, D. O., Marchand, E., Cantereau, A., Raymond, G., and Cognard, C. (2002). Na(+)/Ca(2+) exchange in human myotubes: intracellular calcium rises in response to external sodium depletion are enhanced in DMD. *Neuromuscul. Disord.* 12, 665–673. doi: 10.1016/s0960-8966(02)00022-6

DiFranco, M., Woods, C. E., Capote, J., and Vergara, J. L. (2008). Dystrophic skeletal muscle fibers display alterations at the level of calcium microdomains. *Proc. Natl. Acad. Sci. U.S.A.* 105, 14698–14703. doi: 10.1073/pnas.0802217105

Divet, A., and Huchet-Cadiou, C. (2002). Sarcoplasmic reticulum function in slow- and fast-twitch skeletal muscles from mdx mice. *Pflugers Arch.* 444, 634–643. doi: 10.1007/s00424-002-0854-5

Dowling, P., Lohan, J., and Ohlendieck, K. (2003). Comparative analysis of Dp427-deficient mdx tissues shows that the milder dystrophic phenotype of

extraocular and toe muscle fibres is associated with a persistent expression of beta-dystroglycan. *Eur. J. Cell Biol.* 82, 222–230. doi: 10.1078/0171-9335-00315

Duan, D. (2015). Duchenne muscular dystrophy gene therapy in the canine model. *Hum. Gene Ther. Clin. Dev.* 26, 57–69. doi: 10.1089/humc.2015.006

Duan, D., Goemans, N., Takeda, S. I., Mercuri, E., and Aartsma-Rus, A. (2021). Duchenne muscular dystrophy. *Nat. Rev. Dis. Primers* 7:13. doi: 10.1038/s41572-021-00248-3

Edwards, J. N., Friedrich, O., Cully, T. R., von Wegner, F., Murphy, R. M., and Launikonis, B. S. (2010). Upregulation of store-operated Ca^{2+} entry in dystrophic mdx mouse muscle. *Am. J. Physiol. Cell Physiol.* 299, C42–C50. doi: 10.1152/ajpcell.00524.2009

Eisner, D. A., Caldwell, J. L., Kistamas, K., and Trafford, A. W. (2017). Calcium and excitation-contraction coupling in the heart. *Circ. Res.* 121, 181–195. doi: 10.1161/CIRCRESAHA.117.310230

Endo, M. (2009). Calcium-induced calcium release in skeletal muscle. *Physiol. Rev.* 89, 1153–1176. doi: 10.1152/physrev.00040.2008

Ervasti, J. M., and Campbell, K. P. (1993). A role for the dystrophin-glycoprotein complex as a transmembrane linker between laminin and actin. *J. Cell Biol.* 122, 809–823.

Farini, A., Sitzia, C., Cassinelli, L., Colleoni, F., Parolini, D., Giovanella, U., et al. (2016). Inositol 1,4,5-trisphosphate (IP3)-dependent Ca^{2+} signaling mediates delayed myogenesis in Duchenne muscular dystrophy fetal muscle. *Development* 143, 658–669. doi: 10.1242/dev.126193

Fauconnier, J., Thireau, J., Reiken, S., Cassan, C., Richard, S., Matecki, S., et al. (2010). Leaky RyR2 trigger ventricular arrhythmias in Duchenne muscular dystrophy. *Proc. Natl. Acad. Sci. U.S.A.* 107, 1559–1564. doi: 10.1073/pnas.0908540107

Feno, S., Butera, G., Vecellio Reane, D., Rizzuto, R., and Raffaello, A. (2019). Crosstalk between calcium and ROS in pathophysiological conditions. *Oxid. Med. Cell. Longev.* 2019:9324018. doi: 10.1155/2019/9324018

Ferretti, R., Marques, M. J., Pertille, A., and Santo Neto, H. (2009). Sarcoplasmic-endoplasmic-reticulum Ca^{2+}-ATPase and calsequestrin are overexpressed in spared intrinsic laryngeal muscles of dystrophin-deficient mdx mice. *Muscle Nerve* 39, 609–615. doi: 10.1002/mus.21154

Filippin, L., Magalhaes, P. J., Di Benedetto, G., Colella, M., and Pozzan, T. (2003). Stable interactions between mitochondria and endoplasmic reticulum allow rapid accumulation of calcium in a subpopulation of mitochondria. *J. Biol. Chem.* 278, 39224–39234. doi: 10.1074/jbc.M302301200

Finkel, T., Menazza, S., Holmstrom, K. M., Parks, R. J., Liu, J., Sun, J., et al. (2015). The ins and outs of mitochondrial calcium. *Circ. Res.* 116, 1810–1819. doi: 10.1161/CIRCRESAHA.116.305484

Finsterer, J. (2006). Cardiopulmonary support in duchenne muscular dystrophy. *Lung* 184, 205–215. doi: 10.1007/s00408-005-2584-x

Flis, V. V., and Daum, G. (2013). Lipid transport between the endoplasmic reticulum and mitochondria. *Cold Spring Harb. Perspect. Biol.* 5:a013235. doi: 10.1101/cshperspect.a013235

Franzini-Armstrong, C. (2018). The relationship between form and function throughout the history of excitation-contraction coupling. *J. Gen. Physiol.* 150, 189–210. doi: 10.1085/jgp.201711889

Friedrich, O., Both, M., Gillis, J. M., Chamberlain, J. S., and Fink, R. H. (2004). Mini-dystrophin restores L-type calcium currents in skeletal muscle of transgenic mdx mice. *J. Physiol.* 555(Pt 1), 251–265. doi: 10.1113/jphysiol.2003.054213

Friedrich, O., von Wegner, F., Chamberlain, J. S., Fink, R. H., and Rohrbach, P. (2008). L-type Ca^{2+} channel function is linked to dystrophin expression in mammalian muscle. *PLoS ONE* 3:e1762. doi: 10.1371/journal.pone.0001762

Gailly, P. (2002). New aspects of calcium signaling in skeletal muscle cells: implications in Duchenne muscular dystrophy. *Biochim. Biophys. Acta* 1600, 38–44. doi: 10.1016/s1570-9639(02)00442-9

Gao, Q. Q., and McNally, E. M. (2015). The dystrophin complex: structure, function, and implications for therapy. *Compr. Physiol.* 5, 1223–1239. doi: 10.1002/cphy.c140048

Garcia-Perez, C., Hajnoczky, G., and Csordas, G. (2008). Physical coupling supports the local Ca^{2+} transfer between sarcoplasmic reticulum subdomains and the mitochondria in heart muscle. *J. Biol. Chem.* 283, 32771–32780. doi: 10.1074/jbc.M803385200

Garcia-Perez, C., Schneider, T. G., Hajnoczky, G., and Csordas, G. (2011). Alignment of sarcoplasmic reticulum-mitochondrial junctions with mitochondrial contact points. *Am. J. Physiol. Heart Circ. Physiol.* 301, H1907–H1915. doi: 10.1152/ajpheart.00397.2011

Gehlert, S., Bloch, W., and Suhr, F. (2015). Ca^{2+}-dependent regulations and signaling in skeletal muscle: from electro-mechanical coupling to adaptation. *Int. J. Mol. Sci.* 16, 1066–1095. doi: 10.3390/ijms16011066

Gehrig, S. M., van der Poel, C., Sayer, T. A., Schertzer, J. D., Henstridge, D. C., Church, J. E., et al. (2012). Hsp72 preserves muscle function and slows progression of severe muscular dystrophy. *Nature* 484, 394–398. doi: 10.1038/nature10980

Gervasio, O. L., Whitehead, N. P., Yeung, E. W., Phillips, W. D., and Allen, D. G. (2008). TRPC1 binds to caveolin-3 and is regulated by Src kinase - role in Duchenne muscular dystrophy. *J. Cell Sci.* 121(Pt 13), 2246–2255. doi: 10.1242/jcs.032003

Gillis, J. M. (1996). Membrane abnormalities and Ca homeostasis in muscles of the mdx mouse, an animal model of the Duchenne muscular dystrophy: a review. *Acta Physiol. Scand.* 156, 397–406. doi: 10.1046/j.1365-201X.1996.201000.x

Gillis, J. M. (1999). Understanding dystrophinopathies: an inventory of the structural and functional consequences of the absence of dystrophin in muscles of the mdx mouse. *J. Muscle Res. Cell Motil.* 20, 605–625. doi: 10.1023/a:1005545325254

Gonzalez, D. R., Treuer, A. V., Lamirault, G., Mayo, V., Cao, Y., Dulce, R. A., et al. (2014). NADPH oxidase-2 inhibition restores contractility and intracellular calcium handling and reduces arrhythmogenicity in dystrophic cardiomyopathy. *Am. J. Physiol. Heart Circ. Physiol.* 307, H710–H721. doi: 10.1152/ajpheart.00890.2013

Gonzalez, J. P., Ramachandran, J., Himelman, E., Badr, M. A., Kang, C., Nouet, J., et al. (2018). Normalization of connexin 43 protein levels prevents cellular and functional signs of dystrophic cardiomyopathy in mice. *Neuromuscul. Disord.* 28, 361–372. doi: 10.1016/j.nmd.2018.01.012

Goonasekera, S. A., Lam, C. K., Millay, D. P., Sargent, M. A., Hajjar, R. J., Kranias, E. G., et al. (2011). Mitigation of muscular dystrophy in mice by SERCA overexpression in skeletal muscle. *J. Clin. Invest.* 121, 1044–1052. doi: 10.1172/JCI43844

Gorecki, D. C. (2019). P2X7 purinoceptor as a therapeutic target in muscular dystrophies. *Curr. Opin. Pharmacol.* 47, 40–45. doi: 10.1016/j.coph.2019.02.003

Gorlach, A., Bertram, K., Hudecova, S., and Krizanova, O. (2015). Calcium and ROS: a mutual interplay. *Redox Biol.* 6, 260–271. doi: 10.1016/j.redox.2015.08.010

Grounds, M. D., Radley, H. G., Lynch, G. S., Nagaraju, K., and De Luca, A. (2008). Towards developing standard operating procedures for pre-clinical testing in the mdx mouse model of Duchenne muscular dystrophy. *Neurobiol. Dis.* 31, 1–19. doi: 10.1016/j.nbd.2008.03.008

Head, S. I. (2010). Branched fibres in old dystrophic mdx muscle are associated with mechanical weakening of the sarcolemma, abnormal Ca^{2+} transients and a breakdown of Ca^{2+} homeostasis during fatigue. *Exp. Physiol.* 95, 641–656. doi: 10.1113/expphysiol.2009.052019

Himelman, E., Lillo, M. A., Nouet, J., Gonzalez, J. P., Zhao, Q., Xie, L. H., et al. (2020). Prevention of connexin-43 remodeling protects against Duchenne muscular dystrophy cardiomyopathy. *J. Clin. Invest.* 130, 1713–1727. doi: 10.1172/JCI128190

Hirn, C., Shapovalov, G., Petermann, O., Roulet, E., and Ruegg, U. T. (2008). Nav1.4 deregulation in dystrophic skeletal muscle leads to Na+ overload and enhanced cell death. *J. Gen. Physiol.* 132, 199–208. doi: 10.1085/jgp.200810024

Hopf, F. W., Turner, P. R., Denetclaw, W. F. Jr., Reddy, P., and Steinhardt, R. A. (1996). A critical evaluation of resting intracellular free calcium regulation in dystrophic mdx muscle. *Am. J. Physiol.* 271(4 Pt 1), C1325–C1339. doi: 10.1152/ajpcell.1996.271.4.C1325

Horakova, L., Strosova, M. K., Spickett, C. M., and Blaskovic, D. (2013). Impairment of calcium ATPases by high glucose and potential pharmacological protection. *Free Radic. Res.* 47(Suppl. 1), 81–92. doi: 10.3109/10715762.2013.807923

Houang, E. M., Haman, K. J., Filareto, A., Perlingeiro, R. C., Bates, F. S., Lowe, D. A., et al. (2015). Membrane-stabilizing copolymers confer marked protection to dystrophic skeletal muscle *in vivo*. *Mol. Ther. Methods Clin. Dev.* 2:15042. doi: 10.1038/mtm.2015.42

Hoxha, M. (2019). Duchenne muscular dystrophy: focus on arachidonic acid metabolites. *Biomed. Pharmacother.* 110, 796–802. doi: 10.1016/j.biopha.2018.12.034

Hussain, T., Mangath, H., Sundaram, C., and Anandaraj, M. P. J. S. (2000). Expression of the gene for large subunit of m-calpain is elevated in skeletal muscle from Duchenne muscular dystrophy patients. *J. Genet.* 79, 77–80. doi: 10.1007/Bf02728949

Ismail, H. M., Scapozza, L., Ruegg, U. T., and Dorchies, O. M. (2014). Diapocynin, a dimer of the NADPH oxidase inhibitor apocynin, reduces ROS production… and prevents force loss in eccentrically contracting dystrophic muscle. *PLoS ONE* 9:e110708. doi: 10.1371/journal.pone.0110708

Iwata, Y., Katanosaka, Y., Arai, Y., Komamura, K., Miyatake, K., and Shigekawa, M. (2003). A novel mechanism of myocyte degeneration involving the Ca^{2+}-permeable growth factor-regulated channel. *J. Cell Biol.* 161, 957–967. doi: 10.1083/jcb.200301101

Iwata, Y., Katanosaka, Y., Arai, Y., Shigekawa, M., and Wakabayashi, S. (2009). Dominant-negative inhibition of Ca^{2+} influx via TRPV2 ameliorates muscular dystrophy in animal models. *Hum. Mol. Genet.* 18, 824–834. doi: 10.1093/hmg/ddn408

Iwata, Y., Katanosaka, Y., Hisamitsu, T., and Wakabayashi, S. (2007). Enhanced Na+/H+ exchange activity contributes to the pathogenesis of muscular dystrophy via involvement of P2 receptors. *Am. J. Pathol.* 171, 1576–1587. doi: 10.2353/ajpath.2007.070452

Jiao, Q., Takeshima, H., Ishikawa, Y., and Minamisawa, S. (2012). Sarcalumenin plays a critical role in age-related cardiac dysfunction due to decreases in SERCA2a expression and activity. *Cell Calcium* 51, 31–39. doi: 10.1016/j.ceca.2011.10.003

Jorgensen, L. H., Blain, A., Greally, E., Laval, S. H., Blamire, A. M., Davison, B. J., et al. (2011). Long-term blocking of calcium channels in mdx mice results in differential effects on heart and skeletal muscle. *Am. J. Pathol.* 178, 273–283. doi: 10.1016/j.ajpath.2010.11.027

Jung, C., Martins, A. S., Niggli, E., and Shirokova, N. (2008). Dystrophic cardiomyopathy: amplification of cellular damage by Ca^{2+} signalling and reactive oxygen species-generating pathways. *Cardiovasc. Res.* 77, 766–773. doi: 10.1093/cvr/cvm089

Kang, C., Badr, M. A., Kyrychenko, V., Eskelinen, E. L., and Shirokova, N. (2018). Deficit in PINK1/PARKIN-mediated mitochondrial autophagy at late stages of dystrophic cardiomyopathy. *Cardiovasc. Res.* 114, 90–102. doi: 10.1093/cvr/cvx201

Kho, C., Lee, A., Jeong, D., Oh, J. G., Gorski, P. A., Fish, K., et al. (2015). Small-molecule activation of SERCA2a SUMOylation for the treatment of heart failure. *Nat. Commun.* 6:7229. doi: 10.1038/ncomms8229

Kim, J. H., Kwak, H. B., Thompson, L. V., and Lawler, J. M. (2013). Contribution of oxidative stress to pathology in diaphragm and limb muscles with Duchenne muscular dystrophy. *J. Muscle Res. Cell Motil.* 34, 1–13. doi: 10.1007/s10974-012-9330-9

Kirschner, J., Schessl, J., Schara, U., Reitter, B., Stettner, G. M., Hobbiebrunken, E., et al. (2010). Treatment of Duchenne muscular dystrophy with ciclosporin A: a randomised, double-blind, placebo-controlled multicentre trial. *Lancet Neurol.* 9, 1053–1059. doi: 10.1016/S1474-4422(10)70196-4

Koenig, M., Monaco, A. P., and Kunkel, L. M. (1988). The complete sequence of dystrophin predicts a rod-shaped cytoskeletal protein. *Cell* 53, 219–228.

Koenig, X., Rubi, L., Obermair, G. J., Cervenka, R., Dang, X. B., Lukacs, P., et al. (2014). Enhanced currents through L-type calcium channels in cardiomyocytes disturb the electrophysiology of the dystrophic heart. *Am. J. Physiol. Heart Circ. Physiol.* 306, H564–H573. doi: 10.1152/ajpheart.00441.2013

Kranias, E. G., and Hajjar, R. J. (2012). Modulation of cardiac contractility by the phospholamban/SERCA2a regulatome. *Circ. Res.* 110, 1646–1660. doi: 10.1161/CIRCRESAHA.111.259754

Kuo, I. Y., and Ehrlich, B. E. (2015). Signaling in muscle contraction. *Cold Spring Harb. Perspect. Biol.* 7:a006023. doi: 10.1101/cshperspect.a006023

Kuznetsov, A. V., Winkler, K., Wiedemann, F. R., von Bossanyi, P., Dietzmann, K., and Kunz, W. S. (1998). Impaired mitochondrial oxidative phosphorylation in skeletal muscle of the dystrophin-deficient mdx mouse. *Mol. Cell. Biochem.* 183, 87–96. doi: 10.1023/a:1006868130002

Kwon, H. W., Kwon, B. S., Kim, G. B., Chae, J. H., Park, J. D., Bae, E. J., et al. (2012). The effect of enalapril and carvedilol on left ventricular dysfunction in middle childhood and adolescent patients with muscular dystrophy. *Korean Circ. J.* 42, 184–191. doi: 10.4070/kcj.2012.42.3.184

Kwong, J. Q., and Molkentin, J. D. (2015). Physiological and pathological roles of the mitochondrial permeability transition pore in the heart. *Cell Metab.* 21, 206–214. doi: 10.1016/j.cmet.2014.12.001

Kyrychenko, S., Kyrychenko, V., Badr, M. A., Ikeda, Y., Sadoshima, J., and Shirokova, N. (2015a). Pivotal role of miR-448 in the development of ROS-induced cardiomyopathy. *Cardiovasc. Res.* 108, 324–334. doi: 10.1093/cvr/cvv238

Kyrychenko, V., Polakova, E., Janicek, R., and Shirokova, N. (2015b). Mitochondrial dysfunctions during progression of dystrophic cardiomyopathy. *Cell Calcium* 58, 186–195. doi: 10.1016/j.ceca.2015.04.006

Lamb, G. D. (2000). Excitation-contraction coupling in skeletal muscle: comparisons with cardiac muscle. *Clin. Exp. Pharmacol. Physiol.* 27, 216–224. doi: 10.1046/j.1440-1681.2000.03224.x

Lancel, S., Qin, F., Lennon, S. L., Zhang, J., Tong, X., Mazzini, M. J., et al. (2010). Oxidative posttranslational modifications mediate decreased SERCA activity and myocyte dysfunction in Galphaq-overexpressing mice. *Circ. Res.* 107, 228–232. doi: 10.1161/CIRCRESAHA.110.217570

Lanner, J. T., Georgiou, D. K., Joshi, A. D., and Hamilton, S. L. (2010). Ryanodine receptors: structure, expression, molecular details, and function in calcium release. *Cold Spring Harb. Perspect. Biol.* 2:a003996. doi: 10.1101/cshperspect.a003996

Law, M. L., Prins, K. W., Olander, M. E., and Metzger, J. M. (2018). Exacerbation of dystrophic cardiomyopathy by phospholamban deficiency mediated chronically increased cardiac Ca(2+) cycling *in vivo*. *Am. J. Physiol. Heart Circ. Physiol.* 315, H1544–H1552. doi: 10.1152/ajpheart.00341.2018

Lee, E. H. (2010). Ca^{2+} channels and skeletal muscle diseases. *Prog. Biophys. Mol. Biol.* 103, 35–43. doi: 10.1016/j.pbiomolbio.2010.05.003

Lindahl, M., Backman, E., Henriksson, K. G., Gorospe, J. R., and Hoffman, E. P. (1995). Phospholipase A2 activity in dystrophinopathies. *Neuromuscul. Disord.* 5, 193–199. doi: 10.1016/0960-8966(94)00045-b

Loehr, J. A., Stinnett, G. R., Hernandez-Rivera, M., Roten, W. T., Wilson, L. J., Pautler, R. G., et al. (2016). Eliminating Nox2 reactive oxygen species production protects dystrophic skeletal muscle from pathological calcium influx assessed *in vivo* by manganese-enhanced magnetic resonance imaging. *J. Physiol.* 594, 6395–6405. doi: 10.1113/JP272907

Lohan, J., and Ohlendieck, K. (2004). Drastic reduction in the luminal Ca^{2+} -binding proteins calsequestrin and sarcalumenin in dystrophin-deficient cardiac muscle. *Biochim. Biophys. Acta* 1689, 252–258. doi: 10.1016/j.bbadis.2004.04.002

Lopez, J. R., Uryash, A., Faury, G., Esteve, E., and Adams, J. A. (2020). Contribution of TRPC channels to intracellular Ca(2 +) dyshomeostasis in smooth muscle from mdx mice. *Front. Physiol.* 11:126. doi: 10.3389/fphys.2020.00126

Lyon, A. R., Babalis, D., Morley-Smith, A. C., Hedger, M., Suarez Barrientos, A., Foldes, G., et al. (2020). Investigation of the safety and feasibility of AAV1/SERCA2a gene transfer in patients with chronic heart failure supported with a left ventricular assist device - the SERCA-LVAD TRIAL. *Gene Ther.* 27, 579–590. doi: 10.1038/s41434-020-0171-7

MacLennan, D. H., and Kranias, E. G. (2003). Phospholamban: a crucial regulator of cardiac contractility. *Nat. Rev. Mol. Cell Biol.* 4, 566–577. doi: 10.1038/nrm1151

MacLennan, P. A., McArdle, A., and Edwards, R. H. (1991). Effects of calcium on protein turnover of incubated muscles from mdx mice. *Am. J. Physiol.* 260(4 Pt 1), E594–E598. doi: 10.1152/ajpendo.1991.260.4.E594

Makarewich, C. A., Bezprozvannaya, S., Gibson, A. M., Bassel-Duby, R., and Olson, E. N. (2020). Gene therapy with the DWORF micropeptide attenuates cardiomyopathy in mice. *Circ. Res.* 127, 1340–1342. doi: 10.1161/CIRCRESAHA.120.317156

Makarewich, C. A., Munir, A. Z., Schiattarella, G. G., Bezprozvannaya, S., Raguimova, O. N., Cho, E. E., et al. (2018). The DWORF micropeptide enhances contractility and prevents heart failure in a mouse model of dilated cardiomyopathy. *Elife* 7:e38319. doi: 10.7554/eLife.38319

Mareedu, S., Dwivedi, S., Niranjan, N., and Babu, G. J. (2019). "Sarcolipin knockdown therapy for duchenne muscular dystrophy," in *Muscle Gene Therapy,* eds D. Duan and J. R. Mendell (Cham: Springer International Publishing), 405–415.

Mareedu, S., Pachon, R. E., Jayapalraj, T., Fefelova, N., Balakrishnan, R., Niranjan, N., et al. (2021). Sarcolipin haploinsufficiency prevents dystrophic

cardiomyopathy in mdx mice. *Am. J. Physiol. Heart Circ. Physiol.* 320, H200–H210. doi: 10.1152/ajpheart.00601.2020

Markham, B. E., Kernodle, S., Nemzek, J., Wilkinson, J. E., and Sigler, R. (2015). Chronic dosing with membrane sealant poloxamer 188 NF improves respiratory dysfunction in dystrophic Mdx and Mdx/Utrophin-/- mice. *PLoS ONE* 10:e0134832. doi: 10.1371/journal.pone.0134832

Matsumura, C. Y., Pertille, A., Albuquerque, T. C., Santo Neto, H., and Marques, M. J. (2009). Diltiazem and verapamil protect dystrophin-deficient muscle fibers of MDX mice from degeneration: a potential role in calcium buffering and sarcolemmal stability. *Muscle Nerve* 39, 167–176. doi: 10.1002/mus.21188

Matsumura, C. Y., Taniguti, A. P., Pertille, A., Santo Neto, H., and Marques, M. J. (2011). Stretch-activated calcium channel protein TRPC1 is correlated with the different degrees of the dystrophic phenotype in mdx mice. *Am. J. Physiol. Cell Physiol.* 301, C1344–C1350. doi: 10.1152/ajpcell.00056.2011

Mazala, D. A., Pratt, S. J. P., Chen, D., Molkentin, J. D., Lovering, R. M., and Chin, E. R. (2015). SERCA1 overexpression minimizes skeletal muscle damage in dystrophic mouse models. *Am. J. Physiol. Cell Physiol* 308, C699–C709. doi: 10.1152/ajpcell.00341.2014

Mendell, J. R., and Lloyd-Puryear, M. (2013). Report of MDA muscle disease symposium on newborn screening for Duchenne muscular dystrophy. *Muscle Nerve* 48, 21–26. doi: 10.1002/mus.23810

Millay, D. P., Sargent, M. A., Osinska, H., Baines, C. P., Barton, E. R., Vuagniaux, G., et al. (2008). Genetic and pharmacologic inhibition of mitochondrial-dependent necrosis attenuates muscular dystrophy. *Nat. Med.* 14, 442–447. doi: 10.1038/nm1736

Miyatake, S., Shimizu-Motohashi, Y., Takeda, S., and Aoki, Y. (2016). Anti-inflammatory drugs for Duchenne muscular dystrophy: focus on skeletal muscle-releasing factors. *Drug Des. Dev. Ther.* 10, 2745–2758. doi: 10.2147/DDDT.S110163

Moens, P., Baatsen, P. H., and Marechal, G. (1993). Increased susceptibility of EDL muscles from mdx mice to damage induced by contractions with stretch. *J. Muscle Res. Cell Motil.* 14, 446–451.

Monaco, A. P., Neve, R. L., Colletti-Feener, C., Bertelson, C. J., Kurnit, D. M., and Kunkel, L. M. (1986). Isolation of candidate cDNAs for portions of the Duchenne muscular dystrophy gene. *Nature* 323, 646–650. doi: 10.1038/323646a0

Mondin, L., Balghi, H., Constantin, B., Cognard, C., and Sebille, S. (2009). Negative modulation of inositol 1,4,5-trisphosphate type 1 receptor expression prevents dystrophin-deficient muscle cells death. *Am. J. Physiol. Cell Physiol.* 297, C1133–C1145. doi: 10.1152/ajpcell.00048.2009

Moore, T. M., Lin, A. J., Strumwasser, A. R., Cory, K., Whitney, K., Ho, T., et al. (2020). Mitochondrial dysfunction is an early consequence of partial or complete dystrophin loss in mdx mice. *Front. Physiol.* 11:690. doi: 10.3389/fphys.2020.00690

Morgan, J. E., Prola, A., Mariot, V., Pini, V., Meng, J., Hourde, C., et al. (2018). Necroptosis mediates myofibre death in dystrophin-deficient mice. *Nat. Commun.* 9:3655. doi: 10.1038/s41467-018-06057-9

Morine, K. J., Sleeper, M. M., Barton, E. R., and Sweeney, H. L. (2010). Overexpression of SERCA1a in the mdx diaphragm reduces susceptibility to contraction-induced damage. *Hum. Gene Ther.* 21, 1735–1739. doi: 10.1089/hum.2010.077

Mule, F., D'Angelo, S., Tabacchi, G., Amato, A., and Serio, R. (1999). Mechanical activity of small and large intestine in normal and mdx mice: a comparative analysis. *Neurogastroenterol. Motil.* 11, 133–139. doi: 10.1046/j.1365-2982.1999.00142.x

Mule, F., and Serio, R. (2001). Increased calcium influx is responsible for the sustained mechanical tone in colon from dystrophic (mdx) mice. *Gastroenterology* 120, 1430–1437. doi: 10.1053/gast.2001.24054

Murphy, R. M., Larkins, N. T., Mollica, J. P., Beard, N. A., and Lamb, G. D. (2009). Calsequestrin content and SERCA determine normal and maximal Ca^{2+} storage levels in sarcoplasmic reticulum of fast- and slow-twitch fibres of rat. *J. Physiol.* 587, 443–460. doi: 10.1113/jphysiol.2008.163162

Nakada, T., Kashihara, T., Komatsu, M., Kojima, K., Takeshita, T., and Yamada, M. (2018). Physical interaction of junctophilin and the CaV1.1 C terminus is crucial for skeletal muscle contraction. *Proc. Natl. Acad. Sci. U.S.A.* 115, 4507–4512. doi: 10.1073/pnas.1716649115

Nelson, B. R., Makarewich, C. A., Anderson, D. M., Winders, B. R., Troupes, C. D., Wu, F., et al. (2016). A peptide encoded by a transcript annotated as long noncoding RNA enhances SERCA activity in muscle. *Science* 351, 271–275. doi: 10.1126/science.aad4076

Niranjan, N., Mareedu, S., Tian, Y., Kodippili, K., Fefelova, N., Voit, A., et al. (2019). Sarcolipin overexpression impairs myogenic differentiation in Duchenne muscular dystrophy. *Am. J. Physiol. Cell Physiol.* 317, C813–C824. doi: 10.1152/ajpcell.00146.2019

Olthoff, J. T., Lindsay, A., Abo-Zahrah, R., Baltgalvis, K. A., Patrinostro, X., Belanto, J. J., et al. (2018). Loss of peroxiredoxin-2 exacerbates eccentric contraction-induced force loss in dystrophin-deficient muscle. *Nat. Commun.* 9:5104. doi: 10.1038/s41467-018-07639-3

Pal, R., Palmieri, M., Loehr, J. A., Li, S., Abo-Zahrah, R., Monroe, T. O., et al. (2014). Src-dependent impairment of autophagy by oxidative stress in a mouse model of Duchenne muscular dystrophy. *Nat. Commun.* 5:4425. doi: 10.1038/ncomms5425

Pan, Z., Brotto, M., and Ma, J. (2014). Store-operated Ca^{2+} entry in muscle physiology and diseases. *BMB Rep.* 47, 69–79. doi: 10.5483/bmbrep.2014.47.2.015

Pant, M., Sopariwala, D. H., Bal, N. C., Lowe, J., Delfin, D. A., Rafael-Fortney, J., et al. (2015). Metabolic dysfunction and altered mitochondrial dynamics in the utrophin-dystrophin deficient mouse model of duchenne muscular dystrophy. *PLoS ONE* 10:e0123875. doi: 10.1371/journal.pone.0123875

Patergnani, S., Suski, J. M., Agnoletto, C., Bononi, A., Bonora, M., De Marchi, E., et al. (2011). Calcium signaling around Mitochondria Associated Membranes (MAMs). *Cell Commun. Signal.* 9:19. doi: 10.1186/1478-811X-9-19

Pathak, T., and Trebak, M. (2018). Mitochondrial Ca(2+) signaling. *Pharmacol. Ther.* 192, 112–123. doi: 10.1016/j.pharmthera.2018.07.001

Periasamy, M., and Kalyanasundaram, A. (2007). SERCA pump isoforms: their role in calcium transport and disease. *Muscle Nerve* 35, 430–442. doi: 10.1002/mus.20745

Pertille, A., de Carvalho, C. L., Matsumura, C. Y., Neto, H. S., and Marques, M. J. (2010). Calcium-binding proteins in skeletal muscles of the mdx mice: potential role in the pathogenesis of Duchenne muscular dystrophy. *Int. J. Exp. Pathol.* 91, 63–71. doi: 10.1111/j.1365-2613.2009.00688.x

Petrof, B. J., Shrager, J. B., Stedman, H. H., Kelly, A. M., and Sweeney, H. L. (1993). Dystrophin protects the sarcolemma from stresses developed during muscle contraction. *Proc. Natl. Acad. Sci. U.S.A.* 90, 3710–3714.

Plant, D. R., and Lynch, G. S. (2003). Depolarization-induced contraction and SR function in mechanically skinned muscle fibers from dystrophic mdx mice. *Am. J. Physiol. Cell Physiol.* 285, C522–C528. doi: 10.1152/ajpcell.00369.2002

Prosser, B. L., Ward, C. W., and Lederer, W. J. (2011). X-ROS signaling: rapid mechano-chemo transduction in heart. *Science* 333, 1440–1445. doi: 10.1126/science.1202768

Protasi, F. (2002). Structural interaction between RYRs and DHPRs in calcium release units of cardiac and skeletal muscle cells. *Front. Biosci.* 7, d650–d658. doi: 10.2741/A801

Quinlan, J. G., Wong, B. L., Niemeier, R. T., McCullough, A. S., Levin, L., and Emanuele, M. (2006). Poloxamer 188 failed to prevent exercise-induced membrane breakdown in mdx skeletal muscle fibers. *Neuromuscul. Disord.* 16, 855–864. doi: 10.1016/j.nmd.2006.09.016

Raturi, A., and Simmen, T. (2013). Where the endoplasmic reticulum and the mitochondrion tie the knot: the mitochondria-associated membrane (MAM). *Biochim. Biophys. Acta* 1833, 213–224. doi: 10.1016/j.bbamcr.2012.04.013

Reeve, J. L., McArdle, A., and Jackson, M. J. (1997). Age-related changes in muscle calcium content in dystrophin-deficient mdx mice. *Muscle Nerve* 20, 357–360. doi: 10.1002/(SICI)1097-4598(199703)20:3<357::AID-MUS14>3.0.CO;2-Y

Reutenauer, J., Dorchies, O. M., Patthey-Vuadens, O., Vuagniaux, G., and Ruegg, U. T. (2008). Investigation of Debio 025, a cyclophilin inhibitor, in the dystrophic mdx mouse, a model for Duchenne muscular dystrophy. *Br. J. Pharmacol.* 155, 574–584. doi: 10.1038/bjp.2008.285

Rios, E. (2018). Calcium-induced release of calcium in muscle: 50 years of work and the emerging consensus. *J. Gen. Physiol.* 150, 521–537. doi: 10.1085/jgp.201711959

Rizzuto, R., Pinton, P., Carrington, W., Fay, F. S., Fogarty, K. E., Lifshitz, L. M., et al. (1998). Close contacts with the endoplasmic reticulum as determinants of mitochondrial Ca^{2+} responses. *Science* 280, 1763–1766. doi: 10.1126/science.280.5370.1763

Robert, V., Massimino, M. L., Tosello, V., Marsault, R., Cantini, M., Sorrentino, V., et al. (2001). Alteration in calcium handling at the subcellular

level in mdx myotubes. *J. Biol. Chem.* 276, 4647–4651. doi: 10.1074/jbc.M006337200

Robin, G., Berthier, C., and Allard, B. (2012). Sarcoplasmic reticulum Ca^{2+} permeation explored from the lumen side in mdx muscle fibers under voltage control. *J. Gen. Physiol.* 139, 209–218. doi: 10.1085/jgp.201110738

Rybalka, E., Timpani, C. A., Cooke, M. B., Williams, A. D., and Hayes, A. (2014). Defects in mitochondrial ATP synthesis in dystrophin-deficient mdx skeletal muscles may be caused by complex I insufficiency. *PLoS ONE* 9:e115763. doi: 10.1371/journal.pone.0115763

Sabourin, J., Lamiche, C., Vandebrouck, A., Magaud, C., Rivet, J., Cognard, C., et al. (2009). Regulation of TRPC1 and TRPC4 cation channels requires an alpha1-syntrophin-dependent complex in skeletal mouse myotubes. *J. Biol. Chem.* 284, 36248–36261. doi: 10.1074/jbc.M109.012872

Santulli, G., Nakashima, R., Yuan, Q., and Marks, A. R. (2017). Intracellular calcium release channels: an update. *J. Physiol.* 595, 3041–3051. doi: 10.1113/JP272781

Schiavone, M., Zulian, A., Menazza, S., Petronilli, V., Argenton, F., Merlini, L., et al. (2017). Alisporivir rescues defective mitochondrial respiration in Duchenne muscular dystrophy. *Pharmacol Res.* 125(Pt B), 122–131. doi: 10.1016/j.phrs.2017.09.001

Schneider, J. S., Shanmugam, M., Gonzalez, J. P., Lopez, H., Gordan, R., Fraidenraich, D., et al. (2013). Increased sarcolipin expression and decreased sarco(endo)plasmic reticulum Ca^{2+} uptake in skeletal muscles of mouse models of Duchenne muscular dystrophy. *J. Muscle Res. Cell Motil.* 34, 349–356. doi: 10.1007/s10974-013-9350-0

Selsby, J., Pendrak, K., Zadel, M., Tian, Z., Pham, J., Carver, T., et al. (2010). Leupeptin-based inhibitors do not improve the mdx phenotype. *Am. J. Physiol. Regul. Integr. Comp. Physiol.* 299, R1192–R1201. doi: 10.1152/ajpregu.00586.2009

Shaikh, S. A., Sahoo, S. K., and Periasamy, M. (2016). Phospholamban and sarcolipin: are they functionally redundant or distinct regulators of the Sarco(Endo)Plasmic Reticulum Calcium ATPase? *J. Mol. Cell. Cardiol.* 91, 81–91. doi: 10.1016/j.yjmcc.2015.12.030

Shanmuga Sundaram, J., Mohana Rao, V., Meena, A. K., and Anandaraj, M. P. (2006). Altered expression, intracellular distribution and activity of lymphocyte calpain II in Duchenne muscular dystrophy. *Clin. Chim. Acta* 373, 82–87. doi: 10.1016/j.cca.2006.05.004

Shannon, T. R. (2009). Ryanodine receptor Ca^{2+} sensitivity and excitation-contraction coupling in muscular dystrophy and heart failure: similar and yet different. *Am. J. Physiol. Heart Circ. Physiol* 297, H1965–H1966. doi: 10.1152/ajpheart.00945.2009

Shin, J. H., Bostick, B., Yue, Y., Hajjar, R., and Duan, D. (2011). SERCA2a gene transfer improves electrocardiographic performance in aged mdx mice. *J. Transl. Med.* 9:132. doi: 10.1186/1479-5876-9-132

Shirokova, N., and Niggli, E. (2013). Cardiac phenotype of Duchenne Muscular Dystrophy: insights from cellular studies. *J. Mol. Cell. Cardiol.* 58, 217–224. doi: 10.1016/j.yjmcc.2012.12.009

Silva, M. T., Wensing, L. A., Brum, P. C., Camara, N. O., and Miyabara, E. H. (2014). Impaired structural and functional regeneration of skeletal muscles from beta2-adrenoceptor knockout mice. *Acta Physiol.* 211, 617–633. doi: 10.1111/apha.12329

Simpson, P. B., Mehotra, S., Lange, G. D., and Russell, J. T. (1997). High density distribution of endoplasmic reticulum proteins and mitochondria at specialized Ca^{2+} release sites in oligodendrocyte processes. *J. Biol. Chem.* 272, 22654–22661. doi: 10.1074/jbc.272.36.22654

Simpson, P. B., and Russell, J. T. (1997). Role of sarcoplasmic/endoplasmic-reticulum Ca^{2+}-ATPases in mediating Ca^{2+} waves and local Ca2+-release microdomains in cultured glia. *Biochem. J.* 325 (Pt 1), 239–247. doi: 10.1042/bj3250239

Skura, C. L., Fowler, E. G., Wetzel, G. T., Graves, M., and Spencer, M. J. (2008). Albuterol increases lean body mass in ambulatory boys with Duchenne or Becker muscular dystrophy. *Neurology* 70, 137–143. doi: 10.1212/01.WNL.0000287070.00149.a9

Smani, T., Zakharov, S. I., Csutora, P., Leno, E., Trepakova, E. S., and Bolotina, V. M. (2004). A novel mechanism for the store-operated calcium influx pathway. *Nat. Cell Biol.* 6, 113–120. doi: 10.1038/ncb1089

Smani, T., Zakharov, S. I., Leno, E., Csutora, P., Trepakova, E. S., and Bolotina, V. M. (2003). Ca^{2+}-independent phospholipase A2 is a novel determinant of store-operated Ca^{2+} entry. *J. Biol. Chem.* 278, 11909–11915. doi: 10.1074/jbc.M210878200

Smith, W. N., Dirks, A., Sugiura, T., Muller, S., Scarpace, P., and Powers, S. K. (2002). Alteration of contractile force and mass in the senescent diaphragm with beta(2)-agonist treatment. *J. Appl. Physiol.* 92, 941–948. doi: 10.1152/japplphysiol.00576.2001

Spencer, M. J., Croall, D. E., and Tidball, J. G. (1995). Calpains are activated in necrotic fibers from mdx dystrophic mice. *J. Biol. Chem.* 270, 10909–10914. doi: 10.1074/jbc.270.18.10909

Spencer, M. J., and Mellgren, R. L. (2002). Overexpression of a calpastatin transgene in mdx muscle reduces dystrophic pathology. *Hum. Mol. Genet.* 11, 2645–2655. doi: 10.1093/hmg/11.21.2645

Sperl, W., Skladal, D., Gnaiger, E., Wyss, M., Mayr, U., Hager, J., et al. (1997). High resolution respirometry of permeabilized skeletal muscle fibers in the diagnosis of neuromuscular disorders. *Mol. Cell. Biochem.* 174, 71–78.

Spinazzola, J. M., and Kunkel, L. M. (2016). Pharmacological therapeutics targeting the secondary defects and downstream pathology of Duchenne muscular dystrophy. *Expert Opin. Orphan Drugs* 4, 1179–1194. doi: 10.1080/21678707.2016.1240613

Spurney, C. F., Knoblach, S., Pistilli, E. E., Nagaraju, K., Martin, G. R., and Hoffman, E. P. (2008). Dystrophin-deficient cardiomyopathy in mouse: expression of Nox4 and Lox are associated with fibrosis and altered functional parameters in the heart. *Neuromuscul. Disord.* 18, 371–381. doi: 10.1016/j.nmd.2008.03.008

Sudevan, S., Takiura, M., Kubota, Y., Higashitani, N., Cooke, M., Ellwood, R. A., et al. (2019). Mitochondrial dysfunction causes Ca(2+) overload and ECM degradation-mediated muscle damage in *C. elegans*. *FASEB J.* 33, 9540–9550. doi: 10.1096/fj.201802298R

Szabadkai, G., Bianchi, K., Varnai, P., De Stefani, D., Wieckowski, M. R., Cavagna, D., et al. (2006). Chaperone-mediated coupling of endoplasmic reticulum and mitochondrial Ca^{2+} channels. *J. Cell Biol.* 175, 901–911. doi: 10.1083/jcb.200608073

Tanihata, J., Nagata, T., Ito, N., Saito, T., Nakamura, A., Minamisawa, S., et al. (2018). Truncated dystrophin ameliorates the dystrophic phenotype of mdx mice by reducing sarcolipin-mediated SERCA inhibition. *Biochem. Biophys. Res. Commun.* 505, 51–59. doi: 10.1016/j.bbrc.2018.09.039

Terry, R. L., Kaneb, H. M., and Wells, D. J. (2014). Poloxamer [corrected] 188 has a deleterious effect on dystrophic skeletal muscle function. *PLoS ONE* 9:e91221. doi: 10.1371/journal.pone.0091221

Tidball, J. G., Albrecht, D. E., Lokensgard, B. E., and Spencer, M. J. (1995). Apoptosis precedes necrosis of dystrophin-deficient muscle. *J. Cell Sci.* 108 (Pt 6), 2197–2204.

Touyz, R. M., Anagnostopoulou, A., Rios, F., Montezano, A. C., and Camargo, L. L. (2019). NOX5: molecular biology and pathophysiology. *Exp. Physiol.* 104, 605–616. doi: 10.1113/EP086204

Townsend, D., Turner, I., Yasuda, S., Martindale, J., Davis, J., Shillingford, M., et al. (2010). Chronic administration of membrane sealant prevents severe cardiac injury and ventricular dilatation in dystrophic dogs. *J. Clin. Invest.* 120, 1140–1150. doi: 10.1172/JCI41329

Turner, P. R., Fong, P. Y., Denetclaw, W. F., and Steinhardt, R. A. (1991). Increased calcium influx in dystrophic muscle. *J. Cell Biol.* 115, 1701–1712. doi: 10.1083/jcb.115.6.1701

Turner, P. R., Westwood, T., Regen, C. M., and Steinhardt, R. A. (1988). Increased protein degradation results from elevated free calcium levels found in muscle from mdx mice. *Nature* 335, 735–738. doi: 10.1038/335735a0

Valladares, D., Utreras-Mendoza, Y., Campos, C., Morales, C., Diaz-Vegas, A., Contreras-Ferrat, A., et al. (2018). IP3 receptor blockade restores autophagy and mitochondrial function in skeletal muscle fibers of dystrophic mice. *Biochim. Biophys. Acta* 1864, 3685–3695. doi: 10.1016/j.bbadis.2018.08.042

Vance, J. E. (2015). Phospholipid synthesis and transport in mammalian cells. *Traffic* 16, 1–18. doi: 10.1111/tra.12230

Vandebrouck, A., Sabourin, J., Rivet, J., Balghi, H., Sebille, S., Kitzis, A., et al. (2007). Regulation of capacitative calcium entries by alpha1-syntrophin: association of TRPC1 with dystrophin complex and the PDZ domain of alpha1-syntrophin. *FASEB J.* 21, 608–617. doi: 10.1096/fj.06-6683com

Vandebrouck, C., Martin, D., Colson-Van Schoor, M., Debaix, H., and Gailly, P. (2002). Involvement of TRPC in the abnormal calcium influx observed in

dystrophic (mdx) mouse skeletal muscle fibers. *J. Cell Biol.* 158, 1089–1096. doi: 10.1083/jcb.200203091

Viola, H. M., Davies, S. M., Filipovska, A., and Hool, L. C. (2013). L-type Ca(2+) channel contributes to alterations in mitochondrial calcium handling in the mdx ventricular myocyte. *Am. J. Physiol. Heart Circ. Physiol.* 304, H767–H775. doi: 10.1152/ajpheart.00700.2012

Voit, A., Patel, V., Pachon, R., Shah, V., Bakhutma, M., Kohlbrenner, E., et al. (2017). Reducing sarcolipin expression mitigates Duchenne muscular dystrophy and associated cardiomyopathy in mice. *Nat. Commun.* 8:1068. doi: 10.1038/s41467-017-01146-7

Wang, Q., Wang, W., Wang, G., Rodney, G. G., and Wehrens, X. H. (2015). Crosstalk between RyR2 oxidation and phosphorylation contributes to cardiac dysfunction in mice with Duchenne muscular dystrophy. *J. Mol. Cell Cardiol.* 89(Pt B), 177–184. doi: 10.1016/j.yjmcc.2015.11.009

Wasala, N. B., Yue, Y., Lostal, W., Wasala, L. P., Niranjan, N., Hajjar, R. J., et al. (2020). Single SERCA2a therapy ameliorated dilated cardiomyopathy for 18 months in a mouse model of duchenne muscular dystrophy. *Mol. Ther.* 28, 845–854. doi: 10.1016/j.ymthe.2019.12.011

Whitehead, N. P., Yeung, E. W., and Allen, D. G. (2006). Muscle damage in mdx (dystrophic) mice: role of calcium and reactive oxygen species. *Clin. Exp. Pharmacol. Physiol.* 33, 657–662. doi: 10.1111/j.1440-1681.2006.04394.x

Williams, G. S., Boyman, L., Chikando, A. C., Khairallah, R. J., and Lederer, W. J. (2013). Mitochondrial calcium uptake. *Proc. Natl. Acad. Sci. U.S.A.* 110, 10479–10486. doi: 10.1073/pnas.1300410110

Williams, I. A., and Allen, D. G. (2007a). Intracellular calcium handling in ventricular myocytes from mdx mice. *Am. J. Physiol. Heart Circ. Physiol.* 292, H846–H855. doi: 10.1152/ajpheart.00688.2006

Williams, I. A., and Allen, D. G. (2007b). The role of reactive oxygen species in the hearts of dystrophin-deficient mdx mice. *Am. J. Physiol. Heart Circ. Physiol.* 293, H1969–H1977. doi: 10.1152/ajpheart.00489.2007

Woods, C. E., Novo, D., DiFranco, M., and Vergara, J. L. (2004). The action potential-evoked sarcoplasmic reticulum calcium release is impaired in mdx mouse muscle fibres. *J. Physiol.* 557(Pt 1), 59–75. doi: 10.1113/jphysiol.2004.061291

Yasuda, S., Townsend, D., Michele, D. E., Favre, E. G., Day, S. M., and Metzger, J. M. (2005). Dystrophic heart failure blocked by membrane sealant poloxamer. *Nature* 436, 1025–1029. doi: 10.1038/nature03844

Yeung, E. W., Head, S. I., and Allen, D. G. (2003). Gadolinium reduces short-term stretch-induced muscle damage in isolated mdx mouse muscle fibres. *J. Physiol.* 552(Pt 2), 449–458. doi: 10.1113/jphysiol.2003.047373

Yeung, E. W., Whitehead, N. P., Suchyna, T. M., Gottlieb, P. A., Sachs, F., and Allen, D. G. (2005). Effects of stretch-activated channel blockers on [Ca2+]i and muscle damage in the mdx mouse. *J. Physiol.* 562(Pt 2), 367–380. doi: 10.1113/jphysiol.2004.075275

Young, C. N., Brutkowski, W., Lien, C. F., Arkle, S., Lochmuller, H., Zablocki, K., et al. (2012). P2X7 purinoceptor alterations in dystrophic mdx mouse muscles: relationship to pathology and potential target for treatment. *J. Cell. Mol. Med.* 16, 1026–1037. doi: 10.1111/j.1582-4934.2011.01397.x

Young, C. N. J., Chira, N., Rog, J., Al-Khalidi, R., Benard, M., Galas, L., et al. (2018). Sustained activation of P2X7 induces MMP-2-evoked cleavage and functional purinoceptor inhibition. *J. Mol. Cell Biol.* 10, 229–242. doi: 10.1093/jmcb/mjx030

Yu, L., Zhang, X., Yang, Y., Li, D., Tang, K., Zhao, Z., et al. (2020). Small-molecule activation of lysosomal TRP channels ameliorates Duchenne muscular dystrophy in mouse models. *Sci. Adv.* 6:eaaz2736. doi: 10.1126/sciadv.aaz2736

Zanou, N., Iwata, Y., Schakman, O., Lebacq, J., Wakabayashi, S., and Gailly, P. (2009). Essential role of TRPV2 ion channel in the sensitivity of dystrophic muscle to eccentric contractions. *FEBS Lett.* 583, 3600–3604. doi: 10.1016/j.febslet.2009.10.033

Zsebo, K., Yaroshinsky, A., Rudy, J. J., Wagner, K., Greenberg, B., Jessup, M., et al. (2014). Long-term effects of AAV1/SERCA2a gene transfer in patients with severe heart failure: analysis of recurrent cardiovascular events and mortality. *Circ. Res.* 114, 101–108. doi: 10.1161/CIRCRESAHA.113.302421

Conflict of Interest: The authors declare that the research was conducted in the absence of any commercial or financial relationships that could be construed as a potential conflict of interest.

frontiers in Physiology

ORIGINAL RESEARCH
published: 03 May 2021
doi: 10.3389/fphys.2021.642908

Metformin *I*ncreases *S*arcolemma *I*ntegrity and *A*meliorates *N*euromuscular *D*eficits in a *M*urine *M*odel of Duchenne *M*uscular *D*ystrophy

*Xia Dong[1,2†], Tiankun Hui[2,3†], Jie Chen[2,3], Zheng Yu[2], Dongyan Ren[2,3], Suqi Zou[2,3], Shunqi Wang[2,3], Erkang Fei[2,3], Huifeng Jiao[1] and Xinsheng Lai[2,3]**

[1] School of Basic Medical Sciences, Nanchang University, Nanchang, China, [2] Laboratory of Synaptic Development and Plasticity, Institute of Life Science, Nanchang University, Nanchang, China, [3] School of Life Sciences, Nanchang University, Nanchang, China

OPEN ACCESS

Edited by:
Helen Cristina Miranda,
Case Western Reserve University,
United States

Reviewed by:
Jose R. Lopez,
Mount Sinai Medical Center,
United States
Annamaria De Luca,
University of Bari Aldo Moro, Italy

***Correspondence:**
Xinsheng Lai
laixinsheng@ncu.edu.cn

[†] These authors have contributed equally to this work

Specialty section:
This article was submitted to Striated Muscle Physiology, a section of the journal Frontiers in Physiology

Received: 17 December 2020
Accepted: 12 April 2021
Published: 03 May 2021

Citation:
Dong X, Hui T, Chen J, Yu Z, Ren D, Zou S, Wang S, Fei E, Jiao H and Lai X (2021) Metformin Increases Sarcolemma Integrity and Ameliorates Neuromuscular Deficits in a Murine Model of Duchenne Muscular Dystrophy. Front. Physiol. 12:642908. doi: 10.3389/fphys.2021.642908

Duchenne muscular dystrophy (DMD) is a genetic neuromuscular disease characterized by progressive muscle weakness and wasting. Stimulation of AMP-activated protein kinase (AMPK) has been demonstrated to increase muscle function and protect muscle against damage in dystrophic mice. Metformin is a widely used anti-hyperglycemic drug and has been shown to be an indirect activator of AMPK. Based on these findings, we sought to determine the effects of metformin on neuromuscular deficits in mdx murine model of DMD. In this study, we found metformin treatment increased muscle strength accompanied by elevated twitch and tetanic force of tibialis anterior (TA) muscle in mdx mice. Immunofluorescence and electron microscopy analysis of metformin-treated mdx muscles revealed an improvement in muscle fiber membrane integrity. Electrophysiological studies showed the amplitude of miniature endplate potentials (mEPP) was increased in treated mice, indicating metformin also improved neuromuscular transmission of the mdx mice. Analysis of mRNA and protein levels from muscles of treated mice showed an upregulation of AMPK phosphorylation and dystrophin-glycoprotein complex protein expression. In conclusion, metformin can indeed improve muscle function and diminish neuromuscular deficits in mdx mice, suggesting its potential use as a therapeutic drug in DMD patients.

Keywords: Duchenne muscular dystrophy, metformin, AMP-activated protein kinase, skeletal muscle, neuromuscular junction

Abbreviations: DMD, Duchenne muscular dystrophy; AMPK, AMP-activated protein kinase; TA, tibialis anterior; EDL, extensor digitorum longus; mEPP, miniature endplate potentials; EPPs, endplate potentials; DGC, dystrophin-glycoprotein complex; T2D, type 2 diabetes; NMJ, neuromuscular junction; CK, creatine kinase; EBD, evans blue dye; HE, hematoxylin and eosin; CLN, centrally located nuclei; NF, neurofilament; SYN, synaptophysin; α-BTX, α-bungarotoxin; ROS, reactive oxygen species.

INTRODUCTION

Duchenne muscular dystrophy (DMD), an X-linked recessive neuromuscular disease with an incidence of 1 in 3600–6000 boys (Emery, 1991; Bushby et al., 2010), is caused by loss-of-function mutations or deletions in gene encoding dystrophin. Dystrophin is a plasma membrane protein within the dystrophin-glycoprotein complex (DGC), which forms a bridge between the extracellular matrix and the intracellular cytoskeleton in healthy sarcolemma (Muntoni et al., 2003; Davies and Nowak, 2006; Quan and Gao, 2015). In DMD, lack of dystrophin disrupts this bridge and breaks down the membrane integrity of muscle fiber, leading to muscle wasting and degeneration (Campbell and Kahl, 1989). Mdx (X-linked muscular dystrophy) mouse, which does not express dystrophin, is a well-known mouse model for DMD with a characteristic of muscle weakness (Bulfield et al., 1984; Hoffman et al., 1987b).

AMP-activated protein kinase is a serine/threonine protein kinase and a critical regulator of energy metabolism. It is activated by elevations in cellular ADP and AMP/ATP ratio due to metabolic stress, such as glucose deficiency, hypoxia, and muscle contractile activity (Winder and Hardie, 1996; Salt et al., 1998; Marsin et al., 2000). AMPK activation has been shown to play an essential role in maintaining and remodeling skeletal muscle function (Mounier et al., 2015; Kjøbsted et al., 2018). Muscle-specific AMPK β1β2 double-knockout mice display a significant myopathy with increased split, necrotic myofibers and centrally nucleated myofibers (Thomas et al., 2014). During muscle regeneration, AMPK is critical for the normal process of macrophage skewing, which is required for proper regeneration (Mounier et al., 2013). Chronic activation of AMPK reduces skeletal muscle fragility but enhances the enhances the myogenesis of slow-twitch, oxidative muscle (Ljubicic et al., 2011). In mdx mice, chronic activation of AMPK with AMPK activator AICAR (5-aminoimidazole-4-carboxamide-1-β-D-ribofuranoside) induced a slow oxidative muscle fiber program and improved the dystrophic pathology (Ljubicic et al., 2012; Ljubicic and Jasmin, 2013; Lynch, 2017). These evidences indicate that AMPK activation plays a beneficial role in skeletal muscle function maintenance and the potential therapeutic effect on DMD.

Metformin is a widely used anti-diabetic agent recommended as a first-line oral therapy for type 2 diabetes (T2D) (Inzucchi et al., 2012). Beyond the T2D, metformin has also been shown to be effective for cancer treatment, cardiovascular, anxiety, polycystic ovary syndrome, and other diseases (Barbieri, 2003; Cabreiro et al., 2013; Hong et al., 2013; Bailey, 2017; Zemdegs et al., 2019). Moreover, metformin is an indirect agonist of AMPK by targeting hepatocyte mitochondria, leading to decreased ATP/AMP ratio (Zhou et al., 2001). Considering the beneficial role of AMPK activation in skeletal muscle function, we hypothesized that metformin has a potential therapeutic effect on DMD (Viollet et al., 2012). Recently, some reports support our hypothesis. Metformin protects skeletal muscle from cardiotoxin-induced injury (Langone et al., 2014). Expression of utrophin A, which is autosomal homolog of dystrophin and serves as a compensate functionally target for the lack of dystrophin, increased after 42 days of muscle treatment with metformin in mdx mice (Ljubicic and Jasmin, 2015). More importantly, treatment with L-arginine and metformin clinically delayed the disease progression and effectively prevent the loss of DMD motor function and muscle degeneration in 7–10 years old DMD boys (ClinicalTrials.gov identifier: NCT01995032) (Hafner et al., 2016, 2019).

Here, we studied the effect of metformin on skeletal muscle and neuromuscular junction (NMJ) deficits in mdx mice. We found that metformin increased muscle strength, improved muscle sarcolemma integrity and NMJ transmission in mdx mice. Our results explored the pharmacological action of metformin on dystrophic muscles suggested the potential efficacy of metformin as a metabolic enhancer in DMD treatment.

MATERIALS AND METHODS

Mouse Lines and Drug Treatment Dose

Mdx mice (C57BL/10ScSn-Dmd^{mdx}/J) were purchased from The Jackson Laboratory (stock # 001801). Before treatment, a total of 50 male mdx mice and 20 male wild-type control mice (WT, C57BL/10ScSn/J) aged 4–5 weeks were acclimatized for 1 week in the animal facility before the experimental procedures. For treatment, mdx mice were randomly assigned to two subgroups. One group was intraperitoneally injected with metformin (D150959-5G, Sigma, 200 mg/kg, n = 25) everyday, and the other group was intraperitoneally injected with normal saline (0.9% NaCl, n = 25) everyday. Wild-type mice (n = 20), were intraperitoneally injected with normal saline (0.9% NaCl) everyday. After 30, 60, and 90 days of treatment, six mice from each group were taken out for further experiments (**Figure 1A**). Experimental procedures were approved by the Institutional Animal Care and Use Committee of the Nanchang University.

Reagents and Antibodies

Chemicals were purchased from Sigma-Aldrich unless otherwise indicated. CF568 α-bungarotoxin (α-BTX, #00006, 1:1000 for staining) was purchased from Biotium. Antibodies including AMPKα (2603, 1:1000 for Western blot), phospho-AMPKα (Thr^{172}) (2535, 1:1000 for Western blot), Neurofilament (2837S, 1:1000 for staining) and Synapsin (5297S, 1:1000 for staining) were from Cell Signaling Technology; laminin (#041M4799, 1:200 for staining) from Sigma-Aldrich; GAPDH (HRP-60004; 1:2000 for Western blot) and α-dystroglycan (106110; 1:1000 for Western blot and staining) from Abcam, eMyHC (F1.652; 1:200 for staining) from DSHB. Alex-aFluor-488 goat anti-rabbit IgG (A11034, 1:1000 for staining), AlexaFluor-488 goat anti-mouse IgG (A11029, 1:1000 for staining), and AlexaFluor-568 goat anti-rabbit IgG (A11036,1:1000 for staining) were from Invitrogen. HRP-conjugated goat anti-rabbit IgG (32260), goat anti-mouse IgG (32230) antibodies (1:2000 for Western blot) were from Invitrogen.

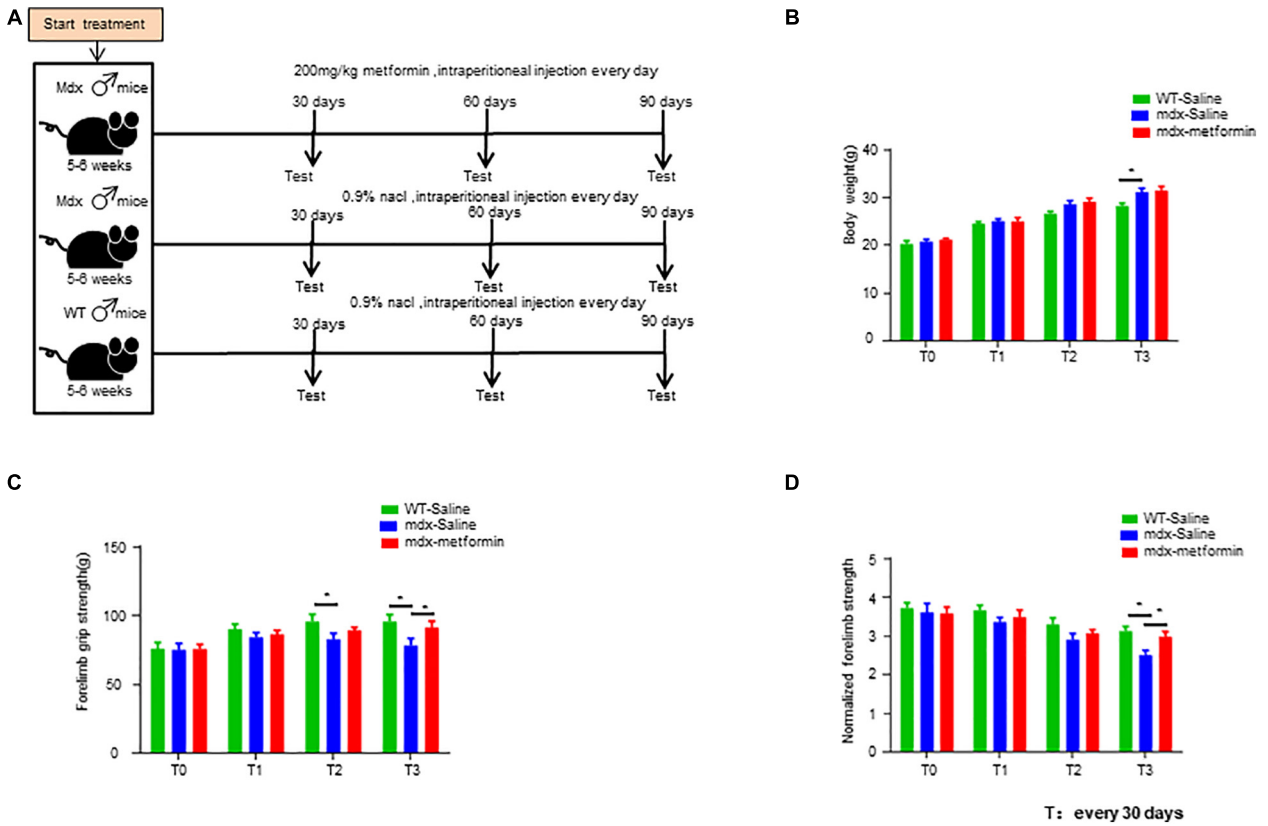

FIGURE 1 | Metformin treatment increased muscle strength in mdx mice. **(A)** Scheme of the metformin treatment in mice. Intraperitoneal injection of metformin (50 μl, 200 mg/kg) or normal saline (50 μl, 0.9% NaCl) for 1–3 months. **(B)** Bodyweight of wild-type (WT) mice and metformin treated/untreated mdx mice at the beginning of treatment (T0) and after 1, 2, and 3 months (T1, T2, T3). Weight was recorded every month. Statistical analysis was conducted using a unpaired *t*-test. $*p < 0.05$, $**p < 0.01$. $N = 6$ mice per group. **(C)** Forelimb grip strength of WT mice and metformin treated/untreated mdx mice at the beginning of treatment (T0) and after 1, 2, and 3 months (T1, T2, T3). Forelimb grip strength was recorded once a month. Statistical analysis was conducted using a unpaired *t*-test. $*p < 0.05$, $**p < 0.01$, $N = 6$ mice per group. **(D)** Normalization of forelimb grip strength by body weight at the beginning of treatment (T0) and at 1, 2, and 3 months after treatment (T1, T2, T3) in WT and metformin treated/untreated mdx mice. Statistical analysis was conducted using a unpaired *t*-test. $*p < 0.05$, $**p < 0.01$, $***p < 0.001$. $N = 6$ mice per group.

Body Weight and Muscle Strength

Body weight was measured by the electronic scale. Muscle strength was measured by SR-1 hanging scale (American Weigh Scales) (Shen et al., 2013; Barik et al., 2014). Briefly, mice were allowed with forelimbs to grasp a grid that was connected to a scale. Their tails were gently pulled until the grid was released by the forelimbs, and readings of the scale were recorded.

In vivo Twitch and Tetanic Force Measurement

Torque muscle tension analysis was performed on male mice as previously reported (Ingalls et al., 1985; Arpke et al., 2013). Briefly, mice were anesthetized with isoflurane continuously supplied by VetFlo anesthesia system (Kent Scientific) and placed on a 37°C heating pad. With gentle pressing the knee clamps, left feet were fixed onto the footplate that was connected to the servomotor (Aurora Scientific 1300A). For muscle stimulation, two needle electrodes were inserted subcutaneously into TA muscle close to the knee. The best position of muscle contraction was found by adjusting the distance between the footplate and the knee and measuring the muscle force by stimulating muscle with a single electrical stimulation (100 mA current, 0.2 ms pulse width). When the muscle force was no longer increasing, the position was the best position of muscle contraction. To identify best stimulation strength, a single muscle electrical stimulation was given starting at 100 mA current, 0.2 ms pulse width in the best position, the muscle force was measured every 30 mA increase, with an interval of 30 s. When the muscle force was no longer increasing, the current was the best stimulation strength. In the best position and the best stimulation strength, twitch force was measured by stimulating muscle with a single electrical stimulation (0.2 ms pulse width), repeating 10 times with an interval of 30 s. Tetanic force was measured by stimulating muscle with 300 ms duration, 0.2 ms pulse width at a series of frequencies from 50 to 150 Hz (50, 100, 150 Hz) with an interval of 2 min. For nerve stimulation, the sciatic nerve was exposed at thigh level and stimulated by two needle electrodes that were close to both sides of the nerve. After finding out the best position

and the best stimulation intensity, nerve-stimulated twitch and tetanic were measured. Twitch and tetanic forces were normalized by body weight.

Electromyography and Electrophysiological Recording

Electrophysiology recording was performed as described previously (Barik et al., 2016; Zhao et al., 2017). Mice were anesthetized with ketamine and xylazine mixture (100 and 10 mg/kg body weight, respectively) on a 37°C heating pad, left hemi-diaphragm together with ribs and phrenic nerves were dissected, mounted on Sylgard gel, and perfused in oxygenated (95% O_2/5% CO_2) Ringer's solution (136.8 mM NaCl, 5 mM KCl, 12 mM $NaHCO_3$, 1 mM NaH_2PO_4, 1 mM $MgCl_2$, 2 mM $CaCl_2$, and 11 mM D-glucose, pH 7.3) at room temperature. To record miniature endplate potentials (mEPPs), microelectrodes with 20–50 MΩ were filled with 3M KCl and pierced into the muscle fiber with the macroscopic adjacent of nerve with the resting potential between –65 and –80 mV. Ten recordings were performed and each last about 3 min. For endplate potentials (EPPs), phrenic nerves were stimulated by a suction electrode with suprathreshold square pulses. Muscle contraction was blocked by adding 2.5 μM μ-Conotoxin. Twenty minutes later the phrenic nerve was sucked into electrode and stimulated. The data was collected with MultiClamp 700B amplifier which digitized (10 kHz low-pass filtered) with Digidata 1550A and analyzed in Clampfit10.5 software.

Serum Creatine Kinase Measurement

Mice were deeply anesthetized with isoflurane, and blood samples were obtained by cardiac puncture. Blood was centrifuged at 10,000 rpm for 10 min at 4°C. Serum creatine kinase (CK) levels were measured using a CK activity assay kit (MAK116-1KT, Sigma) and a spectrophotometer according to the manufacturer's protocol. When measuring CK, the wavelength of the instrument was set to 340 nm.

Immunofluorescence

Muscles were fixed with 4% PFA in PBS at room temperature 20 min, rinsed with 0.1 M glycine in PBS for 30 min, and incubated with the blocking buffer (5% BSA, 2% Triton X-100, 5% goat serum in PBS) for 2 h at room temperature. They were then incubated with primary antibodies in blocking buffer at 4°C overnight. After washing three times for 1 h each with 2% Triton X-100 in PBS, the samples were incubated with fluorescent-labeled secondary antibodies in PBS 2 h at room temperature. Muscle samples were then washed with 2% TritonX-100 in PBS three times for 1 h each and mounted with Vectashield mounting medium (H1200) and coverslip. For muscle cross-section staining, muscles were fixed with 4% PFA in PBS at 4°C overnight. After dehydration by 30% sucrose at 4°C overnight, muscles were frozen at –80°C in Cryo-embedding medium (Ted Pella) and cut into 15 μm sections on a Frozen slicing machine (Leica CM900). Sections were incubated with the blocking buffer for 2 h at room temperature and then with primary antibodies in the blocking buffer at 4°C overnight. After washing three times for 30 min each with 2% Triton X-100 in PBS at room temperature, the samples were incubated with fluorescent-labeled secondary antibodies in PBS 2 h at room temperature. The samples were mounted with Vectashield mounting medium. Z serial images were collected with a Zeiss confocal laser scanning microscope (LSM 700) and collapsed into a single image.

Hematoxylin and Eosin Staining (HE)

Muscle cross sections (15 μm) were stained with hematoxylin and eosin, dehydrated through ascending, graded ethanol washes, cleared with toluene, and then mounted with Permount (Fisher Scientific, Ottawa, Canada). They were visualized at 4.2× magnification using a light microscope and the ratio of myofibers with centralized nuclei to the total number of fibers in the muscle section was counted from the acquired high resolution images.

Evans Blue Dye Staining

Evans blue (EBD) were purchased from Sigma (St. Louis, MO, United States). The dyes were dissolved in phosphate-buffered saline (PBS; 0.15M NaCl, 10 mM phosphate buffer, pH7.0) sterilized by passage through membrane filters with a pore size of 0.2 μm and kept at 4°C. Dye solution was injected intravenously through the celiac vein (1 mg dye/0.1 ml/10 g body weight) and 3–24 h after injection, mice were killed with an over-dose of ether gas. To prepare cryosections, fresh tissues were embedded in OTC compound (Miles, Elkhart, IN, United States) and frozen immediately in isopentane at –70°C. Frozen tissues were then sectioned at a thickness of 15 μm by a cryostat. EBD binds to albumin and is detected by fluorescence microscopy (at 568 nm) in the extracellular space. Presence of the proteinbound dye inside the muscle fiber indicates damage to the sarcolemma. Here, the sections were assessed blindly, and the myofibers were judged in a binary fashion, as positive or negative for intracellular EBD.

Masson's Trichrome Staining

The masson's trichrome staining was conducted using ready-to-use kit (Masson's Trichrome Stain Kit, G1340, Solarbio). Briefly, the muscle tissue cut into 10 μm sections on a Frozen slicing machine (Leica CM900). Sections were then immersed in Bouin's solution (G2331, Solarbio) at room temperature overnight; stained in Weigert's hematoxylin for 5 min, differentiation in acid ethanol solution for 10 s, washing with tap water for 1 min, then used Masson blue solution to return to blue for 5 min and washed again with tap water for 1 min and rinsed in distilled water for 1 min. Next, the sections were stained in Ponceau Magenta staining solution for 5 min, washed with phosphomolybdic acid solution for 1 min, and washed with 0.2% acetic acid for 1 min. Dyed directly in the aniline blue staining solution for 1 min, and washed with 0.2% acetic acid for 1 min. Finally, dehydrated and mounted.

Electron Microscopy

Precooling glutaraldehyde fixative solution before muscle tissue extraction. Removed TA muscle from the body after the mice were deeply anesthetized. the muscle tissue samples were cut into 1 mm^3 pieces and immersed into 0.5% glutaraldehyde

fixative for 2 min. Fixed in 2.5% glutaraldehyde fixative solution at 4°C overnight. Fixed tissues were washed with PBS and rinses with 100% propylene oxide three times. Muscle samples were embedded in plastic resin. Ultrathin cross sections were cut at 80∼100 nm and mounted on 200-mesh unsupported copper grids and stained with a solution containing 50% methanol, 3.5% sodium citrate, 3% uranylacetate, and 2.6% lead nitrate. Micrographs were taken by using JEOL 100CXII operated at 80 KeV.

Western Blot Analysis

Western blot was performed as described previously (Barik et al., 2014). Briefly, each protein sample was separated by SDS-polyacrylamide gel electrophoresis, transferred to a nitrocellulose membrane, blocked with 5% milk in Tris-buffered saline/0.1% Tween 20, and hybridized with the following primary antibodies: anti-α-dystroglycan (1:1000, Abcam), anti-AMPKα (1:1000, Cell Signaling), anti-Phospho-AMPKα (Thr172) (1:1000, Cell Signaling), and GAPDH (1:2000, Abcam). The membranes were then incubated with anti-rabbit or anti-mouse horseradish peroxidase (HRP)-conjugated secondary antibody (1:2000, Invitrogen). Detection of the signal was accomplished using western HRP chemiluminescence (ECL) reagents (Thermo), and imaging of the blots was performed using ChemiDoc^{TM} MP System (Bio-Rad). To analyze the blots, Image Lab^{TM} Software (Bio-Rad) was used to quantify band intensity and calculate the absorbance ratio of the target protein to the loading control.

Quantitative Real-Time PCR Analysis

Total RNA was purified from gastrocnemius with Trizol reagent (Invitrogen, NY, United States), 500 ng of total RNA were converted to cDNA by using a reverse transcription kit (Takara, Japan) and oligo (dT) primers. cDNAs were used as template in qPCR in a 20 μL reaction system containing SYBR GreenER qPCR mix with gene-specific primers (**Table 1**). PCR included an initial step at 95°C (3 min), followed by 40 cycles consisting of denaturation at 95°C (15 s), annealing and extension at 60°C (60 s). Using this method, the GAPDH were used as reference in each sample.

Statistical Analysis

Data were analyzed by unpaired *t*-test, one-way ANOVA, and two-way ANOVA. Unless otherwise indicated, data were shown as mean ± SEM. Statistical difference was considered when $p < 0.05$.

RESULTS

Increased Muscle Strength After Metformin Treatment in mdx Mice

The dose of metformin whas chosen based on previous studies (Mantuano et al., 2018). Here, we opted for intraperitoneal injection for a simpler determination of the daily dose to be administered to each mouse. Male mdx and WT mice aged 5–6 weeks were intraperitoneally injected with metformin (50 μl, 200 mg/kg) or normal saline (50 μl, 0.9% NaCl) for 1–3 months (**Figure 1A**). No differences in bodyweight were found between metformin treated and control group (**Figure 1B**). However, the forelimb grip strength of metformin-treated mdx mice was significantly increased by 8.54 ± 2.733% after 3 months of treatment (T3) (**Figures 1C,D**).

To determine the pathological mechanism of metformin increasing muscle strength, we measured muscle contractions by stimulating nerves and muscles, respectively. Nerve stimulation requires appropriate neuromuscular conduction to cause muscle contraction, whereas direct muscle stimulation does not. As shown in **Figures 2A–D**, by direct muscle stimulation, twitch and tetanic force were increased after metformin treatment in mdx mice, even at 2 months after treatment, earlier than forelimb grip strength increase. However, by nerve stimulation, there was no difference of twitch force between untreated and treated mdx mice, only tetanic force increased in treated mdx mice after 3 months (**Figures 2E–H**). Together, these results suggest that muscle strength improvement in mdx mice by metformin treatment may be mainly due to repaired muscle membrane, because twitch and tetanic force increased more and earlier by direct muscle stimulation.

Improved the Sarcolemma Integrity of Muscle Fibers

In DMD patients and mdx mice, loss of dystrophin leads to muscle sarcolemma fragile due to the disruption of sarcolemma integrity (Campbell and Kahl, 1989; Quan and Gao, 2015). We then asked whether metformin improves the muscle

TABLE 1 | Primer sequence used in the qRT-PCR.

Name	Forward (5′-3′)	Reverse (5′-3′)
GAPDH	GTGAAGGTCGGTGTGAACGG	CAAGCTTCCCATTCTCGGCCT
Dystrobrevin	CGGCTTGATGAAGAACACAGGC	CGATGGTGAAGGAGATGTCAGG
β1-syntrophin	AGCCTCTGTCATCCCAGTCCTT	GTGTGCTTAGCATCTGGCGAGT
β2-syntrophin	GCTGTGACTGAGAAGGACTTGC	GTGACCGACATCCAGAACCTGA
α-syntrophin	CAGTTGGTGGATGGCTGTCATC	GTGAAGCCCTTGTCGATGTGCA
Dystroglycan	GTGGTTGGCATTCCAGACGGTA	CAGTGTAGCCAAGACGGTAAGG
Sarcoglycan α	GGTCGTGTGTTTGTGCATCC	CACGATCTTCTGGAGTGGGG
Sarcoglycan β	GGCAACTTAGCCATCTGCGTGA	GTGGAACTCCATGCTATCACACC
Sarcoglycan γ	GTGACAGTCAGTGCTCGCAACT	GCAGAGAACAGTGGCTTGCCAT
Sarcoglycan δ	TGAGACTGGAGTCCAAGGATGG	CTCGAAGACCTTCTGCCTCGTT

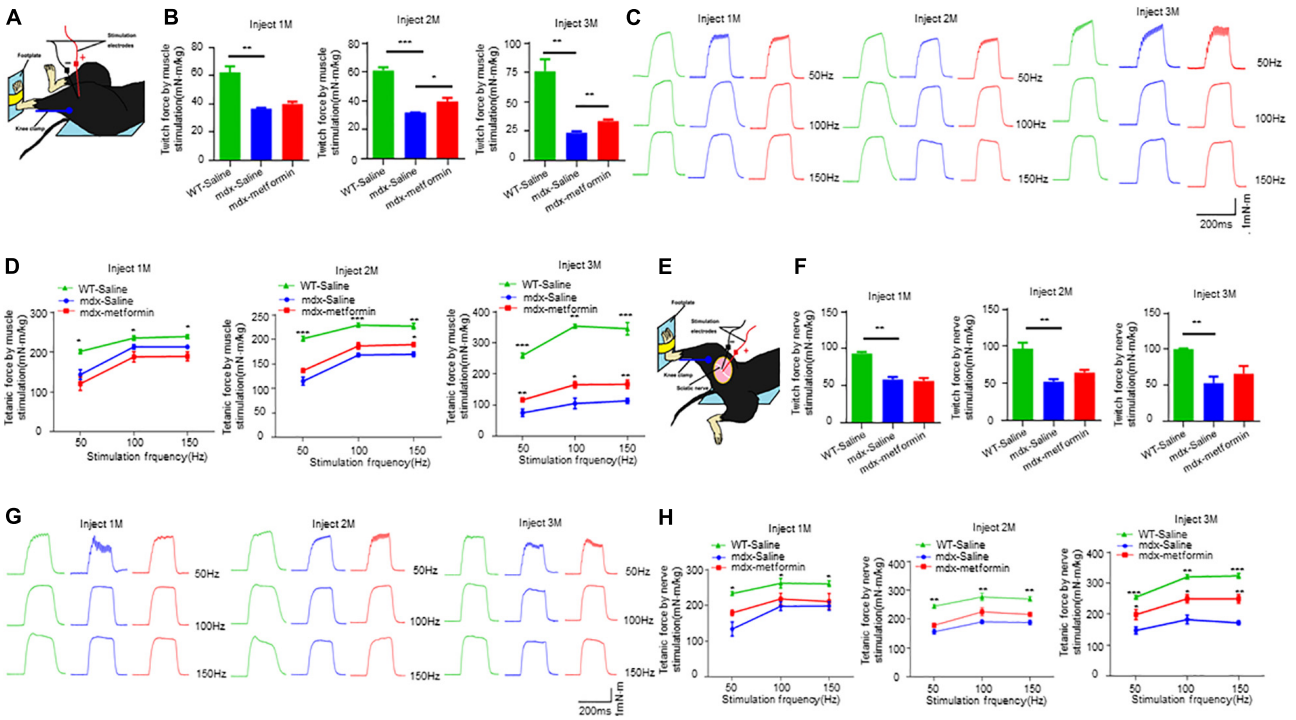

FIGURE 2 | Metformin increased twitch and tetanic force by nerve and muscle stimulation in mdx mice. **(A)** Scheme of in vivo muscle twitch and tetanic force measurement by muscle stimulation. **(B)** After 1, 2, and 3 months of treatment, twitch force between WT mice and metformin treated/untreated mdx mice by muscle stimulation. After 2 and 3 months of treatment with metformin, the twitch force of mdx mice increased. Statistical analysis was conducted using a one-way ANOVA.*$p < 0.05$, **$p < 0.01$, ***$p < 0.001$. $N = 6$ mice per group. **(C)** After 1, 2, and 3 months of treatment, representative tetanic curves at stimulation frequency 50, 100, and 150 Hz by muscle stimulation. **(D)** After 1, 2, and 3 months of treatment, tetanic force between WT mice and metformin treated/untreated mdx mice by muscle stimulation. After treatment with metformin for 3 months, the tetanic force of mdx mice increased. Statistical analysis was conducted using a two-way ANOVA.*$p < 0.05$, **$p < 0.01$, ***$p < 0.001$. $N = 6$ mice per group. **(E)** Scheme of *in vivo* muscle twitch and tetanic force measurement by nerve stimulation. **(F)** After 1, 2, and 3 months of treatment, twitch force between WT mice and metformin treated/untreated mdx mice by nerve stimulation. Statistical analysis was conducted using a one-way ANOVA.**$p < 0.01$. $N = 6$ mice per group. **(G)** After 1, 2, and 3 months of treatment, representative tetanic curves at stimulation frequency 50, 100, and 150 Hz by nerve stimulation. **(H)** After 1, 2, and 3 months of treatment, tetanic force between WT mice and metformin treated/untreated mdx mice by nerve stimulation. After treatment with metformin for 3 months, the tetanic force of mdx mice increased. Statistical analysis was conducted using a two-way ANOVA. *$p < 0.05$, **$p < 0.01$, ***$p < 0.001$. $N = 6$ mice per group.

sarcolemma integrity in mdx mice. Firstly, we analyzed the serum levels of CK, a skeletal muscle enzyme released during fiber degeneration. As shown in **Figure 2**. A, CK levels of mdx mice was expectedly higher than WT mice, but significantly decreased after 3-month metformin treatment (310.2 ± 5.757 vs. 283.2 ± 2.926), suggesting a decrease in severity of muscle damage. Furthermore, tibialis anterior (TA) muscles were stained with HE and analyzed for the presence of centrally located nuclei (CLN). A 6.136 ± 2.124% increase in CLN percentage was observed in the metformin-treated mdx TA muscle compared with control, and the muscle total damage area (necrosis, infiltration, and non-muscle area) decreased by 3.393 ± 1.503%, suggesting promotion of muscle fiber regeneration after metformin treatment (**Figures 3B–E**). Moreover, Masson's trichrome staining was also used to visualize the fibrosis in muscle by detecting collagen fibers. As shown in metformin treatment reduced the area ratio of muscle fibrosis in mdx mice after 3 months (**Figures 3F,G**).

To further determine the effect of metformin on muscle regeneration in mdx mice, we investigated embryonic myosin heavy chain (eMyHC) positive fibers, which represents newly formed muscle fibers, in TA muscle. Consistently, an increased number of eMyHC positive muscle fibers were observed in metformin-treated mdx mice (**Figures 4A,B**). To investigate if metformin can improve the integrity of the muscle membrane by reducing the fragility of the muscle fiber membrane in mdx mice, Evans Blue Dye (EBD) assay was used to evaluate the muscle membrane integrity of TA muscle fiber in mdx mice (Hamer et al., 2002). As shown in **Figures 4C,D**, after metformin treatment, the EBD positive muscle fibers decreased in mdx mice. These results suggest that metformin treatment improved the muscle fiber membrane integrity in mdx mice. To further confirm this, cross sections of TA muscles were collected for electron microscopy examination. As shown in **Figure 4E**, in metformin-treated mdx mice, the muscle basement membrane was significantly thickened and integrated more than that in control mice. Together, these results suggest that metformin treatment significantly improved muscle membrane integrity in mdx mice.

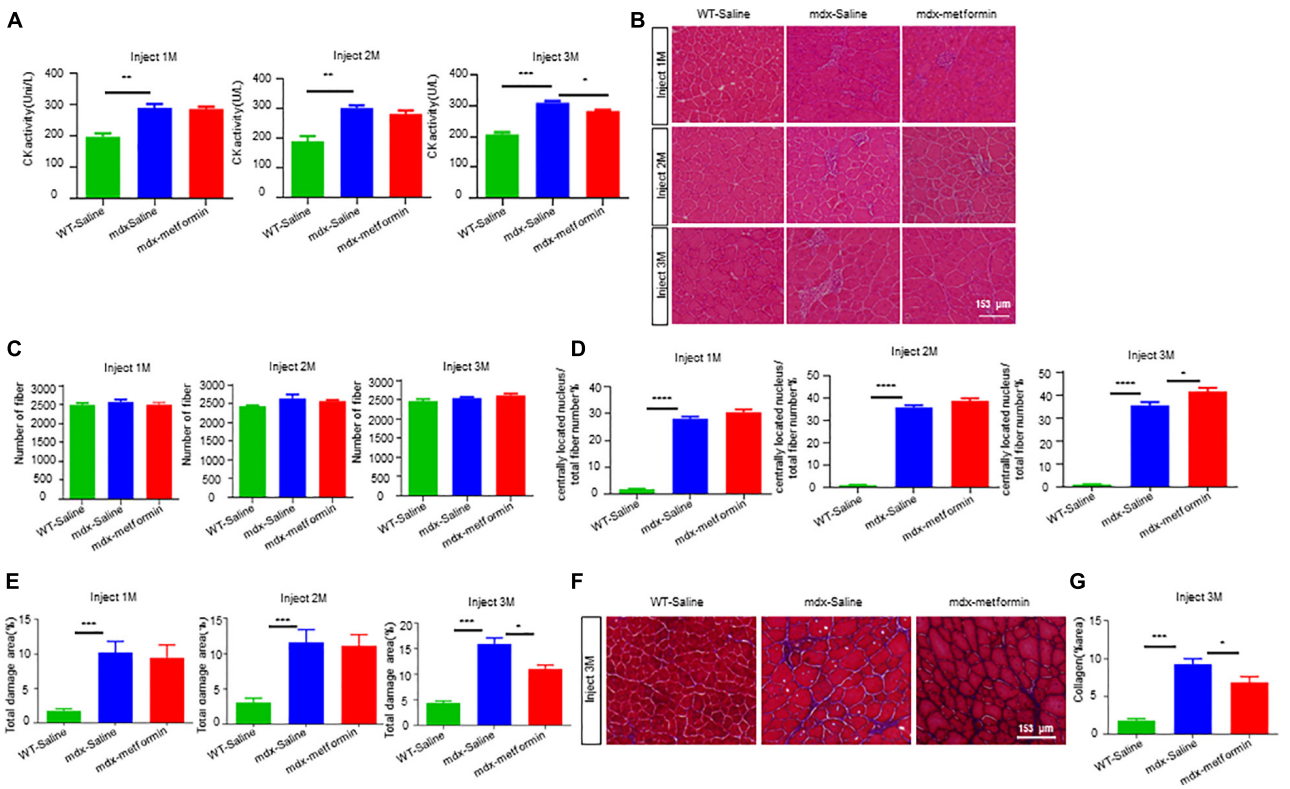

FIGURE 3 | Metformin promoted muscle regeneration in mdx mice. **(A)** Plasma creatine kinase levels in WT mice and metformin untreated/treated mdx mice after 1, 2, and 3 months. Statistical analysis was conducted using a unpaired *t*-test. $^{*}p < 0.05$, $^{**}p < 0.01$, $^{***}p < 0.001$, $^{****}p < 0.0001$. $N = 7$ mice per group. **(B)** Representative images of H&E staining on TA muscle sections of WT mice and metformin untreated/treated mdx mice 1, 2, and 3 months. Scale bar, 153 μm. **(C)** Quantitative analysis of the total number of muscle fibers of TA muscle after 1, 2, and 3 months of WT mice and metformin untreated/treated mdx mice. Statistical analysis was conducted using a unpaired *t*-test. $N = 6$ mice per group. **(D)** Ratio of muscle fibers with central nucleation to total number of muscle fibers. Statistical analysis was conducted using a unpaired *t*-test. $^{*}p < 0.05$, $^{**}p < 0.01$, $^{***}p < 0.001$. $N = 6$ mice per group. **(E)** Percentage of total area of damage area in TA muscles from WT and metformin untreated/treated mdx mice groups. Statistical analysis was conducted using a unpaired *t*-test. $^{*}p < 0.05$, $^{***}p < 0.001$. $N = 6$ mice per group. **(F)** Representative Masson's trichrome staining images of the TA muscles from WT mice, metformin untreated/treated mdx mice for 3 months (collagen fibers were stained blue and muscle red). Scale bar, 153 μm. **(G)** Quantification of the percentage of collagen fiber area in TA muscle after 3 months in WT mice and metformin untreated/treated mdx mice. Statistical analysis was conducted using a unpaired *t*-test. $^{*}p < 0.05$, $^{***}p < 0.001$. $N = 6$ mice per group.

Improved Neuromuscular Transmission

Neuromuscular junction decline is a hallmark of DMD patients and mdx mice. To investigate whether metformin treatment diminishes NMJ structural deficits in mdx mice, extensor digitorum longus (EDL) muscles were stained with α-BTX to label AChR clusters and with anti- Neurofilament (NF)/ Synapsin (SYN) antibodies to label nerve terminals. As expected, NMJs in mdx mice displayed more fragments. However, no difference was observed between metformin-treated and control mdx mice, suggesting metformin treatment did not alter NMJ structure in mdx mice (**Figures 5A–D**).

Neuromuscular junction transmission is impaired in DMD patients and mdx mice with reductions in the amplitudes of mEPP and in AChR density. To test whether metformin treatment ameliorates transmission deficits in mdx mice, we recorded mEPPs and EPPs of muscles in metformin-treated and control mdx mice. mEPPs represents local depolarizations around endplates in response to spontaneous ACh release, as shown in **Figures 6A–C**, mEPP frequency was not altered, but amplitude was increased after 2-month metformin treatment in mdx mice. These results indicate metformin treatment does not affect the presynaptic acetylcholine release but increase the postsynaptic AChR density in mdx mice. After that, we measured EPPs, the local electrical responses in response to nerve stimulation. Accordingly, the EPP amplitude was increased after 2-month metformin treatment in mdx mice (**Figures 6D,E**), suggesting that metformin treatment in mdx mice improved the postsynaptic signal received from nerve stimulation. Together, our findings suggest that metformin improved neuromuscular transmission by postsynaptic, but not presynaptic, component in muscles of mdx mice.

Upregulated AMPK Phosphorylation and DGC Proteins Expression

Previous studies reported metformin indirectly stimulates AMPK signaling in mice. To validate this, we detected the ratio of phosphorylated AMPK (pAMPK)/AMPK in TA muscle samples using western blot (**Figures 7A,B**). Expectedly,

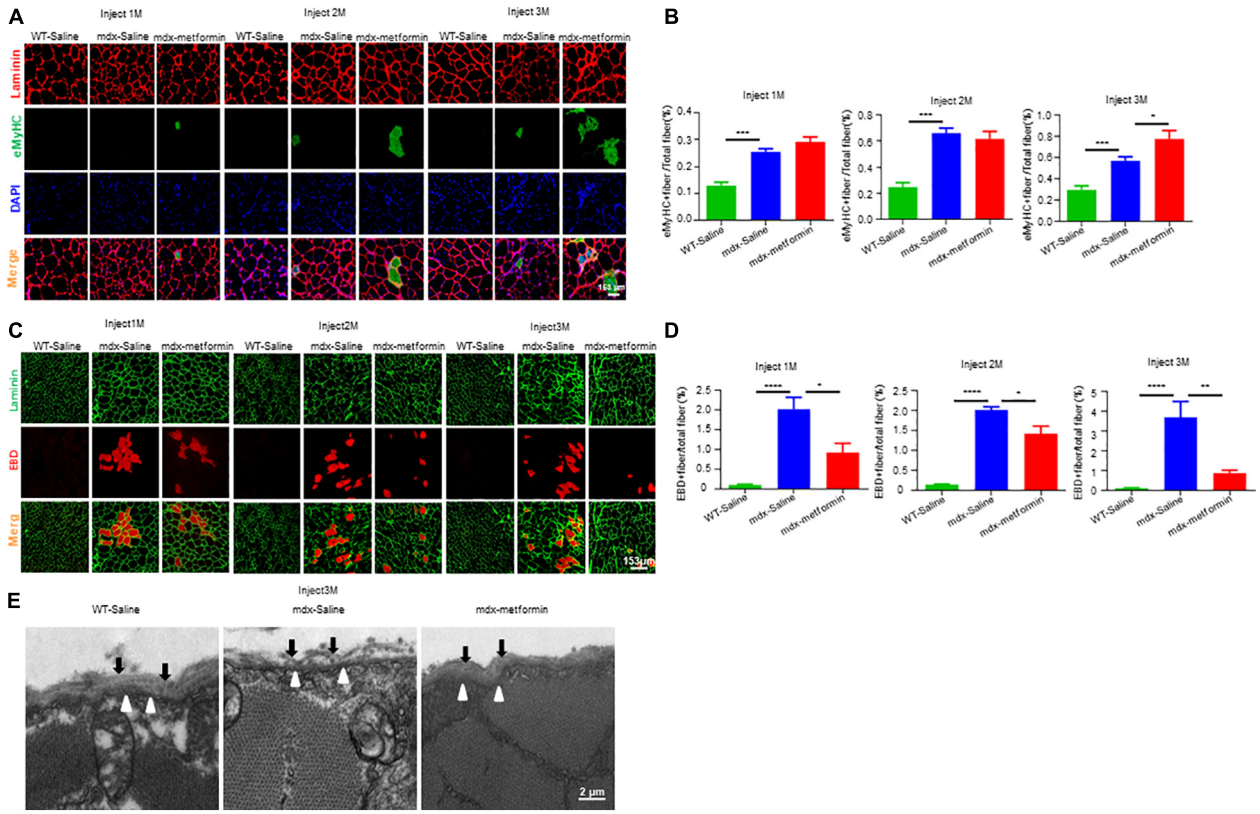

FIGURE 4 | Metformin improved muscle fiber sarcolemma integrity in mdx mice. **(A)** Representative images of TA muscle in WT mice and metformin untreated/treated mdx mice for 1–3 months (eMyHC in green; Laminin in red; DAPI in blue). Scale bar, 153 μm. **(B)** Quantification of eMyHC**+** fiber in TA muscle after 1, 2, and 3 months in WT mice and metformin untreated/treated mdx mice. Statistical analysis was conducted using a unpaired *t*-test. $^{*}p < 0.05$, $^{***}p < 0.001$, $^{****}p < 0.0001$. $N = 6$ mice per group. **(C)** Representative images of Evans blue dye (EBD, red) infiltration in TA muscle after 1, 2, and 3 months in WT mice and metformin untreated/treated mdx mice (laminin in green; EBD in red). Scale bar, 153 μm. **(D)** Quantification of EBD**+** fiber in TA muscle tissue after 1, 2, and 3 months in WT mice and metformin untreated/treated mdx mice. Statistical analysis was conducted using a unpaired *t*-test. $^{*}p < 0.05$, $^{**}p < 0.01$, $^{***}p < 0.001$. $N = 6$ mice per group. **(E)** Representative electron microscopy images of the TA muscles from WT mice, metformin untreated and treated mdx mice for 3 months. The black arrows highlight the substrate structure of the extracellular basement membrane, and the hollow arrows point to the dense plasma membrane. Scale bar, 2 μm.

metformin treatment induced a further increase in the pAMPK/AMPK ratio, and this ratio increased more after the 3-month treatment (T3) (**Figure 7B**). As the results described above, metformin treatment elevated twitch and tetanic contraction by direct muscle stimulation, reduced the muscle membrane's fragility and improved neuromuscular transmission by postsynaptic component (**Figures 2**, **4**, **6**). These results indicate that metformin treatment may increase production of components related to muscle membrane integrity in mdx mice. To test this, we examined mRNA levels of Dystrophin-associated glycoprotein complex (DGC), the protein complex that maintains the stability and functional contraction of the muscle membrane. DGC is composed of transmembrane protein (dystroglycans, sarcoglycans) and intracellular protein (syntrophins, dystrobrevin, dystrophin). β-*syntrophin, dystroglycan and sarcoglycan-a* were upregulated after the 3-month metformin treatment in mdx mice. Notably, mRNA level of *dystroglycan* increased, even in 1-month metformin-treated mdx mice, earlier than other involved proteins (**Figure 7C**). Moreover, immunofluorescence imaging analysis of histological sections from metformin-treated TA muscles showed a noticeable increase in the expression of α-dystroglycan in the sarcolemma (**Figures 7D,E**). Consistently, western blot results also showed that α-dystroglycan protein in the muscles of mdx mice was increased after metformin treatment for 3 months (**Figures 7F,G**).

DISCUSSION

Metformin is one of the most effective and safest agents for anti-hyperglycemic and currently employed as a first-line oral therapy for T2D. It has also demonstrated additional beneficial effects on cancer, cardiovascular disorders, mental disorders, immune and other metabolic diseases (Barbieri, 2003; Hong et al., 2013; Stagi et al., 2017; Ursini et al., 2018; Zemdegs et al., 2019). Previous studies have illustrated the protective effect of metformin on skeletal muscle damage and a potential role in easing DMD patients' symptoms (Langone et al., 2014). In this study, we

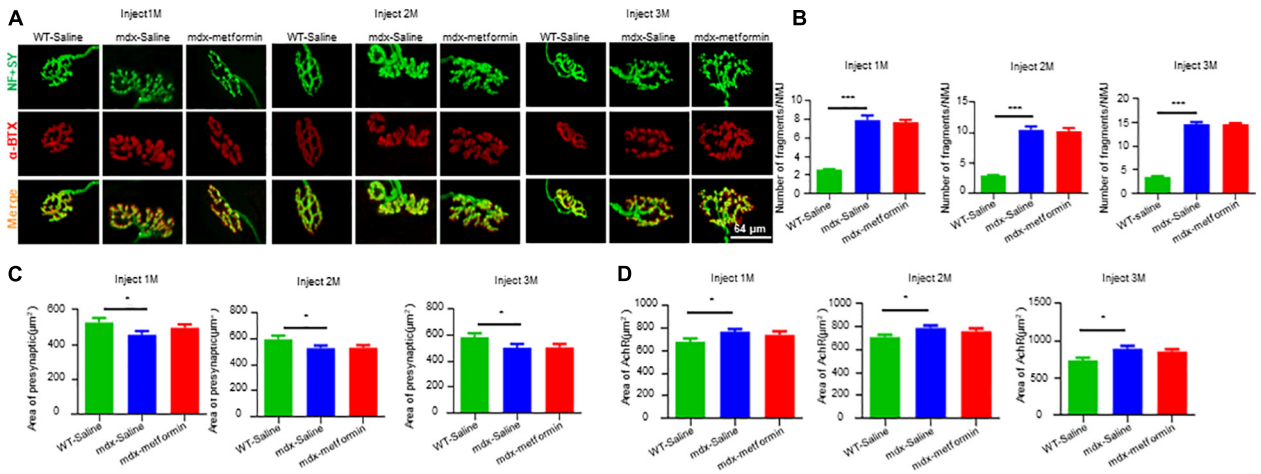

FIGURE 5 | Metformin did not alter NMJ structure in mdx mice. Extensor digitorum longus (EDL) muscle was stained whole-mount with Alexa Fluor 594-conjugated-BTX (red) to label acetylcholine receptor (AChR) and antibodies against NF and SYN (NF/SYN; green) to label axon and terminals. **(A)** Representative images of NMJs after 1, 2, and 3 months in WT and metformin untreated/treated mdx mice. The Scale bar, 64 μm. **(B)** Quantitative analysis of the fragmented number of AChR clusters in EDL muscle tissues of WT mice and metformin untreated/treated mdx mice after 1, 2, and 3 months. Hundred NMJs per mouse were analyzed. Statistical analysis was conducted using a one-way ANOVA. $N = 6$ mice per group. $^{***}p < 0.001$. **(C)** Quantitative analysis of the presynaptic area of NMJs in EDL muscle tissue after 1, 2, and 3 months of WT mice and metformin untreated/treated mdx mice. Twenty NMJs per mouse were analyzed. Statistical analysis was conducted using a one-way ANOVA. $^{*}p < 0.05$. $N = 6$ mice per group. **(D)** Quantitative analysis of NMJs postsynaptic AChR area (AChR area) in EDL muscle tissue of WT mice and metformin untreated/treated mdx mice after 1, 2, and 3 months. Twenty NMJs were analyzed for each mouse. Statistical analysis was conducted using a one-way ANOVA. $^{*}p < 0.05$. $N = 6$ mice per group.

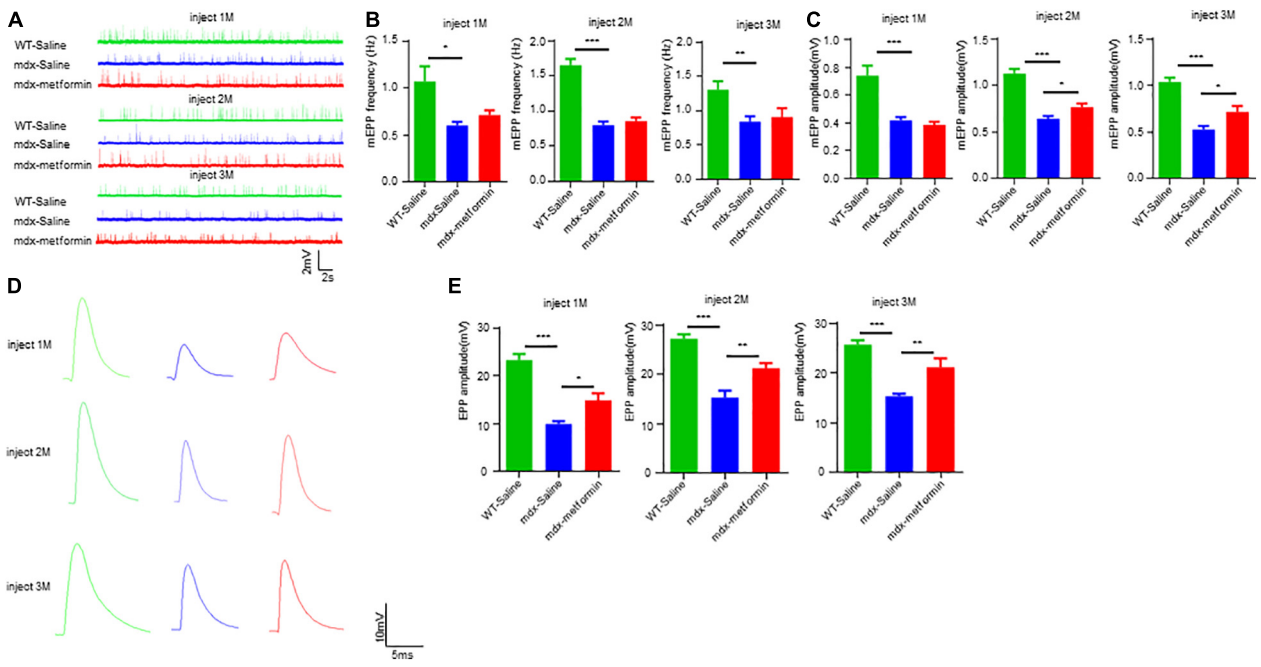

FIGURE 6 | Metformin improved neuromuscular transmission in mdx mice. **(A)** Representative traces of mEPP in WT mice and metformin untreated/treated mdx mice after 1–3 months. **(B)** Quantitative analysis of mEPP frequency in WT mice and metformin untreated/treated mdx mice after 1–3 months. Statistical analysis was conducted using a one-way ANOVA. $^{*}p < 0.05$, $^{**}p < 0.01$, and $^{***}p < 0.001$. $N = 6$ mice per group. **(C)** Quantitative analysis of mEPP amplitude in WT mice and metformin untreated/treated MDX mice after 1–3 months. mEPP amplitude increased after metformin treatment for mdx mice at 2 and 3 months. Statistical analysis was conducted using a one-way ANOVA. $^{*}p < 0.05$, $^{**}p < 0.01$, $^{***}p < 0.001$. $N = 6$ mice per group. **(D)** Representative traces of EPP in WT mice and metformin untreated/treated mdx mice after 1–3 months. **(E)** Quantitative analysis of EPP amplitude in WT mice and metformin untreated/treated MDX mice after 1–3 months. EPP amplitude increased after metformin treatment for mdx mice at 2 and 3 months. Statistical analysis was conducted using a one-way ANOVA. $^{*}p < 0.05$, $^{**}p < 0.01$, $^{***}p < 0.001$. $N = 6$ mice per group.

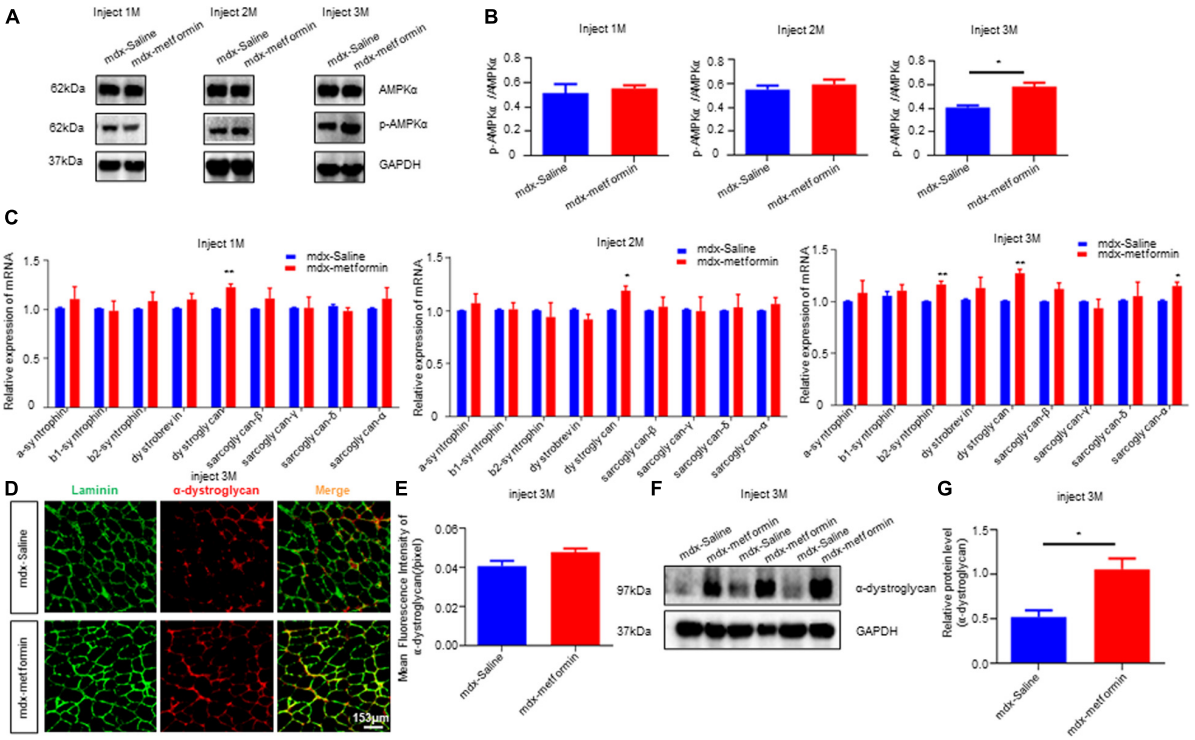

FIGURE 7 | Metformin increased AMPK phosphorylation and DGC proteins expression in mdx mice. **(A)** The figure shows a representative western blot of total AMPKα and phosphorylated AMPKα (p AMPKα) from the tibialis anterior muscle (TA) of metformin treated/untreated mdx mice after 1, 2, and 3 months. *N* = 6 mice per group. **(B)** Quantification of p AMPKα/ AMPKα of **(A)**. *N* = 3 mice group. Statistical analysis was conducted using a unpaired *t*-test. $^{*}P < 0.05$, *N* = 6 mice group. **(C)** Detection of mRNA levels of DGC components in metformin untreated/treated mdx mice after 1, 2, and 3 months. Membrane protein dystroglycan was upregulated after metformin treated. Statistical analysis was conducted using a unpaired *t*-test. $^{*}p < 0.05$, $^{**}p < 0.01$, $^{***}p < 0.001$. *N* = 6 mice per group. **(D)** Representative images of α-dystroglycan immunofluorescence of metformin untreated/treated mdx mice after 3 months. Scale bar, 153 μm. **(E)** Quantitative analysis of α-dystroglycan immunofluorescence intensity in metformin untreated/treated mdx mice after 3 months. Statistical analysis was conducted using a unpaired *t*-test. *N* = 6 mice per group. **(F)** Western blot of α-dystroglycan protein in metformin untreated/treated mdx mice after 3 months. **(G)** Quantitative analysis of the relative expression level of α-dystroglycan protein in metformin untreated/treated mdx mice after 3 months. Statistical analysis was conducted using a unpaired *t*-test. $^{*}p < 0.05$. *N* = 6 mice per group.

investigated the effect of metformin on neuromuscular deficits in the DMD mouse model mdx. Interestingly, we found that metformin treatment alleviates dystrophin deficiency induced muscle weakness. Firstly, metformin treatment in mdx mice increased the forelimb strength force (**Figure 1**), consistent with previous findings that metformin increases muscle strength in the mdx mice (Mantuano et al., 2018). Secondly, after metformin treatment in mdx mice, muscle contraction was significantly increased by muscle stimulation (**Figure 2**). Since the core clinical symptom of DMD is progressive muscle weakness, it first affects the muscles of limb close to the trunk, followed by a gradual loss of muscle strength that usually makes the patient sit in a wheelchair before the age of 13 (Hoffman et al., 1987a). TA muscle, the largest muscle group in the anterior tibia of the lower limbs innervated by the sciatic nerve, was selected for *in vivo* muscle contractions measurement in our present study. Another group also reported that the twitch and tetanic force of isolated diaphragm from metformin-treated mdx mice were significantly improved (Mantuano et al., 2018). Considering muscle weakness is the major cause of dyskinesia in DMD patients, these results can be considered as a potential therapeutic outcome.

Due to the lack of dystrophin, mdx muscle fibers have repeated degeneration/regeneration processes (Torres and Duchen, 1987; Coulton et al., 1988; McGeachie et al., 1993). Our results revealed that the drug significantly improved TA muscle degeneration, decreased the percentage of muscle damage and increased the percentage of central nuclear muscle fibers and eMyHC+ newly formed muscle fibers (**Figure 3**), suggesting that more muscle fiber regeneration occurred after metformin treatment. In addition, the lack of dystrophin leads to improper assembly of DGC to maintain the integrity and stability of the muscle fiber membrane structure, and the muscle fibers become fragile and prone to damage (Campbell and Kahl, 1989). We also showed that metformin significantly improved the incomplete muscle fiber membrane of TA muscles and reduced muscle fragility (**Figure 4**). Our findings add new insights into metformin for the treatment of DMD muscle injury or degeneration. On the other hand, membrane fragility due to dystrophin deficiency causes intracellular Ca^{2+} dysregulation, subsequently results of substantial production of reactive oxygen species (ROS) and mitochondrial dysfunction. While increased oxidative stress results from an unbalance between increased production

of ROS and an insufficient antioxidant response will lead to myonecrosis, inflammatory cell infiltration, adipose tissue accumulation and muscle damage (Whitehead et al., 2010; Pal et al., 2014; Pessina et al., 2015). In particular, increasing oxidative stress was observed in muscle biopsies from DMD patients and reducing ROS level has been recently considered to be one of the treatments for DMD (Scholte et al., 1985; Petrillo et al., 2017). Interestingly, previous studies have shown that metformin has antioxidant properties by enhancing the endogenous cell antioxidant capacity (Onaran et al., 2006; Abd-Elsameea et al., 2014; Zeng et al., 2019). Our results also showed that the percentage of total damage area and the percentage of muscle fibrosis in mdx mice decreased after metformin treatment (**Figure 3**). Future study is needed to determine whether ROS level are also reduced after metformin treated in mdx mice.

The synergy of muscles and nerves regulates muscle strength. NMJ, a synapse between motor neurons and skeletal muscle fibers, is critical for muscle contraction control. Importantly, both human patients and the mouse model for DMD (the mdx mouse) exhibit fragmented NMJ (Kong, 1999; Adams et al., 2000). Studies in mdx mice have revealed presynaptic and postsynaptic abnormalities, nerve terminal discontinuity, as well as related functional changes in neuromuscular transmission and nerve-evoked electromyography (Kong, 1999; Banks et al., 2009; Pratt et al., 2015). Here, we reported for the first time that metformin improved neuromuscular transmission in dystrophic muscles. Meanwhile, we also found that metformin did not improve NMJ structure deficits in mdx mice (**Figure 6**), which is not hard to understand because of the stable NMJ structure. However, it needs a further deep examination of how metformin improves neuromuscular transmission.

AMP-activated protein kinase is a major cellular energy sensor and regulator for metabolic homeostasis. In skeletal muscle, AMPK responds to the deprivation of cellular energy by increasing ATP production, and usually is activated during exercise (Jørgensen et al., 2006). We observed increased activation of AMPKα in the metformin-treated mdx mice by using anti-phospho-AMPKα antibody (**Figure 7**). This finding is consistent with a previous study showing that metformin exerts its effects by activating AMPK in the liver and skeletal muscle (Zhou et al., 2001). The activation of AMPK in dystrophic muscles has great significance for the observed beneficial effects of metformin. Recently, the activation of AMPK has been shown to play an important role in maintaining and remodeling skeletal muscle phenotype in DMD disease (Ljubicic and Jasmin, 2013; Dial et al., 2018a). The chronic induction of skeletal muscle AMPK activity is an attractive treatment for DMD. Activating AMPK mitigates the dystrophic phenotypes and, importantly, can apply to all DMD patients (Ljubicic and Jasmin, 2013; Lynch, 2017). Previous studies have also shown that AMPK activators have beneficial effects in mdx mice. For example, AICAR (an AMPK activator) treatment in mdx mice for 4 weeks significantly improved symptoms including increased overall behavioral activity and limb strength (Jahnke et al., 2012). Our results also suggest that metformin activates AMPK in skeletal muscles of mdx mice. Therefore, the AMPK activation observed in metformin-treated mdx mice may be another potential mechanism for improving dystrophic muscle function (**Figure 7**). Metformin has previously been shown to protect against apoptosis in cardiomyocyte cell, and activating AMPK has been reported to reduce myocardial apoptosis (Morrow et al., 2003; Sasaki et al., 2009). Reducing muscle cell apoptosis in mdx mice might be another possible mechanism of improve muscle function after metformin treatment. However, further investigation on this issue is needed.

The DGC is localized to the muscle membrane and connects the extracellular matrix to the intracellular skeleton, critical for maintaining muscle cells' structural stability (Davies and Nowak, 2006; Quan and Gao, 2015). The DGC promotes muscle NO production by regulating the activity of AMPK as a mechanical sensor (Garbincius and Michele, 2015). On the other hand, AMPK stimulation induces the expression of Dystrophin-associated protein complex (DAPC) in skeletal muscle, and the decrease of AMPK is related to DAPC dysfunction (Dial et al., 2018b). These findings indicate that AMPK is sufficient (but not necessary) to affect DAPC levels. However, in mdx mice, the relationship between AMPK kinase and DGC still unknown. In our present study, we also found that metformin, as an indirect activator of AMPK, up-regulated the expression of DGC components in mdx mice. However, the interaction between AMPK activation and DGC components to improve muscle functions in mdx mice needs to be further explored. Notably, both protein and mRNA levels of α-dystroglycan, a component of DGC, were increased after metformin treatment (**Figure 7**). In DGC, dystroglycan spans the sarcolemma and directly interact with subsarcolemmal proteins and extracellular matrix (ECM) components providing a physical connection between the subsarcolemmal cytoskeleton and basement membrane (Henry and Campbell, 1999; Michele and Campbell, 2003; Lapidos et al., 2004). Studies have shown that the lack of dystroglycan can cause embryonic death in mice (Garbincius and Michele, 2015). When dystroglycan is selectively destroyed in mature muscle fibers, it will lead to fiber instability and degeneration (Dial et al., 2018b). Dystroglycan is cleaved into two subunits after translation, α- and β-dystroglycan. α-dystroglycan is attached to the extracellular cell surface through the transmembrane β-dystroglycan subunit (Ibraghimov-Beskrovnaya et al., 1992; Holt et al., 2000). The polysaccharide carbohydrate moieties of α-dystroglycan are necessary for its binding to ECM proteins such as laminin, agrin, and perlecan (Williamson et al., 1997; Davies and Nowak, 2006; Benziane et al., 2012). Here, our results showed that after metformin treatment in mdx mice, the skeletal muscle membrane's fragility was reduced and the integrity was increased. We hypothesized that these improvements may be resulted from the upregulation of α-dystroglycan on the surface of the muscle membrane.

One of the most notable limitations of the present study was that some protocols used in our study did not follow the international experimental guidelines and standard operating procedures (SOPs) drafted by independent experts engaged in preclinical research of the mdx mouse model[1]. For example, in the test of measuring muscle strength, we did not follow the SOPs due to the limitation of our instrument. Meanwhile, we also have not measured isometric force of isolated mouse skeletal muscles,

[1]https://treat-nmd.org/

which may take advantage on accurate evaluation of muscle contractile function. This may cause some of our data to be unable to be compared with the research of other laboratories, limiting the significance of the present study in pre-clinical research.

In summary, our work showed that metformin enhances muscle functions by affecting the integrity of skeletal muscle cell membranes. The underlying mechanism might mainly rely on the activation of AMPK, the increase of muscle cell regeneration and the decrease of muscle fragility. These findings, combined with the results of recent studies, illustrate the potential efficacy of metformin for DMD treatment, and support the beneficial effects of long-term use of metformin in the treatment of DMD patients with weakened muscle functions. Future research should focus on developing treatment methods to solve the dyskinesia caused by muscle weakness to maximize the recovery of the motor function of DMD patients.

DATA AVAILABILITY STATEMENT

The raw data supporting the conclusions of this article will be made available by the authors, without undue reservation.

ETHICS STATEMENT

The animal study was reviewed and approved by Institutional Animal Care and Use Committee of the Nanchang University.

AUTHOR CONTRIBUTIONS

XL designed and directed the project. XD, TH, and JC performed the research experiments. XD, XL, and EF wrote the manuscript. ZY, DR, SZ, and HJ analyzed the data. SW helped with data interpretation and provided instruction. All the authors contributed to the article and approved the submitted version.

FUNDING

This work was supported by the National Natural Science Foundation of China (31660268, 81601092 to XL, and 81701324 to HJ) and Natural Science Foundation of Jiangxi Province (20181BAB215017).

REFERENCES

Abd-Elsameea, A. A., Moustaf, A. A., and Mohamed, A. M. (2014). Modulation of the oxidative stress by metformin in the cerebrum of rats exposed to global cerebral ischemia and ischemia/reperfusion. *Eur. Rev. Med. Pharmacol. Sci.* 18, 2387–2392.

Adams, M. E., Kramarcy, N., Krall, S. P., Rossi, S. G., Rotundo, R. L., Sealock, R., et al. (2000). Absence of alpha-syntrophin leads to structurally aberrant neuromuscular synapses deficient in utrophin. *J. Cell Biol.* 150, 1385–1398. doi: 10.1083/jcb.150.6.1385

Arpke, R. W., Darabi, R., Mader, T. L., Zhang, Y., Toyama, A., Lonetree, C. L., et al. (2013). A new immuno-, dystrophin-deficient model, the NSG-mdx(4Cv) mouse, provides evidence for functional improvement following allogeneic satellite cell transplantation. *Stem Cells* 31, 1611–1620. doi: 10.1002/stem.1402

Bailey, C. J. (2017). Metformin: historical overview. *Diabetologia* 60, 1566–1576. doi: 10.1007/s00125-017-4318-z

Banks, G. B., Chamberlain, J. S., and Froehner, S. C. (2009). Truncated dystrophins can influence neuromuscular synapse structure. *Mol. Cell. Neurosci.* 40, 433–441. doi: 10.1016/j.mcn.2008.12.011

Barbieri, R. (2003). Metformin for the treatment of polycystic ovary syndrome. *Obstetrics Gynecol.* 101, 785–793. doi: 10.1016/s0029-7844(03)00045-0

Barik, A., Li, L., Sathyamurthy, A., Xiong, W. C., and Mei, L. (2016). Schwann cells in neuromuscular junction formation and maintenance. *J. Neurosci.* 36, 9770–9781. doi: 10.1523/JNEUROSCI.0174-16.2016

Barik, A., Lu, Y., Sathyamurthy, A., Bowman, A., Shen, C., Li, L., et al. (2014). LRP4 is critical for neuromuscular junction maintenance. *J. Neurosci.* 34, 13892–13905. doi: 10.1523/JNEUROSCI.1733-14.2014

Benziane, B., Björnholm, M., Pirkmajer, S., Austin, R. L., Kotova, O., Viollet, B., et al. (2012). Activation of AMP-activated protein kinase stimulates Na+,K+-ATPase activity in skeletal muscle cells. *J. Biol. Chem.* 287, 23451–23463. doi: 10.1074/jbc.M111.331926

Bulfield, G. S. W., Wight, P. A., and Moore, K. J. (1984). X chromosome-linked muscular dystrophy (mdx) in the mouse. *Proc. Natl. Acad. Sci. U.S.A.* 81, 1189–1192. doi: 10.1073/pnas.81.4.1189

Bushby, K., Finkel, R., Birnkrant, D. J., Case, L. E., Clemens, P. R., Cripe, L., et al. (2010). Diagnosis and management of Duchenne muscular dystrophy, part 1: diagnosis, and pharmacological and psychosocial management. *Lancet Neurol.* 9, 77–93. doi: 10.1016/s1474-4422(09)70271-6

Cabreiro, F., Au, C., Leung, K. Y., Vergara-Irigaray, N., Cochemé, H. M., Noori, T., et al. (2013). Metformin retards aging in C. elegans by altering microbial folate and methionine metabolism. *Cell* 153, 228–239. doi: 10.1016/j.cell.2013.02.035

Campbell, K. P., and Kahl, S. D. (1989). Association of dystrophin and an integral membrane glycoprotein. *Nature* 338, 259–262. doi: 10.1038/338259a0

Coulton, G. R., Morgan, J. E., Partridge, T. A., and Sloper, J. C. (1988). The mdx mouse skeletal muscle myopathy: I. A histological, morphometric and biochemical investigation. *Neuropathol. Appl. Neurobiol.* 14, 53–70. doi: 10.1111/j.1365-2990.1988.tb00866.x

Davies, K. E., and Nowak, K. J. (2006). Molecular mechanisms of muscular dystrophies: old and new players. *Nat. Rev. Mol. Cell Biol.* 7, 762–773. doi: 10.1038/nrm2024

Dial, A. G., Ng, S. Y., Manta, A., and Ljubicic, V. (2018a). The role of AMPK in neuromuscular biology and disease. *Trends Endocrinol. Metab.* 29, 300–312. doi: 10.1016/j.tem.2018.02.010

Dial, A. G., Rooprai, P., Lally, J. S., Bujak, A. L., Steinberg, G. R., and Ljubicic, V. (2018b). The role of AMP-activated protein kinase in the expression of the dystrophin-associated protein complex in skeletal muscle. *FASEB J.* 32, 2950–2965. doi: 10.1096/fj.201700868RRR

Emery, A. E. (1991). Population frequencies of inherited neuromuscular diseases–a world survey. *Neuromuscul. Disord.* 1, 19–29. doi: 10.1016/0960-8966(91)90039-u

Garbincius, J. F., and Michele, D. E. (2015). Dystrophin-glycoprotein complex regulates muscle nitric oxide production through mechanoregulation of AMPK signaling. *Proc. Natl. Acad. Sci. U.S.A.* 112, 13663–13668. doi: 10.1073/pnas.1512991112

Hafner, P., Bonati, U., Erne, B., Schmid, M., Rubino, D., Pohlman, U., et al. (2016). Improved muscle function in duchenne muscular dystrophy through L-Arginine and metformin: an investigator-initiated, open-label, single-center, proof-of-concept-study. *PLoS One* 11:e0147634. doi: 10.1371/journal.pone.0147634

Hafner, P., Bonati, U., Klein, A., Rubino, D., Gocheva, V., Schmidt, S., et al. (2019). Effect of Combination l-citrulline and metformin treatment on motor function in patients with duchenne muscular dystrophy: a randomized clinical trial. *JAMA Netw. Open* 2:e1914171. doi: 10.1001/jamanetworkopen.2019.14171

Hamer, P. W. M. J., Davies, M. J., and Grounds, M. D. (2002). Evans Blue Dye as an *in vivo* marker of myofibre damage: optimising parameters for detecting

initial myofibre membrane permeability. *J. Anat.* 200(Pt 1), 69–79. doi: 10.1046/j.0021-8782.2001.00008.x

Henry, M. D., and Campbell, K. P. (1999). Dystroglycan inside and out. *Curr. Opin. Cell Biol.* 11, 602–607. doi: 10.1016/s0955-0674(99)00024-1

Hoffman, E. P., Brown, R. H., and Kunkel, L. M. (1987a). Dystrophin: the protein product of the Duchenne muscular dystrophy locus. *Cell* 51, 919–928. doi: 10.1016/0092-8674(87)90579-4

Hoffman, E. P., Monaco, A. P., Feener, C. C., and Kunkel, L. M. (1987b). Conservation of the Duchenne muscular dystrophy gene in mice and humans. *Science* 238, 347–350. doi: 10.1126/science.3659917

Holt, K. H., Crosbie, R. H., Venzke, D. P., and Campbell, K. P. (2000). Biosynthesis of dystroglycan: processing of a precursor propeptide. *FEBS Lett.* 468, 79–83. doi: 10.1016/s0014-5793(00)01195-9

Hong, J., Zhang, Y., Lai, S., Lv, A., Su, Q., Dong, Y., et al. (2013). Effects of metformin versus glipizide on cardiovascular outcomes in patients with type 2 diabetes and coronary artery disease. *Diabetes Care* 36, 1304–1311. doi: 10.2337/dc12-0719

Ibraghimov-Beskrovnaya, O., Ervasti, J. M., Leveille, C. J., Slaughter, C. A., Sernett, S. W., and Campbell, K. P. (1992). Primary structure of dystrophin-associated glycoproteins linking dystrophin to the extracellular matrix. *Nature* 355, 696–702. doi: 10.1038/355696a0

Ingalls, C. P., Warren, G. L., Zhang, J. Z., Hamilton, S. L., and Armstrong, R. B. (1985). Dihydropyridine and ryanodine receptor binding after eccentric contractions in mouse skeletal muscle. *J. Appl. Physiol.* 96, 1619–1625. doi: 10.1152/japplphysiol.00084

Inzucchi, S. E., Bergenstal, R. M., Buse, J. B., Diamant, M., Ferrannini, E., Nauck, M., et al. (2012). Management of hyperglycaemia in type 2 diabetes: a patient-centered approach. Position statement of the American Diabetes Association (ADA) and the European Association for the Study of Diabetes (EASD). *Diabetologia* 55, 1577–1596. doi: 10.1007/s00125-012-2534-0

Jahnke, V. E., Van Der Meulen, J. H., Johnston, H. K., Ghimbovschi, S., Partridge, T., Hoffman, E. P., et al. (2012). Metabolic remodeling agents show beneficial effects in the dystrophin-deficient mdx mouse model. *Skeletal Muscle* 2:16. doi: 10.1186/2044-5040-2-16

Jørgensen, S. B., Richter, E. A., and Wojtaszewski, J. F. P. (2006). Role of AMPK in skeletal muscle metabolic regulation and adaptation in relation to exercise. *J. Physiol.* 574, 17–31. doi: 10.1113/jphysiol.2006.109942

Kjøbsted, R., Hingst, J. R., Fentz, J., Foretz, M., Sanz, M. N., Pehmoller, C., et al. (2018). AMPK in skeletal muscle function and metabolism. *FASEB J.* 32, 1741–1777. doi: 10.1096/fj.201700442R

Kong, J. A. J. (1999). Dystrophin is required for organizing large acetylcholine receptor aggregates. *Brain Res.* 28, 298–304. doi: 10.1016/s0006-8993(99)01737-0

Langone, F., Cannata, S., Fuoco, C., Lettieri Barbato, D., Testa, S., Nardozza, A. P., et al. (2014). Metformin protects skeletal muscle from cardiotoxin induced degeneration. *PLoS One* 9:e114018. doi: 10.1371/journal.pone.0114018

Lapidos, K. A., Kakkar, R., and McNally, E. M. (2004). The dystrophin glycoprotein complex: signaling strength and integrity for the sarcolemma. *Circ. Res.* 94, 1023–1031. doi: 10.1161/01.RES.0000126574.61061.25

Ljubicic, V., and Jasmin, B. J. (2013). AMP-activated protein kinase at the nexus of therapeutic skeletal muscle plasticity in Duchenne muscular dystrophy. *Trends Mol. Med.* 19, 614–624. doi: 10.1016/j.molmed.2013.07.002

Ljubicic, V., and Jasmin, B. J. (2015). Metformin increases peroxisome proliferator-activated receptor gamma Co-activator-1alpha and utrophin a expression in dystrophic skeletal muscle. *Muscle Nerve* 52, 139–142. doi: 10.1002/mus.24692

Ljubicic, V., Khogali, S., Renaud, J.-M., and Jasmin, B. J. (2012). Chronic AMPK stimulation attenuates adaptive signaling in dystrophic skeletal muscle. *Am. J. Physiol. Cell Physiol.* 302, C110–C121. doi: 10.1152/ajpcell.00183.2011

Ljubicic, V., Miura, P., Burt, M., Boudreault, L., Khogali, S., Lunde, J. A., et al. (2011). Chronic AMPK activation evokes the slow, oxidative myogenic program and triggers beneficial adaptations in mdx mouse skeletal muscle. *Hum. Mol. Genet.* 20, 3478–3493. doi: 10.1093/hmg/ddr265

Lynch, G. S. (2017). "Therapeutic potential of skeletal muscle plasticity and slow muscle programming for muscular dystrophy and related muscle conditions," in *The Plasticity of Skeletal Muscle*, ed. K. Sakuma (Gateway East: Springer Singapore), 277–292. doi: 10.1007/978-981-10-3292-9_13

Mantuano, P., Sanarica, F., Conte, E., Morgese, M. G., Capogrosso, R. F., Cozzoli, A., et al. (2018). Effect of a long-term treatment with metformin in dystrophic mdx mice: a reconsideration of its potential clinical interest in Duchenne muscular dystrophy. *Biochem. Pharmacol.* 154, 89–103. doi: 10.1016/j.bcp.2018.04.022

Marsin, A. S., Bertrand, L., Rider, M. H., Deprez, J., Beauloye, C., Vincent, M. F., et al. (2000). Phosphorylation and activation of heart PFK-2 by AMPK has a role in the stimulation of glycolysis during ischaemia. *Curr. Biol.* 10, 1247–1255. doi: 10.1016/s0960-9822(00)00742-9

McGeachie, J. K., Grounds, M. D., Partridge, T. A., and Morgan, J. E. (1993). Age-related changes in replication of myogenic cells in mdx mice: quantitative autoradiographic studies. *J. Neurol. Sci.* 119, 169–179. doi: 10.1016/0022-510x(93)90130-q

Michele, D. E., and Campbell, K. P. (2003). Dystrophin-glycoprotein complex: post-translational processing and dystroglycan function. *J. Biol. Chem.* 278, 15457–15460. doi: 10.1074/jbc.R200031200

Morrow, V. A., Foufelle, F., Connell, J. M. C., Petrie, J. R., Gould, G. W., and Salt, I. P. (2003). Direct activation of AMP-activated protein kinase stimulates nitric-oxide synthesis in human aortic endothelial cells. *J. Biol. Chem.* 278, 31629–31639.

Mounier, R., Théret, M., Arnold, L., Cuvellier, S., Bultot, L., Göransson, O., et al. (2013). AMPKα1 regulates macrophage skewing at the time of resolution of inflammation during skeletal muscle regeneration. *Cell Metab.* 18, 251–264. doi: 10.1016/j.cmet.2013.06.017

Mounier, R., Théret, M., Lantier, L., Foretz, M., and Viollet, B. (2015). Expanding roles for AMPK in skeletal muscle plasticity. *Trends Endocrinol. Metab.* 26, 275–286. doi: 10.1016/j.tem.2015.02.009

Muntoni, F., Torelli, S., and Ferlini, A. (2003). Dystrophin and mutations: one gene, several proteins, multiple phenotypes. *Lancet Neurol.* 2, 731–740. doi: 10.1016/s1474-4422(03)00585-4

Onaran, I., Guven, G. S., Ozdaş, S. B., Kanigur, G., and Vehid, S. (2006). Metformin does not prevent DNA damage in lymphocytes despite its antioxidant properties against cumene hydroperoxide-induced oxidative stress. *Mutat Res.* 611, 1–8.

Pal, R., Palmieri, M., Loehr, J. A., Li, S., Abo-Zahrah, R., Monroe, T. O., et al. (2014). Src-dependent impairment of autophagy by oxidative stress in a mouse model of Duchenne muscular dystrophy. *Nat. Commun.* 5:4425. doi: 10.1038/ncomms5425

Pessina, P., Kharraz, Y., Jardí, M., Fukada, S.-i, Serrano, A. L., Perdiguero, E., et al. (2015). Fibrogenic cell plasticity blunts tissue regeneration and aggravates muscular dystrophy. *Stem Cell Rep.* 4, 1046–1060. doi: 10.1016/j.stemcr.2015.04.007

Petrillo, S., Pelosi, L., Piemonte, F., Travaglini, L., Forcina, L., Catteruccia, M., et al. (2017). Oxidative stress in Duchenne muscular dystrophy: focus on the NRF2 redox pathway. *Hum. Mol. Genet.* 26, 2781–2790. doi: 10.1093/hmg/ddx173

Pratt, S. J. P., Valencia, A. P., Le, G. K., Shah, S. B., and Lovering, R. M. (2015). Pre- and postsynaptic changes in the neuromuscular junction in dystrophic mice. *Front. Physiol.* 6:252. doi: 10.3389/fphys.2015.00252

Quan, Q., and Gao, E. M. M. (2015). The Dystrophin complex: structure, function, and implications for therapy. *Compr. Physiol.* 5, 1223–1239. doi: 10.1002/cphy.c140048

Salt, I. P., Johnson, G., Ashcroft, S. J., and Hardie, D. G. (1998). AMP-activated protein kinase is activated by low glucose in cell lines derived from pancreatic beta cells, and may regulate insulin release. *Biochem. J.* 335, 533–539. doi: 10.1042/bj3350533

Sasaki, H., Asanuma, H., Fujita, M., Takahama, H., Wakeno, M., Ito, S., et al. (2009). Metformin prevents progression of heart failure in dogs: role of AMP-activated protein kinase. *Circulation* 119, 2568–2577. doi: 10.1161/CIRCULATIONAHA.108.798561

Scholte, H. R., Luyt-Houwen, I. E., Busch, H. F., and Jennekens, F. G. (1985). Muscle mitochondria from patients with Duchenne muscular dystrophy have a normal beta oxidation, but an impaired oxidative phosphorylation. *Neurology* 35, 1396–1397.

Shen, C., Lu, Y., Zhang, B., Figueiredo, D., Bean, J., Jung, J., et al. (2013). Antibodies against low-density lipoprotein receptor-related protein 4 induce myasthenia gravis. *J. Clin. Invest.* 123, 5190–5202. doi: 10.1172/JCI66039

Stagi, S., Ricci, F., Bianconi, M., Sammarco, M., Municchi, G., Toni, S., et al. (2017). Retrospective evaluation of metformin and/or metformin plus a new polysaccharide complex in treating severe hyperinsulinism and insulin resistance in obese children and adolescents with metabolic syndrome. *Nutrients* 9:524. doi: 10.3390/nu9050524

Thomas, M. M., Wang, D. C., D'Souza, D. M., Krause, M. P., Layne, A. S., Criswell, D. S., et al. (2014). Muscle-specific AMPK β1β2-null mice display a myopathy due to loss of capillary density in nonpostural muscles. *FASEB J.* 28, 2098–2107. doi: 10.1096/fj.13-238972

Torres, L. F., and Duchen, L. W. (1987). The mutant mdx: inherited myopathy in the mouse. Morphological studies of nerves, muscles and end-plates. *Brain* 110 (Pt 2), 269–299. doi: 10.1093/brain/110.2.269

Ursini, F., Russo, E., Pellino, G., D'Angelo, S., Chiaravalloti, A., De Sarro, G., et al. (2018). Metformin and autoimmunity: a "new deal" of an old drug. *Front. Immunol.* 9:1236. doi: 10.3389/fimmu.2018.01236

Viollet, B., Guigas, B., Sanz Garcia, N., Leclerc, J., Foretz, M., and Andreelli, F. (2012). Cellular and molecular mechanisms of metformin: an overview. *Clin. Sci. (Lond)* 122, 253–270. doi: 10.1042/CS20110386

Whitehead, N. P., Yeung, E. W., Froehner, S. C., and Allen, D. G. (2010). Skeletal muscle NADPH oxidase is increased and triggers stretch-induced damage in the mdx mouse. *PLoS One* 5:e15354. doi: 10.1371/journal.pone.0015354

Williamson, R. A., Henry, M. D., Daniels, K. J., Hrstka, R. F., Lee, J. C., Sunada, Y., et al. (1997). Dystroglycan is essential for early embryonic development: disruption of Reichert's membrane in Dag1-null mice. *Hum. Mol. Genet.* 6, 831–841. doi: 10.1093/hmg/6.6.831

Winder, W. W., and Hardie, D. G. (1996). Inactivation of acetyl-CoA carboxylase and activation of AMP-activated protein kinase in muscle during exercise. *Am. J. Physiol.* 270, E299–E304. doi: 10.1152/ajpendo.1996.270.2.E299

Zemdegs, J., Martin, H., Pintana, H., Bullich, S., Manta, S., Marqués, M. A., et al. (2019). Metformin promotes anxiolytic and antidepressant-like responses in insulin-resistant mice by decreasing circulating branched-chain amino acids. *J. Neurosci.* 39, 5935–5948. doi: 10.1523/JNEUROSCI.2904-18.2019

Zeng, J., Zhu, L., Liu, J., Zhu, T., Xie, Z., Sun, X., et al. (2019). Metformin protects against oxidative stress injury induced by ischemia/reperfusion via regulation of the lncRNA-H19/miR-148a-3p/Rock2 Axis. *Oxid. Med. Cell Longev.* 2019:8768327. doi: 10.1155/2019/8768327

Zhao, K., Shen, C., Lu, Y., Huang, Z., Li, L., Rand, C. D., et al. (2017). Muscle yap is a regulator of neuromuscular junction formation and regeneration. *J. Neurosci.* 37, 3465–3477. doi: 10.1523/JNEUROSCI.2934-16.2017

Zhou, G., Myers, R., Li, Y., Chen, Y., Shen, X., Fenyk-Melody, J., et al. (2001). Role of AMP-activated protein kinase in mechanism of metformin action. *J. Clin. Invest.* 108, 1167–1174. doi: 10.1172/jci13505

Conflict of Interest: The authors declare that the research was conducted in the absence of any commercial or financial relationships that could be construed as a potential conflict of interest.

frontiers in Physiology

ORIGINAL RESEARCH
published: 08 July 2021
doi: 10.3389/fphys.2021.678974

Circadian Genes as Exploratory Biomarkers in DMD: Results From Both the *mdx* Mouse Model and Patients

Rachele Rossi[1,2†], Maria Sofia Falzarano[1†], Hana Osman[1,3†], Annarita Armaroli[1], Chiara Scotton[1], Paola Mantuano[4], Brigida Boccanegra[4], Ornella Cappellari[4], Elena Schwartz[5], Anton Yuryev[6], Eugenio Mercuri[7], Enrico Bertini[8], Adele D'Amico[8], Marina Mora[9], Camilla Johansson[10], Cristina Al-Khalili Szigyarto[10,11], Annamaria De Luca[4*] and Alessandra Ferlini[1,2*]*

[1] Unit of Medical Genetics, Department of Medical Sciences, University of Ferrara, Ferrara, Italy, [2] The Dubowitz Neuromuscular Centre, Institute of Child Health, London, United Kingdom, [3] Department of Medical Microbiology, Faculty of Medical Laboratory Sciences, University of Khartoum, Khartoum, Sudan, [4] Section of Pharmacology, Department of Pharmacy-Drug Sciences, University of Bari "Aldo Moro", Bari, Italy, [5] Ami-Go-Science LLC, Rockville, MD, United States, [6] Elsevier, Rockville, MD, United States, [7] Pediatric Neurology Unit, Catholic University and Nemo Center, Policlinico Universitario Gemelli, Rome, Italy, [8] Unit of Neuromuscular and Neurodegenerative Disorders, Department of Neurosciences, IRCCS Bambino Gesu Children's Hospital, Rome, Italy, [9] Neuromuscular Diseases and Neuroimmunology Unit, Fondazione IRCCS Istituto Neurologico Carlo Besta, Milan, Italy, [10] School of Chemistry, Biotechnology and Health, Royal Institute of Technology, Stockholm, Sweden, [11] Science for Life Laboratory, Royal Institute of Technology, Stockholm, Sweden

Duchenne muscular dystrophy (DMD) is a rare genetic disease due to dystrophin gene mutations which cause progressive weakness and muscle wasting. Circadian rhythm coordinates biological processes with the 24-h cycle and it plays a key role in maintaining muscle functions, both in animal models and in humans. We explored expression profiles of circadian circuit master genes both in Duchenne muscular dystrophy skeletal muscle and in its animal model, the mdx mouse. We designed a customized, mouse-specific Fluidic-Card-TaqMan-based assay (Fluid-CIRC) containing thirty-two genes related to circadian rhythm and muscle regeneration and analyzed gastrocnemius and tibialis anterior muscles from both unexercised and exercised *mdx* mice. Based on this first analysis, we prioritized the 7 most deregulated genes in mdx mice and tested their expression in skeletal muscle biopsies from 10 Duchenne patients. We found that *CSNK1E, SIRT1*, and *MYOG* are upregulated in DMD patient biopsies, consistent with the mdx data. We also demonstrated that their proteins are detectable and measurable in the DMD patients' plasma. We suggest that *CSNK1E, SIRT1*, and *MYOG* might represent exploratory circadian biomarkers in DMD.

Keywords: circadian rhythm, Duchenne muscular dystrophy (DMD), *mdx* mice, skeletal muscle, RNA analysis, biomarker

OPEN ACCESS

Edited by:
Helen Cristina Miranda, Case Western Reserve University, United States

Reviewed by:
Lucas Robert Smith, University of California, Davis, United States
Yifan Li, University of South Dakota, United States

***Correspondence:**
Rachele Rossi
r.rossi@ucl.ac.uk;
rssrhl@unife.it
Annamaria De Luca
annamaria.deluca@uniba.it
Alessandra Ferlini
fla@unife.it

[†] These authors have contributed equally to this work and share first authorship

Specialty section:
This article was submitted to Striated Muscle Physiology, a section of the journal Frontiers in Physiology

Received: *10 March 2021*
Accepted: *14 June 2021*
Published: *08 July 2021*

Citation:
Rossi R, Falzarano MS, Osman H, Armaroli A, Scotton C, Mantuano P, Boccanegra B, Cappellari O, Schwartz E, Yuryev A, Mercuri E, Bertini E, D'Amico A, Mora M, Johansson C, Al-Khalili Szigyarto C, De Luca A and Ferlini A (2021) Circadian Genes as Exploratory Biomarkers in DMD: Results From Both the mdx Mouse Model and Patients. Front. Physiol. 12:678974. doi: 10.3389/fphys.2021.678974

INTRODUCTION

The dystrophin gene (DMD) (OMIM 300377), located in Xp21.2-p21.1, is a 2,2 Mb gene that encodes for the dystrophin protein (DYS), a subsarcolemmal, rod-shaped protein of 427kDa involved in the formation of the dystrophin-associated protein complex (DAPC) (Ervasti and Campbell, 1993). The DAPC is composed of dystroglycans, sarcoglycans, sarcospan, dystrobrevins,

and syntrophin. This complex exerts the structural function of mechanic-transducer between muscle fibers and the extracellular matrix and controls membrane stability. The multiple binding sites and domains present in the DAPC confer the scaffold of various signaling and channel proteins, which may implicate the DAPC in regulation of signaling (Constantin, 2014).

A large variety of dystrophin gene mutations (approximately 75% of deletions/duplications and 25% of small/atypical mutations) cause dystrophinopathies (see in DMD Leiden pages[1]). Mutations maintaining the reading frame are generally associated with Becker muscular dystrophy (BMD) and other milder or atypical allelic forms of dystrophinopathies (OMIM 300376). In contrast, frameshifting mutations are mainly associated with severe Duchenne muscular dystrophy (DMD OMIM 310200) and cause a complete absence or severe reduction of the dystrophin protein. Some exceptions to the rule occur via diverse mechanisms such as splicing modulation or novel ATG start site use (Gualandi et al., 2006; Ferlini et al., 2013; Wein et al., 2015). Dystrophin-deficient fibers are more prone to membrane damage following muscle contraction. The resulting leaky membrane leads to the onset of a calcium-mediated degenerative process that culminates in inflammation, oxidative stress pathway activation, and consequent muscle fiber necrosis (De Luca et al., 2002). At the early stage, the regenerative process (myoblast recruitment and differentiation) is able to counterbalance the damage. However, after a number of degenerative-regenerative cycles, regeneration fails and there is the complete fibrotic substitution of muscle tissue (Massopust et al., 2020).

Duchenne muscular dystrophy is the most severe form of dystrophinopathies and is clinically characterized by muscle wasting with onset in early childhood (around 3-4 years old) and a progressive course that culminates in death by cardiac or respiratory complications around 20-30 years old (Merlini and Sabatelli, 2015).

In recent years, novel therapeutic approaches have emerged that aim at ameliorating the disease's course, even if an etiologic cure has not been discovered to date (Sun et al., 2020). Steroids (prednisolone and deflazacort) remain, however, the gold-standard drugs.

These new ongoing clinical trials in DMD would greatly benefit from the use of specific biomarkers (Scotton et al., 2014) since reliable biomarkers would facilitate not only correct disease diagnosis, but also disease monitoring and prognosis, patient stratification, and the prevision of an individual drug response. Furthermore, sensitive and feasible biomarkers could improve drug screening and effectiveness evaluations.

The most used animal model of dystrophinopathies is the *mdx* mouse that carries a point mutation in exon 23, leading to a stop codon instead of a glutamine. Despite the absence of dystrophin, the overall phenotype of this mouse model is less severe with respect to Duchenne muscular dystrophy (Lynch et al., 2001).

Evidence highlights the role of exercise in modifying skeletal muscle pathology in *mdx* mice, showing a different impact in different muscle types, that contributes to a worsening of the overall muscle phenotype, prolong the degenerative phase, and enhance DMD-like muscle pathology (Grounds and Torrisi, 2004; Camerino et al., 2014; Capogrosso et al., 2016).

We have identified a relationship between muscle damage and disease severity and circadian genes, suggesting that the *CLOCK* gene represents a disease severity biomarker in collagen VI myopathies (Scotton et al., 2016).

Here, we have investigated circadian gene behavior in Duchenne muscular dystrophy (DMD) and its animal model, the mdx mouse. Both exercised and untrained mdx mice and the skeletal muscle of DMD patients were studied by RNA profiling and a pilot immunoassay study was carried out on selected protein in 10 DMD boys.

We found a general deregulation of circadian key genes in mdx muscles. Based on mice results, we prioritized 7 genes and demonstrated that *CSNK1E*, *SIRT1*, and *MYOG* are invariably upregulated in DMD skeletal muscle and also measurable in plasma. We suggest that these circadian genes may represent exploratory biomarkers for DMD and might underline an interesting link between DMD pathology and circadian rhythm.

MATERIALS AND METHODS

Animal Selection and RNA Extraction

In vivo experiments and animal housing were carried out in conformity with the Italian Guidelines for Care and Use of Laboratory Animals (D.L. 116/92) and with the European Directive (2010/63/UE). The study was approved by the National Ethics Committee for Research Animal Welfare of the Italian Ministry of Health (authorization no. 1119/2020-PR). Experimental procedures were conducted according to standard operating procedures for pre-clinical tests in *mdx* mice, the SOP (ID) Number DMD_M.2.1.001, available at the TREAT NMD website https://treat-nmd.org/wp-content/uploads/2016/08/MDX-DMD_M.2.1.001.pdf.

In this study, a total of 6 male wild type (WT; C57BL/10ScSnJ) and 13 male *mdx* (C57BL/10ScSnDmd<mdx>/J) mice aged 4-5 weeks (Charles River, Italy for Jackson Laboratories) and homogeneous for their body weight, were selected. The *mdx* mice were divided into two groups: the sedentary group consisting of 6 male *mdx* mice and the exercised group consisting of 7 male *mdx* mice. The exercise protocol was performed as previously described (Camerino et al., 2014) by running for 30 min on a horizontal treadmill (Columbus Instruments) at 12 m/min, twice a week (keeping a constant interval of 2–3 days between each trial). Both *wt* and sedentary *mdx* mice were left to move freely in the cage without any exercise. At 8-9 weeks of age, gastrocnemius (GC) muscle was collected from a total of 10 mice, 3 wt and 7 *mdx*. Of the mdx mice, 3 were sedentary and 4 exercised by treadmill exercise for 4 weeks (see **Table 1**).

The fast-twitch tibialis anterior (TA) muscle was collected in the remaining 9 mice at 16 to 17-weeks-old (3 wt, 3 *mdx*, and 3 *mdx* exercised for 12 weeks, see **Table 1**, in the attempt to match pathology phase in the two different muscle types).

Muscles were removed from anesthetized mice (100 mg/kg ketamine and 16 mg/kg xylazine intraperitoneal) at the same

[1]www.dmd.nl

TABLE 1 | Wt and *Mdx* mice cohorts.

Mice cohorts		Gastrocnemius (Age 8-9 weeks)	Tibialis anterior (Age 16-17 weeks)
wt		3	3
mdx	Sedentary	3	3
	Exercised	4	3

A 6 wt and 13 mdx mice were selected. The 13 mdx were divided into 2 groups, sedentary and exercised; in 7 mdx mice, GC muscle was collected at the age of 8-9 weeks, following 4 weeks of exercise; in the other 6 mdx mice, TA muscle was collected at the age of 16-17 weeks, following 12 weeks of exercise.

time frame (8-11 a.m.), washed in PBS, and rapidly frozen in liquid nitrogen-cooled isopentane and stored at -80°C until use. Sampling time has been selected according to ethic rules and approved experimental plan.

Total RNA was isolated using the RNeasy-kit (Qiagen, Chatsworth, CA, United States) according to manufacturer's instructions and treated twice with DNase (RNase free DNAse set Qiagen kit) to exclude possible genomic contamination. A DNA contamination check was performed using a Real-time PCR system designed on murine actin-b exon 3. Nucleic acid concentration was quantified using a Nanodrop (Thermo Fisher Scientific) spectrophotometer.

Custom Fluidic Cards Exploring Circadian Genes (Mus Musculus Fluid-CIRC) Design and Circadian Gene Expression Analysis in *mdx* Mice

To test in mouse model the effect of DMD disease on circadian rhythm, we selected murine genes for the sub-network enrichment analysis base on the Kotelnikova work (Kotelnikova et al., 2012).

Specifically, the 32 murine genes chosen (**Table 2**) are involved in circadian rhythm, muscle regeneration, metabolism, apoptosis, immune reaction, and cellular proliferation.

We created a specific, custom TaqMan Low Density Array (TLDA) micro fluidic-card, Fluid-CIRC, combining ABI TaqMan gene assays (Applied Biosystems, Foster City, CA, United States) inventoried for the 32 selected murine gene with *GAPDH*, β-*actin* (*Actb*), and *18s* as reference genes. In the chosen design, all genes were run in triplicate and 4 samples were run in each card (**Supplementary Figure 1**).

For each muscle sample of all mice cohorts, a total of 300 ng of RNA were reverse-transcribed using the High-capacity cDNA Reverse Transcription Kit (Applied Biosystems) and then added to 100 μl of Real-time Universal PCR Master mix. Sterile water was added to reach a total volume of 200 μl and the final solution was loaded in 2 ports (100 μl each) of the Fluid-CIRC and run on ABI 7900HT System Fast Real-time PCR System (Applied Biosystems) using the following conditions: 2 min. at 50°C, 10 min. at 95°C, 40 cycles at 97°C for 15 s. then 1 min. at 60°C (Applied Biosystems TaqMan Array Micro Fluidic Cards user Guide).

Normalization was performed using Actn-B as housekeeping reference. For both muscles (gastrocnemious and tibialis anterior) the average of the DCt of the total number of samples was calculated for each mice cohort (wt, *mdx*, and *mdx* exercised, **Table 1**) and the statistical analysis was performed using Graphpad calculator[2]. For each gene the mean standard error (SEM) was calculated as shown in **Supplementary Figure 2**, and t-test was performed to determine statistically significant gene expression variation (p-Value < 0.05) (**Supplementary Figure 2**).

Mice were subdivided into 2 age-matched cohorts, wild type (WT) and *mdx* exercised (*mdx-exe*) for the two muscles (GC and TA), and were compared as *mdx* vs. WT and *mdx*-exe vs. *mdx*.

Gene Prioritization Analysis

Gene prioritization analysis was performed using Gene Set Enrichment Analysis based on the well-established approach of ranking genes by p-Values associated with the phenotype (a uniform distribution using a weighted Kolmogorov-Smirnov test as previously described in Kotelnikova et al., 2012). Using a sub-network enrichment analysis (SNEA), significantly deregulated genes based on p-Values and concordant in terms of side of expression change were identified and selected relative to their crucial role as downstream effectors in the core clock circadian network. Interactome was implemented in Pathway Studio.

DMD Patient Studies

Expression Analysis of Prioritized Genes in DMD Patients' Muscle

Patient selection, RNA extraction, and real-time PCR analysis

Ten DMD patients with different mutation types and with variable severity phenotypes were enrolled in this study. Mutations and clinical characteristics are detailed in **Table 3**. From each DMD subject, we obtained a muscle biopsy (tibialis anterior) either by in-house diagnostic procedures or via the Telethon biobank. In all cases, written informed consent was obtained and specific approval of this research study from the S. Anna University Hospital of Ferrara Ethics Committee (no. 02/2009, 26th February 2009) was achieved. This research was conducted following the Declaration of Helsinki's rules concerning human subject research. As a control, we used a pool of RNA extract from 3 healthy control samples [Control 1: commercial human skeletal muscle total RNA (Ambion) male, 71 years; Control 2: healthy donor male, 9 years; Control 3: healthy donor male, 37 years].

Muscle sample collecting procedures were carried out following local standard surgical procedures between 8 and 10 a.m. (CET) and frozen shortly afterward in liquid nitrogen until use. The concordance of collection time for each sample allowed us to correctly analyze and compare molecular clock component genes.

Total RNA was isolated from all muscle specimens using an RNeasy-kit (Qiagen, Chatsworth, CA) according to the manufacturer's instructions, double-treated with DNase (RNase free DNAse set Qiagen kit) and reverse-transcribed using the HighCapacity cDNA Reverse Transcription Kit (Applied Biosystems). DNA contamination checks were performed using

[2]https://www.graphpad.com/quickcalcs/ttest1/

TABLE 2 | Selected genes for Fluid-CIRC design.

Gene code	Gene name	Function
Arntl1	Aryl Hydrocarbon Receptor Nuclear Transclocator-Like1	Transcription factor, CCGs component of positive loop
Arntl2	Aryl Hydrocarbon Receptor Nuclear Transclocator-Like2	Transcription factor, CCGs component of positive loop
Atf5	Activating Transcription Factor 5	Transcriptional repressor; blocks the differentiation of neuronal progenitor cells
18s rRNA	ribosomal RNA 18s	Component of 40s minor subunit of ribosome
Ccrn4l	Carbon Catabolite Repressor 4-like (Nocturnin)	Deadenylase: plays an important role in post-transcriptional regulation of metabolic genes under circadian control.
Clock	Circadian Locomotor Output Cycles Kaput	Core clock gene, involved in the positive arm of the transcriptional-translational feedback loop.
Dbp	D-Site Binding Protein	Transcriptional activator, not crucial for circadian rhythm but modulates important clock output genes
Egr1	Early Growth Response 1	Transcriptional regulator
Fkbp5	Fk506 Binding Protein 5	Regulator of trafficking of steroid receptor containing vesicles
Per1	Period circadian clock 1	CCGs component of the negative transcriptional-translational regulatory negative loop
Per2	Period circadian clock 2	CCGs component of the negative transcriptional-translational regulatory negative loop
Per3	Period circadian clock 3	CCGs component of the negative transcriptional-translational regulatory negative loop
Cry1	Cryptochrome Circadian Clock1	Transcriptional repressor of circadian positive loop. It translocates PER proteins into the nucleus
Cry2	Cryptochrome Circadian Clock1	Transcriptional repressor of circadian positive loop. It translocates PER proteins into the nucleus
Rorα	RAR-Related Orphan Receptor A	Transcriptional factor that regulates lipid metabolism, circadian rhythm, and skeletal muscle differentiation
Nr1d1	Nuclear Receptor Subfamily 1, Group D, Member 1	Transcriptional repressor of Clock, Arntl1, Cry1
Nr1d2	Nuclear Receptor Subfamily 1, Group D, Member 2	Transcriptional repressor of Clock, Arntl1, Cry1
Csnk1ε	Casein Kinase 1, Epsilon	Kinase that phosphorylates many proteins, among which circadian proteins Per1 and 2
Csnk1δ	Casein Kinase 1, Delta	Kinase that phosphorylates many proteins, among which circadian proteins Per1 and 2
Bhlhe40	Basic Helix-Loop-Helix Family, Member E40	Transcriptional Factor which interacts with Arntl and indirectly modulates Per1 transactivation via Clock/Arntl1
Bhlhe41	Basic Helix-Loop-Helix Family, Member E41	Transcriptional repressor
Tim	Timeless circadian clock	Transcriptional repressor of circadian genes involved in the positive loop
Sirt1	Sirtuin1	Deacetylase involved in many different functions such as DNA repair, metabolism, apoptosis, and autophagy
Myod1	Myogenicenic Differentiation 1	Transcriptional activator of muscle-specific genes mainly involved in muscle differentiation. It regulates myogenesis
Myog	Myogenin (Myogenic factor 4)	Transcriptional activator of many muscle-specific genes. It plays a role in end-stage muscle differentiation and adult muscle phenotype
Dmd	Dystrophin	Muscle specific structural protein
Ppargc1α	Peroxisome Proliferator Activated Receptor Gamma, Coactivator 1α	Transcriptional co-activator of steroid and nuclear receptors; has a role in fatty acid and glucose metabolism
Tgfb1	Transforming Growth factor, Beta 1	Controls cellular proliferation and differentiation
Gapdh	Glyceraldehyde-3-Phosphate dehydrogenase	Role in glycolysis, transcription, RNA transport, DNA replication, and apoptosis
ActB	Actin, Beta	Globular protein, it forms thin filaments of sarcomere

Gene-specific functions are listed; CCGs, core clock gene components.

a Real-time PCR system designed in intron 14 of the dystrophin gene. Nucleic acid concentration was quantified using the Nanodrop (Thermo Fisher Scientific) spectrophotometer.

Transcript quantification of the 7 selected circadian genes *CNSK1E, SIRT1*, *MYOG, MYOD1, CRY1, CRY2*, and *ARNTL* was obtained using commercially available TaqMan expression assays (Applied Biosystems): CSNK1E, NM_001894.4, Hs00266431_m1, exon boundaries 6-7; SIRT1, NM_001142498.1, Hs01009006_m1, exon boundaries 7-8; MYOG, NM_002479.5, Hs01072232_m1, exon boundaries 2-3;MYOD1, NM_002478.4, Hs02330075_g1, exon boundaries 1-2; CRY1, NM_004075.4, Hs00172734_m1 exon boundaries 2-3; CRY2, NM_001127457.1, Hs00323654_m1, exon boundaries 5-6; ARNTL, NM_001030272.1, Hs00154147_m1, exon boundaries 8-9. Genes were selected according to the most deregulated genes observed in the mice Fluidic cards data.

β-actin was selected as a housekeeping reference gene (ACTB Endogenous Control). All Real-Time reactions were run in triplicate. Data were analyzed according to the comparative CT method ($2^{-\Delta\Delta Ct}$ method). and statistical analyses were performed with students'*t*-test using the technical replicates for both control and DMD patients.

TABLE 3 | Duchenne muscular dystrophy patients selected for expression analysis of the 7 most deregulated genes.

Patient	Mutation	Phenotype	Age at muscle biopsy sampling
PT1	Deletion exons 46-55	DMD	13 years
PT2	Deletion exons 61-63	DMD	11 years
PT3	Duplication exons 5-7	DMD	11 years
PT4	c.2950-2A > G	DMD	7 years
PT5	c.9808-1G > A	DMD	4 years
PT6	c.3655-3656indelGG > TT, p.E1150X	DMD	4 years
PT7	c.2510C > T, p.R768X	DMD	8 years
PT8	c.158T > A c.2971G > C	DMD	4 years
PT9	c.8027 + 2T > A	DMD	4 years
PT10	c.10223 + 2T > C	DMD	4 years

Age at muscle biopsy sampling and mutation are detailed.

CSNK1E, SIRT1, and MYOG Protein Quantification in Plasma

CSNK1E ELISA assay

Plasma samples from 16 patients (2 BMDs and 14 DMDs) with 6 age-matching control males, were collected after written informed consent and approval by the Ethics Committee of S. Anna University Hospital of Ferrara (no. 02/2009, Feburary 26, 2009, BIO-NMD European Union Seventh Framework Programme). Genotypic and phenotypic information are summarized in **Table 4**.

Plasma was isolated from peripheral blood after a single centrifugation within 2 h after sampling at 1500 g for 10 min at 4°C and immediately stored at -80°C in 400 ul aliquots.

ELISA assay was performed using the CSNK1E ELISA kit (My BioSource) according to the manufacturer's instructions. In brief, a total of 100 μl of standard and samples (in triplicate) were added to a pre-coated microplate (96 wells) with the antibody specific for CSNK1E and incubated for 2 h at 37°C. Following incubation, steps were performed with100 μl of Biotin-antibody (1×), 100 μl of HRP-avidin (1×), and 90 μl of TMB substrate. All the incubations were at 37°C, the first two for 1 h and the last one for 15 min. Finally, 50 μl of stop solution was added and the optical density of each well was determined using a microplate reader at 450 nm within 5 min.

For data analysis, a standard curve was constructed using "Curve expert 1.3" software, according to the manufacturer's instructions. CSNK1E concentration was calculated based on the absorbance value in relation to the calculated standard curve according to the equation of [CSNK1E] = (mean absorbance - 0,0391)/0,0013 and finally expressed in pg/ml.

CSNK1E data analysis was performed using R software.

SIRT1 and MYOG detection by suspension bead assays

A 44 DMD, 9 BMD, and 28 control plasma samples, coming from the large BIO-NMD cohort already reported (Ayoglu et al., 2014), were analyzed to assay SIRT1 and MYOG using the suspension bead array (LUMINEX Corp.). Two antibodies toward SIRT1 (HPA006295 and HPA007016) and one toward MYOG (HPA038093) (Uhlén et al., 2015) were diluted to a 17.5 μg antibody per ml in a 0.1 M 2-(N-morpholino) ethanesulfonic acid (MES) buffer (pH 4.5). Antibodies were then coupled to carboxylated, fluorescently labeled, magnetic beads (MagPlex-C, Luminex Corp.) according to previously established protocol (Ayoglu et al., 2014) with minor changes. After the coupling of antibodies, the beads were re-suspended in a 50 μl storage buffer containing 5% w/v bovine serum albumin (Albumin fraction V from bovine serum, Merck KGaA, 1.12018.0100) 0.05% v/v Tween 20 in PBS and incubated for 2 h at room temperature. Raw plasma samples from DMD and BMD patients, as well as healthy control samples, were biotinylated according to previously described protocols (Ayoglu et al., 2014) and diluted to a final dilution of 1:708 in 50 μl of an assay buffer containing 0.52 mg/ml bovine IgG (I-5506, Sigma) and 0.01% v/v ProClin^{TM} 300 (48912-U, Sigma) in PBST. The diluted samples were incubated together with beads overnight at 4°C, followed by isolation and washing of the beads in PBST. Streptavidin R-phycoerythrin conjugate was used for detection. Analysis was performed using a Luminex 100/200 instrument (Luminex Corp.) with Luminex xPONENT software. Statistical analysis of mean fluorescence intensity (MFI) was performed using packages *ggsignif* and *ggplot2* in R (Gatto et al., 2015). Wilcoxon ranked sum test was performed to assess differences in MFI between patient groups. Assays were performed in triplicates. Reproducibility was assessed at three different concentrations.

RESULTS

Circadian Genes Are Invariantly Deregulated in *mdx*

In order to explore the involvement of circadian genes in dystrophinopathies, we designed a custom TaqMan Low Density Array (TLDA) micro fluidic-card, Fluid-CIRC, to obtain the transcriptional profiling of two different *mdx* muscles: gastrocnemius (GC) and tibialis anterior (TA) derived from both sedentary and trained mice. These muscles were selected because of their involvement in *mdx* pathology and, for GC in particular, its muscle fiber composition (both fast and slow fibers are represented) and its large and early functional involvement in horizontal treadmill exercise as applied in our study (Camerino et al., 2014, TREAT-NMD[3]).

Sedentary *mdx* vs. Sedentary WT Mice

Gastrocnemius and TA muscles from 3 different *mdx* were compared with age-matched (8-9 weeks for GC and 16-17 weeks for TA) WT muscles (all sedentary), for the differential expression of selected circadian genes (**Table 1**).

As shown in **Supplementary Figure 2A** (sedentary *mdx* mice vs. sedentary WT mice) there is a general trend toward a downregulation of all core clock genes. In particular, a statistically significant (p-Value < 0.05) downregulation affects Ccrn4l, Fkbp5, Per3, Cry1, Ror-α, Nr1d1, Nr1d2, Csnk1ε, Sirt1, and Dmd genes, with the only exception of Myog and Timeless (Tim),

[3]www.treat-nmd.eu

TABLE 4 | Selected patients for Csnk1ε protein quantification in plasma.

Code	Mutation	DMD/BMD	Age at loss of ambulation	Age at plasma sampling
A	del exons 3-7 (out of frame)	BMD	20 years	33 years 7 m
B	del exon 13	BMD	Ambulant at sampling	7 years 2 m
C	del exon 43	DMD	Ambulant at sampling	8 years
D	del exon 45	DMD	Ambulant at sampling	9 years
E	del exon 45	DMD	Ambulant at sampling	9 years
F	del exon 45	DMD	Ambulant at sampling	6 years
G	del exon 45	DMD	Ambulant at sampling	7 years
H	del exon 45	DMD	Ambulant at sampling	6 years
I	del exon 45-50	DMD	Ambulant at sampling	10 years
L	del exon 45-50	DMD	Ambulant at sampling	12 years
M	del exon 45-50	DMD	Ambulant at sampling	7 years
N	del exon 49-50	DMD	Ambulant at sampling	7 years
O	del 50	DMD	Ambulant at sampling	10 years
P	dup exons 65-79	DMD	Ambulant at sampling	19 years
Q	c.4117c > T, p.Q1373X	DMD	Ambulant at sampling	6 years
R	c.9204-9207del,p.N3068K, fs*20	DMD	Ambulant at sampling	8 years

Mutation, phenotype and age at sampling are listed.

which are upregulated genes, with Myog as the most expressed one (p-Value = 0.0085; Camerino et al., 2014).

The same trend toward down-regulation is present in the TA muscle obtained at 16-17 weeks of age, when the muscle pathology reaches a stable level; genes with a statistically significant variation are: Arntl2, Ccrn4l, Clock, Egr1, Ror-α, Nr1d2, Csnk1ε, Bhlhe41, Tim, Ppargc1α, and Dmd. Consistently to GC, Myog and Tim showed a statistically significant upregulation, with Myog as the most upregulated gene (p-Value = 0.0005, **Supplementary Figure 2B**). In GC we also observed the loss of mutual variability of expression among Core Clock genes (CCGs).

Mdx Exercised vs. *mdx* Sedentary

As anticipated before, specific scheduling of exercise could have a damaging effect on the muscle of the mild *mdx* phenotype, leading to a model that better mimics the Duchenne disease. Consequently, a similar comparative analysis was done for exercised *mdx* vs. sedentary *mdx*. Interestingly, an opposite trend of the GC with respect to the TA was found as a main result.

Particularly for GC, exercise deeply changes the signature of all genes compared to untrained *mdx*.

Gastrocnemius muscles show a trend toward upregulation with a statistically significant (p-Value < 0.05) variation in: Ccrn4l, Clock, Dbp, Fkbp5, Per2, Per3, Cry1, Ror-α, Nr1d1, Csnk1ε, Csnk1δ, Bhlhe41, Tim, Sirt1, Ppargc1α, and Dmd. Oppositely, the TA muscle gene expression trend shows circadian genes downregulation (**Supplementary Figures 2A,B**) with statistically significant variation in the following genes: Arntl1, Atf5, Ccrn4l, Dbp, Per3, Cry1, Cry2, Nr1d1, Tim, Sirt1, Ppargc1α .

The different behavior in these two muscles might be explained by the different fiber type composition and different pathology course of the two muscles and their response to the different solicitation of the exercise schedule.

Gene Prioritization Analysis

Figure 1 shows the results of Pathway Studio analysis on circadian rhythm-related genes global deregulation in muscles of *mdx* mice and its effect on muscle differentiation and atrophy. We adopted this tool to build up a gene interactome and compare expression of gene groups between mdx and WT mice in order to prioritized selected genes to be further studied in DMD patients. In the **Figure 1** the downregulated genes in *mdx* mice are highlighted with a blue circle while the upregulated gens are highlighted with a red circle; we prioritized only genes with more than 2-fold of deregulation in both groups.

To determine the genes with a statistically significant differential expression (p-Value < 0.05), each muscle type (either separately or in pools) was analyzed and the 7 genes that were strongly deregulated in both gastrocnemius and tibialis between *mdx* and WT mice were selected (*Csnk1e, Sirt1, Myog, Myod1, Cry1, Cry2*, and *Arntl*).

Human Studies

Prioritized Circadian Genes: CSNK1E, MYOG, and SIRT1 Are Upregulated in DMD Patients' Muscle

To evaluate the expression profile of the 7 prioritized genes from mice studies in DMD patients, muscle biopsies from 10 DMD patients with different mutation types and heterogeneous for both age and phenotype severity were selected.

When comparing all DMD muscles with the healthy control, the 7 prioritized genes were deregulated (**Figure 2**), with levels varying among different samples, possibly due to muscle quality, muscle fiber composition, and disease stage. Specifically, *CSNK1E* (P-value = 0.0168), *SIRT1* (P-value = 0.0095), and *MYOG* (P-value = 0.0072) were significantly upregulated in all DMD muscles, with PT8 and PT10 the only exceptions. The tested genes show a variable level of expression, as expected considering the low number of muscles we studied, however *CSNK1E* and *MYOG* are consistently upregulated in all patients, especially this

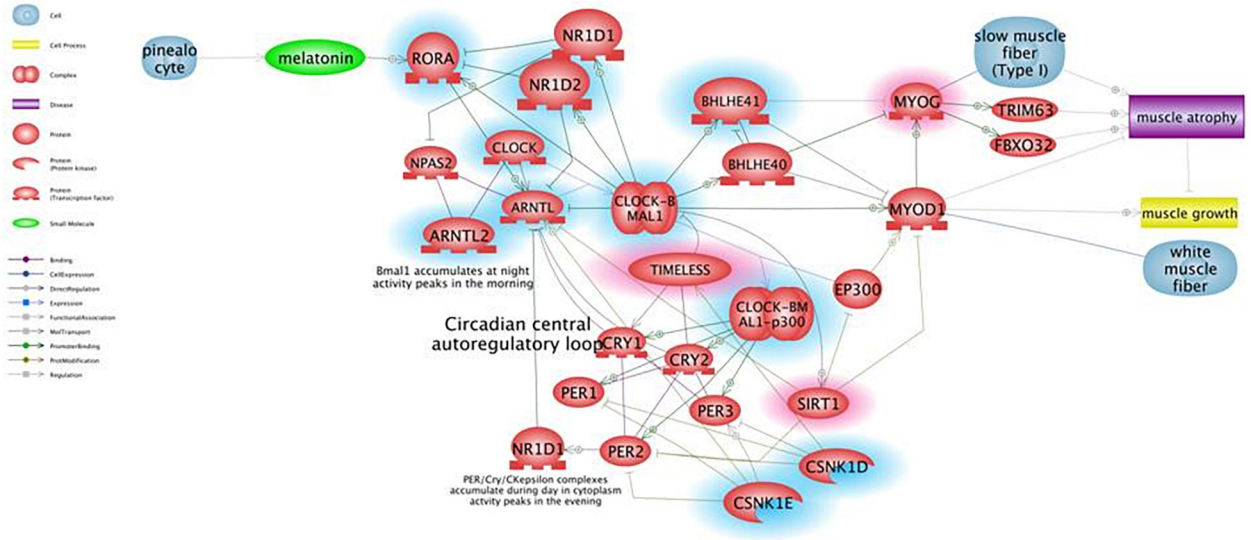

FIGURE 1 | Pathway for circadian rhythm regulation in skeletal muscles and its effect on muscle differentiation and atrophy. Genes that are downregulated in *mdx* mice more than 2-fold are shown in blue, genes upregulated more than 2-fold are shown in red. Pathway Studio analysis shows that downregulation of the ARNTL1 gene leads to upregulation of MYOG, which is known to be involved in muscle atrophy due to increased expression of ubiquitin ligases TRIM63 and FBXO32, rather than being a clear marker of ongoing regeneration. The ARNTL1-CLOCK1 complex is also repressed by upregulation of the Timeless protein that directly binds and represses CLOCK1, and by downregulation of CSNK1E that activates ARNTL1 directly by phosphorylation and through destabilization of PER1/2 proteins.

last one with PT5, PT6, and PT9 reaching levels up to 30 times more with respect to WT. Moreover, a general upregulation of CRY proteins was clearly visible and reflects the downregulation trend seen for ARNTL as part of the negative feedback loop, as already described.

CSNK1E Plasma Levels Are Slightly Elevated in Duchenne Patients

Expression data in patients, and in particular upregulation of primarily *MYOG* and then *CSNK1ε* and *SIRT1*, together with the absence of specific studies in Duchenne patients in literature, prompted us to further explore if these deregulated transcripts could reflect in the plasma of patients affected by dystrophinopathies.

For proteomic studies, plasma samples from a total of 16 patients were obtained (14 DMD and 2 BMD), as well as 6 controls were selected and analyzed with CSNK1E-specific ELISA. All DMD patients were ambulant at sampling and homogeneous for age (around 9-10 years on average), except for patient P, who was 19 years old.

Becker muscular dystrophy patients were less homogeneous, as patient A lost ambulation at age 20, while patient B was still ambulant but very young (4 years old).

To draw a standard curve, the mean absorbance of each standard was plotted on the y-axis against the concentration on the x-axis and the best-fit line drawn through the points on the graph.

CSNK1E protein concentrations of both DMD and controls were depicted in **Figure 3A**. **Figure 3A** demonstrated, in general, a slightly elevated plasma level of CSNK1E in all DMD plasma samples with respect to controls.

In order to evaluate a possible relationship between plasma protein levels and other phenotype variables, we checked if phenotype severity (DMD/BMD) mutation types and the age at sampling correlate to CSNK1E protein expression. No meaningful correlations were observed (**Supplementary Figure 3**).

Nevertheless, three DMD patients (G, H, and I) have about twice the CSNK1E plasma levels, as shown in **Supplementary Figure 4A**. Notably, higher levels of CSNK1E were seen in two patients with the deletion of exon 45, one of the most frequent mutations localized in one of the well-known mutational hot spots of the dystrophin gene (**Supplementary Figure 4B**).

To verify if this protein could be a marker of disease severity, plasma concentrations were also evaluated based on age at plasma sampling, but no specific correlation with age, and therefore disease worsening, was shown (**Supplementary Figure 4C**). However, the sample's cohort, analyzed for both BMD and DMD patients and healthy controls, proves to be rather limited and an enlargement of the number of the samples could lead to a better definition of a CSNK1E protein profile.

SIRT1 and MYOG Plasma Levels Do Not Vary in DMDs/BMDs

Myog and Sirt1 were analyzed in 44 DMD, 9 BMD, and 28 control plasma samples using a suspension bead array assay due to the unavailability of ELISA assays. **Figures 3B-D** show the abundance of the proteins by mean fluorescence intensity (MFI) for Sirt1, HPA006295 antibody (**Figure 3B**), and HPA007016 antibody (**Figure 3C**) and for Myog, HPA038093 antibody (**Figure 3D**) in DMD, BMD, and controls. Wilcoxon ranked sum test was performed to assess differences in MFI between patient groups.

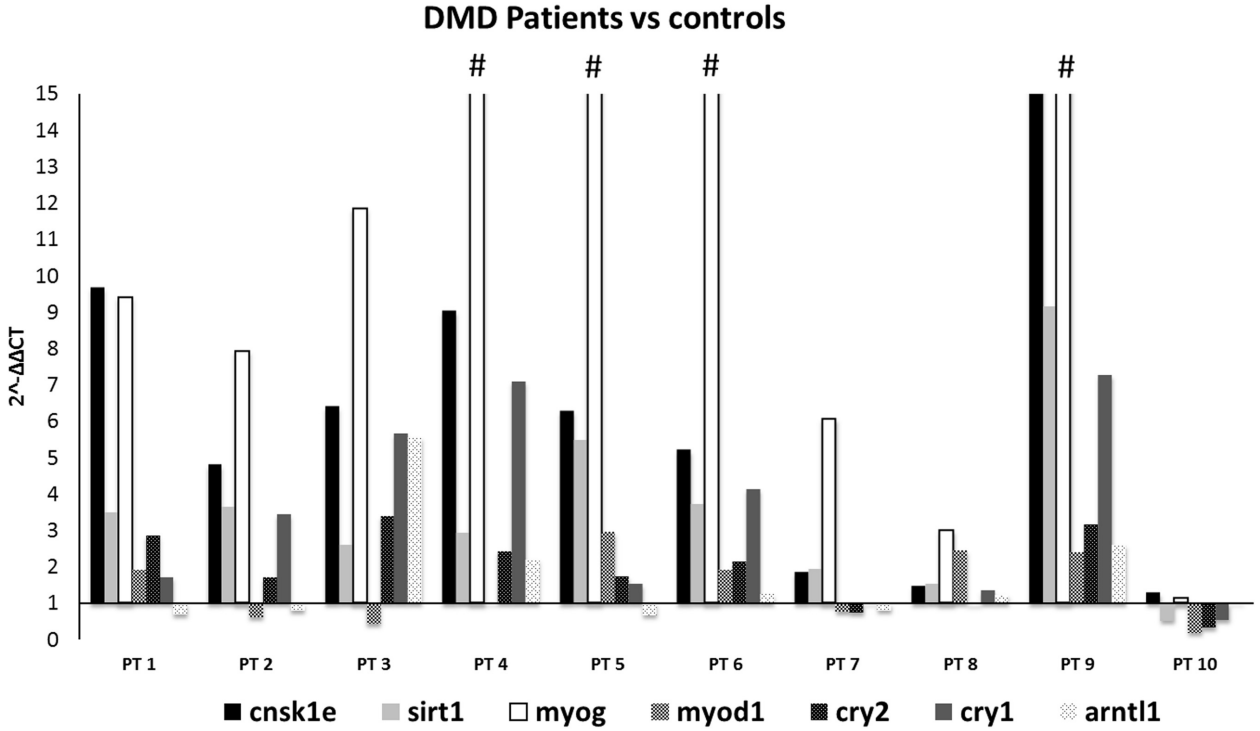

FIGURE 2 | Expression profiling of 7 deregulated genes in muscle samples from DMD patients (n = 10). Note the great upregulation of MYOG. (#): indicates that the expression level of MYOG is more than 15-fold, in PT4:25, PT5:34.7, PT6:43, and PT9:34.7. CSNK1E, SIRT1, and MYOG genes were significantly upregulated in all DMD muscles except for PT8 and PT10.

Both proteins were detected in plasma samples but differences between the patient groups were not significant. The large variation of Sirt1 and Myog within patient groups indicates that analyzing a larger cohort would be beneficial. Plasma samples were collected in the morning (8-10 a.m.) and, therefore, we do not expect that a circadian variation might influence the results since release into the blood stream has a circadian pattern.

DISCUSSION

The *mdx* mouse model of DMD has been widely utilized in evaluating the potential of therapeutic regimens in term of efficacy, efficiency, and side effects. Exploratory biomarkers were extensively searched in the *mdx* mice but also in DMD patients since having available robust biomarkers would greatly benefit the optimization of patient treatments.

Links between circadian rhythms and muscle metabolism are known and rhythmic expression of metabolic factors is common in myogenic homeostatic processes.

Some studies in *mdx* mice are available and pinpoint the role of the circadian clock in muscle differentiation and regeneration. For example, myogenic factors such as *MYOD* and *MYOG* are upregulated in muscle during dark hours and their over expression is suppressed by fasting (Shavlakadze et al., 2013).

Also, MuRF1, Akt1, and ribosomal protein S6 are upregulated in muscles in both fed and fasted mice and for Fbxo32 in fed mice (Chatterjee et al., 2015). Although it is known that skeletal muscle possesses intrinsic functional clocks, it is unclear how it is affected by dystrophinopathy. Asynchrony in fiber regeneration was indeed observed in mdx (Dadgar et al., 2014). Authors found that asynchronously regenerating microenvironments occurred in mice and it may drive fibrosis and regeneration failure. Treatment with either prednisone or Valmorolone (VBP15) mitigated the asynchrony.

Our RNA profiling, using Fluid-CIRC containing 32 genes related to circadian rhythms and muscle regeneration, showed that the majority of the explored circadian genes were profoundly downregulated in sedentary animals with a similar trend in the gastrocnemius and tibialis muscles.

We also observed the upregulation of *Tim* in both TA and GC, and we hypothesize that this might occur via *Per1* and *Per2* deep downregulation, as seen in the Fluid-CIRC. Indeed, Tim is part of the negative loop of inhibition of Clock/Arntl1-activated PER proteins.

Tibialis anterior and GC in untrained mice behave similarly. We showed that both GC and TA lack the physiological mutual expression variability among Core Clock Genes (CCGs), which is due to the network regulation based on feedback loops. It is true that different ages of TA and GC muscles may reflect different stages of disease (early in GC and later in TA), nevertheless, gene expression tendency is similar.

Underlining muscle-specific differences, circadian genes were highly upregulated in gastrocnemius but mainly downregulated

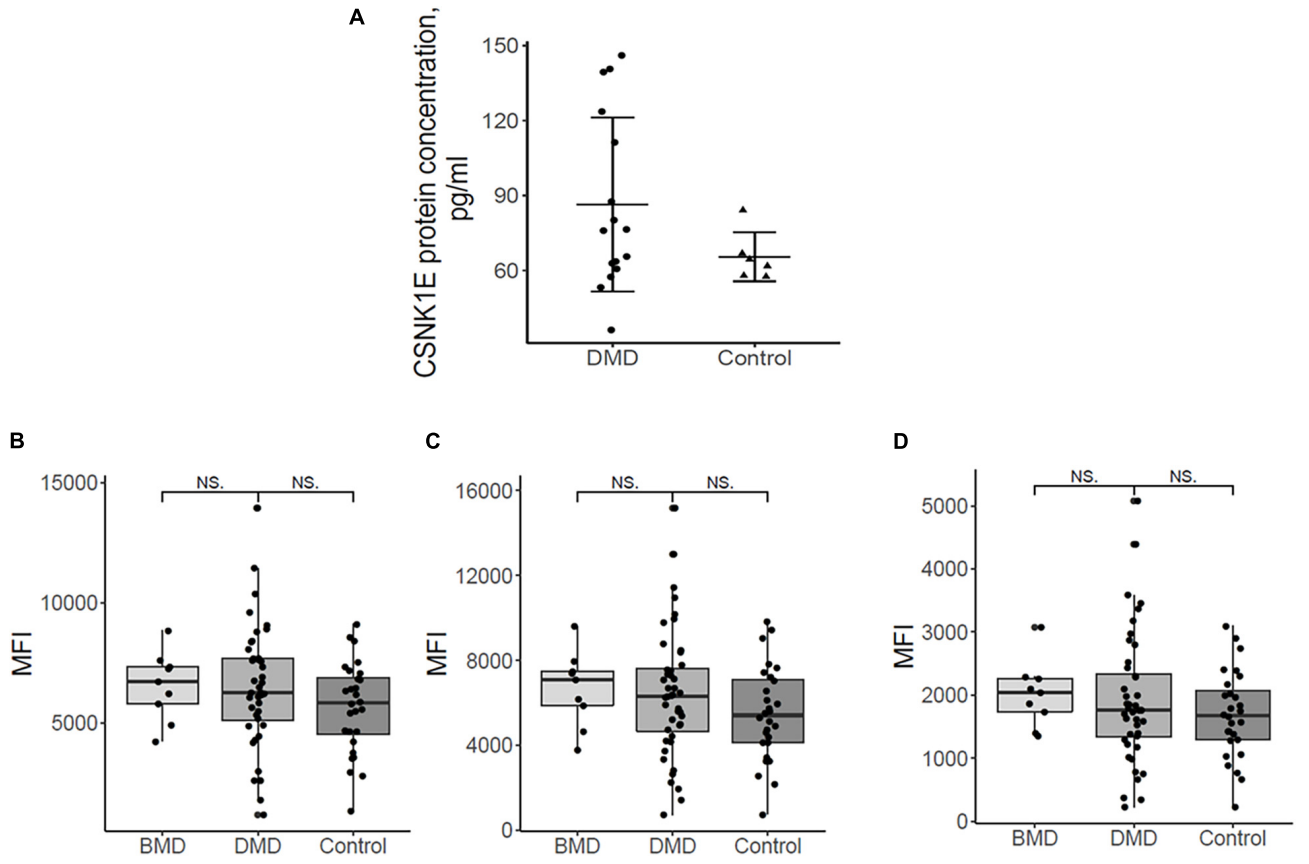

FIGURE 3 | (A) Plasma protein dosing of selected upregulated DMD genes. Csnk1ε protein plasma levels in DMD patients (n = 16) are slightly elevated with respect to controls (n = 6). **(B)** the mean fluorescence intensity (MFI) for sirtuin 1, HPA006295 antibody, and **(C)** MFI for sirtuin 1, HPA007016 antibody. **(D)** MFI for MYOGenin, HPA038093 antibody in DMD, BMD, and controls. Differences between the patient groups are not significant.

in tibialis in exercised mice. The very different fiber composition of these two muscles may also account for this opposite sign of expression in trained animals (Schiaffino and Reggiani, 2011; Bloemberg and Quadrilatero, 2012). Considering the consistent pattern between TA and GC that we observed in untrained *mdx* and the deregulation of their expression in the exercised GC muscle, we prioritized 7 genes as the most profoundly affected: *CSNK1E, SIRT1, MYOG, MYOD, CRY1, CRY2*, and *ARNTL1* (Bmal). Realtime assay in 10 DMD patient muscle biopsies showed that all of these genes were persistently upregulated and have tight interactions within the circadian pathway, which is shown in **Figure 2**. SNEA enrichment analysis underlines a major role of genes involved in muscle mass maintenance. This function is exerted through the central circadian feedback loop (Per and Cry circuit under Clock and Bmal oscillators), which influences muscle growth mainly on fast type fibers (FIGURE muscle) via *MYOD* positive regulation. Slow fibers are mainly under the influence of *MYOG*, which is directly and positively regulated by *MYOD*, but also indirectly interacts with Clock/Bmal oscillators (Aoyama and Shibata, 2017). The upregulation of *MYOG* may also contribute to causing muscle atrophy due to increased expression of ubiquitin ligases *TRIM63* and *FBXO32* (Moresi et al., 2010; Macpherson et al., 2011). Additional repression of ARNTL1-CLOCK1 complex is achieved by upregulation of Tim protein that directly binds and represses *CLOCK1*, and by downregulation of *CSNK1E* that activates *ARNTL1* directly by phosphorylation and through destabilization of PER1/2 proteins. The master clock transcription activator, *ARNT*-like 1 (*BMAL1*), which shows a clear upregulation trend in the muscle of both exercised *mdx* mice and patients, has a very important role in muscle, not only by participating in the maintenance of muscle mass but also in fiber regeneration. Indeed, genetic ablation of *BMAL1* in engineered injured muscle significantly impairs fiber regeneration with markedly suppressed new myofiber formation and attenuated myogenic induction (Chatterjee et al., 2015) and, specifically in *mdx* mice, it was demonstrated that the loss of Bmal1 aggravates the disease phenotype by increasing creatin kinase levels and injury areas and decreasing muscular force (Hongbo et al., 2020).

A lower satellite cell number (regeneration block) was observed in Bmal1-null mice but also in skin (Plikus et al., 2015), cardiomyocytes (Durgan and Young, 2010), and hepatocytes (Yan et al., 2010). The observed upregulation of *MYOD* and *MYOG* in DMD muscles is interesting and predicts to force up

muscle differentiation and regeneration (Ji et al., 2009; Cappellari et al., 2020). *MYOG* is an extremely well-known transcription factor that modulates muscle regeneration. Together with *MYF5*, *MYOD*, and *MRF*, *MYOG* promotes specification of the muscle satellite cell lineage. These cells are vital for muscle since they become the resident stem cell compartment in adult tissue and, therefore, the source of regeneration. It is conceivable that severe damage in DMD muscle activates a compensating upregulation of *MYOD* and *MYOG* in order to allow more muscle fiber replacement. However, while *MYOG* upregulation may result in the activation of satellite cells, it may also be detrimental to muscle since forcing myogenesis may inhibit the satellite cells' self-renewing process (Almada and Wagers, 2016). Also, *SIRT1* and *CSNK1E* were upregulated in DMD muscles. *SIRT1* is a histone deacetylase acting on stress resistance and cell survival. In *mdx*, *Sirt1* activation induces a series of positive effects such as reduction of both oxidative stress and inflammation, fast to slow myofiber switching and less fibrosis. *Sirt1* is under direct control of Clock/Bmal and its expression/activation may also represent a compensatory response of myofiber to ongoing oxidative stress and inflammation. Nothing is known about Csnk1ε protein and skeletal muscle interaction; it positively influences *Per* and *Cry* genes and is thought to negatively affect the transcription-translation-based clock auto-regulatory loop (Liu et al., 2016).

Observing the RNA profile in untrained *mdx*, the 7 selected genes are downregulated. Similarly to DMD, these genes are also involved in muscle differentiation and regeneration in mice (Almada and Wagers, 2016). The opposite sign of expression in humans and sedentary mice might be linked to the nature of myofiber in *mdx* and DMD, as well as to the (partial) preservation of satellite fibers in *mdx*, although in an age-dependent manner. The protocol of forced treadmill exercise moved the expression profile of mdx GC muscle toward that observed in DMD patients, supporting that the failure in mechanical-metabolic signaling and function is a hallmark of dystrophic severity (Camerino et al., 2014; Capogrosso et al., 2016) and is also related to deregulation in clock gene expression.

Based on the data we obtained in DMD patients' muscle, we evaluated if RNA deregulation might also be mirrored in protein from plasma samples. We showed that CSNK1E, MYOG, and SIRT1 are all detectable in human (control and DMD) plasma but only CSNK1E abundance differs slightly between DMD patients and healthy individuals, especially for DMDs carrying deletions involving exon 45. Although the concentration of CSNK1E varies within both the patient group and the control group, these findings suggest that CSNK1E might be an exploratory circadian biomarker for DMD, measurable in plasma. Circadian gene products such as blood biomarkers and their diurnal fluctuations have never been described and remain deserving of further investigation.

CONCLUSION

In conclusion, our study underlines upregulation of *CSNK1E*, *SIRT1*, and *MYOG* in both mdx and DMD skeletal muscle, suggesting that alterations of circadian circuits may activate a more severe and dystrophic-like muscle pathology. We also have shown that CSNK1E, MYOG, and SIRT1 circadian proteins are measurable in plasma. Circadian genes deserve to be further studied as disease-related readout parameters linked to disease status or disease severity. Due to their tight link to muscle differentiation and regeneration, they may also be relevant drug targets in DMD.

DATA AVAILABILITY STATEMENT

The authors acknowledge that the data presented in this study must be deposited and made publicly available in an acceptable repository, prior to publication. Frontiers cannot accept a manuscript that does not adhere to our open data policies.

ETHICS STATEMENT

The studies involving human participants were reviewed and approved by the S. Anna University Hospital of Ferrara Ethics Committee (no. 02/2009, 26th February 2009). Written informed consent to participate in this study was provided by the participants' legal guardian/next of kin. The animal study was reviewed and approved by Department of Pharmacy-Drug Sciences, University of Bari (Italy).

AUTHOR CONTRIBUTIONS

HO and CS performed the mice experiments. HO, RR, and MF performed the human muscle experiments. PM and AD performed the mice *in vivo* studies. ES and AY performed the bioinformatics analysis and gene prioritization. EM, EB, AA, and AD'A performed the patient clinical studies. MF, RR, CJ, and CA-K performed the immunoassay studies. MM provided the muscle samples from the Telethon Biobank. RR, AD, and AF wrote the manuscript. AF conceived and supervised the work. All authors contributed to the article and approved the submitted version.

FUNDING

This study was funded by the BIO-NMD FP7 EU project 241665 (to AF). The contribution of PRIN MIUR to the project n. Prot. 2017FJSM9S_005 to AD is also acknowledged.

ACKNOWLEDGMENTS

We thank the EuroBioBank and Telethon Network of Genetic Biobanks for providing biological samples. Special thanks are due to Duchenne Parent Project Italia Onlus for granting parts of the immunoassay studies. Olga Calabrese and Rossella Tupler (Policlinico di Modena, and University of Modena, respectively,

Modena Italy) are acknowledged for having referred patients 3 and 4 (in **Table 4**) for diagnostic procedures. Dr. Alexandra McPherron (Ami-Go-Science LLC, MD, United States) is acknowledged for critical review of this manuscript.

SUPPLEMENTARY MATERIAL

The Supplementary Material for this article can be found online at: https://www.frontiersin.org/articles/10.3389/fphys.2021.678974/full#supplementary-material

Supplementary Figure 1 | Design of the TaqMan Low Density Array (TLDA) micro fluidic-card (Fluid-CIRC). The Fluid-CIRC is a 384-count well plate pre-loaded with TaqMan gene expression assays of 32 murine genes involved in circadian rhythm, muscle regeneration, metabolism, apoptosis, immune reaction, and cellular proliferation, plus ACTIN-B and GAPDH as reference genes.

Supplementary Figure 2 | Fluid-CIRC expression data of Gastrocnemius GC **(A)**, and Tibialis anterior TA **(B)** of WT (blue bars), *mdx* sedentary (red bars) and *mdx* exercised (green bars) samples. Mean standard error (SEM) is indicated with error bars. In *mdx* CCGs are deregulated with a trend through a general downregulation. Genes with a statistically significant variation (p-Value < 0.05) are indicated with asterisk (*). Only MYOG is consistently upregulated in both muscle types. Comparing mdx-sedentary vs. mdx-exercised, we can observe an opposite behavior of the two selected muscle types. MYOG and MYOD don't show a consistent change of expression with respect to *mdx*.

Supplementary Figure 3 | Csnk1ε protein plasma levels in DMD patients analyzed with respect to phenotype **(A)**, mutation type **(B)**, and age **(C)**. White bars are averaged controls (protein concentrations measured in the 6 controls were averaged and used for the comparison), gray bars are BMD patients ($n = 2$) and black bars are DMD patients ($n = 14$).

REFERENCES

Almada, A. E., and Wagers, A. J. (2016). Molecular circuitry of stem cell fate in skeletal muscle regeneration, ageing and disease. *Nat. Rev. Mol. Cell Biol.* 17, 267–279. doi: 10.1038/nrm.2016.7

Aoyama, S., and Shibata, S. (2017). The role of circadian rhythms in muscular and osseous physiology and their regulation by nutrition and exercise. *Front. Neurosci.* 11:63.

Ayoglu, B., Chaouch, A., Lochmüller, H., Politano, L., Bertini, E., Spitali, P., et al. (2014). Affinity proteomics within rare diseases: a BIO-NMD study for blood biomarkers of muscular dystrophies. *EMBO Mol. Med.* 6, 918–936. doi: 10.15252/emmm.201303724

Bloemberg, D., and Quadrilatero, J. (2012). Rapid determination of myosin heavy chain expression in rat, mouse, and human skeletal muscle using multicolor immunofluorescence analysis. *PLoS One* 7:e35273. doi: 10.1371/journal.pone.0035273

Camerino, G. M., Cannone, M., Giustino, A., Massari, A. M., Capogrosso, R. F., Cozzoli, A., et al. (2014). Gene expression in mdx mouse muscle in relation to age and exercise: aberrant mechanical-metabolic coupling and implications for pre-clinical studies in Duchenne muscular dystrophy. *Hum. Mol. Genet.* 23, 5720–5732. doi: 10.1093/hmg/ddu287

Capogrosso, R. F., Cozzoli, A., Mantuano, P., Camerino, G. M., Massari, A. M., Sblendorio, V. T., et al. (2016). Assessment of resveratrol, apocynin and taurine on mechanical-metabolic uncoupling and oxidative stress in a mouse model of duchenne muscular dystrophy: a comparison with the gold standard, α-methyl prednisolone. *Pharmacol. Res.* 106, 101–113. doi: 10.1016/j.phrs.2016.02.016

Cappellari, O., Mantuano, P., and De Luca, A. (2020). "The social network" and muscular dystrophies: the lesson learnt about the niche environment as a target for therapeutic strategies. *Cells* 9:1659. doi: 10.3390/cells9071659

Chatterjee, S., Yin, H., Nam, D., Li, Y., and Ma, K. (2015). Brain and muscle Arnt-like 1 promotes skeletal muscle regeneration through satellite cell expansion. *Exp. Cell Res.* 331, 200–210. doi: 10.1016/j.yexcr.2014.08.041

Constantin, B. (2014). Dystrophin complex functions as a scaffold for signalling proteins. *Biochim. Biophys. Acta* 1838, 635–642. doi: 10.1016/j.bbamem.2013.08.023

Dadgar, S., Wang, Z., Johnston, H., Kesari, A., Nagaraju, K., Chen, Y. W., et al. (2014). Asynchronous remodeling is a driver of failed regeneration in Duchenne muscular dystrophy. *J. Cell Biol.* 207, 139–158. doi: 10.1083/jcb.201402079

De Luca, A., Pierno, S., Liantonio, A., and Conte, C. D. (2002). Pre-clinical trials in Duchenne dystrophy: what animal models can tell us about potential drug effectiveness. *Neuromuscul. Disord.* 12(Suppl. 1), S142–S146.

Durgan, D. J., and Young, M. E. (2010). The cardiomyocyte circadian clock: emerging roles in health and disease. *Circ. Res.* 106, 647–658. doi: 10.1161/circresaha.109.209957

Ervasti, J. M., and Campbell, K. P. (1993). A role for the dystrophin-glycoprotein complex as a transmembrane linker between laminin and actin. *J. Cell Biol.* 122, 809–823. doi: 10.1083/jcb.122.4.809

Ferlini, A., Neri, M., and Gualandi, F. (2013). The medical genetics of dystrophinopathies: molecular genetic diagnosis and its impact on clinical practice. *Neuromuscul. Disord.* 23, 4–14. doi: 10.1016/j.nmd.2012.09.002

Gatto, L., Breckels, L. M., Naake, T., and Gibb, S. (2015). Visualisation of proteomics data using R and bioconductor. *Proteomics* 15, 1375–1389. doi: 10.1002/pmic.201400392

Grounds, M. D., and Torrisi, J. (2004). Anti-TNFalpha (Remicade) therapy protects dystrophic skeletal muscle from necrosis. *FASEB J.* 18, 676–682. doi: 10.1096/fj.03-1024com

Gualandi, F., Rimessi, P., Trabanelli, C., Spitali, P., Neri, M., Patarnello, T., et al. (2006). Intronic breakpoint definition and transcription analysis in DMD/BMD patients with deletion/duplication at the 5′ mutation hot spot of the dystrophin gene. *Gene* 370, 26–33. doi: 10.1016/j.gene.2005.11.002

Hongbo, G., Xuekai, X., Yayu, L., Somik, C., and Ke, M. (2020). The clock regulator Bmal1 protects against muscular dystrophy. *Exp. Cell Res.* 397:112348. doi: 10.1016/j.yexcr.2020.112348

Ji, Z. X., Du, C., Wu, G. S., Li, S. Y., An, G. S., Yang, Y. X., et al. (2009). Synergistic up-regulation of muscle LIM protein expression in C2C12 and NIH3T3 cells by MYOGenin and MEF2C. *Mol. Genet. Genomics* 281, 1–10. doi: 10.1007/s00438-008-0393-7

Kotelnikova, E., Shkrob, M. A., Pyatnitskiy, M. A., Ferlini, A., and Daraselia, N. (2012). Novel approach to meta-analysis of microarray datasets reveals muscle remodeling-related drug targets and biomarkers in Duchenne muscular dystrophy. *PLoS Comput. Biol.* 8:e1002365. doi: 10.1371/journal.pcbi.1002365

Liu, J., Zhou, B., Yan, M., Huang, R., Wang, Y., He, Z., et al. (2016). CLOCK and BMAL1 regulate muscle insulin sensitivity via SIRT1 in male mice. *Endocrinology* 157, 2259–2269. doi: 10.1210/en.2015-2027

Lynch, G. S., Hinkle, R. T., Chamberlain, J. S., Brooks, S. V., and Faulkner, J. A. (2001). Force and power output of fast and slow skeletal muscles from mdx mice 6-28 months old. *J. Physiol.* 535(Pt 2), 591–600. doi: 10.1111/j.1469-7793.2001.00591.x

Macpherson, P. C., Wang, X., and Goldman, D. (2011). Myogenin regulates denervation-dependent muscle atrophy in mouse soleus muscle. *J. Cell Biochem.* 112, 2149–2159. doi: 10.1002/jcb.23136

Massopust, R. T., Lee, Y. I., Pritchard, A. L., Nguyen, V. M., McCreedy, D. A., and Thompson, W. J. (2020). Lifetime analysis of mdx skeletal muscle reveals a progressive pathology that leads to myofiber loss. *Sci. Rep.* 10:17248.

Merlini, L., and Sabatelli, P. (2015). Improving clinical trial design for Duchenne muscular dystrophy. *BMC Neurol.* 15:153.

Moresi, V., Williams, A. H., Meadows, E., Flynn, J. M., Potthoff, M. J., McAnally, J., et al. (2010). Myogenin and class II HDACs control neurogenic muscle atrophy by inducing E3 ubiquitin ligases. *Cell* 143, 35–45. doi: 10.1016/j.cell.2010.09.004

Plikus, M. V., Van Spyk, E. N., Pham, K., Geyfman, M., Kumar, V., Takahashi, J. S., et al. (2015). The circadian clock in skin: implications for adult stem cells, tissue regeneration, cancer, aging, and immunity. *J. Biol. Rhythms* 30, 163–182. doi: 10.1177/0748730414563537

Schiaffino, S., and Reggiani, C. (2011). Fiber types in mammalian skeletal muscles. *Physiol. Rev.* 91, 1447–1531. doi: 10.1152/physrev.00031.2010

Scotton, C., Bovolenta, M., Schwartz, E., Falzarano, M. S., Martoni, E., Passarelli, C., et al. (2016). Deep RNA profiling identified CLOCK and molecular clock genes as pathophysiological signatures in collagen VI myopathy. *J. Cell Sci.* 129, 1671–1684.

Scotton, C., Passarelli, C., Neri, M., and Ferlini, A. (2014). Biomarkers in rare neuromuscular diseases. *Exp. Cell Res.* 325, 44–49. doi: 10.1016/j.yexcr.2013.12.020

Shavlakadze, T., Anwari, T., Soffe, Z., Cozens, G., Mark, P. J., Gondro, C., et al. (2013). Impact of fasting on the rhythmic expression of myogenic and metabolic factors in skeletal muscle of adult mice. *Am. J. Physiol. Cell Physiol.* 305, C26–C35.

Sun, C., Shen, L., Zhang, Z., and Xie, X. (2020). Therapeutic strategies for duchenne muscular dystrophy: an update. *Genes* 11:837. doi: 10.3390/genes11080837

Uhlén, M., Fagerberg, L., Hallström, B. M., Lindskog, C., Oksvold, P., Mardinoglu, A., et al. (2015). Tissue-based map of the human proteome. *Science* 347:1260419.

Wein, N., Vulin, A., Falzarano, M. S., Szigyarto, C. A., Maiti, B., Findlay, A., et al. (2015). Translation from a DMD exon 5 IRES results in a functional dystrophin isoform that attenuates dystrophinopathy in humans and mice. *Nat. Med.* 21, 992–1000. doi: 10.1038/nm.3628

Yan, B. C., Gong, C., Song, J., Krausz, T., Tretiakova, M., Hyjek, E., et al. (2010). Arginase-1: a new immunohistochemical marker of hepatocytes and hepatocellular neoplasms. *Am. J. Surg. Pathol.* 34, 1147–1154. doi: 10.1097/PAS.0b013e3181e5dffa

Conflict of Interest: ES was employed by company Ami-Go-Science LLC. AY was employed by company Elsevier.

The remaining authors declare that the research was conducted in the absence of any commercial or financial relationships that could be construed as a potential conflict of interest.

frontiers in Physiology

ORIGINAL RESEARCH
published: 20 August 2021
doi: 10.3389/fphys.2021.697139

Downregulation of let-7 by Electrical Acupuncture Increases Protein Synthesis in Mice

Ying Huang[1,2†], Manshu Yu[1,3†], Akihiro Kuma[1,4], Janet D. Klein[1], Yanhua Wang[1], Faten Hassounah[1], Hui Cai[1,5] and Xiaonan H. Wang[1]**

[1] Renal Division, Department of Medicine, Emory University, Atlanta, GA, United States, [2] Department of Nephrology, The Second Xiangya Hospital of Central South University, Changsha, China, [3] Renal Division, Affiliated Hospital of Nanjing University of Chinese Medicine, Nanjing, China, [4] Second Department of Internal Medicine, School of Medicine, University of Occupational and Environmental Health, Kitakyushu, Japan, [5] Section of Nephrology, Atlanta VA Medical Center, Decatur, GA, United States

OPEN ACCESS

Edited by:
Helen Cristina Miranda, Case Western Reserve University, United States

Reviewed by:
Somasish Dastidar, Manipal Academy of Higher Education, India
Jeffrey J. Brault, Indiana University Bloomington School of Medicine, United States

***Correspondence:**
Hui Cai
hcai3@emory.edu
Xiaonan H. Wang
xwang03@emory.edu

† These authors have contributed equally to this work

Specialty section:
This article was submitted to Striated Muscle Physiology, a section of the journal Frontiers in Physiology

Received: *18 April 2021*
Accepted: *21 July 2021*
Published: *20 August 2021*

Citation:
Huang Y, Yu M, Kuma A, Klein JD, Wang Y, Hassounah F, Cai H and Wang XH (2021) Downregulation of let-7 by Electrical Acupuncture Increases Protein Synthesis in Mice. Front. Physiol. 12:697139. doi: 10.3389/fphys.2021.697139

Background: Our previous study found that acupuncture with low frequency electrical stimulation (Acu/LFES) prevents muscle atrophy by attenuation of protein degradation in mice. The current study examines the impact of Acu/LFES on protein synthesis.

Method: C57/BL6 mice received Acu/LFES treatment on hindlimb for 30 min once. Acu/LFES points were selected by WHO Standard Acupuncture Nomenclature and electric stimulation applied using an SDZ-II Electronic acupuncture instrument. Muscle protein synthesis was measured by the surface-sensing of translation (SUnSET) assay. Exosomes were isolated using serial centrifugation and concentration and size of the collected exosomes were measured using a NanoSight instrument. The mature microRNA library in serum exosomes was validated using a High Sensitivity DNA chip.

Results: Protein synthesis was enhanced in the both hindlimb and forelimb muscles. Blocking exosome secretion with GW4869 decreased the Acu/LFES-induced increases in protein synthesis. MicroRNA-deep sequencing demonstrated that four members of the Let-7 miRNA family were significantly decreased in serum exosomes. Real time qPCR further verified Acu/LFES-mediated decreases of let-7c-5p in serum exosomes and skeletal muscles. In cultured C2C12 myotubes, inhibition of let-7c not only increased protein synthesis, but also enhanced protein abundance of Igf1 and Igf1 receptors. Using a luciferase reporter assay, we demonstrated that let-7 directly inhibits Igf1.

Conclusion: Acu/LFES on hindlimb decreases let-7-5p leading to upregulation of the Igf1 signaling and increasing protein synthesis in both hindlimb and forelimb skeletal muscles. This provides a new understanding of how the electrical acupuncture treatment can positively influence muscle health.

Keywords: Acu/LFES, exosome, IGF-1 signaling, microRNA, mTOR, skeletal muscle

HIGHLIGHTS

- Protein synthesis is a core physiologic and biological process, occurring inside cells, balancing the loss of cellular proteins through the production of new proteins and degradation of old proteins.
- Proteins perform a number of critical physiologic functions as enzymes, structural proteins or hormones. Protein synthesis plays a key role in many diseases.
- Acupuncture is a form of alternative medicine and a simple and safe treatment. It has been used to treat a wide range of diseases or disorder conditions.
- Our group found that acupuncture plus low frequency electrical stimulation (Acu/LFES) can limit muscle wasting.
- We have evidence that Acu/LFES can increase protein synthesis through decreases in let-7-5p microRNA.
- Since let-7 directly targets and inhibits Igf-1, the decrease in let-7 could lead to Igf1 signaling, which could be the foundation for the rise in protein synthesis.
- Our study provides evidence for a muscle atrophy treatment—a simple method for increasing muscle protein synthesis.

INTRODUCTION

Numerous studies have demonstrated that acupuncture with low frequency electrical stimulation (Acu/LFES) can correct muscle atrophy in human and animals with various diseases, including diabetes and chronic kidney disease-induced muscle wasting (Hu et al., 2015; Su et al., 2015), hindlimb suspension induced muscle loss (Onda et al., 2011), facioscapulohumeral muscle dystrophy (Liu et al., 2019), and amyotrophic lateral sclerosis or sciatic nerve injury caused muscle atrophy (Su et al., 2016; Sudhakaran, 2017; Yu et al., 2017). Acu/LFES is used worldwide as a therapeutic intervention to reduce stress and other health problems (NIH Consensus Conference, 1998). However, little is known regarding the precise mechanisms of this treatment on protein metabolism in muscle.

Skeletal muscle protein metabolism accounts for the major change of the total body protein pool and a fine balance between protein synthesis and protein breakdown regulates skeletal muscle mass (Mitch and Goldberg, 1996). Important determinants of protein synthesis are the key anabolic hormone insulin, insulin-like growth factor 1 (Igf1) and the insulin/Igf1 pathway. Activation of this pathway will upregulate PI3K-Akt-mTOR leading to phosphorylation of mechanistic target of rapamycin complex 1 (mTORC1), and subsequent downstream 4E-binding protein-1 (4EBP1), and the ribosomal protein of 70-kDa S6 kinase 1 (p70S6K1) (Holz et al., 2005). As the name suggests, p70S6K's target substrate is the S6 ribosomal protein. Phosphorylation of S6 initiates protein synthesis at the ribosome and proliferation of satellite cells results to muscle mass increase (Chung et al., 1992). The phosphorylation of p70S6K at threonine 389 has been used as a hallmark of activation by mTOR. It is well known that resistance exercise stimulates mTORC1 activity, promoting increases in the rates of myofibrillar protein synthesis.

Muscle is recognized as an endocrine organ. Contracting skeletal muscles have the capacity to communicate with other organs through the release of factors, such as myokines and exosomes for intercellular and inter-organ communication (Wang B. et al., 2019; Wang H. et al., 2019). Exosomes are small membranous vesicles that are secreted from muscle fibers inside multivesicular bodies. The release of exosomes is a common cellular function in living biological systems (Kim et al., 2015). The exosomes could act as messengers in tissue crosstalk since these muscle-derived nano-sized vesicles have the ability to deliver useful or harmful molecules (such as cytokines, proteins and miRNAs) to distant organs as well as distant muscles. Both pre-miRNAs and mature miRNAs packaged in exosomes are quite stable (Li et al., 2015). These miRs play an important regulatory role in the mechanisms of adaptation to physiology and pathology conditions. Our previous studies of exosomes following Acu/LEFS found that this treatment alters the expression of multiple miRNAs that are capable of regulating the physiology in distant organs, including decreased let-7 miRNA (Su et al., 2018).

Lethal-7 (let-7) was the second microRNAs (miRNA) to ever be identified. It was originally discovered in the nematode elegans in 2000 (Reinhart et al., 2000). Later, let-7 miRNAs were found in various animal species, including human. Unlike the nematode and fruit fly, which have a single isoform, the let-7 family is composed of nine mature let-7 miRNAs encoded by 12 different genomic loci, some of which are clustered together in the human (Roush and Slack, 2008). Let-7 miRNAs have been the focus of a variety of approaches for therapy and diagnosis. For example, Let-7 has been widely studied in oncogene, cell cycle and immunology fields. Many studies showed that let-7 enhances antitumor responses by directly targeting the high mobility group A2 oncogenes and RAS genes (Johnson et al., 2005; Mayr et al., 2007). Let-7 has been reported to be closely associated with regulation of cell cycle and leads to inhibitor cell proliferation (Johnson et al., 2007). Studies have revealed that let-7 family members act as key regulators for immune response to pathogenic agents in various diseases (Zhi et al., 2017; Gilles and Slack, 2018). Altogether, the let-7 family provides multiple possible strategies for developing approaches of diagnosis markers and therapy.

In this study, we hypothesize that Acu/LFES increases protein synthesis not only in local muscle, but also in distant muscle, through serum-derived exosomes-encapsulated microRNA. For proof of this hypothesis we: (1) measured protein synthesis in the muscle with or without Acu/LFES treatment and found increased synthesis with treatment; (2) measured exosome cargoes after Acu/LFES, and found that four members of the Let-7 family were significantly decreased by Acu/LFES; and (3) tested the impact of let-7 on the Igf1 signaling pathway and protein synthesis and found that Igf1 is the direct target of let-7.

RESULTS

Acu/LFES in Hindlimb Significantly Increases Protein Synthesis in Both Gastrocnemius and Triceps Brachii Muscles

Our previous studies have found that Acu/LFES decreases diabetes-induced protein degradation and improves muscle function (Hu et al., 2015; Su et al., 2015). To investigate whether Acu/LFES alters protein synthesis, we verified the protein synthesis in C57BL/6 mice after Acu/LFES. Acu/LFES mice received needles in point GB34 and S36 of hindlimb using a constant pulse for a one-time 30 min of electrical stimulation. In gastrocnemius muscle, Acu/LFES increased protein synthesis by 1.7-fold immediately after treatment and protein synthesis continued to increase up to the last experimental reading at 48-h (**Figure 1A**). Protein synthesis signaling proteins phosphorylated mTORC1, p70S6, and 4EBP1 also increased significantly. The increase was apparent immediately (0-h) after treatment through the terminal 24– or 72-h time points in gastrocnemius muscle (**Figure 1B**). Interestingly, protein synthesis also significantly increased in triceps brachii muscle, which is not near the electrically stimulated area (**Figure 1C**). These protein synthesis markers increased at 0-h after Acu/LFES until 72 h in triceps brachii muscles (**Figure 1D**). Acu/LFES did not change the protein degradation markers TRIM63/MuRF1, FBXO32/atrogin-1 and myostatin in these mice (**Supplementary Figure 1**).

Blocking Exosome Secretion Limited the Acu/LFES-Induced Increase in Protein Synthesis

Our previous research found that Acu/LFES increases exosome secretion (Su et al., 2018). To explore whether the increasing protein synthesis in triceps brachii is due to exosome-mediated regulation, we used GW4869 to inhibit exosome secretion. GW4869 is the most widely used pharmacological agent for blocking exosome generation. It inhibits the ceramide-mediated inward budding of multivesicular bodies and prevents release of mature exosomes from multivesicular bodies (Kosaka et al., 2010). Mice were injected with 1 μg/g body weight of GW4869 16-h before Acu/LFES. To elucidate the role of exosomes in Acu/LFES, we isolated exosomes from both sham and Acu/LFES-treated mice with or without GW4869 treatment. A Nanosight instrument was used to measure exosome amounts. We found that Acu/LFES changed exosome distribution in the serum (**Figure 2A**). The concentration of exosomes was increased 1.7-fold by Acu/LFES (**Figure 2B**). GW4869 decreased serum exosome concentration by 61% in sham mice, and 73% in Acu/LFES mice. There was no significant difference in either exosome mean size or mode size in each group (**Figures 2C,D**). In gastrocnemius muscle from mice treated with GW4869, Acu/LFES-induced protein synthesis was apparent at the 6-and 24-h point but not at any later time points (**Figure 3A**). In triceps brachii muscle, protein synthesis only increased at the 6-h time point after Acu/LFES treatment (**Figure 3B**). The phosphorylated mTORC1 and 4EBP1 increased at 6– and 24-h time points after treatment, and phosphorylated p70S6 only increased at 6-h′ time point in gastrocnemius muscle (**Figure 3C**). In triceps brachii muscles p70S6 phosphorylation only increased at the 6-h time point and mTORC1 increased at 0– and 6-h time points (**Supplementary Figure 5**). These results suggest that Acu/LFES-induced increase in muscle protein synthesis is associated with exosome secretion.

Acu/LFES Decreased let-7 in Serum Exosomes and Skeletal Muscles

The Acu/LFES induced increase in protein synthesis in distant muscle could be due to circulating exosomes carrying microRNAs. To explore this possibility, miRNA deep sequencing was performed on serum exosomes from both sham- and Acu/LFES-treated mice. We found that four members of the let-7 miRNA family were significantly decreased by Acu/LFES (**Supplementary Figure 2**). The largest change was in Let-7c-5p, which was 79% decreased by Acu/LFES treatment. In addition, the expressions of Let-7b-5p, let-7e-5p, let-7a-5p and let-7f-5p were also significantly decreased by 78, 71, 78, and 75% respectively (**Table 1**). To verify the deep-sequence data, we measured let-7c-5p miRNA by real time qPCR in RNA from serum exosomes of sham and Acu/LFES mice. The expression of let-7c-5p was decreased 75% in the serum exosomes from Acu/LFES mice vs. sham mice (**Figure 4A**). To validate whether Acu/LFES also altered let-7 miRNA in muscle tissue, the expression of let-7c-5p was measured in skeletal muscle of mice. In gastrocnemius, the expression of let-7c-5p was significantly decreased at 0–, 6–, 24– and 48-h after treatment (**Figure 4B**). In triceps brachii muscle decrease of let-7 in response to Acu/LFES was apparent at 0–, 6– and 24-h points but not at later time points (**Figure 4C**).

According to a miRNA database search, let-7-5p targets insulin-like growth factor 1, and Igf1 receptor (Igf1r) (Lewis et al., 2005). Since microRNA inhibits protein translation of their targets mRNA, a decrease of let-7 could release the inhibition of protein translation and results to increase targeted proteins, Igf-1 in this case. To identify whether Acu/LFES alters the translation of Igf-1, the amount of Igf1 and Igf1 receptor α and β subunits were measured by western blot (**Figure 4D**). Igf-1 was significantly increased immediately after Acu/LFES and persisted to the 72-h point. The increase in Igf-1r α subunit was detected from 6– to 72-h, and β subunit was from 0– to 48-h after Acu/LFES.

Overexpressing let-7c-5p Decreased Protein Synthesis in Cultured C2C12 Myotubes

To examine whether let-7 could change protein synthesis, we transfected let-7c-5p miRNA mimic or its inhibitor into cultured C2C12 cells. First, we tested whether let-7c-5p was successfully overexpressed. The expression of let-7 was increased 10.2-fold in the cells transfected with let-7c-5p mimic, and 15% decreased following transfection of the let-7 inhibitor compared with the control mimic group (**Figure 5A**). Second, we measured protein synthesis using puromycin incorporation and found that overexpressing let-7 significantly decreased protein synthesis.

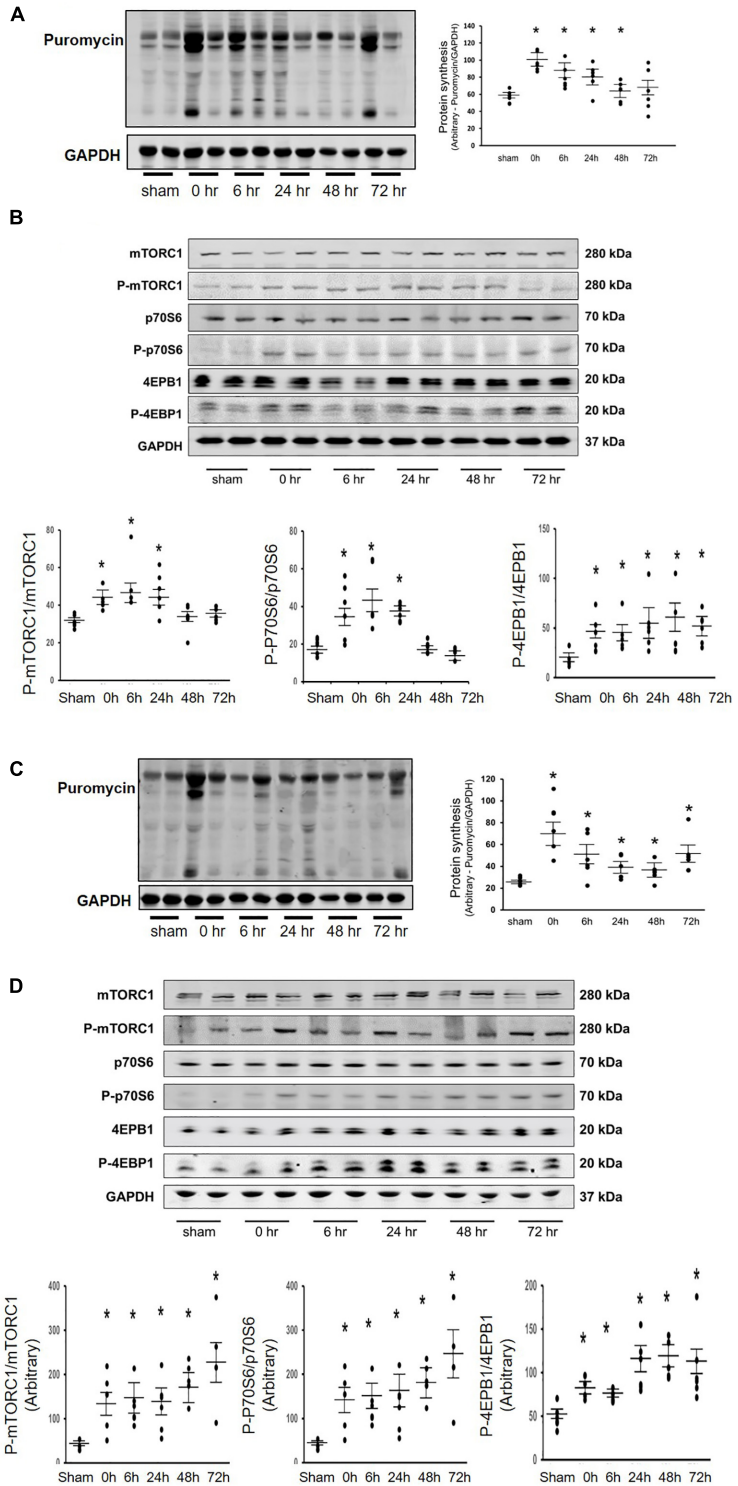

FIGURE 1 | Acu/LFES in hindlimb increased protein synthesis in both gastrocnemius and triceps brachii muscles. Experiments were performed in the sham and Acu/LFES treated mice. Puromycin was injected 30 min before harvest. Protein was isolated from the muscle of mice immediately (0), and 6–, 24–, 48– and 72-h after Acu/LFES. Puromycin in tissue lysates of gastrocnemius muscle **(A)** and triceps brachii muscle **(C)** was measured by Western blots. The point graphs show the change in incorporated puromycin normalized to their corresponding GAPDH protein (n = 6/group; $^*p < 0.05$ vs. sham). The proteins mTORC1, 4EBP1 and P70S6 were measured by Western blotting in gastrocnemius muscle **(B)** and triceps brachii muscle **(D)** of sham and Acu/LFES mice. The bottom point graphs show the ratio of phosphorylated protein to total protein, each normalized to the GAPDH from the same sample. Data is provided in arbitrary units (n = 6/group; $^*p < 0.05$ vs. sham).

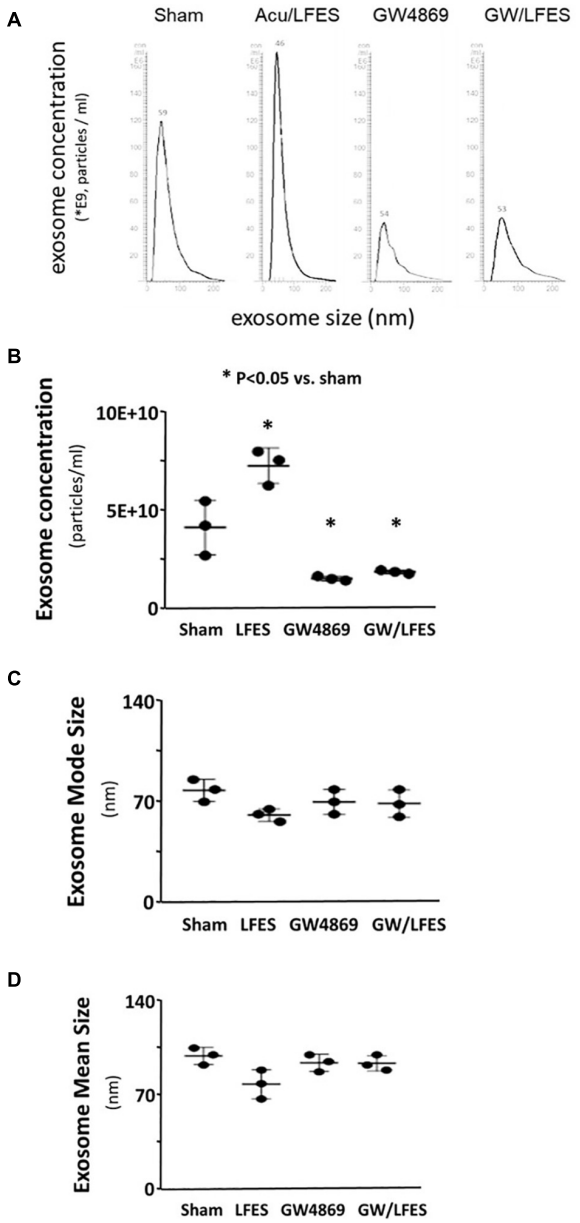

FIGURE 2 | GW4869 limited exosome secretion. Exosomes were isolated from sham, Acu/LFES, GW4869 and Acu/LFES+GW4869 treated mice. The exosome distribution **(A)**, concentration **(B)**, mode size **(C)** and mean size **(D)** were measured using a NanoSight instrument (means ± SE; n = 3/group; *$p < 0.05$ vs. sham).

Inhibition of endogenous let-7c-5p increased protein synthesis 1.28-fold (**Figure 5B**).

Provision of let-7 Inhibited Insulin/Igf-1 Signaling Pathway Components in Cultured C2C12 Myotubes

Since decreasing let-7-5p showed upregulation of insulin/Igf1 signaling pathway in animals, the protein and mRNA levels of these targets were investigated in the cultured cells. Providing let-7c-5p to the C2C12 myotubes in culture resulted in a decline in the protein abundance of Igf1, Igf1r α and β subunits (**Figure 5C**). Conversely, decreasing endogenous let-7 expression by transfection of the let-7 inhibitor raised the amount of Igf1 and Igf receptorα (**Figure 5C**). The 3′-UTR of Igf1 contains a conserved binding site for let-7 miRNA according to a consensus sequence search. To experimentally confirm that let-7c-5p directly interacts with the Igf1 mRNA. The Igf1 target site of let-7 (1,360–1,367 nt on Igf1 3′-UTR) was cloned into a luciferase reporter construct (pLUC-Igf1/3UTR). When cells were transfected with pLUC-Igf1/3UTR along with let-7c-5p miRNA, luciferase activity was decreased. However, when cells were transduced with an Igf1-luciferase construct along with let-7c inhibitor, luciferase activity was enhanced (**Figure 5D**). These results confirmed that let-7-5p directly targets Igf1 and blocks its translation.

DISCUSSION

In this study, we provide evidence showing that Acu/LFES administered to the hind limb muscles results in enhanced protein synthesis in both hindlimb and forelimb of mice. In addition, we showed that the treatment decreases circulation of let-7 miRNA in exosomes, which has the potential to influence distant muscles. A decrease in let-7 would increase the production of Igf-1 and Igf-1r; therefore, the consequence of let-7 inhibition would be increased protein synthesis.

It is well known that resistance exercise increases muscle mass through upregulation of the IGF-1 signaling pathway. Many tissues secrete Igf-1, including liver and skeletal muscle. Circulating Igf1 is largely contributed by the liver. However, skeletal muscle protein synthesis does not depend on plasma Igf1 (Sjogren et al., 1999). Instead, intrinsic secretion of muscle Igf-1 is a key determinant for activation of protein synthesis in muscle. Activation of the Igf-1 pathway results in phosphorylation of Akt, followed by upregulation of the mechanistic target of rapamycin complex 1 (mTORC1) (Morton et al., 2016). In our study, we found that Acu/LFES mimics resistance exercise, in that it upregulates the Igf-1 signaling pathway for at least 48 h leading to increased protein synthesis. The half-life of IGF-1 is only 5–10 min (Morimoto et al., 2005), so how is the increased protein synthesis supported for 48–72 h? We believe the key is the Acu/LFES -induced decrease in let-7 (**Figure 4A**) that results in increased levels of Igf-1 for 48–72 h and the consequent activation of protein synthesis (**Figure 1A**). The lower level of circulating let-7 would remove a repressive effect resulting in activation of Igf-1/Akt/mTORC1 signaling in distant muscles. In addition, the mTOR-dependent protein synthesis pathway is upregulated in 24-h, but increased protein synthesis persists for up to 72-h. We don't have an explanation for this phenomenon. Possibilities are that the Acu/LFES upregulation of protein synthesis levels are related to an mTOR-independent regulation. Alternatively, they may reflect a process that is begun by increasing mTOR that remains in effect beyond the initial stimulation. This is suggested by the fact that the protein synthesis levels, while significantly

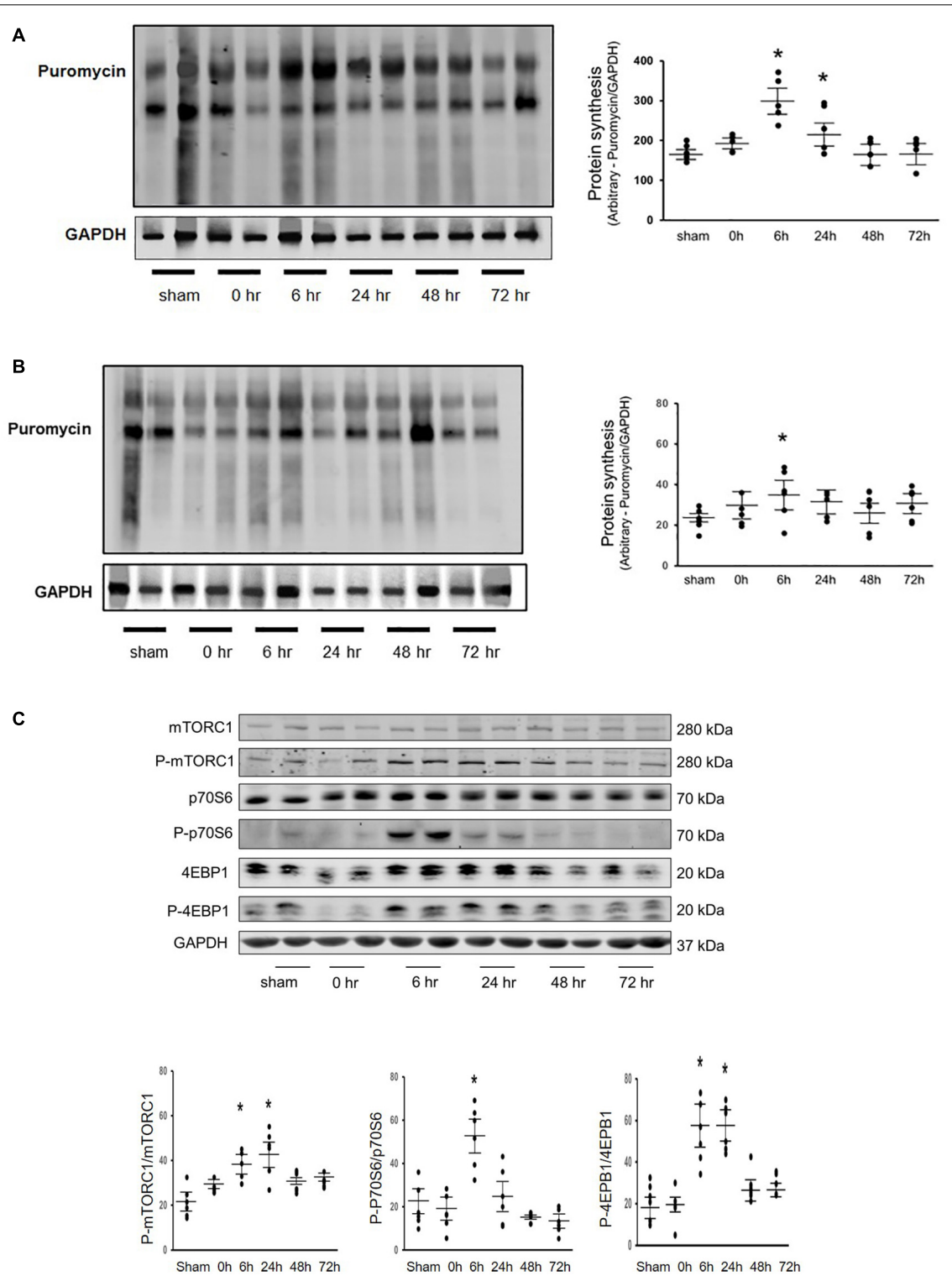

FIGURE 3 | Blocking exosome secretion limited the Acu/LFES-induced increase in protein synthesis. Experiments were performed in the sham and Acu/LFES treated mice. GW4869 was injected 16 h before Acu/LFES and puromycin was injected 30 min before harvest. Protein was isolated from the muscle of mice immediately (0), 6–, 24, 48 and 72 h after Acu/LFES. Puromycin in tissue lysates was measured by Western blots. The point graph of incorporate puromycin into gastrocnemius muscle **(A)** and triceps brachii muscle **(B)** show the change of the density of puromycin protein normalized to their corresponding GAPDH protein (n = 6/group; *p < 0.05 vs. sham). The proteins mTORC1, 4EBP1 and P70S6 were measured by Western blotting in gastrocnemius muscle **(C)** of sham and Acu/LFES mice. The bottom point graphs show the ration of phosphate protein to total protein normalized to the same sample GAPDH. Data is provided in arbitrary units (n = 6/group; *p < 0.05 vs. sham).

TABLE 1 | Let-7s are decreased by Acu/LFES in serum exosome.

miRNA	Base mean	Log2 fold change (control/ACU-LFES)	LfcSE*	Stat**	*p* value***
mmu-let-7c-5p	28,184.6	0.928507	0.218726	4.24507	2.19E-05
mmu-let-7b-5p	18,811.7	0.853183	0.225057	3.79096	0.00015006
mmu-let-7e-5p	480.613	1.01145	0.297435	3.40058	0.00067243
mmu-let-7a-5p	7,705.88	0.640478	0.213673	2.99747	0.00272233
mmu-let-7f-5p	4,335.76	0.590771	0.271134	2.17889	0.0293401
mmu-let-7k	40.8737	0.819582	0.484445	1.6918	0.0906847
mmu-let-7f-5p	4,335.76	0.590771	0.271134	2.17889	0.0293401
mmu-let-7d-3p	2,012.34	0.501061	0.273758	1.83031	0.0672043
mmu-let-7k	40.8737	0.819582	0.484445	1.6918	0.0906847
mmu-let-7d-5p	3,591.96	0.338747	0.229611	1.47531	0.14013
mmu-let-7f-1-3p	3.59731	−0.580753	0.45081	−1.28824	0.197661
mmu-let-7e-3p	17.7148	−0.61289	0.583092	−1.0511	0.293212
mmu-let-7a-1-3p	153.433	−0.368842	0.396564	−0.930093	0.352323
mmu-let-7a-1-3p	153.433	−0.368842	0.396564	−0.930093	0.352323
mmu-let-7c-2-3p	153.433	−0.368842	0.396564	−0.930093	0.352323
mmu-let-7a-2-3p	1.01045	−0.241443	0.324752	−0.743471	0.457197
mmu-let-7f-2-3p	1.05089	−0.243161	0.325405	−0.747256	0.454909
mmu-let-7j	7.3655	−0.38925	0.59186	−0.657673	0.510748
mmu-let-7b-3p	44.5565	0.32332	0.567	0.57023	0.568522
mmu-let-7g-5p	10,722.1	0.148303	0.295198	0.502383	0.615398
mmu-let-7i-3p	5.12321	−0.181665	0.503983	−0.360458	0.718505
mmu-let-7c-1-3p	5.37882	−0.140332	0.513847	−0.273101	0.784776
mmu-let-7i-5p	9,099.88	−0.116069	0.257261	−0.45117	0.865412
mmu-let-7g-3p	0	0	0	0	0

**LfcSE is the standard error of log2 fold change estimate. **Stat = Wald statistic. ***p value = Wald test.*

elevated, are not at as high a level as when mTOR is activated. Unraveling how mTOR signaling contributes to the protein synthesis during Acu/LFES needs further study. The important point is that patients with severe diseases that have muscle wasting frequently are unable to exercise to stimulate protein synthesis so it is important to explore other treatments that will provide them with a similar benefit. Acu/LFES will help them to increase muscle protein synthesis and prevent muscle wasting.

The let-7 family is involved with maintenance of muscle mass. An increase in let-7 is often associated with muscle loss. Oculopharyngeal muscle dystrophy patients have significantly increased expression of let-7 (Cappelletti et al., 2019). Muscle biopsy studies found that the expression of let-7s was increased in the skeletal muscle in humans with lower limb immobilization (D'Souza et al., 2018). However, there is some controversy about this role. In healthy men with 21-days bed rest let-7 was increased (Rullman et al., 2016); but in another study, the expression of let-7 was decreased in skeletal muscle at 10-days of bed rest in healthy man (Rezen et al., 2014). Our current study found that four members of the let-7 family were decreased in Acu/LFES mice. These changes were associated with an increase in protein synthesis and upregulation of the Igf-1 signaling pathway.

The impact of let-7 on the Igf1 signaling pathway could differ in various tissues. Our current study indicates that let-7c-5p directly targets Igf1 and inhibits its translation in skeletal muscle. The consequence of inhibiting Igf1 is inhibition of the downstream signaling pathway. For example, decreasing the activity or availability of the signaling pathway component mTORC1 would suppress protein synthesis, which is what we see in our Acu/LFESmice. The mTORC1 complex is a key player in nutrient status, and when activated, mTORC1 promotes protein synthesis, lipogenesis, and energy metabolism (Laplante and Sabatini, 2012). Some investigators have demonstrated that let-7 represses mTOR activation without turning off the insulin-signaling pathway in brain (Dubinsky et al., 2014). However, other recent articles describe let-7 directly targeting Igf-1 and/or Igf-1 receptor in human colorectal cancer cell proliferation (Samadi et al., 2019) in endometrial stromal cells (Ghazal et al., 2015) and in cultured testicular fragments (Shen et al., 2014). Another study showed that elevated let-7 expression increased insulin resistance while inhibition of the let-7 reduced insulin resistance and improved glucose uptake in the diabetic myocardium through Akt and mTOR pathways (Li et al., 2016). In our hands, Acu/LFES-induced decreased let-7 at 48 h, but increased Igf-1 for up to 72-h. This could suggest that Acu/LFES-mediated upregulation of Igf-1 is not only dependent on let-7 but has multiple regulatory pathways. This needs further investigation. Acu/LFES uses low-voltage electric currents in acupuncture points to treat a wide range of conditions. We used Acu/LFES for treat CKD-induced muscle wasting. Several alternate electric stimulations have also been used in clinical settings to treat different diseases, including muscle atrophy (Doucet et al., 2012). Transcutaneous electrical nerve stimulation (TENS) therapy involves the use of low-voltage electric currents

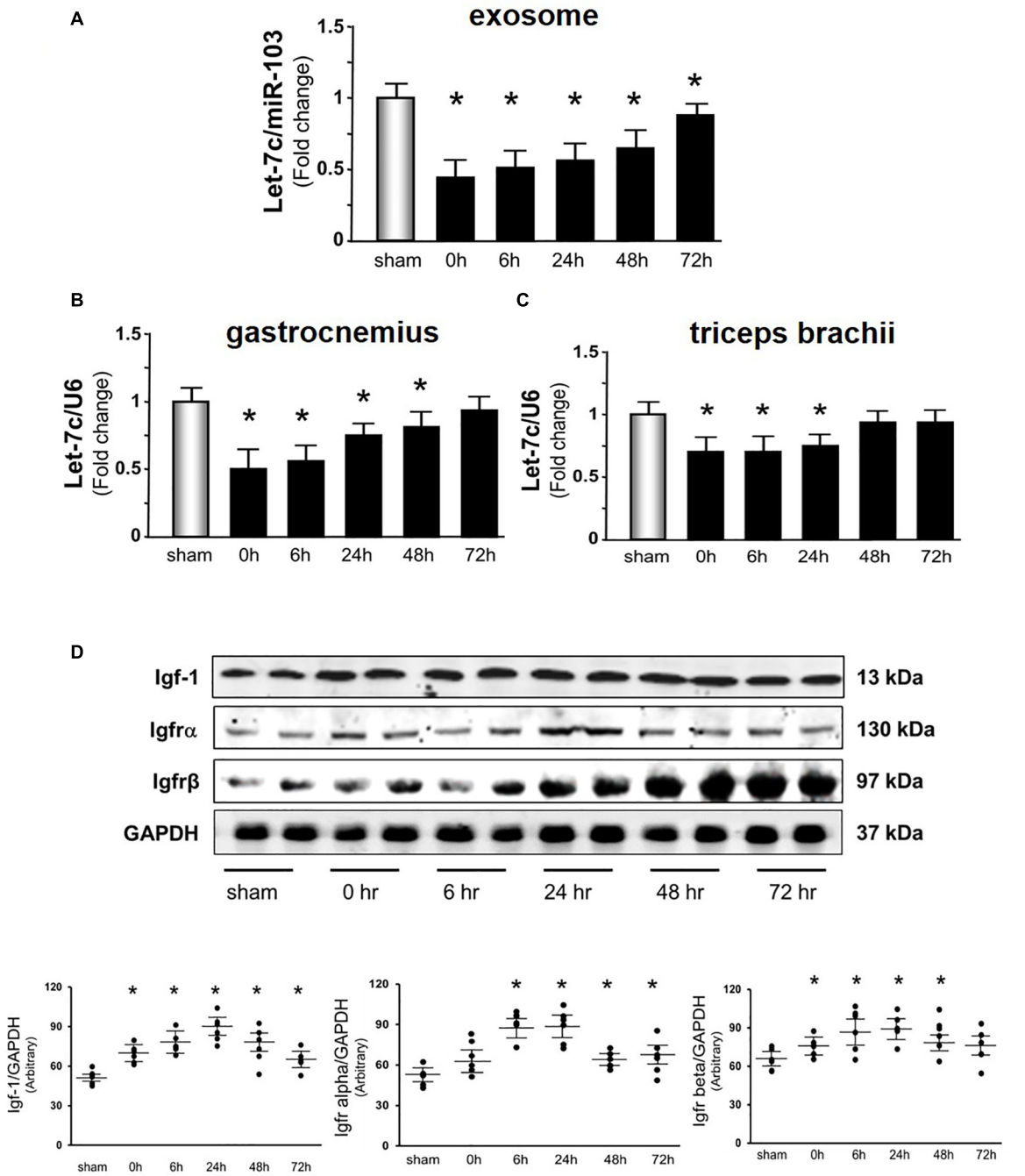

FIGURE 4 | Acu/LFES decreased let-7 in serum exosome and skeletal muscles. Total RNA was isolated from serum exosomes **(A)**, gastrocnemius muscle **(B)** and triceps brachii muscles **(C)** of sham and Acu/LFES treated mice. The expression of let-7c-5p was assayed by real time qPCR. The bar graph shows microRNA from the exosomes of Acu/LFES mice compared with levels in shams (defined as onefold). Results are normalized to miR-103a for serum and U6 for muscle (Bars: mean ± SE.; n = 6/group; *$p < 0.05$ vs. sham). **(D)** Protein was isolated from gastrocnemius muscle. Igf1, Igfrα and Igfrβ measured by Western blots. The point graph of protein showed the change of the density of proteins normalized to their corresponding GAPDH protein Data is provided in arbitrary units. (n = 6/group; *$p < 0.05$ vs. sham).

to treat pain (Gibson et al., 2017). Neuromuscular electrical stimulation (NMES) was used to build muscle strength after surgery or a period of disuse (Doucet et al., 2012). However, these treatments are different from Acu/LFES. Both TENS and NMES are non-invasive while Acu/LFES employs a direct insertion of a needle into the muscle. They also have different targets. TENS is specifically targeting the sensory nerves, which are responsible for sending pain-stop signals to the brain. NMES

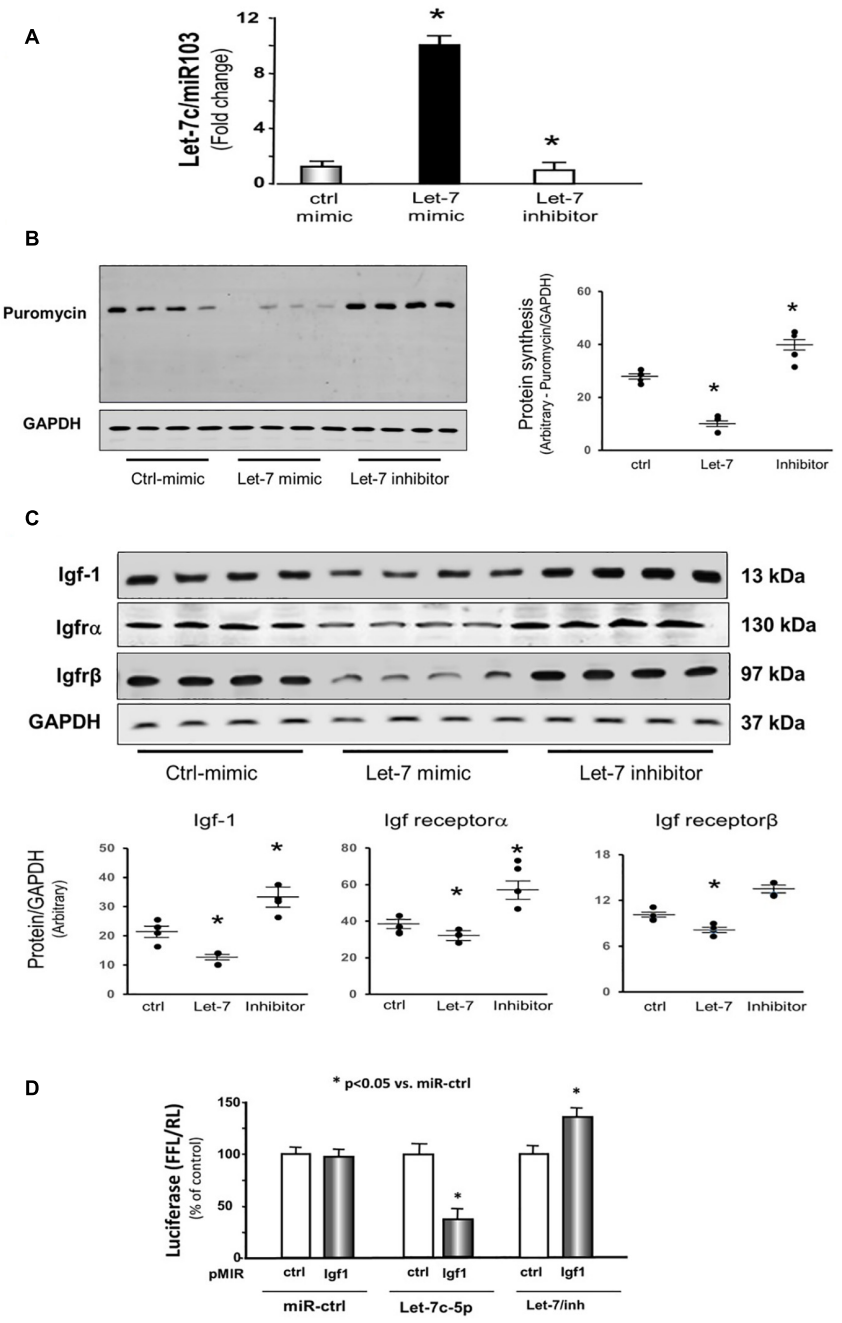

FIGURE 5 | Provision of let-7 inhibited Igf-1, Igfrα and Igfrβ in cultured C2C12 myotubes. **(A)** Total RNA was isolated from C2C12 myotubes transfected with control/mimic, let-7-5p/mimic and let-7/inhibitor. The expression of let-7-5p was assayed by real time qPCR. The bar graph shows let-7-5p from different group compared with levels in control/mimic (defined as onefold). Results are normalized to miR103 (Bars: mean ± SE; n = 4/group; *$p < 0.05$ vs. control/mimic). **(B)** Protein was isolated from the C2C12 myotubes transfected with control/mimic, let-7-5p/mimic and let-7/inhibitor. Puromycin was added into cell culture medium (1 μg final concentration) exactly 30 min before harvesting the cells. Puromycin in cell lysates was measured by Western blots. The point graph of incorporate puromycin into myotube shows the change of the density of puromycin protein normalized to their corresponding GAPDH protein (n = 4/group; *$p < 0.05$ vs. sham). **(C)** Protein was isolated from the C2C12 myotubes transfected with control/mimic, let-7-5p/mimic and let-7/inhibitor. Igf-1, Igfrα and Igfrβ in myotube lysates was measured by Western blots. The point graph showed the change of the density of each protein normalized to their corresponding GAPDH protein. Data is provided in arbitrary units. (n = 6/group; *$p < 0.05$ vs. control/mimic). **(D)** C2C12 cells were transfected with luciferase pMIR–ctrl vector (white bars) or the vector containing the 3′-UTR of Igf1 (pMIR-Igf: black bars). Cells were co-transfected with control mimic (miR-ctrl), let-7c-5p or let-7 inhibitor. Luciferase activity in cells that received the pMIR–ctrl with miR-ctrl was designated as the 100% (far left white bar). The other bars show the response to let-7 expressed as a percent of this control. Triplicate determinations were made in each condition and each experiment was repeated twice; the firefly luciferase (FFL) results were normalized by renilla luciferase (RL) activity. Data: mean ± SE; n = 9; * = $p < 0.05$ vs. pMIR-ctrl + miR-ctrl.

targets the muscle itself, specifically through the motor nerves to improve muscle regeneration. Acu/LFES targets acupuncture points (explained in the next paragraph). Some investigators performed NMES in hemodialysis patients and found that NMES increased quadriceps muscle area and maximum quadriceps extension strength compared with control patients (Esteve et al., 2017). However, there has been no study that directly compares Acu/LFES with NMES, and there is no study that examines the impact of the NMES on exosome release or exosome carried microRNA. Therefore, we cannot exclude the possibility that external electrical stimulation such as NMES may have beneficial effects similar as Acu/LFES. In this work we provide evidence that Acu/LFES can improve muscle health and may offer therapeutic options in the clinic.

Electrical Acupuncture involves the insertion of very thin needles through the skin at strategic points on the body; it is part of the ancient practice of Traditional Chinese Medicine. The most common role of acupuncture is to treat pain, for stress management and for overall wellness. Traditional Chinese Medicine practitioners believe the human body has more than 2,000 acupuncture points connected by channels or meridians, named Jing-Luo (collaterals). These channels create an energy flow (Qi, pronounced "chee," which means energy flow) through the body that is responsible for overall health. Disruption of the energy flow can cause disease. By applying Acu/LFES to certain points, it is thought to improve the flow of Qi, thereby improving health for distant organs. However, no anatomy study has identified structural components of the Jing-Luo in the human body. In this study, we found that electrical acupuncture changes the exosome concentration, size, and cargo, such as microRNA, that is in the circulation. We believe that muscle-derived exosomes in circulation play a role in Jing-Luo and exosome-carried cargo plays a role in Qi. This is a new concept to explain ancient medicine.

A consideration in this study is that we used GW4869 to inhibit exosome secretion, since it is the most widely used pharmacological agent for blocking exosome generation. However, GW4869 inhibits sphingolipid metabolism. Sphingolipids are capable of modulating multiple cell functions, such as apoptosis, cell proliferation, differentiation, and inflammation and have a broad role in skeletal muscle (Tan-Chen et al., 2020). Therefore, the potential of the Acu/LFES to influence muscle that is distant from the Acu/LFES origin site through a non-exosome mechanism needs further study.

Conclusion

Acu/LFES in the hindlimb releases exosomes into the circulation where it could move to and influence distant muscle and increase protein synthesis. The increase in protein synthesis in response to Acu/LFES is a consequence of the decrease in exosome-carried let-7-5p miRNA. Since let-7 targets and inhibits Igf-1 signaling pathway, limitation of let-7 upregulates this pathway and leads to increased protein synthesis. Our study provides strong mechanistic insight for understanding the benefits of treating muscle atrophy with Acu/LFES.

MATERIALS AND METHODS

Animals

These experiments were approved by the Emory University IACUC (protocol 4000152). The mice (C57BL/6J) were purchased from Jackson Laboratories (Bar Harbor, ME, United States) and were housed with a 12-h light/12-h dark cycle. GW4869, an inhibitor of exosome release, was purchased from Sigma-Aldrich. GW4869 was initially dissolved in DMSO into a stock solution of 200 mM before dilution in PBS to 20 μM for final injection and final DMSO concentration is 0.01%. The impact of vehicle (0.01% DMSO) on exosome secretion has also be tested in mice (**Supplementary Figure 4**).

Acu-LFES Treatment

The mice were kept in specially designed restraints so that they would remain in a recumbent position during Acu-LFES treatment. Mice were awake without any anesthesia and appeared to be comfortable throughout the treatments. Electrical acupuncture points were according to the WHO Standard Acupuncture guidelines (Lim, 2010). The positive point (anode: Yang-Ling-Quan, GB34) is in the hollow of the exterior-inferior of the caput fibulae about 6 mm deep. This position is close to the superficial fibular nerve and deep fibular nerve. The negative point (cathode: Zu-San-Li, ST36) is 5 mm beneath the capitulum fibulae and located laterally and posterior to the knee-joint about 7 mm deep and close to fibular nerve. The impulses were delivered between the two electrical acupuncture needles. Disposable sterile needles with a diameter of 0.25 mm (Shen Li Medical and Health Material Co., Ltd., Wujiang, China) were used. The needles were connected into an SDZ-II Electronic acupuncture instrument using consistent pulse, electric frequency 20 Hz, electric current 1 mA for 30 min (Hu et al., 2015). Sham mice had Acu/LFES needles inserted in close proximity to the ACU/LFES insertion position, needles were connected to the LFES device, but electrical stimulation was not applied.

Determination of Protein Synthesis by Puromycin Incorporation

To determine the rate of protein synthesis we utilized surface sensing of translation (SUnSET) methodology (Goodman et al., 2011). *In vivo*, 0.04 μmol/g puromycin (Calibiochem, Catalog #: 540222) was injected intraperitoneally into mice 30 min before harvest of skeletal muscle. Muscle was harvested at 0, 6, 24, 48 and 72 h after treatment and homogenized in Mueller's Buffer (50 mM HEPES, 0.1% Triton-X100, 4 mM EGTA, 10 mM EDTA, 15 mM Na4P2O7, 100 mM β-glycerophosphate, 20 mM NaF, 5 mM NaVO4 and 1% protease inhibitor cocktail). *In vitro*, C2C12 myotubes were grown in 6-well plates. Puromycin was added into the cell culture medium (1 μM final concentration) exactly 30 min before harvesting the cells. Cells were scraped into ice-cold RIPA buffer (100 μl for one well of a 6-well plate) followed by ultrasound sonication on ice. Puromycin-containing proteins were analyzed by Western blot. Proteins were separated on 10% SDS-PAGE gels. Anti-puromycin antibody was

purchased from Millipore (Catalog #: MABE343; Burlington, MA, United States).

Western Blot and Antibodies

Skeletal muscle or cells were homogenized in Gentle Lysis Buffer (10 mM Tris–HCl, 10 mM NaCl, 2 mM EDTA, 0.5% NP-40, 1% glycerol, and fresh added: 1 mM Na3VO4; 10 μg/ml PMSF; 5 μg/ml Aprotinin; 1 μg/ml Leupeptin) with phosphatase inhibitors cocktail 1 and 2 (Sigma). Protein concentration was measured using a RC-PC protein assay kit (Bio-Rad). Equal amounts of protein were loaded on the acrylamide/bis SDS-PAGE gel. Protein was transferred to a PVDF membrane and blotted with a specific primary antibody. Primary antibodies: (1:1,000 dilution except where indicated) that we used included mTOR (cat# 2972), p-mTOR (Ser2448; cat# 2481), 70S6K (cat# 9202); p-p70S6K (Thr389; cat# 9205), 4E-BP1 (53H11; cat# 9644); phospho-4E-BP1 (Thr37/46; Cat# 2855) from Cell Signaling; GAPDH (SC-365062), igfra (SC-712) and igfrb (SC-713) from Santa Cruz). Anti-IGF1 antibody (ab9572) was purchased from Abcam). Protein bands were scanned and quantified using the Li-cor Odyssey infrared scanning system (Li-COR Biosciences, Lincoln, Nebraska).

Isolation of Exosome

Exosomes were harvested from mice serum or conditional medium of cultured C2C12 myotubes. Mice sera were obtained from heart puncture. 0.5 ml serum from each mouse was diluted 5-times with PBS before isolation of exosomes. For purification and characterization of exosomes from serum or conditional medium, cell debris and organelles were eliminated by centrifugation at 1,000 *g* for 10 min, 4°C. The supernatant fraction was further centrifuged at 16,000 *g* for 30 min. The second supernatant was sterile filtered through a 0.22 μm filter. Exosomes were pelleted at 120,000 *g* for 90 min at 4°C (L8-70M ultracentrifuge, Beckman-Coulter, Indianapolis, IN, United States). Finally, the exosome pellet was re-suspended in 100-400 μl RNA stabilization reagent (Qiagen, Germantown, MD, United States) for RNA extraction or sterile PBS for other experiments. Exosomal size and concentration were verified using a NanoSight instrument (Malvern, Westborough, MA, United States) and an exosome marker (TSG101) was assessed by Western blot (Su et al., 2018) and exosome images taken by electro-microscopy (**Supplementary Figure 3**). Exosomes were also isolated from serum of vehicle (0.01% DMSO) injected mice. There are no significant differences in exosome size and concentration between vehicle injected and non-injected mice (**Supplementary Figure 4**).

Reverse Transcription and Quantitative PCR (q-PCR) for MicroRNA and mRNA

Total RNA was extracted using Tri-Reagent (Molecular Research Inc., Cincinnati, OH, United States). For miRNA, the miRCURY LNA™ Universal cDNA Synthesis kit (Exiqon Inc., Woburn, MA, United States) was used for reverse transcription of miRNA. The primers were purchased from Exiqon. The miRCURY LNA microRNA PCR SYBR Green master mix (Exiqon Inc.) was used for qPCR with the following cycle parameters: 95°C for 10 min and 40 cycles at 95°C for 10 s and 60°C for 60 s. Expression of individual microRNA was standardized to the mouse U6 gene (tissue) or miR103 (serum) (Hu et al., 2015; Su et al., 2017). For mRNA we used a Thermoscript RT-PCR kit (Invitrogen, Carlsbad, CA, United States). Real-time qPCR was performed with SYBR Green PCR Reagents (Bio-Rad, Hercules, CA, United States) using the following cycle parameters: 94°C for 2 min and 40 cycles at 94°C for 15 s, 55°C for 30 s, 72°C for 30 s with final extension at 72°C for 10 min. The quantification cycle (Cq) values were defined as the number of cycles required for the fluorescence signal to exceed the detection threshold. Individual miRNA or mRNA expression was calculated as the difference between the threshold values of the two genes ($2\text{-}\Delta cq$). Melting curve analysis was routinely performed to verify the specificity of the reaction. Let-7-5p (YP00204767) was ordered from Qiagen (Germantown, MD, United States).

miRNA-Seq Library Preparation and Sequencing

Qualitative and quantitative analysis of the total RNA was performed using the Thermo Nanodrop 2000 and Agilent 2100 Bioanalyzer respectively. Small RNA libraries were prepared using the SeqMatic tailormix miRNA sample preparation kit (SeqMatic. Union City, CA, United States) as per manufacturer's instructions. Briefly, 100 ng of total RNA was used for library preparation. Small RNA's were ligated with Illumina compatible adapters and each sample was tagged with a unique barcode to allow multiplexing. The adapter-ligated libraries were then enriched using PCR amplification followed by gel enrichment for mature miRNA library. The amplified library was validated using a High Sensitivity DNA chip on the Agilent Bioanalyzer. The libraries were further quantified on Qubit® 2.0 Fluorometer (Life Technologies, Grand Island, NY, United States) using the High Sensitivity dsDNA assay. Libraries from all the samples were multiplexed and run in a single lane of Illumina 3K flowcell. PhiX was used as an internal control on each lane to monitor the error statistics. Cluster generation was performed on the v3 flowcell on the Illumina cBot. The clustered flowcell was sequenced on the Illumina HiSeq3000 system as a 100-cycle single read multiplexed run.

Cell Culture

C2C12 cells (ATCC, Manassas, VA, United States), studied between passages 3 and 9, were cultured in growth medium (Dulbecco's Modified Eagle's Medium (DMEM) with 10% fetal bovine serum, 10% cow serum, 25 mM glucose, 100 u/ml penicillin, 100 μg/ml streptomycin, and 2 mM L-glutamine). Myotube differentiation was induced by replacing growth medium with differentiation media (FBS and cow serum was replaced by 2% horse serum). For *in vitro* let-7 overexpression and inhibition, mmu-let-7c-5p mimic (miRBase Accession #: MIMAT0000523; cat: 4464066), mmu-let-7c-5p inhibitor (Catalog #: 4464084), miRNA mimic negative control #1 and miRNA inhibitor negative control #1 were purchased from Thermo Fisher Scientific (Waltham, MA, United States). For

transfection, C2C12 cells in growth medium were seeded in 6-well plates and transfected using Effectene transfection reagent (Qiagen, Valencia, CA, United States). Cells were harvested 48 h after transfection and assayed for microRNA, mRNA and protein.

Luciferase Reporter Assay and Transfection

Effectene transfection reagent was used for transfection (Qiagen). Renilla luciferase vector was used for transfection efficiency control. Firefly and Renilla luciferase activities were measured by dual-luciferase assays (Promega) using TD-20/20 Luminometer (Turner designs, Sunnyvale, CA, United States) (Du et al., 2014). The luciferase report vectors (pMIR-REPORT Luciferase) were purchase from Applied BIOSYSTEMS (Cat#: AM5795; Waltham, MA, United States). The construct was made by Emory Integrated Genomics Core. Since the Let-7c miRNA binding site on the 3′-UTR of Igf1 is located at 1,360–1,367, the custom-made vector (pLuc-Igf1-3 UTR) containing the firefly luciferase gene and the 3-UTR (1310-1417) of Igf1. The insert was cloned between the *Spe*I and *Hin*dIII of the multiple cloning sites.

Statistical Analysis

Data are presented as mean ± se. To identify significant differences between two groups, comparisons were made by using the Student's *t*-test. When multiple treatments were compared, ANOVA was performed with a *post hoc* analysis by the Student–Newman–Keuls test. Differences with P values < 0.05 were are considered significant.

DATA AVAILABILITY STATEMENT

The datasets presented in this study can be found in online repositories. The names of the repository/repositories and accession number(s) can be found below: https://www.ncbi.nlm.nih.gov/, GSE176530.

ETHICS STATEMENT

The animal study was reviewed and approved by Emory University IACUC.

AUTHOR CONTRIBUTIONS

XW, CH, YH, and MY: conceptualization. CH, MY, and YH: methodology. XW, YH, MH, YW, and FH: validation. YH and MY: formal analysis. YH, MY, AK, HC, YW, and FH: investigation. XW and HC: resources. XW, YH, and MY: data curation. YH and MY: writing—original draft preparation. XW and JK: writing—review and editing. XW and HC: visualization and funding acquisition. XW: supervision. All authors contributed to the article and approved the submitted version.

FUNDING

Research reported in this publication was supported by the National Institute of Arthritis and Musculoskeletal and Skin Diseases (NIAMS) of the National Institutes of Health under Award Number R01 AR060268 to XW; and by the Department of Veteran Affairs MERIT Award 5I01BX000994 to HC. This research project was also supported in part (microRNA deep sequencing) by the Genomics core of Yerkes National Primate Research Center under Award Number NIH ORIP/OD P51OD011132.

SUPPLEMENTARY MATERIAL

The Supplementary Material for this article can be found online at: https://www.frontiersin.org/articles/10.3389/fphys.2021.697139/full#supplementary-material

REFERENCES

Cappelletti, C., Galbardi, B., Bruttini, M., Salerno, F., Canioni, E., Pasanisi, M. B., et al. (2019). Aging-associated genes and let-7 microRNAs: a contribution to myogenic program dysregulation in oculopharyngeal muscular dystrophy. *FASEB J.* 33, 7155–7167. doi: 10.1096/fj.201801577rr

Chung, J., Kuo, C. J., Crabtree, G. R., and Blenis, J. (1992). Rapamycin-FKBP specifically blocks growth-dependent activation of and signaling by the 70 kd S6 protein kinases. *Cell* 69, 1227–1236. doi: 10.1016/0092-8674(92)90643-q

Doucet, B. M., Lam, A., and Griffin, L. (2012). Neuromuscular electrical stimulation for skeletal muscle function. *Yale J. Biol. Med.* 85, 201–215.

D'Souza, R. F., Zeng, N., Figueiredo, V. C., Markworth, J. F., Durainayagam, B. R., Mitchell, S. M., et al. (2018). Dairy protein supplementation modulates the human skeletal muscle microRNA response to lower limb immobilization. *Mol. Nutr. Food Res.* 62:e1701028.

Du, J., Klein, J. D., Hassounah, F., Zhang, J., Zhang, C., and Wang, X. H. (2014). Aging increases CCN1 expression leading to muscle senescence. *Am. J. Physiol. Cell Physiol.* 306, C28–C36.

Dubinsky, A. N., Dastidar, S. G., Hsu, C. L., Zahra, R., Djakovic, S., Duarte, S., et al. (2014). Let-7 coordinately suppresses components of the amino acid sensing pathway to repress mTORC1 and induce autophagy. *Cell Metab.* 20, 626–638. doi: 10.1016/j.cmet.2014.09.001

Esteve, V., Carneiro, J., Moreno, F., Fulquet, M., Garriga, S., Pou, M., et al. (2017). The effect of neuromuscular electrical stimulation on muscle strength, functional capacity and body composition in haemodialysis patients. *Nefrologia* 37, 68–77. doi: 10.1016/j.nefroe.2017.01.011

Ghazal, S., McKinnon, B., Zhou, J., Mueller, M., Men, Y., Yang, L., et al. (2015). H19 lncRNA alters stromal cell growth via IGF signaling in the endometrium of women with endometriosis. *EMBO Mol. Med.* 7, 996–1003. doi: 10.15252/emmm.201505245

Gibson, W., Wand, B. M., and O'Connell, N. E. (2017). Transcutaneous electrical nerve stimulation (TENS) for neuropathic pain in adults. *Cochrane Database Syst. Rev.* 9:CD011976.

Gilles, M. E., and Slack, F. J. (2018). Let-7 microRNA as a potential therapeutic target with implications for immunotherapy. *Expert Opin. Ther. Targets* 22, 929–939. doi: 10.1080/14728222.2018.1535594

Goodman, C. A., Mabrey, D. M., Frey, J. W., Miu, M. H., Schmidt, E. K., Pierre, P., et al. (2011). Novel insights into the regulation of skeletal muscle protein synthesis as revealed by a new nonradioactive in vivo technique. *FASEB J.* 25, 1028–1039. doi: 10.1096/fj.10-168799

Holz, M. K., Ballif, B. A., Gygi, S. P., and Blenis, J. (2005). mTOR and S6K1 mediate assembly of the translation preinitiation complex through dynamic protein interchange and ordered phosphorylation events. *Cell* 123, 569–580. doi: 10.1016/j.cell.2005.10.024

Hu, L., Klein, J. D., Hassounah, F., Cai, H., Zhang, C., Xu, P., et al. (2015). Low-frequency electrical stimulation attenuates muscle atrophy in CKD-a potential treatment strategy. *J. Am. Soc. Nephrol.* 26, 626–635. doi: 10.1681/asn.2014020144

Johnson, C. D., Esquela-Kerscher, A., Stefani, G., Byrom, M., Kelnar, K., Ovcharenko, D., et al. (2007). The let-7 microRNA represses cell proliferation pathways in human cells. *Cancer Res.* 67, 7713–7722. doi: 10.1158/0008-5472.can-07-1083

Johnson, S. M., Grosshans, H., Shingara, J., Byrom, M., Jarvis, R., Cheng, A., et al. (2005). RAS is regulated by the let-7 microRNA family. *Cell* 120, 635–647. doi: 10.1016/j.cell.2005.01.014

Kim, D. K., Lee, J., Simpson, R. J., Lotvall, J., and Gho, Y. S. (2015). EVpedia: a community web resource for prokaryotic and eukaryotic extracellular vesicles research. *Semin. Cell Dev. Biol.* 40, 4–7. doi: 10.1016/j.semcdb.2015.02.005

Kosaka, N., Iguchi, H., Yoshioka, Y., Takeshita, F., Matsuki, Y., and Ochiya, T. (2010). Secretory mechanisms and intercellular transfer of microRNAs in living cells. *J. Biol. Chem.* 285, 17442–17452. doi: 10.1074/jbc.m110.107821

Laplante, M., and Sabatini, D. M. (2012). mTOR signaling in growth control and disease. *Cell* 149, 274–293. doi: 10.1016/j.cell.2012.03.017

Lewis, B. P., Burge, C. B., and Bartel, D. P. (2005). Conserved seed pairing, often flanked by adenosines, indicates that thousands of human genes are microRNA targets. *Cell* 120, 15–20. doi: 10.1016/j.cell.2004.12.035

Li, J., Ren, Y., Shi, E., Tan, Z., Xiong, J., Yan, L., et al. (2016). Inhibition of the Let-7 family MicroRNAs induces cardioprotection against ischemia-reperfusion injury in diabetic rats. *Ann. Thor. Surg.* 102, 829–835. doi: 10.1016/j.athoracsur.2016.02.016

Li, Y., Shen, Z., and Yu, X. Y. (2015). Transport of microRNAs via exosomes. *Nat. Rev. Cardiol.* 12:198. doi: 10.1038/nrcardio.2014.207-c1

Lim, S. (2010). WHO standard acupuncture point locations. *Evidence Based Complement. Altern. Med.* 7, 167–168. doi: 10.1093/ecam/nep006

Liu, Y., Xiao, F., and Liang, X. (2019). Acupuncture improves the facial muscular function in a case of facioscapulohumeral muscular dystrophy. *J. Acupunct. Merid. Stud.* 12, 73–76. doi: 10.1016/j.jams.2018.11.001

Mayr, C., Hemann, M. T., and Bartel, D. P. (2007). Disrupting the pairing between let-7 and Hmga2 enhances oncogenic transformation. *Science* 315, 1576–1579. doi: 10.1126/science.1137999

Mitch, W. E., and Goldberg, A. L. (1996). Mechanisms of muscle wasting. The role of the ubiquitin-proteasome pathway. *N. Engl. J. Med.* 335, 1897–1905. doi: 10.1056/nejm199612193352507

Morimoto, L. M., Newcomb, P. A., White, E., Bigler, J., and Potter, J. D. (2005). Variation in plasma insulin-like growth factor-1 and insulin-like growth factor binding protein-3: genetic factors. *Cancer Epidemiol. Biomark. Prevent.* 14, 1394–1401. doi: 10.1158/1055-9965.epi-04-0694

Morton, R. W., Oikawa, S. Y., Wavell, C. G., Mazara, N., McGlory, C., Quadrilatero, J., et al. (2016). Neither load nor systemic hormones determine resistance training-mediated hypertrophy or strength gains in resistance-trained young men. *J. Appl. Physiol.* 121, 129–138. doi: 10.1152/japplphysiol.00154.2016

NIH Consensus Conference (1998). NIH consensus conference. Acupuncture. *JAMA* 280, 1518–1524.

Onda, A., Jiao, Q., Nagano, Y., Akimoto, T., Miyamoto, T., Minamisawa, S., et al. (2011). Acupuncture ameliorated skeletal muscle atrophy induced by hindlimb suspension in mice. *Biochem. Biophys. Res. Commun.* 410, 434–439. doi: 10.1016/j.bbrc.2011.05.152

Reinhart, B. J., Slack, F. J., Basson, M., Pasquinelli, A. E., Bettinger, J. C., Rougvie, A. E., et al. (2000). The 21-nucleotide let-7 RNA regulates developmental timing in Caenorhabditis elegans. *Nature* 403, 901–906. doi: 10.1038/35002607

Rezen, T., Kovanda, A., Eiken, O., Mekjavic, I. B., and Rogelj, B. (2014). Expression changes in human skeletal muscle miRNAs following 10 days of bed rest in young healthy males. *Acta Physiol.* 210, 655–666. doi: 10.1111/apha.12228

Roush, S., and Slack, F. J. (2008). The let-7 family of microRNAs. *Trends Cell Biol.* 18, 505–516. doi: 10.1016/j.tcb.2008.07.007

Rullman, E., Mekjavic, I. B., Fischer, H., and Eiken, O. (2016). PlanHab (Planetary Habitat Simulation): the combined and separate effects of 21 days bed rest and hypoxic confinement on human skeletal muscle miRNA expression. *Physiol. Rep.* 4:e12753. doi: 10.14814/phy2.12753

Samadi, P., Afshar, S., Amini, R., Najafi, R., Mahdavinezhad, A., Sedighi Pashaki, A., et al. (2019). Let-7e enhances the radiosensitivity of colorectal cancer cells by directly targeting insulin-like growth factor 1 receptor. *J Cell Physiol.* 234, 10718–10725. doi: 10.1002/jcp.27742

Shen, G., Wu, R., Liu, B., Dong, W., Tu, Z., Yang, J., et al. (2014). Upstream and downstream mechanisms for the promoting effects of IGF-1 on differentiation of spermatogonia to primary spermatocytes. *Life Sci.* 101, 49–55. doi: 10.1016/j.lfs.2014.02.016

Sjogren, K., Liu, J. L., Blad, K., Skrtic, S., Vidal, O., Wallenius, V., et al. (1999). Liver-derived insulin-like growth factor I (IGF-I) is the principal source of IGF-I in blood but is not required for postnatal body growth in mice. *Proc. Natl. Acad. Sci. U.S.A.* 96, 7088–7092. doi: 10.1073/pnas.96.12.7088

Su, Z., Hu, L., Cheng, J., Klein, J. D., Hassounah, F., Cai, H., et al. (2016). Acupuncture plus low-frequency electrical stimulation (Acu-LFES) attenuates denervation-induced muscle atrophy. *J. Appl. Physiol.* 120, 426–436. doi: 10.1152/japplphysiol.00175.2015

Su, Z., Klein, J. D., Du, J., Franch, H. A., Zhang, L., Hassounah, F., et al. (2017). Chronic kidney disease induces autophagy leading to dysfunction of mitochondria in skeletal muscle. *Am. J. Physiol. Renal Physiol.* 312, F1128–F1140.

Su, Z., Robinson, A., Hu, L., Klein, J. D., Hassounah, F., Li, M., et al. (2015). Acupuncture plus low-frequency electrical stimulation (Acu-LFES) attenuates diabetic myopathy by enhancing muscle regeneration. *PLoS One* 10:e0134511. doi: 10.1371/journal.pone.0134511

Su, Z., Yuan, Y., Yu, M., Liu, Y., Klein, J. D., and Wang, X. H. (2018). Electrically stimulated acupuncture increases renal blood flow through exosomes-carried miR-181. *Am. J. Physiol. Renal Physiol.* 315, F1542–F1549.

Sudhakaran, P. (2017). Amyotrophic lateral sclerosis: an acupuncture approach. *Med. Acupunct.* 29, 260–268. doi: 10.1089/acu.2017.1241

Tan-Chen, S., Guitton, J., Bourron, O., Le Stunff, H., and Hajduch, E. (2020). Sphingolipid metabolism and signaling in skeletal muscle: from physiology to physiopathology. *Front. Endocrinol.* 11:491.

Wang, B., Zhang, A., Wang, H., Klein, J. D., Tan, L., Wang, Z. M., et al. (2019). miR-26a limits muscle wasting and cardiac fibrosis through exosome-mediated microRNA transfer in chronic kidney disease. *Theranostics* 9, 1864–1877. doi: 10.7150/thno.29579

Wang, H., Wang, B., Zhang, A., Zhang, A., Hassounah, F., Seow, Y., et al. (2019). Exosome-mediated miR-29 transfer reduces muscle atrophy and kidney fibrosis in mice. *Mol. Ther.* 27, 571–583. doi: 10.1016/j.ymthe.2019.01.008

Yu, J., Wang, M., Liu, J., Zhang, X., and Yang, S. (2017). Effect of electroacupuncture on the expression of agrin and acetylcholine receptor subtypes in rats with tibialis anterior muscular atrophy induced by sciatic nerve injection injury. *Acupunct. Med.* 35, 268–275. doi: 10.1136/acupmed-2015-011005

Zhi, L., Yu, Y., Li, X., Wang, D., and Wang, D. (2017). Molecular control of innate immune response to *Pseudomonas aeruginosa* infection by intestinal let-7 in *Caenorhabditis elegans*. *PLoS Pathog.* 13:e1006152. doi: 10.1371/journal.ppat.1006152

Author Disclaimer: The content is solely the responsibility of the authors and does not necessarily reflect the official views of the NIH, the Department of Veterans Affairs, or the United States Government.

Conflict of Interest: The authors declare that the research was conducted in the absence of any commercial or financial relationships that could be construed as a potential conflict of interest.

Publisher's Note: All claims expressed in this article are solely those of the authors and do not necessarily represent those of their affiliated organizations, or those of the publisher, the editors and the reviewers. Any product that may be evaluated in this article, or claim that may be made by its manufacturer, is not guaranteed or endorsed by the publisher.

frontiers in Physiology

ORIGINAL RESEARCH
published: 13 October 2021
doi: 10.3389/fphys.2021.689179

Fine Tuning of Phosphorothioate Inclusion in 2′-O-Methyl Oligonucleotides Contributes to Specific Cell Targeting for Splice-Switching Modulation

Yoshitsugu Aoki[1,2], Cristina S. J. Rocha[3], Taavi Lehto[3], Shouta Miyatake[1], Henrik Johansson[4], Yasumasa Hashimoto[1], Joel Z. Nordin[1,3], Imre Mager[2], Misako Aoki[2], McClorey Graham[2], Chaitra Sathyaprakash[1], Thomas C. Roberts[2], Matthew J. A. Wood[2], Mark A. Behlke[5] and Samir El Andaloussi[2,3]**

[1] Department of Molecular Therapy, National Institute of Neuroscience, National Center of Neurology and Psychiatry (NCNP), Tokyo, Japan, [2] Department of Paediatrics, University of Oxford, Oxford, United Kingdom, [3] Department of Laboratory Medicine, Clinical Research Center, Karolinska Institutet, Karolinska University Hospital, Huddinge, Sweden, [4] Department of Oncology-Pathology, Clinical Research Center, Karolinska Institutet, Karolinska University Hospital, Huddinge, Sweden, [5] Integrated DNA Technologies, Inc., Coralville, IA, United States

OPEN ACCESS

Edited by:
Wataru Aoi, Kyoto Prefectural University, Japan

Reviewed by:
Demetrios A. Arvanitis, Biomedical Research Foundation, Greece
Abitha Sukumaran, Cincinnati Children's Hospital Medical Center, United States

***Correspondence:**
Samir El Andaloussi
samir.el-andaloussi@ki.se
Yoshitsugu Aoki
tsugu56@ncnp.go.jp

Specialty section:
This article was submitted to Striated Muscle Physiology, a section of the journal Frontiers in Physiology

Received: *31 March 2021*
Accepted: *06 September 2021*
Published: *13 October 2021*

Citation:
Aoki Y, Rocha CSJ, Lehto T, Miyatake S, Johansson H, Hashimoto Y, Nordin JZ, Mager I, Aoki M, Graham M, Sathyaprakash C, Roberts TC, Wood MJA, Behlke MA and Andaloussi SE (2021) Fine Tuning of Phosphorothioate Inclusion in 2′-O-Methyl Oligonucleotides Contributes to Specific Cell Targeting for Splice-Switching Modulation. Front. Physiol. 12:689179. doi: 10.3389/fphys.2021.689179

Splice-switching antisense oligonucleotide- (SSO-) mediated correction of framedisrupting mutation-containing premessenger RNA (mRNA) transcripts using exon skipping is a highly promising treatment method for muscular diseases such as Duchenne muscular dystrophy (DMD). Phosphorothioate (PS) chemistry, a commonly used oligonucleotide modification, has been shown to increase the stability of and improve the pharmacokinetics of SSOs. However, the effect of PS inclusion in 2′-O-methyl SSOs (2OMe) on cellular uptake and splice switching is less well-understood. At present, we demonstrate that the modification of PS facilitates the uptake of 2OMe in H2k-*mdx* myoblasts. Furthermore, we found a dependency of SSO nuclear accumulation and high splice-switching activity on PS inclusion in 2OMe (2OMePS), as tested in various reporter cell lines carrying pLuc/705. Increased exon-inclusion activity was observed in muscle, neuronal, liver, and bone cell lineages *via* both the gymnotic uptake and lipofection of 2OMePS. Using the photoactivatable ribonucleoside-enhanced crosslinking and a subsequent proteomic approach, we identified several 2OMePS-binding proteins, which are likely to play a role in the trafficking of 2OMePS to the nucleus. Ablation of one of them, *Ncl* by small-interfering RNA (siRNA) enhanced 2OMePS uptake in C2C12 myoblasts and upregulated luciferase RNA splicing in the HeLa Luc/705 reporter cell line. Overall, we demonstrate that PS inclusion increases nuclear delivery and splice switching in muscle, neuronal, liver, and bone cell lineages and that the modulation of 2OMePS-binding partners may improve SSO delivery.

Keywords: skeletal muscle, Duchenne muscular dystrophy, splice-switching oligonucleotide (SSO), phosphorothioate, 2OMePS

INTRODUCTION

In the last few decades, numerous studies have demonstrated the potential of using splice-switching antisense oligonucleotides (SSOs). SSOs are typically 15–25 mers, short oligonucleotides, designed to target pre-messenger RNA (mRNA) and modulate the splicing patterns of target transcripts by blocking Watson–Crick RNA–RNA base-pairing or RNA–protein-binding interactions (Zamecnik and Stephenson, 1978; Dominski and Kole, 1993). This function gives SSOs a solid therapeutic potential, particularly, for exon skipping in Duchenne muscular dystrophy (DMD). SSOs using 2′-O-methyl RNA (2OMe) chemistry designed to restore dystrophin were the first oligonucleotides tested in DMD (Cirak et al., 2011). However, they failed at trials due to only a marginal clinical benefit for patients, including low efficiency of dystrophin restoration to the muscle. However, 2OMe SSOs have a tremendous promise as a treatment, and further optimisation and understanding of its delivery mechanism and action are crucial for use in related diseases.

A major limitation of the unmodified SSO using 2OMe in a therapeutic context is its instability in biological fluids due to susceptibility to nuclease digestion. The introduction of phosphorothioate (PS) linkages, replacing a phosphodiester backbone, was a commonly used oligonucleotide modification, which dramatically increased SSO stability and improved their ability to interact with serum proteins, including albumin, increasing their half-life and bioavailability (Dias and Stein, 2002). Subsequent SSO designs typically display 2′ modifications in the ribose ring, such as a naturally occurring methyl group. Most of these modifications further increase oligonucleotide stability and significantly enhance their binding affinity toward complementary RNAs. For *in vitro* and *in vivo* splice-switching applications, 2OMe has been extensively used with full PS modifications (Heemskerk et al., 2010; Ezzat et al., 2012; Flanigan et al., 2014). It has been shown that three-terminal PS entities on each side of SSOs are sufficient to confer exonuclease resistance (Mathy et al., 2007). However, the optimal modifications of PS inclusion in 2OMe to improve the splicing efficiency of SSO are not well-understood.

The activity of 2OMePS depends on numerous factors, including RNA secondary and tertiary structures, protein binding with target RNAs, the subcellular localization of 2OMePS, the interaction of 2OMePS with endogenous intracellular proteins and cellular machinery, and cellular uptake. An understanding of the interaction of 2OMePS with proteins may facilitate the development of more efficacious SSOs. PS-modified 2OMe is known to bind more proteins and to have a higher affinity than 2OMe with a phosphodiester backbone (Dias and Stein, 2002). Differences in protein binding can result in different pharmacological profiles and alter the subcellular distribution of SSOs (Weidner et al., 1995; Baltz et al., 2012). Although some proteins, such as nucleolin (NCL), albumin, and chaperonin T-complex 1 (TCP1) that interact with 2OMePS, have been previously identified (Liang et al., 2014), the effects of these proteins on 2OMePS activity and subcellular localization remain elusive.

Here, we aimed to fine-tune PS inclusion in 2OMe to improve SSO splicing efficiency in several cell types. Muscle, neuronal, liver, and bone cell lines were investigated to understand whether different target cell types would pose respective challenges in the case of the same SSO. We further investigated the interaction of PS-modified 2OMe with the other cellular proteins in C2C12 myoblasts.

MATERIALS AND METHODS

Splice-Switching Antisense Oligonucleotides

All SSOs targeting the donor splice site of exon 23 of the mouse *Dmd* pre-mRNA with PS- and end2OMePS modifications (5′-GGCCAAACCUCGGCUUACCU-3′) were synthesized by Integrated DNA Technologies (IDT, Coralville, IA, USA). Cy3- or FITC-conjugated 2OMePS and 2OMe-endPS were also synthesized by IDT. The nomenclature, size, and sequence of all SSOs used in this study are summarized in **Table 1**.

Cell Line Culture Conditions

C2C12 and HeLa cells were grown in Dulbecco's Modified Eagle Medium (DMEM), high glucose, GlutaMAX media (Life Technologies, Carlsbad, CA, USA) with 10% fetal bovine serum (FBS) (Life Technologies, Carlsbad, CA, USA) and 1% penicillin/streptomycin (Life Technologies, Carlsbad, CA, USA). Murine H2k-*mdx* myoblasts were cultured in gelatin- (0.01%) coated flasks at 33°C, under 10% CO_2 in DMEM supplemented with 20% heat-inactivated FBS (FBS Gold, PAA Laboratories, Pasching, Austria), 2% chicken embryo extract (Seralab, Sussex, UK), 1% penicillin/streptomycin-neomycin antibiotic mixture (Life Technologies, Carlsbad, CA, USA), and 3 pg/ml γ-interferon (PeproTech, Rehovot, Israel). For differentiation, the cells (1×10^5) were seeded into the wells of a 24-well plate, and the medium was changed after 24 h into a differentiation medium consisting of DMEM containing 2% horse serum (Life Technologies, Carlsbad, CA, USA) and was differentiated for 3–4 days before experimentation. For the SSO treatment, the cells were treated in the serum-free Opti-MEM® medium for 4 h, the medium was then changed for a differentiation medium, and incubation continued for 20 h. Reporter cell lines HeLa Luc/705, HuH7_705, C2C12_705, Neuro-2a_705, and U-2 OS_705 were cultivated and maintained in DMEM, high glucose plus 10% FBS with 200 (U-2 OS_705) or 400 (Huh7_705, C2C12_705, and Neuro-2a_705) μg/ml G418 (Life Technologies, Carlsbad, CA, USA) at 37°C, 5% CO_2 in 95% humidity (Rocha et al., 2016).

SSO or Small-Interfering RNA Delivery

Transfection with different concentrations of SSOs was performed with PepFect14 (Psyclo Peptide, Inc., Shanghai, China) (Ezzat et al., 2011) or Lipofectamine® 2000 (LF2000) (Life Technologies, Invitrogen, CA, USA) or OptiMEM (gymnotic delivery), which was formulated in OptiMEM for 15 min at room temperature according to the protocols of the manufacturer, and was then added to the cells cultured in DMEM + 10% FBS. The complexes were left in the culture for 24 h, after which the cells were harvested for RNA isolation or luciferase

TABLE 1 | Nomenclature, size, and sequence of oligonucleotides.

Name	Size (mers)	Sequence (5′-3′)
PS25	25 (+7,−18)	G*G*C*C*A*A*A*C*C*U*C*G*G*C*U*U*A*C*C*U*G*A* A*A*U
PS20	20 (+2,−18)	G*G*C*C*A*A*A*C*C*U*C*G*G*C*U*U*A*C*C*U
endPS20	20 (+2,-18)	G*G*C*CAAACCUCGGCUUA*C*C*U
PS18 (705)	18	C*C*U*C*U*U*A*C*C*U*C*A*G*U*U*A*C*A
endPS18 (705)	18	C*C*U*CUUACCUCAGUU*A*C*A
PS18-alt (705)	18	C*CU*CU*UA*CC*UC*AG*UU*AC*A
PS18-11 (705)	18	C*C*U*C*U*U*ACCUCAG*U*U*A*C*A
PS18-9 (705)	18	C*C*U*C*U*UACCUCAGU*U*A*C*A
PS16 (705)	16	C*U*C*U*U*A*C*C*U*C*A*G*U*U*A*C
endPS16 (705)	16	C*U*C*UUACCUCAGU*U*A*C
PS-4-thiodT	20 (+2,−18)	Biotinylated 5′-G*G*C*C*A*A*A*C*C*U*C*G*G*C*U*U*A*C*C*U−3′−4-thiodT
2OMe endPS-4-thiodT	20 (+2,−18)	Biotinylated 5′-G*G*C*CAAACCUCGGCUUA*C*C*U-3′−4-thiodT

*Phosphorothioate linkage.

measurement. Transfection with 5 nM of Silencer Select siRNA® (Life Technologies, Carlsbad, CA, USA), including NCL s70420 and TCP1 s224715, was performed with LF2000, formulated in OptiMEM 15 min at room temperature, according to the protocols of the manufacturer, and was then added to the cells cultured in DMEM + 10% FBS. The complexes were left in the culture for 48 h, after which the cells were harvested for RNA isolation.

RNA Expression Analysis

Total RNA was isolated using Tri-Reagent® (Sigma-Aldrich, St. Louis, MO, USA) according to the protocol of the manufacturer. Total RNA quantity and quality were analyzed by NanoDrop 2000 (Thermo Scientific, Waltham, MA, USA). For complementary DNA (cDNA) synthesis, 500 ng of total RNA was used with the High-Capacity cDNA Reverse Transcription kit (Applied Biosystems, Warrington, UK) according to the protocol of the manufacturer. Reverse transcription PCR (RT-PCR) was performed with 12.5 ng of cDNA in each reaction (the total volume per reaction was 25 μl) using the HotStarTaq Plus DNA polymerase kit (QIAGEN, Hilden, Germany) following the protocol of the manufacturer. Primers targeting luciferase mRNA had the following sequences. Forward primer 5′-TTGATATG TGGATTTCGAGTCGTC-3′; reverse primer 5′-TGTCAATC AGAGTGCTTTTGGCG-3′ (CyberGene, Solna, Sweden); and the PCR program employed was 5 s 95°C; 30 s 95°C, 30 s 55°C, 30 s 72°C for 29 cycles; and 10 min at 72°C for the final extension. The PCR products were analyzed on a 2% agarose gel in 0.5× Tris-Borate-EDTA buffer and visualized by SYBRsafe (Invitrogen, Carlsbad, CA, USA) staining. Gel images were captured on a Fluor-S gel documentation system (Bio-Rad, Hercules, CA, USA) with the Quantity One software (Bio-Rad, Hercules, CA, USA). Quantitative PCR (qPCR) analysis was performed on cDNA from C2C12 and H2k-*mdx* cells using the cDNA template (25 ng) and amplified by the TaqMan Gene Expression Master Mix (Applied Biosystems, Waltham, MA, USA) on a StepOne Plus Thermocycler (Applied Biosystems, Waltham, MA, USA). TaqMan probes targeting Ncl1 and Tcp1 (Life Technologies, Carlsbad, CA, USA) were used, and murine glyceraldehyde 3-phosphate dehydrogenase (Gapdh) probes were used as an internal control for cDNA levels.

Luciferase Assay

To measure luciferase activity, the medium was removed, the wells were washed two times with 1 × phosphate-buffered saline (PBS), and the cells were lysed in 150 or 25 ml of 1 × PBS with 0.1% Triton-X 100 per well for 24- or 96-well plates, respectively. The cells were incubated for 20 min at 4°C, followed by a frost/defrost cycle at −80°C. After this, the lysates were kept on ice until use. About 20 μl of the lysates were mixed by an injector with 100 ml of the luciferase assay reagent (1 mM EDTA pH 8.0, 20 mM Tricine pH 7.8, 1 mM $MgCO_3$ pH 7.8, 5 mM $MgSO_4$, 25 mM 1,4-dithiothreitol, 1 mM adenosine 5′-triphosphate disodium salt hydrate, 25 mM coenzyme A, and 1 mM d-luciferin). The relative light units of luciferase were determined using the GloMax® 96 Microplate Luminometer (Promega, Madison, Wisconsin, USA) with an integration time of 10 s. The values were normalized by the total protein quantity that was determined using the DC Protein Assay (Bio-Rad, Hercules, CA, USA).

Immunostaining and Fluorescence Microscopy

For immunofluorescence, the cells were treated with Cy3- or FITC-conjugated 2OMePS oligonucleotides for 4 h, washed three times with PBS containing Ca^{2+} and Mg^{2+} solution, and fixed with methanol at −20°C for 10 min. Then, the cells were washed and stored in PBS at 4°C for future immunofluorescence analysis. For colocalisation, the cells were treated with 0.1% Triton-X100 (Sigma-Aldrich, München, Germany) in PBS for 10′, washed three times with PBS plus, and then blocked with PBS containing 1% bovine serum albumin (BSA, Sigma-Aldrich, St. Louis, MO, USA) for 1 h. After this, the cells were incubated with rat anti-mouse NCL antibody (1:200 dilution, Bio-Rad, Hercules, CA, USA), washed three times with PBS plus, and treated with 1:500 Alexa Fluor 488 goat anti-rat antibody (Life Technologies,

Carlsbad, CA, USA) for 1 h. 4′,6-diamidino-2-phenylindole (DAPI) (1:5000 dilution, Sigma-Aldrich, St. Louis, MO, USA) staining, which was then performed for 2′, after which the cells were washed and mounted with the fluorescent mounting medium S3023 (Dako, Tokyo, Japan) onto glass slides. The visualization was carried out on a Leica fluorescent microscope, and the pictures were taken by an Axiovision fluorescent camera and the Axiovision software (Zeiss, Oberkochen, Germany).

UV Crosslinking, Immunoprecipitation, and Nano-High Performance Liquid Chromatography

We applied only the photoactivatable ribonucleoside-enhanced crosslinking and immunoprecipitation (PAR-CLIP) protocol that uses photoactivatable 4-Thio-Dthymidine (4ThioT). C2C12 myoblasts (1×10^7 cells) were transfected with 5′-biotin-2OMePS-4ThioT-3′ or 5′-biotin-2OMe-endPS-4ThioT-3′ (100 nM as the final concentration) under gymnotic uptake settings for 30 min and then rinsed to remove excess oligo. UV crosslinking was performed using Stratalinker® 2400 Bulbs, 365 nm (Stratagene, San Diego, CA, USA). The cells were harvested using a silicon scraper and lysed in the plate with lysis buffer 1 (LB1: 10 mM of 1 M Hepes-KOH, pH 7.5, 100 mM of 5 M NaCl, 1 mM of 0.5 M EDTA, 0.5 mM of 0.5 M EGTA, 0.1% of sodium-deoxycholate, and 0.5% of sodium lauroyl sarcosinate) using a protease inhibitor cocktail tablet from Complete. The cell pellet was resuspended in 1 ml LB1 and sonicated [six cycles of 30 s with 1-min intervals at power 7.0 (∼40 watts)]. Streptavidin beads (Dynabeads MyOne Streptavidin C1, Thermo Fisher, Waltham, MA, USA) were mixed with the supernatant at 4°C O/N. The beads were washed, transferred to a clean 1.5 ml tube, and boiled in lithium dodecyl sulfate loading buffer, and the supernatant was collected in a new 1.5 ml, following the instructions of the manufacturer.

The supernatant was fractionated and analyzed on a nano-high performance liquid chromatography system (Proxeon, Seattle, WA, USA) coupled directly to a Linear Trap Quadrupole Orbitrap Velos (Thermo Fisher Scientific, Waltham, MA, USA). The identification and quantification of proteins were processed by standard protocols. A detailed description of the protein identification and quantification can be found in the **Supplemental Material**.

Biolayer Interferometry and Dissociation Constant (KD) Calculation

The BioLayer Interferometry technology (BLItz) uses optical biosensors to measure multiple interactions in parallel without detection agents. Recombinant NCL (RPC242Mu01, Cloud-Clone Corp, Katy, TX, USA), a fusion protein of Tyr353–Ser568 of NCL and an N-terminal His-Tag (NCL-His), was used for this BLItz label-free protein assay. Before its use, biosensors were soaked in the BLItz assay buffer (20 mM Tris-HCl, pH 8.0, 150 mM KCl, 0.02% Tween 20, 2 mM DTT, and 1 mg/ml BSA) for at least 10 min. Biolayer interferometry assays consisted of five steps, all performed in the BLItz assay buffer: initial baseline (30 s), loading (120 s), baseline (120 s), association (120 s), and dissociation (120 s). NCL-His was immobilized on the Ni-NTA biosensor. For the loading step, biotinylated 2OMePS and 2′OMe concentrations (0, 1.56, 3.13, 6.25, 12.5, 25, and 50 mM) were adjusted to yield a signal intensity in the range of 0–0.1 nm, thereby ensuring that the sensors were not saturated. Control values, measured using empty (no NCL-His loaded) sensors, were subtracted from experimental values before data processing. Initial experiments indicated that empty sensors and sensors loaded with control biotin-labeled DNA yielded similar values in binding experiments with MBP-R1c. The equilibrium KD rate constant was calculated.

Data Analysis

Data were expressed as mean ± SEM. Values were tested for normality by the D'Agostino-Pearson normality test (omnibus K2). Statistical significance was determined by one-way ANOVA followed by a comparison of each treatment group with the control group by Fisher's least significance difference (LSD) test (GraphPad Prism 6 Software, GraphPad Software, Inc., San Diego, CA, USA). In all cases, $p < 0.05$ was defined as significant. The detection of differentially expressed proteins is based on a 5% false discovery rate (5% FDR).

RESULTS

Splice Switching Is Dependent on PS Inclusion in 2OMe Upon Lipofection in Muscle, Neuronal, Liver, and Bone Reporter Cell Lineages

To date, exon-skipping SSOs with PS modifications have been primarily studied in muscle cells due to their clinical relevance in neuromuscular diseases. However, their application to other cell types has been overlooked. Thus, we briefly investigated whether the PS-dependent activity remains consistent in a greater variety of relevant reporter cell lines to enhance tissue-specific uptake. This may provide a better understanding of whether SSOs require specific chemical modifications for tissue targeting, in addition to enhancing stability and half-life. To this end, we used the four pLuc/705 splice-switching reporter cell lines derived from muscle, neuronal, liver, and bone cell lineages (C2C12, Neuro-2a, HuH7, and U-2 OS, respectively; Rocha et al., 2016), carrying the pLuc/705 splice-switching reporter (**Supplementary Figure 1**). In this reporter system, the presence of a defective intronic 5′ splice site that activates a cryptic 3′ splice site results in aberrant splicing of luciferase pre-mRNA and the translation of a non-functional luciferase reporter. An SSO targeted to the 5′ splice site masks the mutation, allowing the splicing machinery to be redirected and generating the corrected mRNA to restore luciferase activity. To investigate the optimal modifications of PS inclusion in 2OMe to improve the splicing efficiency of SSO, 16- and 18-mer 2OMe with PS or endPS modification at a final concentration of 50 or 100 nM were transfected into the reporter cell lines by PepFect14 following our previously published protocols (Ezzat et al., 2011; Rocha et al., 2016). We found that the percentage of the corrected luciferase transcript compared with total pLuc705 mRNA transcript (**Figures 1A–D**) and the

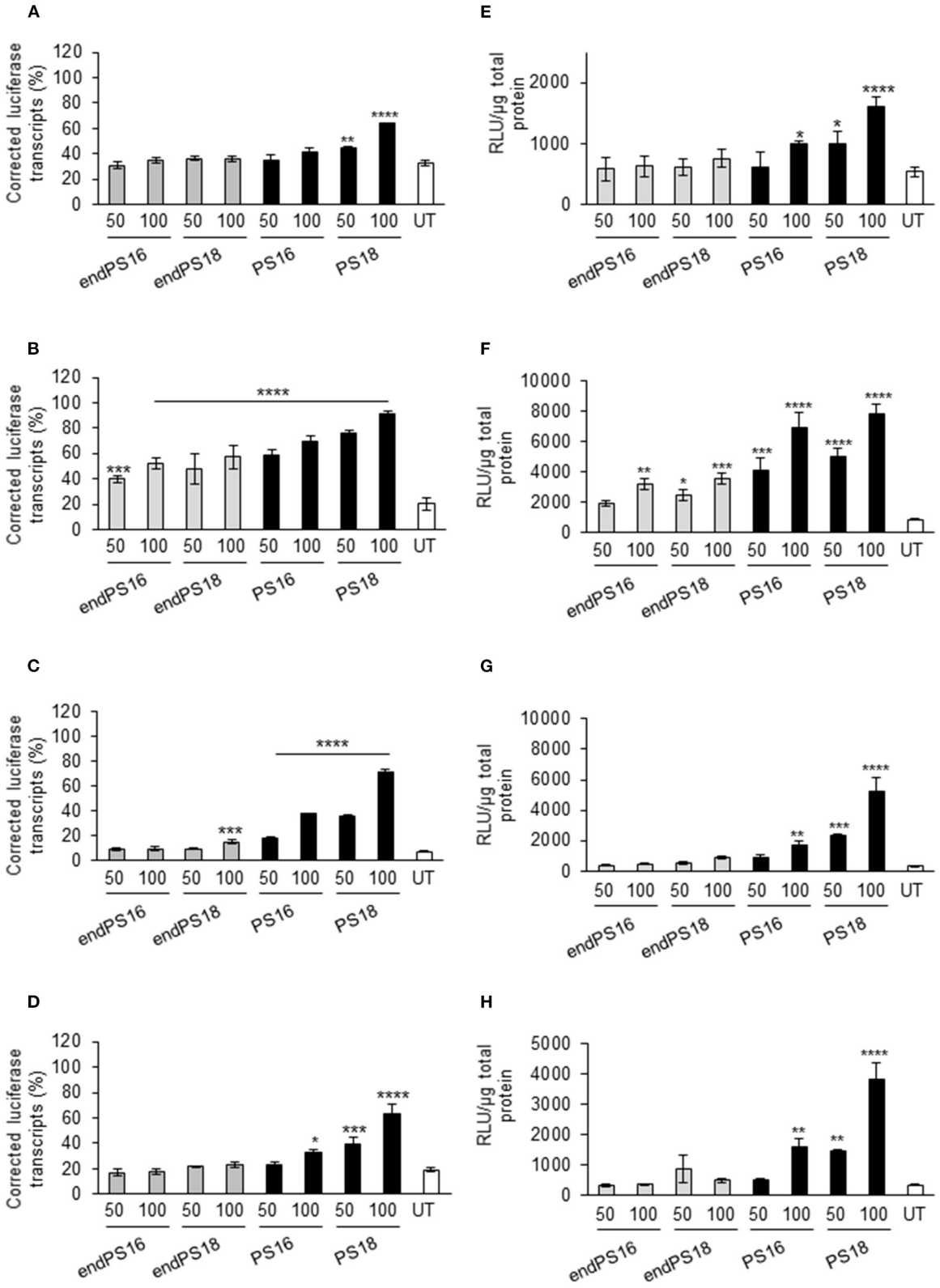

FIGURE 1 | Phosphorothioate (PS) modification modulates the splice-switching activity in different cellular models. Reverse transcription PCR of aberrant and correct luciferase mRNA and 18S RNA in all reporter cell lines when the concentrations of 50 and 100 nM of 18 or 16 mers were modified with full PS vs. endPS 2OMe were

(Continued)

FIGURE 1 | delivered by PepFect14 nanoparticles and the effect measured after 24 h. Graphs represent the percentage of correct transcript compared with total pLuc705 mRNA transcribed after 24 h post-treatment in C2C12 _705 **(A)**, U-2 OS_705 **(B)**, Neuro-2a_705 **(C)**, and HuH7_705 **(D)** reporter cell lines when transfected with the concentrations of 50 and 100 nM of endPS or PS 2OMe. Graphs represent the relative luminescence units (RLU) normalized by micrograms of total protein from C2C12 _705 **(E)**, U-2 OS_705 **(F)**, Neuro-2a_705 **(G)**, and HuH7_705 **(H)** reporter cell lines when transfected at the concentrations of 50 and 100 nM of endPS or PS 2OMe. Data represent the mean ± SEM obtained from the three independent experiments. UT: Untreated. $p < 0.05$ was defined as statistically significant. $^{*}p < 0.05$; $^{**}p \leq 0.01$, $^{***}p \leq 0.001$; $^{****}p \leq 0.0001$.

relative luminescence units (RLU) normalized by micrograms of total protein (**Figures 1E–H**) were quantitatively increased relatively in a dose-dependent manner in C2C12_705, Neuro-2a_705, HuH7_705, and U-2 OS_705 cell lines. Notably, exon-skipping was far more efficient in the U-2 OS_705 line across all the examined PS-SSOs compared with C2C12_705, suggesting that myoblasts might contain an inherent hurdle for SSOs. We also found that 2OMePS with 18 mers rather than with 16 mers resulted in increased splice switching. Furthermore, splice switching in the HeLa_705 cell line was highly dependent on the PS substitution degree in 2OMe (**Supplementary Figure 2A**), and the effects were mediated in a dose-dependent manner (**Supplementary Figure 2B**).

Overall, 2OMePS oligonucleotides are taken up and efficacious at inducing splice switching in various reporter lines, with a moderate variability between lines. This suggests that subtle differences in chemical modifications in SSOs may be crucial in modulating the transcript correction though the experiments have given now cannot predict how more complex cellular interactions may affect them *in vivo*.

PS Modification Facilitates the Uptake of 2OMe in Skeletal Muscle Cells

As a next step, to further assess the impact of PS modification on the uptake and exon-skipping activity of 2OMe in dystrophic muscle cells, we chose to use murine H2k-*mdx* myoblast, a widely studied myoblast model of DMD. We used a 20-mer sequence (Ex23D +2–18), previously optimized in mice, as a parent sequence for our modified SSO designs (Mann et al., 2002) before applying our findings to mice *in vivo* as a future study.

It has been indicated that only three-terminal PS modifications are necessary to confer the full exonuclease stability of 2OMe (Lennox et al., 2013). 2OMe SSO is also known to distribute differently within the cells depending on the applied delivery method (Dias and Stein, 2002). We synthesized both Cy3-labeled 20-mer 2OMePS containing a full PS backbone (Cy3-PS20) and Cy3-labeled low-PS-versions (Cy3-endPS20). We transfected H2k-*mdx* myoblasts with Cy3-endPS20 or Cy3-PS20 using either LF2000, which was previously optimized for the cells, or on gymnosis (Ezzat et al., 2011). Their uptake and cellular localization were observed by fluorescent microscopy.

Cy3-PS20 was rapidly taken up by H2k-mdx myoblasts, 4h post-transfection (**Figure 2A**). Fluorescence microscopy revealed primary accumulation at the nucleus, in a diffuse form or a distinct nuclear dot-like pattern, known as PSbodies. However, endPS20 showed negligible uptake. We then transduced H2k-*mdx* myoblasts with endPS20 or PS20 at a final concentration of 50, 100, or 200 nM, and exon 23 skipping efficiency was evaluated by RT-PCR after 48- h incubation. We found that endPS20 remained completely inactive, but PS20 induced 40–100% exon 23 skipping dose-dependently in H2k-*mdx* myoblasts (**Figure 2B**).

Next, we sought to carry out similar uptake and exon-skipping assessments in the context of gymnotic cellular uptake. In contrast to lipofection, 4 h after gymnotic uptake Cy3-PS20 exhibited a predominant cytosolic distribution in H2k-mdx myoblasts, examined by fluorescence microscopy while endPS20 showed negligible uptake (**Figure 2C**). We then transduced H2k-*mdx* myoblasts with endPS20 or PS20 at a final concentration of 200, 400, or 600 nM, and exon 23 skipping efficiency was evaluated by RT-PCR after 48 h incubation. We found that endPS20 remained completely inactive, but PS20 induced 20–50% exon 23 skipping dose-dependently in H2k-*mdx* myoblasts (**Figure 2D**).

Collectively, these data support the hypothesis that the full PS modification of 2OMe is a key in facilitating the uptake and activity on both lipofection and gymnotic transfection in H2k-*mdx* myoblasts. Furthermore, the lipofection and gymnotic transfection of 2OMe might lead to a predominant nuclear and cytosolic distribution in the cells, respectively.

Determination of 2OMePS-Binding Proteins by Interactome Capture Studies in Living C2C12 Myoblasts

To provide better insights into the potential cellular uptake mechanisms of 2OMePS, we sought to identify the endogenous proteins that are in association with 2OMePS by using photoactivatable-ribonucleoside-enhanced crosslinking and immunoprecipitation (PAR-CLIP) to define the SSO interactome of uptake-permissive cells in a physiological environment (Castello et al., 2012, 2013). PAR-CLIP was originally developed to identify RNA-binding proteins and microRNA target sites. We have adapted it to identify the proteins interacting with SSOs, by performing UV crosslinking of 2OMePS-binding proteins to a 3′-4ThioT-coupled biotinylated 2OMePS (5′-biotin-2OMePS-4ThioT-3′) in living C2C12 myoblasts (as opposed to lysed cell-incubating 2OMePS) and captured the covalently bound proteins with magnetic Streptavidin-Dynabeads (Castello et al., 2013). After stringent washes, interacting proteins were detected by nano-high performance liquid chromatography. We identified and further validated 574 2OMePS-binding proteins (**Supplementary Table 1**) while we identified 32 proteins in the control group. In parallel, we confirmed that the biotinylated 2OMePS with photocrosslinking agents was able to induce efficient exon-23 skipping in C2C12 myoblasts with the same doses as nonbiotinylated 2OMePS without photocrosslinking agents (**Supplementary Figure 3**).

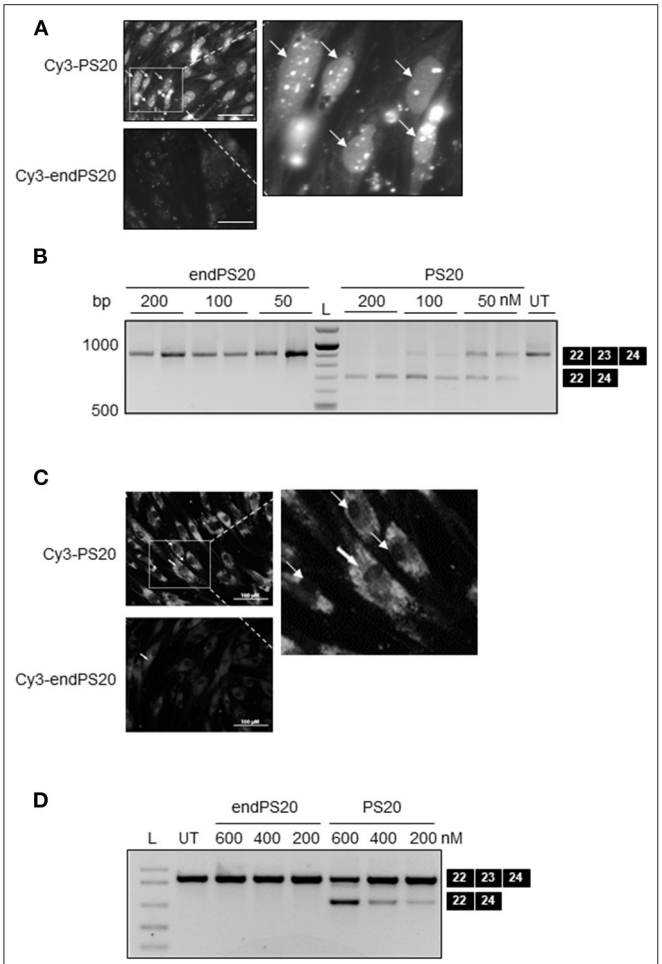

FIGURE 2 | PS-dependent cellular uptake and nuclear accumulation of 2OMe modified splice-switching antisense oligonucleotides (SSOs) in H2k-*mdx* myoblasts. Cy3-conjugated 2OMePS or 2OMe-endPS SSO with 20 mers were delivered either through gymnotic uptake or by LF2000. **(A)** Fluorescence microscopy images depicting the cellular uptake of 2OMePS or 2OMe-endPS SSO (200 μM final concentration) complexed with Lipofectamine 2000 in H2k-*mdx* myoblasts after 4 h post-transfection. Bar = 15 μm. **(B)** RT-PCR depicting splice-switching activity of 2OMePS or 2OMe-endPS SSO in H2k-*mdx* myoblasts targeting exon 23 skipping of dystrophin with LF2000. UT: untreated. **(C)** Fluorescent microscopy images depicting the gymnotic cellular uptake of 2OMePS or 2OMe-endPS SSO (200 μM final concentration) in H2k-*mdx* myoblasts 4 h post-transfection. Bar = 15 μm. **(D)** RT-PCR depicting the splice-switching activity of 2OMePS or 2OMe-endPS SSO in H2k-*mdx* myoblasts targeting exon 23 skipping of dystrophin upon gymnotic uptake. L, DNA ladder; endPS, 2OMe-endPS. PS20 denotes 2OMePS with 20 mers.

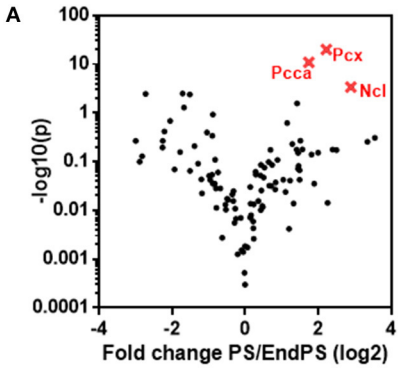

B

Gene name	Fold change PS/endPS	P-value
Ncl	7.42	4.2E-04
Pcx	4.65	0.0E-00
Pcca	3.33	1.3E-11

FIGURE 3 | Crosslinking and proteomic analysis of proteins responsible for PS binding. **(A)** Comparison of PS and endPS UV+ sample interactome by a volcano plot analysis. **(B)** List of three statistically differentially expressed proteins (nucleolin (NCL), pyruvate carboxylase (PCX), and propionyl-CoA carboxylase subunit alpha (PCCA), which are found to be explicitly enriched in PS interactome as compared to endPS interactome. The most significantly enriched partners of the 2OMePS analog were identified by a volcano plot.

Following the differential expression analysis between PS20 and endPS20 UV+ samples, the most significantly enriched interacting partners of the 2OMePS analog were identified by a volcano plot (**Figure 3A**). We found that Ncl (fold change 7.42, $p \leq 0.0005$), an abundant nucleolar phosphoprotein, was strongly associated with PS20 (**Figure 3B**). Mitochondrial enzymes, including pyruvate carboxylase (PCX) (fold change: 4.65, $p \leq 0.0001$) involved in gluconeogenesis, adiposity, and insulin resistance in type 2 diabetes (Schär et al., 2010), and PCCA (fold change: 3.33, $p \leq 0.0001$) (**Figure 3B**), were also the strong candidates for a PS20 interaction. Due to the supporting data from previous studies and the enrichment of Ncl being the highest among the three identified proteins, we focused our further investigations on unraveling the link between Ncl and PS20.

Ncl Interacts With 2OMePS and May Regulate Its Antisense Activity

Ncl and Tcp1 have previously been shown to interact with 2OMePS and to colocalise in induced nuclear bodies in mammalian cells (Liang et al., 2014). Therefore, to study the role of Ncl in the uptake and biological activity of PS20, we treated the C2C12 myoblasts with small-interfering RNAs (siRNAs) targeting *Ncl* or *Tcp1* transcripts to deplete the expression of these proteins. It was reported that the estimated half-life of the surface Ncl was about 45 min and that of nuclear Ncl is more than 8 h (Hovanessian et al., 2010). Therefore, the treatment with siRNAs was performed 24 h prior to PS20 to confirm the effects resulting from Ncl depletion. Subsequently, C2C12 myoblasts were transfected with FITC-labeled PS20 (FITC-PS20) for 4 h, and the cellular uptake of FITC-PS20 was evaluated by fluorescent microscopy. The knockdown level of *Ncl* by qPCR was 67%, accompanied by the reduced expression of Ncl protein

in *Ncl* siRNA-treated C2C12 myoblasts compared to the scramble treated ones (**Supplementary Figures 4A,B**).

Interestingly, FITC-PS20 uptake was significantly increased in the Ncl-depleted myoblasts while *Tcp1* silencing did not affect the uptake as measured by relative fluorescence intensity (**Figures 4A,B**). Splicing efficiency in a HeLa_705 luciferase reporter cell line transfected with siRNAs targeting Ncl 24 h prior to PS20 treatment was also correspondingly increased compared to control scramble-treated cells (**Figure 4C**). To further confirm the impact of Ncl on PS20 activity, HeLa_705 cells were transfected with a DNA plasmid encoding for Ncl overexpression for 24 h and subsequently treated with PS20 *via* lipofection (LF2000) for 24 h, after which the splice-switching activity was measured. Corroborating the siRNA data, we found that increased levels of Ncl have a negative impact on the splice-switching activity of PS20 in HeLa_705 cells (**Figure 4D**). We further confirmed the binding of a recombinant protein of Tyr353-Ser568 of Ncl with an NCL-His, which contains the RNA recognition motifs (Weidner et al., 1995), to PS20 using the BLItz (**Figure 4E**). We measured the equilibrium dissociation constant (Kd) between Ncl and PS20 and confirmed that the Kd value between Ncl and PS20 was 6.29E-07 M (**Figure 4E**). The data suggest an interaction between Ncl and PS20, which is compatible with the previous report that the binding of 2OMePS to Ncl occurs in a non-sequence-specific manner (Weidner et al., 1995). Together, our data indicate that Ncl interacts with 2OMePS and could negatively regulate the cellular uptake of 2OMePS and the splicing efficiency in mouse C2C12 myoblasts and human HeLa_705 cells.

DISCUSSION

Phosphorothioate modification of 2OMe is promising therapeutically and can create more effective drugs for antisense oligonucleotide-targeted treatments. The optimisation of PS inclusion in 2OMe could improve its splicing efficiency in several different tissue types, and aid a deeper understanding of the pharmacological effects and side effects of 2OMePS (Flanigan et al., 2014).

Three-terminal PS modifications (2OMe-endPS) are sufficient to give full exonuclease stability to 2OMe despite showing reduced uptake, cellular distribution, and negligible nuclear localization, and splice-switching activity in several muscle cell lines and reporter cells. On the other hand, splice switching was highly enhanced by the full PS modification in 2OMe, in a relatively dose-dependent manner, with subtle differences pertaining to SSO length and modification between different cell types. Using lipofection, 2OMePS was rapidly taken up by the cells that are primarily accumulated in the nucleus. Following gymnotic uptake, 2OMePS displayed a predominant cytosolic distribution, and a relatively shorter length (20 mers) of SSO was vital in facilitating the uptake and activity in mouse myoblasts because 25 mers had almost zero activity. Accordingly, we confirmed that full PS modification could facilitate the uptake of 2OMe in different cellular splice-switching models of neuromuscular, hepatic, and bone diseases. Critically, it has been shown that the cellular distribution of 2OMePS could be regulated in the nucleus upon lipofection and the cytosol after gymnotic uptake, highlighting that the mechanism of cell entry is crucial for correct delivery-efficient splice switching.

In this study, we have confirmed Ncl protein to be a key player in this regulation, substantiating previous findings. Ncl has multiple proposed functions within and outside of the nucleoli. For example, it is involved in ribosome biogenesis, including the first processing step of pre-ribosomal RNA (rRNA) maturation, DNA repair, mRNA metabolism, an internalization of growth significant factors and viral ligands, and virus replication (Orrick et al., 1973). It has also been reported that Ncl and nucleophosmin disperse into the nucleoplasm during heat shock stress and reaccumulate in the nucleolus within an hour after release from the stress in normal cells; however, this reaccumulation of Ncl is strongly inhibited in cells lacking Hikeshi, a nuclear import carrier for Hsp70s (Kose et al., 2012).

It has been shown that 2OMePS enters the cells *via* endocytosis and accumulates in endosome-related structures in the cytoplasm (Marcusson et al., 1998). The interaction between Ncl and 2OMePS affected the potency of 2OMePS. The depletion of Ncl enhanced the splice-switching activity of 2OMePS, and our dissociation data suggest that the protein may decrease the splice-switching activity through direct interaction with 2OMePS (**Figures 4C,E**). These findings support the hypothesis that Ncl functions in the form of a heteromultimeric receptor complex (signalosomes) that may include other chaperones such as Tcp1 and other receptor proteins, including scavenger receptors (Ezzat et al., 2015). Tcp1 complex proteins are reported to interact with 2OMePS and colocalise in oligonucleotide-induced nuclear bodies in mammalian cells (Liang et al., 2014), but we were unable to reproduce these data in this study. It should be noted that Ncl shuttles between the nucleus, cytoplasm, and cell surface, and has been implicated in controlling regulatory processes and may play a role in pathogen infection and autoimmune diseases (Chen et al., 2008).

Furthermore, Ncl was reported to act as a scavenger receptor for acetylated low-density lipoproteins on macrophages (Canton et al., 2013; Ezzat et al., 2015; Miki et al., 2015), and other receptor proteins may be involved in signalosomes. Thus, it is possible that Ncl interacts with 2OMePS, leading to reduced 2OMePS activity upon diminishing of a particular 2OMe-binding protein. How Ncl reduces 2OMePS activity is still unclear. The binding of Ncl to 2OMePS likely prevents the binding of other proteins that would enhance its SSO activity. Ncl may be involved in the nuclear import of 2OMePS or simply act as a sequestering factor for 2OMePS competing with binding to its target RNA. In addition, the protein may also play a role in 2OMePS uptake and/or in the exchange between endocytosis-related organelles and the cytosol environment. Finally, we cannot rule out the possibility that Ncl may help to melt the intramolecular structures of 2OMePS to increase their base-pairing potential with target RNAs (Tosoni et al., 2015). Similarly, a minor modification to the 2OMePS may help circumvent this barrier. Proteomics following PAR-CLIP was only performed using one type of 2OMePS in C2C12 wild-type cells, not a disease model. These results do not show that DMD disease models would uptake SSOs and process them in

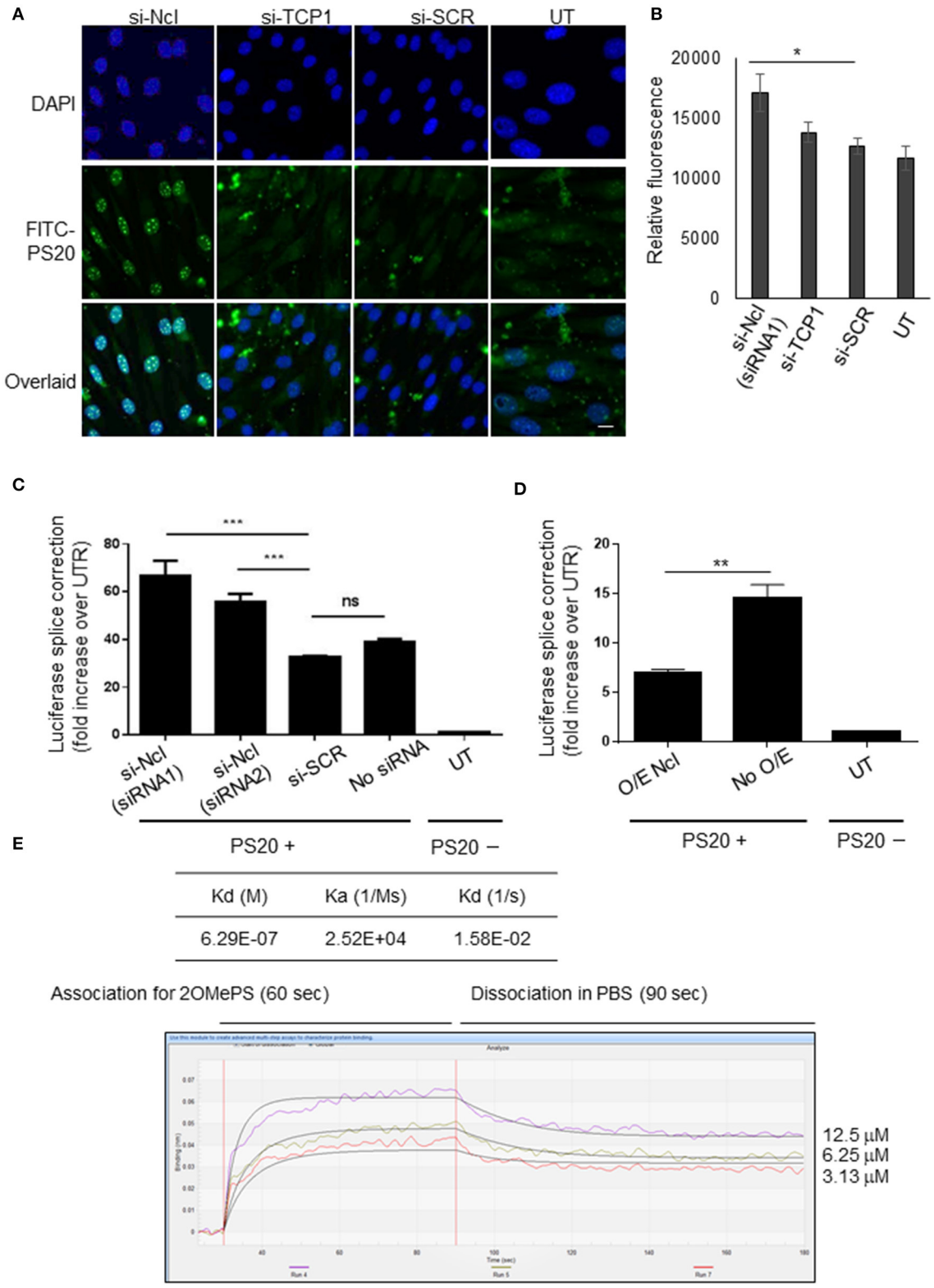

FIGURE 4 | Nucleolin negatively regulates the cellular uptake and splicing efficiency of PS-modified 2OMe SSOs. **(A)** Nucleolin knockdown by siRNA enhances the cellular uptake of FITC-conjugated 2OMe splice-switching oligonucleotides (SSOs) in C2C12 myoblasts. Cells are incubated with FITC-conjugated 2OMePS for 4 h

(Continued)

FIGURE 4 | followed by an analysis using a fluorescent microscope. Bar = 15 μm. UT, untreated cells. **(B)** Relative fluorescent units of FITC-conjugated 2OMePS 4 h post-treatment in C2C12 myoblasts pretreated with siRNA against *Ncl* or *Tcp1*. **(C)** Effect of knockdown of *Ncl* or *Tcp1* on splicing efficiency in HeLa_705 with 2OMe SSO. **(D)** Ncl protein overexpression and impact on SSO activity upon lipofection. HeLa_705 cells are transfected with Ncl-encoding plasmid DNA (pDNA) for 24 h. Then, these and control cells are further treated with 2'-OMePS for 24 h, after which splice-switching activity was measured. O/E Ncl: the activity of lipofected SSOs in Ncl overexpressing cells. $P < 0.05$ was defined as statistically significant. $^{*}p < 0.05$; $^{**}p \leq 0.01$, $^{***}p \leq 0.001$. **(E)** BLItz label-free protein assays. The recombinant Ncl (RPC242Mu01, Cloud-Clone Corp, Katy, TX, USA), a recombinant protein of amino acids Tyr353–Ser568 of Ncl and an N-terminal His-Tag (NCL-His), was used for these assays. KD, the equilibrium dissociation constant between an antibody and its antigen.

the same way. Thus, the optimisation of the chemistry is crucial for the targeted tissue delivery, uptake, cellular localization, and effective splice-switching activity.

Ncl depletion could enhance the activity of 2OMePS and facilitate the cellular uptake of 2OMePS from extracellular environments and/or the release of 2OMePS from endosomes or lysosomes. Further investigation of the underlying mechanisms of how Ncl depletion improves 2OMePS drug potency will be necessary for a better drug design. It would be interesting to test if NCL aptamer, AS1411 (Carvalho et al., 2019), or surface NCL antagonists, HB-19-N6L (Verhaart and Aartsma, 2019), may affect 2OMePS and other SSOs' function.

CONCLUSION

We found that PS modification facilitates the gymnotic uptake of 2OMe in myoblasts. We also found that splice switching is dependent on PS inclusion in 2OMe upon the lipofection in muscle, neuronal, liver, and bone cell lineages. Ncl could interact with 2OMePS and influence cellular uptake and intracellular distribution and display differential activity depending on the RNA target.

DATA AVAILABILITY STATEMENT

The raw data supporting the conclusions of this article will be made available by the authors, without undue reservation.

AUTHOR CONTRIBUTIONS

SA, YA, MB, and MW: conceptualization. YA, HJ, IM, MB, and TR: methodology. MA, CSJR, CS, TL, YH, JN, SM, and IM: investigation. YA: writing the original draft. TR, TL, CS, JN, MG, and SA: writing the review and editing. SA, YA, MW, and TL: funding acquisition. SA and MW: supervision. All authors contributed to the article and approved the submitted version.

FUNDING

SA was supported by the Swedish Research Council and the Swedish Society of Medical Research (SSMF). This work was supported by the Swedish Medical Research Council, the MRC Confidence in Concept award (grant to YA and MW), the Japan Society for the Promotion of Science Grant-in-Aid for Scientific Research (C) (Grant No. 18K07544 to YA), Grants-in-Aid for Research on Nervous and Mental Disorders (Grant No. 2–6 to YA), the Japan Agency for Medical Research and Development (AMED) (Grant Nos. 19ek0109239h0003 and 19lm0203069h0002 to YA), and the Estonian Research Council (Grant No. PSG226 to TL).

ACKNOWLEDGMENTS

We thank MB for his support and material supply, Dr. Janne Lehtiö for technical assistance, and Dr. Suzan Hammond for insightful discussions about this study.

SUPPLEMENTARY MATERIAL

The Supplementary Material for this article can be found online at: https://www.frontiersin.org/articles/10.3389/fphys.2021.689179/full#supplementary-material

REFERENCES

Baltz, A. G., Munschauer, M., Schwanhäusser, B., Vasile, A., Murakawa, Y., Schueler, M., et al. (2012). The mRNA-bound proteome and its global occupancy profile on protein-coding transcripts. *Mol. Cell.* 46:674–90. doi: 10.1016/j.molcel.2012.05.021

Canton, J., Neculai, D., and Grinstein, S. (2013). Scavenger receptors in homeostasis and immunity. *Nat. Rev. Immunol.* 13, 621–634. doi: 10.1038/nri3515

Carvalho, J., Paiva, A., Paula, M., Campello, C., Paulo, A., Mergny, J., et al. (2019). Aptamer-based targeted delivery of a G-quadruplex ligand in cervical cancer cells. *Sci. Rep.* 9:7945. doi: 10.1038/s41598-019-44388-9

Castello, A., Fischer, B., Eichelbaum, K., Horos, R., Beckmann, B. M., Strein, C., et al. (2012). Insights into RNA biology from an atlas of mammalian mRNA-binding proteins. *Cell* 149, 1393–1406. doi: 10.1016/j.cell.2012.04.031

Castello, A., Horos, R., Strein, C., Fischer, B., Eichelbaum, K., Steinmetz, L. M., et al. (2013). System-wide identification of RNA-binding proteins by interactome capture. *Nat. Protoc.* 8, 491–500. doi: 10.1038/nprot.2013.020

Chen, X., Kube, D. M., Cooper, M. J., and Davis, P. B. (2008). Cell surface nucleolin serves as receptor for DNA nanoparticles composed of pegylated polylysine and DNA. *Mol. Ther.* 16, 333–342. doi: 10.1038/sj.mt.6300365

Cirak, S., Arechavala-Gomeza, V., Guglieri, M., Feng, L., Torelli, S., Anthony, K., et al. (2011). Exon skipping and dystrophin restoration in patients with Duchenne muscular dystrophy after systemic phosphorodiamidate morpholino oligomer treatment: an open-label, phase 2, dose-escalation study. *Lancet* 378, 595–605. doi: 10.1016/S0140-6736(11)60756-3

Dias, N., and Stein, C. A. (2002). Antisense oligonucleotides : basic concepts and mechanisms minireview antisense oligonucleotides : basic concepts and mechanisms. *Mol. Cancer Ther.* 1, 347–355.

Dominski, Z., and Kole, R. (1993). Antisense. *Oligonucleotides*. 90, 8673–8677. doi: 10.1073/pnas.90.18.8673

Ezzat, K., Andaloussi, S. E. L., Zaghloul, E. M., Lehto, T., Lindberg, S., Moreno, P. M. D., et al. (2011). PepFect 14, a novel cell-penetrating peptide for oligonucleotide delivery in solution and as solid formulation. *Nucl. Acids Res.* 39, 5284–5298. doi: 10.1093/nar/gkr072

Ezzat, K., Aoki, Y., Koo, T., McClorey, G., Benner, L., Coenen-Stass, A., et al. (2015). Self-assembly into nanoparticles is essential for receptor mediated uptake of therapeutic antisense oligonucleotides. *Nano Lett.* 15, 4364–4373. doi: 10.1021/acs.nanolett.5b00490

Ezzat, K., Helmfors, H., Tudoran, O., Juks, C., Lindberg, S., Padari, K., et al. (2012). Scavenger receptor-mediated uptake of cell-penetrating peptide nanocomplexes with oligonucleotides. *FASEB J.* 26, 1172–1180. doi: 10.1096/fj.11-191536

Flanigan, K. M., Voit, T., Rosales, Z. Q., Servais, L., Kraus, J. E., Wardell, C., et al. (2014). Pharmacokinetics and safety of single doses of drisapersen in non-ambulant subjects with Duchenne muscular dystrophy: results of a double-blind randomized clinical trial. *Neuromuscul. Disord.* 24, 16–24. doi: 10.1016/j.nmd.2013.09.004

Heemskerk, H., de Winter, C., van Kuik, P., Heuvelmans, N., Sabatelli, P., Rimessi, P., et al. (2010). Preclinical PK and PD studies on 2'-O-methyl-phosphorothioate RNA antisense oligonucleotides in the mdx mouse model. *Mol. Ther.* 18, 1210–1217. doi: 10.1038/mt.2010.72

Hovanessian, A. G., Soundaramourty, C., El Khoury, D., Nondier, I., Svab, J., and Krust, B. (2010). Surface expressed nucleolin is constantly induced in tumor cells to mediate calcium-dependent ligand internalization. *PLoS ONE* 5:15787. doi: 10.1371/journal.pone.0015787

Kose, S., Furuta, M., and Imamoto, N. (2012). Hikeshi, a nuclear import carrier for Hsp70s, protects cells from heat shock-induced nuclear damage. *Cell* 149, 578–589. doi: 10.1016/j.cell.2012.02.058

Lennox, K. A., Owczarzy, R., Thomas, D. M., Walder, J. A., and Behlke, M. A. (2013). Improved performance of anti-miRNA oligonucleotides using a novel non-nucleotide modifier. *Mol. Ther. Nucl. Acids* 2:e117. doi: 10.1038/mtna.2013.46

Liang, X. H., Shen, W., Sun, H., Prakash, T. P., and Crooke, S. T. (2014). TCP1 complex proteins interact with phosphorothioate oligonucleotides and can co-localize in oligonucleotide-induced nuclear bodies in mammalian cells. *Nucl. Acids Res.* 42, 7819–7832. doi: 10.1093/nar/gku484

Mann, C. J., Honeyman, K., McClorey, G., Fletcher, S., and Wilton, S. D. (2002). Improved antisense oligonucleotide induced exon skipping in themdx mouse model of muscular dystrophy. *J. Gene Med.* 4, 644–654. doi: 10.1002/jgm.295

Marcusson, E. G., Bhat, B., Manoharan, M., Bennett, C. F., and Dean, N. M. (1998). Phosphorothioate oligodeoxyribonucleotides dissociate from cationic lipids before entering the nucleus. *Nucl. Acids Res.* 26, 2016–2023. doi: 10.1093/nar/26.8.2016

Mathy, N., Bénard, L., Pellegrini, O., Daou, R., Wen, T., and Condon, C. (2007). 5′-to-3′ exoribonuclease activity in bacteria: role of RNase J1 in rRNA maturation and 5′ stability of mRNA. *Cell* 129, 681–692. doi: 10.1016/j.cell.2007.02.051

Miki, Y., Tachibana, Y., Ohminato, Y., and Fujiwara, Y. (2015). Nucleolin acts as a scavenger receptor for acetylated low-density lipoprotein on macrophages. *Biol. Pharm. Bull.* 38, 1420–1424. doi: 10.1248/bpb.b15-00260

Orrick, L. R., Olson, M. O., and Busch, H. (1973). Comparison of nucleolar proteins of normal rat liver and Novikoff hepatoma ascites cells by two-dimensional polyacrylamide gel electrophoresis. *Proc. Natl. Acad. Sci. U. S. A.* 70, 1316–1320. doi: 10.1073/pnas.70.5.1316

Rocha, C. S. J., Lundin, K. E., Behlke, M. A., Zain, R., E. L., Andaloussi, S., et al. (2016). Four Novel splice-switch reporter cell lines: distinct impact of oligonucleotide chemistry and delivery vector on biological activity. *Nucl. Acid Ther.* 26, 381–391. doi: 10.1089/nat.2016.0631

Schär, J., Stoll, R., Schauer, K., Loeffler, D. I. M., Eylert, E., Joseph, B., et al. (2010). Pyruvate carboxylase plays a crucial role in carbon metabolism of extra- and intracellularly replicating Listeria monocytogenes. *J. Bacteriol.* 192, 1774–1784. doi: 10.1128/JB.01132-09

Tosoni, E., Frasson, I., Scalabrin, M., Perrone, R., Butovskaya, E., Nadai, M., et al. (2015). Nucleolin stabilizes G-quadruplex structures folded by the LTR promoter and silences HIV-1 viral transcription. *Nucl. Acids Res.* 43, 8884–8897. doi: 10.1093/nar/gkv897

Verhaart, I. E. C., and Aartsma, A. (2019). Therapeutic developments for Duchenne muscular dystrophy. *Nat. Rev. Neurol.* doi: 10.1038/s41582-019-0203-3

Weidner, D. A., Valdez, B. C., Henning, D., Greenberg, S., and Busch, H. (1995). Phosphorothioate oligonucleotides bind in a non sequence-specific manner to the nucleolar protein C23/nucleolin. *FEBS Lett.* 366, 146–150. doi: 10.1016/0014-5793(95)00517-D

Zamecnik, P. C., and Stephenson, M. L. (1978). Inhibition of *Rous sarcoma* virus replication and cell transformation by a specific oligodeoxynucleotide. *Proc. Natl. Acad. Sci. U. S. A.* 75, 280–284. doi: 10.1073/pnas.75.1.280

Conflict of Interest: MA was employed by Integrated DNA Technologies, Inc.

The remaining authors declare that the research was conducted in the absence of any commercial or financial relationships that could be construed as a potential conflict of interest.

Publisher's Note: All claims expressed in this article are solely those of the authors and do not necessarily represent those of their affiliated organizations, or those of the publisher, the editors and the reviewers. Any product that may be evaluated in this article, or claim that may be made by its manufacturer, is not guaranteed or endorsed by the publisher.

frontiers in Physiology

ORIGINAL RESEARCH
published: 20 October 2021
doi: 10.3389/fphys.2021.716471

Urine-Derived Stem Cells Express 571 Neuromuscular Disorders Causing Genes, Making Them a Potential *in vitro* Model for Rare Genetic Diseases

Maria Sofia Falzarano[1†], Rachele Rossi[1,2†], Andrea Grilli[3], Mingyan Fang[4], Hana Osman[1,5], Patrizia Sabatelli[6,7], Manuela Antoniel[6,7], Zhiyuan Lu[4], Wenyan Li[4], Rita Selvatici[1], Cristina Al-Khalili[8], Francesca Gualandi[1], Silvio Bicciato[3], Silvia Torelli[2,9‡] and Alessandra Ferlini[1,2*‡]*

[1] UOL (Unità Operativa Logistica) of Medical Genetics, University of Ferrara, Ferrara, Italy, [2] The Dubowitz Neuromuscular Centre, UCL Great Ormond Street Institute of Child Health, London, United Kingdom, [3] Department of Life Sciences, University of Modena and Reggio Emilia, Modena, Italy, [4] Beijing Genomics Institute (BGI)-Shenzhen, Shenzhen, China, [5] Department of Medical Microbiology, Faculty of Medical Laboratory Sciences, University of Khartoum, Khartoum, Sudan, [6] CNR-Institute of Molecular Genetics "Luigi Luca Cavalli-Sforza"- Unit of Bologna, Bologna, Italy, [7] Istituto di Ricovero e Cura a Carattere Scientifico (IRCCS) Istituto Ortopedico Rizzoli, Bologna, Italy, [8] Department of Proteomics, KTH Royal Institute of Technology, Stockholm, Sweden, [9] National Institute for Health Research, Great Ormond Street Institute of Child Health Biomedical Research Centre, University College London, London, United Kingdom

OPEN ACCESS

Edited by:
Carlo Rinaldi,
University of Oxford, United Kingdom

Reviewed by:
Xiongwen Chen,
Temple University, United States
Raquel Manzano,
University of Zaragoza, Spain

***Correspondence:**
Silvia Torelli
s.torelli@ucl.ac.uk
Alessandra Ferlini
fla@unife.it

[†] These authors have contributed equally to this work and share first authorship

[‡] These authors have contributed equally to this work and share last authorship

Specialty section:
This article was submitted to Striated Muscle Physiology, a section of the journal Frontiers in Physiology

Received: 28 May 2021
Accepted: 21 September 2021
Published: 20 October 2021

Citation:
Falzarano MS, Rossi R, Grilli A, Fang M, Osman H, Sabatelli P, Antoniel M, Lu Z, Li W, Selvatici R, Al-Khalili C, Gualandi F, Bicciato S, Torelli S and Ferlini A (2021) Urine-Derived Stem Cells Express 571 Neuromuscular Disorders Causing Genes, Making Them a Potential in vitro Model for Rare Genetic Diseases. Front. Physiol. 12:716471. doi: 10.3389/fphys.2021.716471

Background: Neuromuscular disorders (NMDs) are a heterogeneous group of genetic diseases, caused by mutations in genes involved in spinal cord, peripheral nerve, neuromuscular junction, and muscle functions. To advance the knowledge of the pathological mechanisms underlying NMDs and to eventually identify new potential drugs paving the way for personalized medicine, limitations regarding the availability of neuromuscular disease-related biological samples, rarely accessible from patients, are a major challenge.

Aim: We characterized urinary stem cells (USCs) by in-depth transcriptome and protein profiling to evaluate whether this easily accessible source of patient-derived cells is suitable to study neuromuscular genetic diseases, focusing especially on those currently involved in clinical trials.

Methods: The global transcriptomics of either native or MyoD transformed USCs obtained from control individuals was performed by RNA-seq. The expression of 610 genes belonging to 16 groups of disorders (http://www.musclegenetable.fr/) whose mutations cause neuromuscular diseases, was investigated on the RNA-seq output. In addition, protein expression of 11 genes related to NMDs including *COL6A*, *EMD*, *LMNA*, *SMN*, *UBA1*, *DYNC1H1*, *SOD1*, *C9orf72*, *DYSF*, *DAG1,* and *HTT* was analyzed in native USCs by immunofluorescence and/or Western blot (WB).

Results: RNA-seq profile of control USCs shows that 571 out of 610 genes known to be involved in NMDs, are expressed in USCs. Interestingly, the expression levels of the

majority of NMD genes remain unmodified following USCs MyoD transformation. Most genes involved in the pathogenesis of all 16 groups of NMDs are well represented except for channelopathies and malignant hyperthermia related genes. All tested proteins showed high expression values, suggesting consistency between transcription and protein representation in USCs.

Conclusion: Our data suggest that USCs are human cells, obtainable by non-invasive means, which might be used as a patient-specific cell model to study neuromuscular disease-causing genes and that they can be likely adopted for a variety of *in vitro* functional studies such as mutation characterization, pathway identification, and drug screening.

Keywords: neuromuscular disorders, neurodegenerative disorders, urine derived stem cells, RNA-seq, western blot (WB), immunofluorescence

INTRODUCTION

Neuromuscular diseases (NMDs) are a broadly defined collection of rare inherited degenerative diseases affecting spinal cord, peripheral nerve, neuromuscular junction and muscle. The genetic diagnosis for NMDs has rapidly improved, due to the recent development of technologies such as next-generation sequencing (NGS) that accelerated the discovery of novel NMD phenotypes and genotypes associated with new classes of mutations (Tian et al., 2015). To date, more than 600 genes have been reported to cause NMDs[1] and are a potential target for personalized medicine. Indeed, the consequent identification of new pathogenic targets and the related biological processes led to the discovery of novel therapeutic strategies for disorders that have been considered, for a long time, untreatable. Among 200 molecules in preclinical and clinical stages for NMDs, the majority target Duchenne muscular dystrophy (DMD) and amyotrophic lateral sclerosis (ALS) (Cowling and Thielemans, 2019). Gene therapy approaches are being tested in clinical trials for patients with mutations in *DMD*, *SOD1* (Superoxide dismutase 1, soluble) or *C9orf72* (Chromosome 9 open reading frame 72) genes[2] (Cappella et al., 2019; Fortunato et al., 2021). Multiple FDA-approved *SMN* (Survival of motor neuron)-targeting treatments have been also developed for spinal muscular atrophy (SMA) (Dowling et al., 2018; Al-Zaidy and Mendell, 2019).

Despite these recent developments, potential drugs are not available for most NMDs. The progress in this field is strictly dependent on and supported by preclinical studies, and the availability of cellular and animal models to accurately recapitulate the disease phenotype is a crucial and limiting aspect for discovering and developing drugs for NMDs.

Different cellular models have been characterized to improve molecular diagnosis and functional studies in these disorders. Currently procedures used to generate patient-specific cells such as myogenic cells, fibroblasts, and induced pluripotent stem cells (iPSCs) are mainly based on invasive methods (i.e., skin and muscle biopsies) (Speciale et al., 2020). Increased attention has been focused on stem cells derived from urine specimens (USCs) that now are used in a broad field of applications and, in some cases, are replacing the traditional cell sources obtained with invasive and time-consuming methods (Falzarano and Ferlini, 2019). USCs are a subpopulation of urinary system derived cells with stem cell properties including high proliferative capacity, multipotency, and immunomodulatory ability.

Native USCs, direct reprogrammed USCs, and especially USCs-induced pluripotent stem cells were used for studying several genetic diseases. Interestingly, native USCs obtained from patients affected by Fabry disease, inherited epidermolysis bullosa, or spinal muscular atrophy exhibited typical disease markers (Schosserer et al., 2015; Zhang et al., 2017; Slaats et al., 2018).

Despite these previous studies showed great interest in the USCs model, few data are available in the NMD field regarding their detailed transcription and protein characterization. It has been shown that USCs represent an ideal source for studying DMD and limb-girdle muscular dystrophy (LGMD) type 2 diseases (Falzarano et al., 2016; Kim et al., 2016), suggesting that they might have great potential for modeling other neuromuscular diseases.

Here, we have specifically interrogated the RNA-seq output for the expression of 610 genes in which mutations cause NMDs. We showed that the vast majority of NMD genes (93%) are transcribed in both native and MyoD transformed USCs, and that different groups of NMDs are overall represented with different gene expression rates. Following the myogenic transformation of USCs, the expression of only a few genes is modified.

We then validated RNA-seq data by immunofluorescence and/or western blotting (WB) for some selected genes causing muscular dystrophies such as *COL6A* (Collagen Alpha 1, 2, and 3 type), *EMD (*Emerin), *LMNA (*Lamin A/C), *DYSF* (Dysferlin), and *DAG1 (*Dystroglycan 1), and another set of genes causing motor neuron diseases such as *SMN*, *UBA1* (Ubiquitin-activating enzyme 1), *DYNC1H1* (Dynein, cytoplasmic 1, heavy chain 1), *SOD1*, and *C9orf72*.

By immunofluorescence, we found that COL6A protein is deposited in the extracellular matrix (ECM), and by WB analysis we confirmed that it is secreted in the cell medium. WB also

[1] http://www.musclegenetable.fr/

[2] https://www.clinicaltrials.gov/

demonstrated the translation of all the other tested genes, including those with lower transcriptional expression levels such as *SMN* and *C9orf72*.

Lastly, we extended the protein analysis to the *HTT* (Huntingtin) gene causing Huntington's disease (HD), as an example of a neurodegenerative disorder for which modeling pathological processes in patient-specific cells is not without challenges. Interestingly, we found that USCs also synthesize the HTT protein.

The results of our work demonstrate that USCs could be considered an appropriate *in vitro* model to test COL6-myopathies (Bethlem myopathy and Ullrich congenital muscular dystrophy), Emery-Dreifuss muscular dystrophies, SMA, ALS, Charcot-Marie-Tooth disease, Muscular dystrophy-dystroglycanopathy, and HD, and we suggest that their use could be expanded to more than 90% of known NMDs if further studies on patients' USCs will confirm our results.

The availability of a new *in vitro* model, easily obtainable from NMDs patients and able to recapitulate the hallmark features of the diseases, should accelerate the discovery of new candidate therapeutic molecules in pre-clinical stages and translate them into clinical studies.

MATERIALS AND METHODS

Isolation of Human Urinary Stem Cells

Urine samples were obtained from three healthy controls (age of subjects: 42, 49, and 29) and USCs were derived and cultured as previously described (Falzarano et al., 2016).

Briefly, urine samples were obtained from each subject and processed within 4 h from the collection.

The urine specimens were centrifuged at 400 × g for 10 min at room temperature, and washed with phosphate-buffered saline (PBS; Thermo Fisher Scientific, Waltham, MA) supplemented with an antibiotic/antimycotic solution (Sigma-Aldrich, St. Louis, MO). After discarding the supernatant, 1 ml of primary medium was added, and each sample was plated into a coated plate with 0.1% gelatin (Millipore, Billerica, MA). The primary medium was removed 96 h after plating, and 1 ml of proliferation medium was added to 1 ml of primary culture medium in each well.

Primary medium: Dulbecco's modified Eagle's medium (DMEM)/high glucose (EuroClone, Pero, Italy) and Gibco Ham's F12 nutrient mix (1:1; Thermo Fisher Scientific), supplemented with 10% (v/v) fetal bovine serum (FBS), antibiotic/antimycotic solution (Sigma-Aldrich), and an REGM (renal epithelial cell growth medium) SingleQuot kit (Lonza, Basel, Switzerland).

Proliferation medium: REGM BulletKit + RE cell basal medium (Lonza) and mesenchymal proliferation medium [DMEM/high glucose, 10% (v/v) FBS, 1% (v/v) Gibco GlutaMAX, 1% (v/v) non-essential amino acids (Gibco NEAA), 1% antibiotic/antimycotic solution, basic fibroblast growth factor (bFGF, 5 ng/ml; ProSpec, Rehovot, Israel), platelet-derived growth factor (PDGF-AB, 5 ng/ml; ProSpec), epidermal growth factor (EGF, 5 ng/ml; Lonza)] mixed at a 1:1 ratio.

The three native control USCs were used for both RNA-seq and protein analysis.

Myogenesis of native USCs was induced by infection with an adenovirus serotype 5 (Ad5)-derived, EA1-deleted adenoviral vector carrying the MyoD gene, as previously described (Spitali et al., 2009).

Transcriptional Profiling of Urinary Stem Cells by RNA-Seq Analysis

We analyzed the gene expression levels of native USCs (WT-n) and MyoD-USCs (WT-m) in RNA derived from a pool of the three healthy controls.

We analyzed a pool of three different donors in order to reduce the biological variations among samples and to be sure that the transcriptional profile was not affected by the variability among donors. Total RNA was isolated using the RNeasy-kit (Qiagen, Chatsworth, CA) according to the manufacturer's instructions. Libraries were prepared using TruSeq Kit (Illumina) according to the manufacturer's instructions. The quality and quantity of the RNA library was assessed using the Agilent 2100 Bioanalyzer and the ABI StepOnePlus Real-Time-PCR System. RNA-seq was carried out with the Illumina HiSeq4000 at the Beijing Genomics Institute (BGI, Beijing). Read quality was verified using fastQC (v. 0.11.3).[3] Raw reads were trimmed for adapters and for length at 100 bp with Trimmomatic, resulting in about 22 M (range 14.8–31.7 M) trimmed reads per sample. Reads were subsequently aligned to the human reference genome (GRCh38) using STAR (v. 2.5.3a; Dobin et al., 2013). Raw gene counts were obtained in R-3.4.4 using the *featureCounts* function of the *Rsubread* R package (v. 1.30.3; Liao et al., 2014) and the Gencode gene annotation. Raw counts were normalized to FPKM (Fragment Per Kilobase Million) using the edgeR package (Robinson et al., 2010).

Genes were categorized into four groups based on the quantiles of the FPKM distributions. Specifically, we defined high those genes with FPKM values higher than the 90th percentile of the distribution of FPKM values; middle those genes with FPKM values comprised between the 80th and the 90th percentile; low those genes with FPKM values comprised between the 50th and the 80th percentile, and not expressed the remaining genes with FPKM lower than the median FPKM values.

Immunofluorescence

Control USCs were grown until confluent onto coverslips, and the medium was supplemented with 0.25 mM ascorbic acid 24 h before cell harvesting. For long-term cultures, confluent cells were grown for 6 days in the presence of 0.25 mM ascorbic acid, the medium being changed every 2 days. The immunofluorescence analysis of collagen VI was performed using an antibody against the collagen VI α3 chain, globular domain (Squarzoni et al., 2006) (clone 3C4, Millipore) and two polyclonal anti-collagen VI antibodies (70R-CR009X, Fitzgerald; ab6588, Abcam) followed by incubation with anti-rabbit and anti-mouse FITC-conjugated antibodies (DAKO). Samples were observed with a Nikon epifluorescence microscope.

[3] http://www.bioinformatics.babraham.ac.uk/projects/fastqc/

TABLE 1 | List of antibodies targeting the NMD genes studied by Immunofluorescence (IF) and Western blot (WB).

Gene	Human Disease	OMIM	Primary antibody	Specie	Catalogue#	Dilution
COL6A1	– Bethlem myopathy – Ullrich congenital muscular dystrophy	# 158810 # 254090	(a) COL6A1 (b) Col6A1-A3 (c) Collagen VI (d) Collagen VI	(a) Rabbit polyclonal (b) Rabbit polyclonal (c) Rabbit polyclonal (d) Mouse monoclonal	(a) sc-20649 (b) 70R-CR009X (c) ab6588 (d) MAB1944	(a) 1:1000 (WB) (b) 1:1000 (WB) 1:100 (IF) (c) 1:100 (IF) (d) 1:50
C9orf72	Amyotrophic lateral sclerosis and/or frontotemporal dementia	# 105550	C90rf72	Mouse IgG2a	GTX634482	1:500
SMN1	Spinal muscular atrophy	# 253300 # 253550 # 253400 # 271150	SMN	Mouse IgG1	610647	1:500
DYNC1H1	– Charcot-Marie-Tooth disease, axonal, type 20 – Spinal muscular atrophy, lower extremity, autosomal dominant	# 614228 # 158600	DYNC1H1	Rabbit polyclonal	ABT266	1:5000
UBA1	Spinal muscular atrophy, distal, Xlinked, related to UBA1	# 301830	UBA1	Rabbit polyclonal	Orb411973	1:1000
SOD1	Amyotrophic lateral sclerosis	# 105400	SOD1	Rabbit polyclonal	10269-1-AP	1:1000
DAG1	– Muscular dystrophy-dystroglycanopathy (limb-girdle) – Congenital muscular dystrophy with hypoglycosylation of dystroglycan type A9	# 613818 # 616538	αDG IIH6 βDG	Mouse IgM Mouse IgG2a	05-593 B-DG-CE	1:2000 1:100
DYSF	– Miyoshi myopathy – Muscular; dystrophy, limb-girdle, type 2B	# 254130 # 253601	Dysferlin	Mouse IgG1	NCL-Hamlet	1:2000
HTT	Huntington Disease	# 143100	Huntingtin	Rabbit polyclonal	EPR5526	1:10000
EMD	Emery-dreifuss muscular dystrophy 1	# 310300	Emerin	Mouse IgG1	ab204987	1:1000
LMNA	– Charcot-Marie-Tooth disease, axonal, type 2B1 – Hutchinson-Gilford progeria syndrome – Mandibuloacral dysplasia with type a lipodystrophy – Restrictive dermopathy; lipodystrophy, familial partial, type 2 – Cardiomyopathy, dilated, 1A – Emery-Dreifuss muscular dystrophy, autosomal dominant.	# 605588 # 176670 # 248370 # 275210 # 151660 # 115200 # 181350	Lamin A/C	Rabbit monoclonal	ab108595	1:10000

 # phenotype description, molecular basis known.

Western Blot Analysis

WB analysis of COL6A, USC culture medium (treated for 24 h with 0.25 mM ascorbic acid in the absence of FBS) was resolved by standard SDS–PAGE, electro-blotted onto a nitrocellulose membrane and incubated with the 70R-CR009X and a specific anti-α1 chain antibody (sc-20649, Santa Cruz), followed by incubation with anti-mouse or anti-rabbit horseradish peroxidase (HRP)-conjugated secondary antibodies. Chemiluminescent detection was carried out with the ECL detection reagent Kit (GE Healthcare Amersham) according to the supplier's instructions.

All the other analyses were performed using the following method. USCs cells from the three healthy controls (ctrl1, ctrl2, ctrl3) were collected in lysis buffer (urea 4 M, Tris 125 mM pH6.8, SDS 4%) containing protease and phosphatase inhibitors (Roche, Merck United Kingdom). Protein quantification was performed using the Pierce BCA kit (Thermo Fisher Scientific, United States). Proteins were separated using NuPAGE 3–8% tris-acetate or NuPAGE 4–12% Bis-Tris gradient gels (Thermo Fisher Scientific) and transferred onto nitrocellulose membrane (Amersham Protran, GE Healthcare, United Kingdom). Membranes were blocked for 1 h at room temperature (RT) in 10% non-fat milk TBS-T (TRIS buffered saline + 0.1% Tween20) or in 3% BSA in 100 mM NaCl, 20 mM Tris pH 7.4. They were then incubated overnight at 4°C with primary antibodies (detailed in **Table 1**).

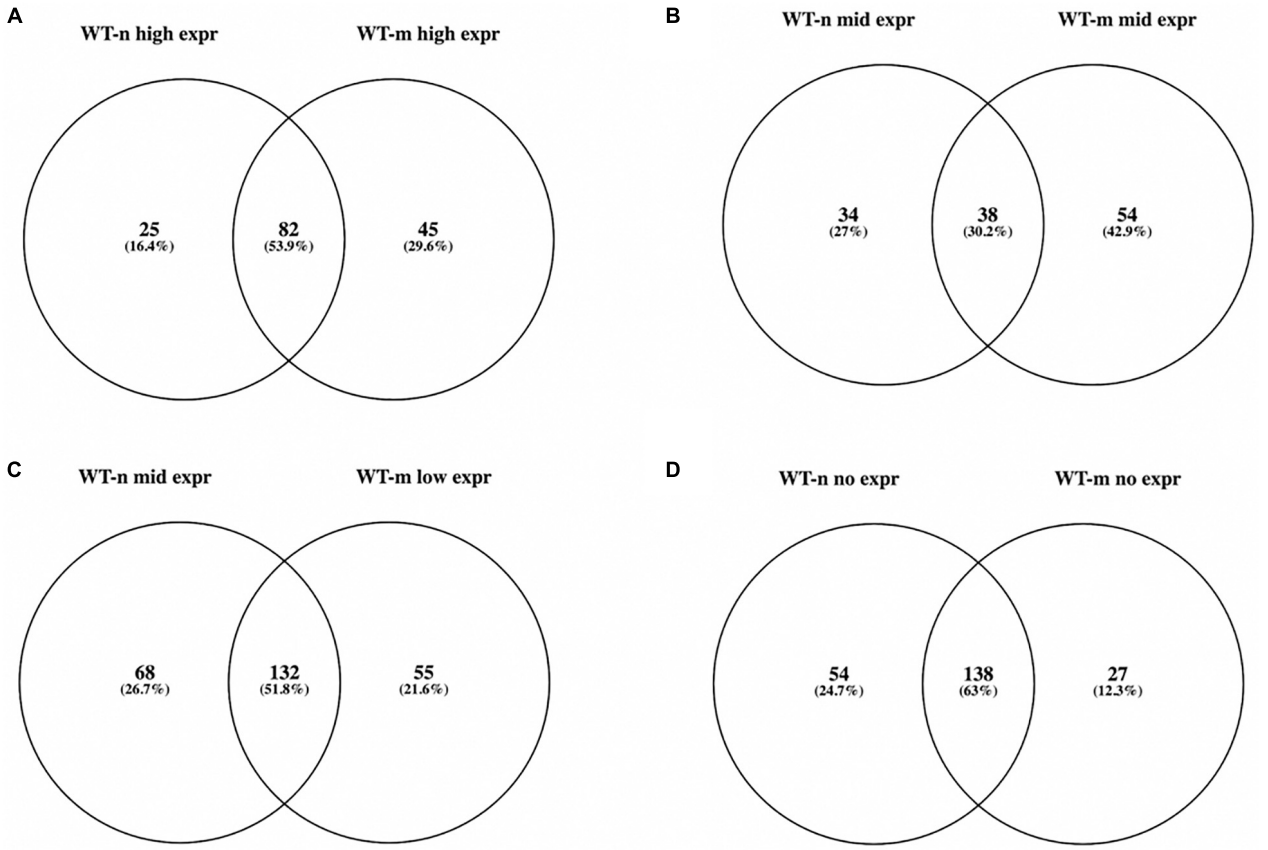

FIGURE 1 | Venn diagram showing overlap of expressed NMD genes belonging to the four groups of expression in WT-n and WT-m USCs (**A:** high; **B:** mid; **C:** low; **D:** no expr). More than 50% of NMD genes at high and low expression were shared between WT-n and WT-m **(A,C)**, while only the 30% of NMD genes at middle expression were in common in both samples **(B)**.

The following day, after 3 × 10 min washes in buffer at room temperature, membranes were incubated with the appropriate secondary antibodies: donkey anti-rabbit or donkey anti-mouse IRDye® (1:10,000, Li-Cor, United States) for 1 h at RT. After 3 × 10 min washes in buffer at RT, membranes were imaged using the Odyssey infrared imaging system (Li-Cor, United States). Since the main aim was to investigate if there was or not protein expression, only one or two gels were run for each antibody with one replicate for each individual.

RESULTS

Expression Profiling of Neuromuscular Genes

In total, we identified the transcripts of 20,716 genes in the two conditions, WT-n (native) and WT-m (MyoD) USCs. These 20,716 genes were categorized into four groups based on the distributions of the FPKM values. Specifically, we identified 2,071 genes with high expression (i.e., with FPKMs higher than 31.19 and 27.16 for WT-n and WT-m, respectively), 2,071 genes with middle expression (i.e., with FPKM values in the range 31.19–15.54 and 27.16–13.26 for WT-n and WT-m, respectively), 6,215 genes with middle expression (i.e., with FPKM values in the range 15.54–2.73 and 13.26–2.76 for WT-n and WT-m, respectively), and 10,358 not expressed genes (i.e., with FPKM values lower than 2.73 and 2.76 for WT-n and WT-m, respectively). All genes with the respective FPKM values and expression categories are listed in **Supplementary Table 1**.

We then focused on 610 genes known to cause neuromuscular diseases and belonging to 16 different groups of disorders (see text footnote 1, accessed 16 March 2021; **Supplementary Table 2**). We found that 571 of these NMD genes were present in the WT USCs gene expression data matrix (**Supplementary Table 3**) and that 379 and 406 of them were at high, middle, and low expression in WT-n and WT-m USCs, respectively. In particular, WT-n and WT-m had in common more than 50% of NMD genes at high and low expression, while only the 30% of NMD genes at middle expression were shared by both samples (**Figures 1A–C**). Interestingly, WT-m modified the expression levels of 154 genes (about 25% of total NMD genes) that resulted over-represented following the myogenic differentiation. Among the NMD genes that resulted not expressed in WT USCs, 138 were not expressed in both WT-n and WT-m, while 54 and

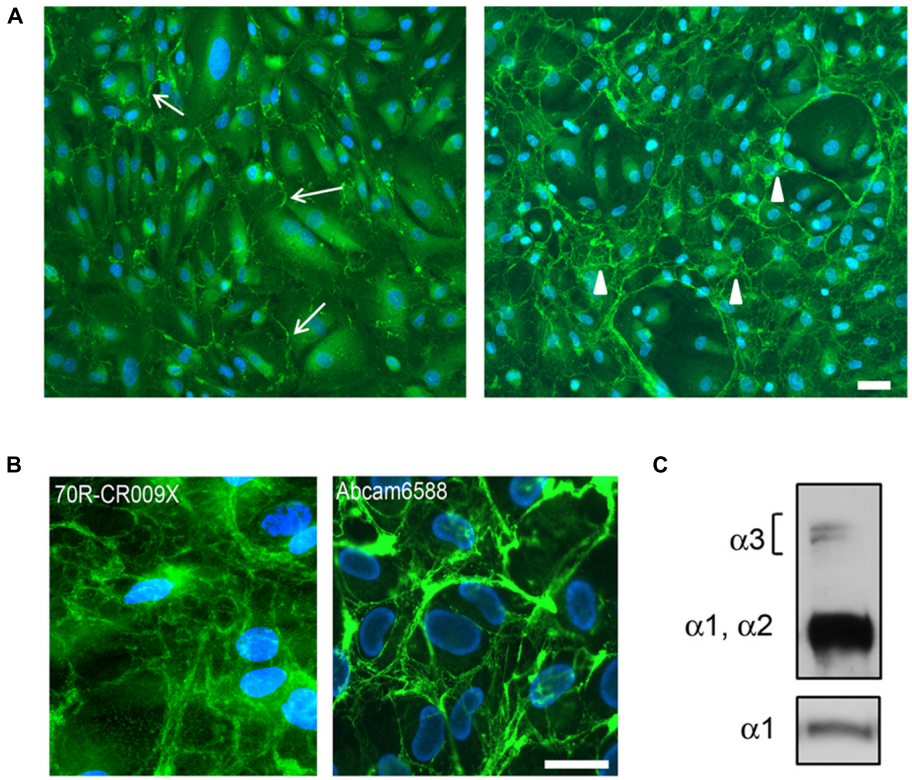

FIGURE 2 | (A) Immunofluorescence analysis of COL6A protein in control USC cultures after L-ascorbate treatment for 24 h (left panel) and 6 days (right panel), with 70R-CR009X antibody showing filamentous (arrows) and web-like arrangement (arrowheads) of protein deposited in the extracellular matrix. Nuclei were stained with DAPI. Scale bar, 40 μm. **(B)** High magnification of COL6A protein obtained with two different antibodies, as indicated, showing the organization in web-like structures. Nuclei were stained with DAPI. Scale bar, 20 μm. **(C)** WB analysis of USC culture medium after treatment with L-ascorbate. COL6A protein was detected by immunoblotting with antibodies recognizing either all COL6A chains (Fitzgerald 70XR95) or the α1chain (Santa Cruz sc-20649).

27 genes were specifically not expressed in WT-n and WT-m, respectively (**Figure 1D**).

The expression of few NMD genes (n = 43) either not expressed or with a weak expression in native USCs was restored following the myogenic differentiation such as *DES* (Desmin), *SGCD* (Delta-sarcoglycan), *SGCA* (Alpha sarcoglycan), *DTNA* (Dystrobrevin, alpha), *MYL1* (Myosin, light polypeptide 1, alkali, skeletal fast), *STAC3* (SH3 and cysteine rich domain 3) (**Supplementary Table 3**). Conversely, some genes that normally are not expressed in myogenic cells were, as expected, downregulated by myogenic differentiation as *COL6A* (Braghetta et al., 2008), *PLEKHG5* (Pleckstrin homology and RhoGEF domain containing G5) (Kim et al., 2013), and *SPTBN2* (Spectrin beta, non-erythrocytic 2) (Perkins et al., 2016) genes (**Supplementary Table 3**).

Transcripts related to the vast majority of disease groups were well represented in both native and myogenic USCs except for those associated with ion channel muscle diseases and malignant hyperthermia that were not expressed in either cell type as shown in **Supplementary Table 4**. Specifically, both WT-n and WT-m USCs did not express genes encoding sodium channel (*SCN4A*), chloride channel (*CLCN1*), calcium channel (*CACNA1S, CACNA1A*), potassium channel (*KCNJ18, KCNA, KCNE3*) and Na^+/K^+-ATPases (*ATP1A2*).

Among muscular dystrophies, LGMD and Emery-Dreifuss (EDMD) dystrophies are examples of diseases whose majority of the genes was expressed in native and/or MyoD USCs like *DES* and *TTN* (Titin) causing LGMD, *SYNE1* (Spectrin repeat-containing nuclear envelope protein) involved in the EDMD, *DYSF* (Dysferlin) associated with LGMD2B and Miyoshi myopathy (**Supplementary Table 4**).

The genes related to SMA and ALS, included in the Motor Neuron Diseases group, are all expressed in WT USCs. In particular, *SMN1*, that causes the most common form of SMA (types 1–4), is expressed in both native and myogenic-induced USCs. *UBA1* (Ubiquitin-activating enzyme 1) (Baumbach-Reardon et al., 2008), *DYNC1H1* (Dynein cytoplasmic 1 heavy chain 1) (Juntas Morales et al., 2017), *ASAH1* (N-acylsphingosine amidohydrolase (acid ceramidase) 1) (Topaloglu and Melki, 2016), and *GARS* (Glycyl-tRNA synthetase) (Antonellis et al., 2003) genes related to other SMA phenotypes showed high expression levels in both native and myogenic USCs.

Regarding ALS, most genes involved in the different phenotypes are very well expressed such as *SOD1*, *VCP* (Valosin-containing protein), *SQSTM1* (Sequestosome 1),

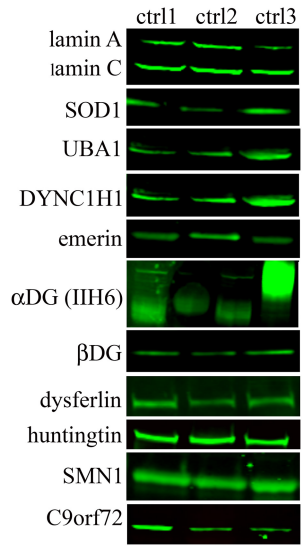

FIGURE 3 | Protein expression in native USCs from three control individuals (ctrl1, ctrl2, and ctrl3) on WB. A representative image of protein results are shown from the top to the bottom based on their transcript expression (from the highest to the lowest FPKM value, **Table 2**). For DAG1, two antibodies (IIH6 and βDG) were used since this gene encodes for two proteins, α- and β-dystroglycan. IIH6 antibody binds to a specific glycan epitope on α-DG. For comparison, in the 4th lane the glycosylation in human skeletal muscle is shown.

HNRNPA1 (Heterogeneous nuclear ribonucleoprotein A1), and *PFN1* (Profilin 1).

Protein Analysis

To assess the dynamics of the extracellular assembly of collagen VI protein, native USC cultures were grown to confluence and treated for 24 h (short-term) or 6 days (long-term) with ascorbate. Using a polyclonal antibody (70R-CR009X), immunofluorescence microscopy revealed that collagen VI was already present in the matrix of USCs after short-term treatment, however, an extensive filamentous network was only apparent in long-term cultures (**Figures 2A,B**). A similar pattern was obtained with the ab6588 polyclonal antibody (**Figure 2B**), while the anti-α3 chain antibody (1944 Millipore) and an anti-N2-N7 α3(VI) antibody (Sabatelli et al., 2011) (data not shown) did not recognize COL6A protein in USCs. On the other hand, evidence of COL6A heterotrimer secretion was confirmed by WB analysis of the cell medium, which demonstrated the presence of clear bands at the predicted molecular weights of the α3, α1, and α2 chains (**Figure 2C**).

The WB analysis on native USCs (**Figure 3**) for all the other selected genes (**Table 1**) showed bands, at the molecular weight predicted, for all the antibodies tested. We detected the proteins for all the four categories of expression (**Table 2**), including the genes belonging to the group with the lower FPKM values. Since the *DAG1* genes encodes for dystroglycan, a protein that is then cleaved into two proteins (α- and β- dystroglycan) (Brancaccio, 2019), we tested the expression of both proteins. To assess α-DG, an antibody (IIH6) that binds to a specific glycan epitope on α-DG was used and for comparison a skeletal muscle lysate was also loaded (4th bands, **Figure 3**).

TABLE 2 | List of genes included in the protein analysis.

GeneSymbol	WT-n FPKM	WT-n expression level
LMNA	192.47	High
SOD1	185.79	High
UBA1	124.49	High
COL6A2	49.10	High
COL6A1	49.10	High
COL6A3	43.59	High
DYNC1H1	48.84	High
EMD	46.75	High
COL6A3	43.59	High
DAG1	30.48	Middle
DYSF	23.77	Middle
HTT	11.79	Low
SMN1	3.92	Low
C9orf72	1.46	Not expressed

Genes were categorized into four groups based on the quantiles of the FPKM distribution, i.e., high (dark gray), medium (gray) and low (light gray) expression and not expressed (white).

CONCLUSION

Understanding the pathophysiologic mechanisms underlying rare genetic diseases is essential for the development of new therapeutic approaches. Therefore, a realistic disease model able to faithfully recapitulate the pathology is crucial. Unfortunately, the lack of *in vitro* human disease or even patient-specific models often forces the use of animal models, mostly mice, which present challenges due to genetic and physiological differences between humans and animals, resulting in poor efficacy and safety in clinical trials (Sato et al., 2019). In addition, the EC Directorate has strongly encouraged the use of non-animal models and it has recently published the first review of strict legislation designed to protect research animals.[4]

Finding an easily obtainable source of patient-specific cells, especially for diseases involving inaccessible tissues such as skeletal and cardiac muscles and the central nervous system, would overcome these limitations and improve the progress in the field of a personalized therapy.

In a previous study, we demonstrated the applicability of USCs as a non-invasive and unlimited cell source modeling DMD (Falzarano et al., 2016), but only a few studies have evaluated the usefulness of USCs in modeling other NMDs (Falzarano et al., 2016; Sato et al., 2019).

The aim of our study was to determine whether USCs might represent a cellular model for other NMDs.

We characterized the gene expression profile of 610 genes causing NMDs in native and myogenic transformed WT USCs. Interestingly, we found that 571 transcripts were expressed

[4]https://www.nature.com/articles/d41586-020-00352-6

in WT USCs, suggesting that USCs have the potential to model a variety of NMDs, at least at the transcriptional level. Indeed, the vast majority of NMD groups were well represented, and a few genes only showed a weak or absent expression in both WT-n and WT-m. Examples of these are ion channel muscle disease genes and malignant hyperthermia-related genes. Both native and MyoD cells did not express sodium, chloride, calcium, and potassium channel mRNAs. Therefore, USCs are not an appropriate tool to study pathogenic pathways or mutation effects of these genes. Nevertheless, it has been reported that USCs from a patient with a mild form of type 2 long QT syndrome can be reprogrammed in iPSCs that differentiate in functional cardiomyocytes recapitulating cardiac arrhythmia phenotypes caused by mutation in *KCNH2* gene (Jouni et al., 2015). Accordingly, USCs can be considered an attractive source to generate iPSCs for studying human ion channel diseases and other diseases as well.

When grouping genes based on their expression levels, we found that the myogenic transformation of USCs modified the expression levels of a limited set of high, middle, and low expression genes, and only a few genes that were not expressed in native USCs reverted to a positive expression. These genes, such as *DES*, *SGCD* and *SGCA*, *DTNA*, *MYL1*, *STAC3*, are, unsurprisingly, related to muscle function. This finding suggests that direct reprogramming of USCs into a myogenic cell line is required for some transcripts closely related to muscle function to be produced. Conversely, native USCs represent an ideal cell model for genes mainly expressed in the extracellular matrix, that are poorly represented in myogenic cells, such as *COL6A,* pathogenic variations in which cause Bethlem and Ulrich diseases (Tagliavini et al., 2014). This speculation is corroborated by our immunofluorescence and WB data, suggesting that USCs are a potential *in vitro* tool to study *COL6A*, as they are able to produce and secrete the fibrillary collagen VI protein.

In addition, differently from skin fibroblasts, antibodies against the α3 chain (N2–N7, and globular domain) did not recognize collagen VI in USCs. On the other hand, the α3 chain was secreted, as confirmed by WB analysis under denaturating conditions, which showed a doublet at 250 kD. These data point to additional post-translational modifications or conformational changes of α3(VI) in USC cultures. The expression of collagen VI chains is highly regulated at different levels and the α3(VI) N-terminus has several potential glycosylation sites which could generate additional molecular heterogeneity by attachment of branched oligosaccharides (Lampe and Bushby, 2005).

A similar finding was obtained using the antibody against alpha-dystroglycan (IIH6) directed against a carbohydrate epitope (Ervasti et al., 1997) that gives a band at a lower molecular weight in the USCs compared to muscle tissue, showing that a less glycosylated form of α-dystroglycan is expressed in the USCs. These modifications may be tissue/cell-type specific and, as for the different transcript levels, related to the differentiation state of the cells.

The protein analysis of all the other selected genes showed no differences of expression among genes belonging to the four categories of expression (high, medium, low expression or not expressed). Moreover, cells in which genes had a weak transcript expression produced the protein with a clear and intense signal, such as SMN1 and C9orf72 proteins. To expand the disease spectrum beyond the NMD field, we studied the *HTT* gene, mutations in which cause HD, an autosomal dominant, lethal, neurodegenerative disease (Hong et al., 2021). We showed that the *HTT* gene was well represented both at the transcript and protein level. This finding is very relevant, since USC might be used to model HD, perhaps without any reprogramming (Csobonyeiova et al., 2020).

To conclude, we show for the first time that a variety of NMDs diseases could be successfully studied in USCs. Among 610 NMD genes interrogated by RNA-seq, 93% of them were highly transcribed, and, consistently, all 11 proteins we tested were expressed. The *HTT* gene transcript and protein positivity strongly suggest USCs as a cell tool to study other central nervous system degenerative diseases.

This study shows that USCs may be adopted for basic research and might be also used if validated for diagnostics and clinical applications in the context of rare disease. However, since we focused our study on healthy donors only, further in depth studies are needed to overcome this limitation and to demonstrate that USCs obtained from patients affected with different diseases and carrying specific genes' mutations may recapitulate the disease-specific cellular phenotype.

We expect that these novel data will provide a resource for developing a new USCs *in vitro* model for several NMDs that will contribute to the understanding of some pathological mechanisms and to the discovery of new therapeutic approaches.

DATA AVAILABILITY STATEMENT

RNA-seq data for this study have been deposited in the GEO database under accession number GSE162108.

ETHICS STATEMENT

The studies involving human participants were reviewed and approved by the UNIFE Ethical Committee approval, No. 161299 (20/05/2020). The patients/participants provided their written informed consent to participate in this study.

AUTHOR CONTRIBUTIONS

MSF and AF designed the study. MSF and RR wrote the manuscript. HO conducted the cell isolation and culturing. MF, ZL, and WL performed RNA-seq raw data analysis. AG, SB, and RR performed bioinformatics and statistical analysis of RNA-seq outputs. ST, PS, and MA performed protein analysis. FG, RS, and CA-K critically revised the manuscript. ST and AF finalized the

manuscript. All authors contributed to the article and approved the submitted version.

FUNDING

This study was financially supported by Duchenne Parent Project Italy (Urinary Stem Cell biobank, grant no. 11/2018 to AF). This work was supported by the National Institute for Health Research Biomedical Research Centre at Great Ormond Street Hospital for Children NHS Foundation Trust and University College London and the MRC Centre for Neuromuscular Diseases Biobank.

ACKNOWLEDGMENTS

We would like to thank Jennifer E. Morgan (University College London, London, United Kingdom) for her critical reading of the manuscript and for English revision and Pierpaolo Ala (University College London, London, United Kingdom) for his technical assistance.

SUPPLEMENTARY MATERIAL

The Supplementary Material for this article can be found online at: https://www.frontiersin.org/articles/10.3389/fphys.2021.716471/full#supplementary-material

Supplementary Table 1 | List of identified 20,716 genes expressed in WT-n and WT-m USCs. Genes were categorized into four groups based on FPKM quantiles, i.e., high if the FPKM values were higher than the 90th percentile of the distribution of FPKM values; middle if the FPKM values were comprised between the 80th and the 90th percentile; low if the FPKM values were comprised between the 50th and the 80th percentile; and not expressed if the FPKM values were lower than the median FPKM.

Supplementary Table 2 | List of genes causing NMDs (http://www.musclegenetable.fr/, accessed 16 March 2021).

Supplementary Table 3 | List of NMD genes expressed in both WT-n and WT-m USCs. The table shows the 571 NMD transcripts expressed in WT USCs with the relative FPKM value, rank and expression category extrapolated from **Supplementary Table 1**.

Supplementary Table 4 | List of 16 categories (A-R) of NMDs. The table shows the FPKM value and the expression category of all genes belonging to the 16 groups of NMDs, comparing WT-n and WT-m USCs.

REFERENCES

Al-Zaidy, S. A., and Mendell, J. R. (2019). From Clinical Trials to Clinical Practice: practical Considerations for Gene Replacement Therapy in SMA Type 1. *Pediatr. Neurol.* 100, 3–11. doi: 10.1016/j.pediatrneurol.2019.06.007

Antonellis, A., Ellsworth, R. E., Sambuughin, N., Puls, I., Abel, A., Lee-Lin, S. Q., et al. (2003). Glycyl tRNA synthetase mutations in Charcot-Marie-Tooth disease type 2D and distal spinal muscular atrophy type V. *Am. J. Hum. Genet.* 72, 1293–1299. doi: 10.1086/375039

Baumbach-Reardon, L., Hunter, J. M., Ahearn, M. E., and Pfautsch, M. (2008). "Spinal Muscular Atrophy, X-Linked Infantile," in *GeneReviews§* , et al Edn, eds M. P. Adam, H. H. Ardinger, R. A. Pagon, S. E. Wallace, L. J. H. Bean, G. Mirzaa, et al. (Seattle: University of Washington).

Braghetta, P., Ferrari, A., Fabbro, C., Bizzotto, D., Volpin, D., Bonaldo, P., et al. (2008). An enhancer required for transcription of the Col6a1 gene in muscle connective tissue is induced by signals released from muscle cells. *Exp. Cell Res.* 314, 3508–3518. doi: 10.1016/j.yexcr.2008.08.006

Brancaccio, A. (2019). A molecular overview of the primary dystroglycanopathies. *J. Cell. Mol. Med.* 23, 3058–3062. doi: 10.1111/jcmm.14218

Cappella, M., Ciotti, C., Cohen-Tannoudji, M., and Biferi, M. G. (2019). Gene Therapy for ALS-A Perspective. *Int. J. Mol. Sci.* 20:4388. doi: 10.3390/ijms20184388

Cowling, B. S., and Thielemans, L. (2019). Translational medicine in neuromuscular disorders: from academia to industry. *Dis. Model Mech.* 13:dmm041434. doi: 10.1242/dmm.041434

Csobonyeiova, M., Polak, S., and Danisovic, L. (2020). Recent Overview of the Use of iPSCs Huntington's Disease Modeling and Therapy. *Int. J. Mol. Sci.* 21:2239. doi: 10.3390/ijms21062239

Dobin, A., Davis, C. A., Schlesinger, F., Drenkow, J., Zaleski, C., Jha, S., et al. (2013). STAR: ultrafast universal RNA-seq aligner. *Bioinformatics* 29, 15–21. doi: 10.1093/bioinformatics/bts635

Dowling, J. J., D Gonorazky, H., Cohn, R. D., and Campbell, C. (2018). Treating pediatric neuromuscular disorders: the future is now. *Am. J. Med. Genet. Part A* 176, 804–841. doi: 10.1002/ajmg.a.38418

Ervasti, J. M., Burwell, A. L., and Geissler, A. L. (1997). Tissue-specific heterogeneity in alpha-dystroglycan sialoglycosylation. Skeletal muscle alpha-dystroglycan is a latent receptor for Vicia villosa agglutinin b4 masked by sialic acid modification. *J. Biol. Chem.* 272, 22315–22321. doi: 10.1074/jbc.272.35.22315

Falzarano, M. S., D'Amario, D., Siracusano, A., Massetti, M., Amodeo, A., La Neve, F., et al. (2016). Duchenne Muscular Dystrophy Myogenic Cells from Urine-Derived Stem Cells Recapitulate the Dystrophin Genotype and Phenotype. *Hum. Gene Ther.* 27, 772–783. doi: 10.1089/hum.2016.079

Falzarano, M. S., and Ferlini, A. (2019). Urinary Stem Cells as Tools to Study Genetic Disease: overview of the Literature. *J. Clin. Med.* 8:627. doi: 10.3390/jcm8050627

Fortunato, F., Rossi, R., Falzarano, M. S., and Ferlini, A. (2021). Innovative Therapeutic Approaches for Duchenne Muscular Dystrophy. *J. Clin. Med.* 10:820. doi: 10.3390/jcm10040820

Hong, E. P., MacDonald, M. E., Wheeler, V. C., Jones, L., Holmans, P., Orth, M., et al. (2021). Huntington's Disease Pathogenesis: two Sequential Components. *J. Huntingtons Dis.* 10, 35–51. doi: 10.3233/JHD-200427

Jouni, M., Si-Tayeb, K., Es-Salah-Lamoureux, Z., Latypova, X., Champon, B., Caillaud, A., et al. (2015). Toward Personalized Medicine: using Cardiomyocytes Differentiated From Urine-Derived Pluripotent Stem Cells to Recapitulate Electrophysiological Characteristics of Type 2 Long QT Syndrome. *J. Am. Heart Assoc.* 4:e002159. doi: 10.1161/JAHA.115.002159

Juntas Morales, R., Pageot, N., Taieb, G., and Camu, W. (2017). Adult-onset spinal muscular atrophy: an update. *Rev. Neurol.* 173, 308–319. doi: 10.1016/j.neurol.2017.03.015

Kim, E. Y., Page, P., Dellefave-Castillo, L. M., McNally, E. M., and Wyatt, E. J. (2016). Direct reprogramming of urine-derived cells with inducible MyoD for modeling human muscle disease. *Skeletal Muscle* 6:32. doi: 10.1186/s13395-016-0103-9

Kim, H. J., Hong, Y. B., Park, J. M., Choi, Y. R., Kim, Y. J., Yoon, B. R., et al. (2013). Mutations in the PLEKHG5 gene is relevant with autosomal recessive intermediate Charcot-Marie-Tooth disease. *Orphanet J. Rare Dis.* 8:104. doi: 10.1186/1750-1172-8-104

Lampe, A. K., and Bushby, K. M. (2005). Collagen VI related muscle disorders. *J. Med. Genet.* 42, 673–685. doi: 10.1136/jmg.2002.002311

Liao, Y., Smyth, G. K., and Shi, W. (2014). featureCounts: an efficient general purpose program for assigning sequence reads to genomic features. *Bioinformatics* 30, 923–930. doi: 10.1093/bioinformatics/btt656

Perkins, E. M., Suminaite, D., Clarkson, Y. L., Lee, S. K., Lyndon, A. R., Rothstein, J. D., et al. (2016). Posterior cerebellar Purkinje cells in an SCA5/SPARCA1 mouse model are especially vulnerable to the synergistic effect of loss of β-III spectrin and GLAST. *Hum. Mol. Genet.* 25, 4448–4461. doi: 10.1093/hmg/ddw274

Robinson, M. D., McCarthy, D. J., and Smyth, G. K. (2010). edgeR: a Bioconductor package for differential expression analysis of digital gene expression data. *Bioinformatics* 26, 139–140. doi: 10.1093/bioinformatics/btp616

Sabatelli, P., Gara, S. K., Grumati, P., Urciuolo, A., Gualandi, F., Curci, R., et al. (2011). Expression of the collagen VI α5 and α6 chains in normal human skin and in skin of patients with collagen VI-related myopathies. *J. Invest. Dermatol.* 131, 99–107. doi: 10.1038/jid.2010.284

Sato, M., Takizawa, H., Nakamura, A., Turner, B. J., Shabanpoor, F., and Aoki, Y. (2019). Application of Urine-Derived Stem Cells to Cellular Modeling in Neuromuscular and Neurodegenerative Diseases. *Front. Mol. Neurosci.* 12:297. doi: 10.3389/fnmol.2019.00297

Schosserer, M., Reynoso, R., Wally, V., Jug, B., Kantner, V., Weilner, S., et al. (2015). Urine is a novel source of autologous mesenchymal stem cells for patients with epidermolysis bullosa. *BMC Res. Notes* 8:767. doi: 10.1186/s13104-015-1686-7

Slaats, G. G., Braun, F., Hoehne, M., Frech, L. E., Blomberg, L., Benzing, T., et al. (2018). Urine-derived cells: a promising diagnostic tool in Fabry disease patients. *Sci. Rep*. 8:11042. doi: 10.1038/s41598-018-29240-w

Speciale, A. A., Ellerington, R., Goedert, T., and Rinaldi, C. (2020). Modelling Neuromuscular Diseases in the Age of Precision Medicine. *J. Pers. Med.* 10:178. doi: 10.3390/jpm10040178

Spitali, P., Rimessi, P., Fabris, M., Perrone, D., Falzarano, S., Bovolenta, M., et al. (2009). Exon skipping-mediated dystrophin reading frame restoration for small mutations. *Hum. Mutat.* 30, 1527–1534. doi: 10.1002/humu.21092

Squarzoni, S., Sabatelli, P., Bergamin, N., Guicheney, P., Demir, E., Merlini, L., et al. (2006). Ultrastructural defects of collagen VI filaments in an Ullrich syndrome patient with loss of the alpha3(VI) N10-N7 domains. *J. Cell. Physiol.* 206, 160–166. doi: 10.1002/jcp.20443

Tagliavini, F., Sardone, F., Squarzoni, S., Maraldi, N. M., Merlini, L., Faldini, C., et al. (2014). Ultrastructural changes in muscle cells of patients with collagen VI-related myopathies. *Muscles Ligaments Tendons J.* 3, 281–286.

Tian, X., Liang, W. C., Feng, Y., Wang, J., Zhang, V. W., Chou, C. H., et al. (2015). Expanding genotype/phenotype of neuromuscular diseases by comprehensive target capture/NGS. *Neurol. Genet.* 1:e14. doi: 10.1212/NXG.0000000000000015

Topaloglu, H., and Melki, J. (2016). Spinal muscular atrophy associated with progressive myoclonus epilepsy. *Epileptic Disord.* 18, 128–134. doi: 10.1684/epd.2016.0858

Zhang, Q. J., Lin, X., Li, J. J., Lu, Y. Q., Guo, X. X., Dong, E. L., et al. (2017). Application of urine cells in drug intervention for spinal muscular atrophy. *Exp. Ther. Med.* 14, 1993–1998. doi: 10.3892/etm.2017.4791

Conflict of Interest: AF is the principal investigator of Sarepta Therapeutics Essence and MIS51ON clinical trial for DMD and is the PI of ongoing grants on DMD diagnosis funded by PTC Therapeutics and Sarepta Therapeutics.

The remaining authors declare that the research was conducted in the absence of any commercial or financial relationships that could be construed as a potential conflict of interest.

Publisher's Note: All claims expressed in this article are solely those of the authors and do not necessarily represent those of their affiliated organizations, or those of the publisher, the editors and the reviewers. Any product that may be evaluated in this article, or claim that may be made by its manufacturer, is not guaranteed or endorsed by the publisher.

frontiers in Physiology

ORIGINAL RESEARCH
published: 12 January 2022
doi: 10.3389/fphys.2021.698166

Lipidomic Analyses Reveal Specific Alterations of Phosphatidylcholine in Dystrophic *Mdx* Muscle

William J. Valentine[1,2], Sherif A. Mostafa[2,3], Suzumi M. Tokuoka[4], Fumie Hamano[2,5], Natsuko F. Inagaki[2], Joel Z. Nordin[1,6], Norio Motohashi[1], Yoshihiro Kita[5], Yoshitsugu Aoki[1]*, Takao Shimizu[2] and Hideo Shindou[2,7]**

[1] Department of Molecular Therapy, National Center for Neurology and Psychiatry (NCNP), National Institute of Neuroscience, Kodaira, Tokyo, Japan, [2] Department of Lipid Signaling, National Center for Global Health and Medicine (NCGM), Shinjuku-ku, Japan, [3] Weill Cornell Medicine—Qatar, Doha, Qatar, [4] Department of Lipidomics, Graduate School of Medicine, The University of Tokyo, Bunkyo-ku, Japan, [5] Life Sciences Core Facility, Graduate School of Medicine, The University of Tokyo, Bunkyo-ku, Japan, [6] Department of Laboratory Medicine, Centre for Biomolecular and Cellular Medicine, Karolinska Institutet, Huddinge, Sweden, [7] Department of Medical Lipid Science, Graduate School of Medicine, The University of Tokyo, Bunkyo-ku, Japan

OPEN ACCESS

Edited by:
Helen Cristina Miranda,
Case Western Reserve University,
United States

Reviewed by:
Constanza J. Cortes,
University of Alabama at Birmingham,
United States
Abitha Sukumaran,
Cincinnati Children's Hospital Medical Center, United States

***Correspondence:**
William J. Valentine
wvalentine@ncnp.go.jp
Yoshitsugu Aoki
tsugu56@ncnp.go.jp
Hideo Shindou
hshindou@ri.ncgm.go.jp

Specialty section:
This article was submitted to Striated Muscle Physiology, a section of the journal Frontiers in Physiology

Received: 20 April 2021
Accepted: 06 December 2021
Published: 12 January 2022

Citation:
Valentine WJ, Mostafa SA, Tokuoka SM, Hamano F, Inagaki NF, Nordin JZ, Motohashi N, Kita Y, Aoki Y, Shimizu T and Shindou H (2022) Lipidomic Analyses Reveal Specific Alterations of Phosphatidylcholine in Dystrophic Mdx Muscle. Front. Physiol. 12:698166. doi: 10.3389/fphys.2021.698166

In Duchenne muscular dystrophy (DMD), lack of dystrophin increases the permeability of myofiber plasma membranes to ions and larger macromolecules, disrupting calcium signaling and leading to progressive muscle wasting. Although the biological origin and meaning are unclear, alterations of phosphatidylcholine (PC) are reported in affected skeletal muscles of patients with DMD that may include higher levels of fatty acid (FA) 18:1 chains and lower levels of FA 18:2 chains, possibly reflected in relatively high levels of PC 34:1 (with 16:0_18:1 chain sets) and low levels of PC 34:2 (with 16:0_18:2 chain sets). Similar PC alterations have been reported to occur in the *mdx* mouse model of DMD. However, altered ratios of PC 34:1 to PC 34:2 have been variably reported, and we also observed that PC 34:2 levels were nearly equally elevated as PC 34:1 in the affected *mdx* muscles. We hypothesized that experimental factors that often varied between studies; including muscle types sampled, mouse ages, and mouse diets; may strongly impact the PC alterations detected in dystrophic muscle of *mdx* mice, especially the PC 34:1 to PC 34:2 ratios. In order to test our hypothesis, we performed comprehensive lipidomic analyses of PC and phosphatidylethanolamine (PE) in several muscles (extensor digitorum longus, gastrocnemius, and soleus) and determined the *mdx*-specific alterations. The alterations in PC 34:1 and PC 34:2 were closely monitored from the neonate period to the adult, and also in mice raised on several diets that varied in their fats. PC 34:1 was naturally high in neonate's muscle and decreased until age ∼3-weeks (disease onset age), and thereafter remained low in WT muscles but was higher in regenerated *mdx* muscles. Among the muscle types, soleus showed a distinctive phospholipid pattern with early and diminished *mdx* alterations. Diet was a major factor to impact PC 34:1/PC 34:2 ratios because *mdx*-specific alterations of PC 34:2 but not PC 34:1 were strictly dependent on diet. Our study identifies high PC 34:1 as a consistent biochemical feature of regenerated *mdx*-muscle and indicates nutritional approaches are also effective to modify the phospholipid compositions.

Keywords: *mdx*, Duchenne, phospholipid, phosphatidylcholine, oleic acid, muscular dystrophy, skeletal muscle

INTRODUCTION

Phosphatidylcholine (PC) is a main component of the lipid bilayer in plasma cell membranes that surrounds muscle fibers. This bilayer forms a hydrophobic barrier that functions to prevent the unregulated passage of ions and other charged molecules, which would otherwise lead to myofiber death and muscle wasting. Duchenne muscular dystrophy (DMD) is a progressive wasting muscle disease characterized by fragile plasma membranes due to a lack of the structural protein dystrophin in myofibers. An unexplained lipid alteration has been observed for over 50 years in muscles of patients with DMD that involves a large increase in fatty acid (FA) 18:1/oleic-acid chains and a relative decrease in FA 18:2/linoleic-acid chains in PC (Takagi et al., 1968; Kunze et al., 1975; Pearce et al., 1981). In more recent studies, a related alteration was suggested to be reflected in higher ratios of PC 34:1 (containing 16:0_18:1 chain sets) to PC 34:2 (containing 16:0_18:2 chain sets) in the affected muscles (Tahallah et al., 2008; **Table 1**). In DMD muscle fibers, enhanced susceptibility to contraction-induced membrane stress results in loss of barrier function of the plasma membranes and unregulated influx of calcium, leading to muscle degeneration (Turner et al., 1988; Menke and Jockusch, 1991; Straub et al., 1997). The biological origin and meaning of the altered PC in DMD muscles has been unknown, however, considering the role of acyl chains of phospholipid in biomembrane integrity, the replacement of FA 18:2 chains with FA 18:1 chains is of considerable interest, especially because mono-unsaturated chains like FA 18:1 are more conformationally stable than polyunsaturated chains like FA 18:2 (Feller et al., 2002), and large alterations of the PC 34:1/PC 34:2 ratios may affect biophysical properties of the membranes that impact the disease course.

The *mdx* mouse, with a stop codon mutation in exon 23 of the dystrophin gene, is a valuable DMD disease model (Hoffman et al., 1987). Despite generally milder course than in human DMD disease, *mdx* mice replicate many DMD-like biochemical and genetic features associated with dystrophin loss including myofiber membrane instability and enhanced permeability which drives progressive muscle wasting (Straub et al., 1997). A similarity in the PC alterations was also suggested by that increased ratios of PC 34:1/PC 34:2 were detected in affected *mdx* mouse muscles (Touboul et al., 2004; Benabdellah et al., 2009) in a similar manner as was detected in DMD patients' muscles (Tahallah et al., 2008; **Table 1**). However, other studies indicate that both PC 34:1 and PC 34:2 may be equally elevated in affected *mdx* muscle, in which case the PC 34:1/PC 34:2 ratios would be unchanged (Senoo et al., 2020), which we also observed.

We hypothesized that several experimental factors, including muscle types sampled, mouse ages, and mouse diets, may strongly affect the PC alterations detected in mdx muscles, including the PC 34:1/PC 34:2 ratios. In order to test our hypothesis, we performed lipidomic analyses to detect changes in the abundant membrane phospholipids PC and phosphatidylethanolamine (PE) in several muscles of wild-type (WT) and *mdx* mice during different stages of growth and development, and in mice raised on different diets. Multiple *mdx*-specific alterations were detected in muscles after the initial wave of degeneration at age ∼3 weeks, but with an early and diminished pattern occurring in soleus (SOL) compared to the other muscles sampled extensor digitorum longus (EDL) and gastrocnemius (GAS). Diet was also a critical factor, and high PC 34:1 occurred in *mdx* muscle independently of diets while high PC 34:2 occurred strictly in a diet-dependent manner. Our study identifies high levels of PC 34:1 as a specific biochemical feature of regenerated *mdx* muscles and indicates muscle type age, and diet also strongly impact phospholipid alterations, including PC 34:1/PC 34:2 ratios, in dystrophic muscles.

TABLE 1 | Phosphatidylcholine alterations reported in the literature.

Subjects	Changes in dystrophic muscle	References
DMD patients	Increased FA 18:1 and decreased FA 18:2 in PC	Takagi et al., 1968
DMD patients	Increased FA 18:1 and decreased FA 18:2 in PC	Kunze et al., 1975
DMD patients	Increased FA 18:1 in PC	Pearce et al., 1981
DMD patients	Increased PC 34:1/PC 34:2 ratio	Tahallah et al., 2008
DMD patients	Increased PC 34:1	Dabaj et al., 2021
mdx mice	Increased PC 34:1/PC 34:2 ratio	Touboul et al., 2004
mdx mice	Increased PC 34:1/PC 34:2 ratio	Benabdellah et al., 2009
mdx mice	Increased FA 18:1 in total phospholipids	Tuazon and Henderson, 2012
mdx mice	Increased PC 34:1	Paran et al., 2015
mdx mice	PC 34:1 and PC 34:2 both increased (EDL) or unchanged (SOL)	Senoo et al., 2020

MATERIALS AND METHODS

Animals Studies

All studies using mice were conducted in accord with the Public Health Service (PHS) Policy on Humane Care and Use of Laboratory Animals. Maintenance of the animal facility and use of animals was in full compliance with the Ethics Committee for animal experiments of the National Center for Global Health and Medicine, Tokyo, Japan.

Mice

Wild-type C57BL/6N, B10-ScN, and B10-ScSn-Dmd (*mdx*) mice were obtained from CLEA Japan, Inc. (Tokyo, Japan). B10-ScN and *mdx* mice were crossed and female offspring in successive generations heterozygous for the X-linked *mdx* mutation were bred to produce litters containing both B10-wild-type (WT) and -*mdx* male mice, and these male littermates were used for all comparative analyses of WT and *mdx* tissues. The original B10-ScN strain, but not B10-*mdx* strain, harbored a TLR4 deletion mutation which inhibits lipopolysaccharide signaling in a recessive manner (Coutinho and Meo, 1978; Vogel et al., 1979; Du et al., 1999). In the crossing of the strains, the inheritance of the mutated TLR4 allele was monitored and WT and *mdx* mice containing only non-mutant TLR4 alleles were generated,

and matched cohorts of heterozygous mice were also used for comparative analyses. All mice were housed in an air-conditioned animal room under specific-pathogen-free (SPF) conditions, with a 12-h light/dark cycle. Mice had *ad libitum* access to food and water and were fed CE-2 standard rodent chow diet (CLEA Japan, Inc., Tokyo, Japan) or custom research diets (described below).

Genotyping

Genotyping of WT and *mdx* mice was performed from mouse tail genomic DNA extracts. *Mdx* genotyping was performed by primer competition PCR (Shin et al., 2011) using the three-primer set common-forward (5′-GCG CGA AAC TCA TCA AAT ATG CGT GTT AG TGT-3′), WT-reverse (5′-GAT ACG CTG CTT TAA TGC CTT TAG TCA CTC AGA TAG TTG AAG CCA TTT TG-3′), and *mdx*-reverse (5′-CGG CCT GTC ACT CAG ATA GTT GAA GCC ATT TTA-3′) to detect WT (134 base pairs) and *mdx* alleles (117 base pairs). TLR4 genotyping was performed according to the Jackson Laboratory protocol using the primer set mutant forward (5′-GCA AGT TTC TAT ATG CAT TCT C -3′) and mutant reverse (5′-CCT CCA TTT CCA ATA GGT AG-3′) to detect mutant alleles (140 base pairs) and the primer set wild-type forward (5′-ATA TGC ATG ATC AAC ACC ACA G -3′) and wild-type reverse (5′-TTT CCA TTG CTG CCC TAT AG -3′) to detect wild-type alleles (390 base pairs).

Phospholipid Analysis by LC-MS

Tissue samples (∼5–25 mg) were isolated from the mid-belly region of muscles and stored at −80°C. Tissues were pulverized in a frozen state using a Tokken Automill cryogenic pulverizer (Tokken, Japan). After adding methanol to the crushed frozen tissues and incubating at 4°C for 1 h, methanolic extracts of the pulverized samples were collected and centrifuged at 14,000 rpm for 10 min at 4°C. The supernatants were collected, diluted with methanol to a concentration corresponding to ∼3 mg of original tissue/ml, and stored at −80°C. For lipidomic analyses, samples were further diluted with methanol ∼20-fold before LC-selected reaction monitoring (SRM)-MS analyses were performed using a Nexera UHPLC system and LCMS-8050 triple quadrupole mass spectrometers (Shimadzu, Japan). An Acquity UPLC BEH C8 column (1.7 μm, 2.1 mm × 100 mm, Waters) was used with the following ternary mobile phase compositions: 5 mM NH_4HCO_3/water (mobile phase A), acetonitrile (mobile phase B), and isopropanol (mobile phase C). The pump gradient [time (%A/%B/%C)] was programmed as follows: 0 min (50/45/5)-10 min (20/75/5)-20 min (20/50/30)-27.5 min (5/5/90)-28.5 min (5/5/90)-28.6 min (50/45/5). The flow rate was 0.35 ml/min and the column temperature was 47°C. The injection volume was 5 μl.

Comprehensive LC-SRM-MS analysis was performed in the positive ion mode electrospray ionization with the transitions $[M + H]^+ \rightarrow 184$ for PC and $[M + H]^+ \rightarrow [M + H\text{-}141]^+$ for PE to detect all diradyl PC and PE species possessing two even number carbon chains each 14–24 carbons in length. Peak areas of all identified species within PC or PE were summed to obtain the total PC or PE signal. Peak areas of individual PC or PE species were normalized to this sum, and peak values were expressed as the percentage of the total. For each analysis, the seven most abundant peaks and all major species beyond this which comprised at least 5% of total PC or PE signals in any group were plotted. Although plasmalogen-type PC and PE are abundant in various tissues, they were not detected above the criteria we set to be plotted in our graphs, possibly due to inefficient detection under our assay conditions (Zemski Berry and Murphy, 2004).

Semi-Quantitative qPCR

Total RNA was isolated from tissues using RNeasy and RNeasy fibrous tissue Kits (Qiagen, Valencia, CA, United States). cDNAs were synthesized using random primers and SuperScript III reverse transcriptase (Invitrogen, Carlsbad, CA, United States) or High-Capacity cDNA Reverse Transcription kit (Applied Biosystems, Waltham, MA, United States). Semi-quantitative qPCR analysis was performed using a StepOnePlus Real-Time PCR System and Fast SYBR Green Master Mix (Applied Biosystems, Waltham, MA, United States). mRNA expression was normalized to 18S rRNA and fold-changes were calculated using the $2^{-\Delta\Delta CT}$ method. Gene expression levels in EDL, GAS, and SOL were compared to EDL (values arbitrarily set to one) to determine statistical variations among the muscle types. The qPCR primer sequences are shown in **Table 2**.

Western Blots

Frozen muscle sections were homogenized in 2 × SDS-gel-loading buffer (4% SDS, 20% glycerol, and 0.125 M Tris pH to 6.8) by four cycles of bead-bashing, each for 120 s at 2,500 rpm, in a refrigerated Bead Smash12 (Wakenyaku). Cellular debris was pelleted at 12,000 × g for 15 min at room temperature; the supernatants were diluted 1:1 with water and protein concentrations were determined using a Pierce BCA Protein Assay kit (Thermo Fisher Scientific, Waltham, MA, United States). Then, 2-mercaptoethanol (5% final concentration) and bromophenol blue were added to the samples. After incubation at 95°C for 5 min, proteins (15 μg) were resolved by 4–20% SDS-PAGE and then transferred to Immobilon-P transfer

TABLE 2 | List of primers used for qPCR.

Gene	Forward primer	Reverse primer
Agpat1	AAACGAGGCGCCT TCCA	GGAGTAGAAGTCTTGATAGGAG GACATG
Agpat2	TGTGGGCCTCATCATGTACCT	AGGTCGGCCATCACAGACA
Agpat3	AAGCACCTATACCGCCGTATCA	GACCACCACTCCAGGAGCAT
Agpat4	AAGCAGCTGTTCCGCAAGA	CCACCACTCCAGAAGCATCA
Agpat5	AATGAGAAAGGTTCAGGAAAAT ACTCA	TGAATATGAAGTTTTGGGC ACTGT
Tnnc1	CTGTGAGCTGTCGCCAGAATG	CAGCATCCTCATCACCTTGCC
Tnni1	CCTAGCTCCACGAGGACTAAAC	CTGCTCCCAACACTCCTTGG
Tnnt1	GGACCCAGCCTTAGGTCTCT	CCCTTCTGGAATCTTCGGGG
Tnni2	TGCAAACAACTGCATGCGAA	TTGAACTTGCCCCTCAGGTC
Tnnc2	ATGGTGCGCCAGATGAAAGA	CCCAGAAGCCCGGAAAATCT
Ppara	CGTGGTGCATTTGGGCGTAT	CCATGTTGGATGGATGTGGC
Ppard	TCTCCCAGAATTCCTCCCCT	GAGCTTCATGCGGATTGTCC
Pparg	TGACAGGAGCCTGTGAGACC	GAATGGCATCTCTGTGTCAACC
Pgc1a	GGTGTAGCGACCAATCGGAA	TCTTCATCCACGGGGAGACT
18S	CTCAACACGGGAAACCTCAC	AGACAAATCGCTCCACCAAC

membranes (Millipore, Burlington, MA, United States) using a semidry transfer cell. Membranes were blocked in 5% ECL Prime Blocking Agent in TBS containing 0.1% Tween 20 (TBS-T) and probed with anti-TnnI1 (Proteintech #16102-1-AP, Rosemont, IL, United States) or anti TnnI2 (Proteintech #22130-1-AP, Rosemont, IL, United States) rabbit polyclonal antibodies. After incubation at room temperature for 60 min, the blots were washed three times for 5 min each with TBS-T and then incubated with horseradish peroxidase-conjugated anti-rabbit IgG (Cytiva #NA9340, Marlborough, MA, United States) for 30–60 min. Detection was performed with ECL Prime Western Blotting Detection Reagent (GE Healthcare, Chicago, IL, United States) and imaged using a Bio-Rad ChemiDoc MP Imaging System. Following detection, the blots were incubated for 15 min in Restore PLUS Western Blot Stripping Buffer (Thermo Fisher Scientific, Waltham, MA, United States) and re-blocked overnight then probed with anti-alpha-Tubulin antibody (Sigma #T6199, St. Louis, MO, United States) followed by horseradish peroxidase-conjugated anti-mouse IgG (Cytiva #NA9310, Marlborough, MA, United States).

Animal Diets

For studies comparing effects of feeding CE-2 standard chow (CLEA Japan, Inc., Tokyo, Japan) to custom research diets (Research Diets, Inc., New Brunswick, NJ, United States), diets were fed from the first day after birth, starting with to their nursing mothers (Oosting et al., 2015). The custom diet formulations are based on the common AIN-93G rodent growth diet, but with the fat sources substituted so as to modify the fatty chain compositions to be relatively rich in FA 18:1/oleic acid chains or FA 18:2/linoleic acid chains. Unlike the CE-2 standard chow which contains appreciable levels of FA 20:5/eicosapentaenoic acid (EPA) and FA 22:6/docosahexaenoic acid (DHA) fish oils, both custom diets lack appreciable levels of EPA and DHA, and they differ from CE-2 standard chow in nutritional energy contents as well. Estimates of the fatty chain compositions of CE-2 standard chow and both custom diets are shown in **Table 3** and the nutritional estimates are shown in **Table 4**, and nutritional estimates of the AIN-93G diet are also included for reference. Fatty chain composition estimates of custom research diets were reported by the manufacturer, and the fatty chain compositions of CE-2 standard chow were determined by GC-FID. Traditional Atwater formula was used to calculate estimation of metabolizable energy (ME): ME(kcal/kg) = [4 × CP(%) + 4 × NFE(%) + 9 × crude fat(%)] × 10 (Bielohuby et al., 2010; Asaro et al., 2017), based on the nutritional components reported by the manufacturers.

Statistical Analysis

Reverse transcription (RT)-PCR expression values were log-transformed before statistical analyses (Derveaux et al., 2010). All *t*-tests (unpaired, 2-tailed), Dunnett's multiple comparison tests, and two-way ANOVA with Sidak's post-tests were performed as indicated in figure legends. For multiple unpaired *t*-tests (more than two), the false discovery rate (FDR) was controlled by the Benjamini, Krieger, and Yekutieli method (FDR < 5%).

TABLE 3 | Estimation of fatty acid compositions of diets (% by weight of total fatty acids).

	CE-2 chow	Oleic custom diet	Linoleic custom diet
FA 16:0	18.2	12.8	13.2
FA 16:1	1.0	0.1	0.1
FA 18:0	2.5	3.8	3.2
FA 18:1	22.3	55.0	19.7
FA 18:2	46.0	24.2	59.6
FA 18:3	3.4	3.0	3.1
FA 20:5	2.4	0.0	0.0
FA 22:6	2.2	0.0	0.0
Saturates	21.6	17.6	17.4
Monounsaturates	23.8	55.1	19.9
Polyunsaturates	54.6	27.2	62.7
n-3	8.5	3.0	3.1
n-6	46.2	24.2	59.6

Fatty acids comprising ≥ 0.5% in any diet are shown. Custom diet values reported by manufacturer. CE-2 standard chow values measured by GC-FID.

TABLE 4 | Nutrition of diets.

	CE-2 chow	Custom diets	AIN-93G
kcal% protein	30.1	20.1	20.3
kcal% fats	12.2	15.8	15.8
kcal% carbs	57.7	64.2	63.9
kcal/100 g	339	399	399

Based on nutritional components reported by manufacturers. Energy contents were estimated by Atwater equations. AIN-93G is shown for reference.

All statistical analyses were performed using GraphPad Prism 9 software (GraphPad Software, La Jolla, CA, United States).

RESULTS

Phosphatidylcholine and Phosphatidylethanolamine Profiles of Healthy Skeletal Muscles of C57BL/6 Mice

To determine the variables, other than loss of dystrophin, which may cause PC 34:1/PC 34:2 ratios in muscles to differ between studies, we first examined how phospholipid profiles vary in different muscles of healthy adults C57BL/6 mice. Initial studies indicated that PC and PE compositions were dynamically regulated until age 6-weeks but highly stable in the adult tissues from ages 12- until at least 24-weeks, thus we analyzed muscle tissues from 15-week-old C57BL/6 mice. We consider this timepoint and others between 12- and 18-weeks of age nearly equivalent for adult mouse muscle tissues in terms of their phospholipid profiles. We measured PC and PE compositions in four muscles that vary in their metabolic capacities—tibialis anterior (TA), EDL, GAS, and SOL, with SOL being the most oxidative. The peak areas of each PC or PE species were normalized against the sum of all peak areas within that class

to determine the relative abundances (expressed as a percent of total PC or PE), and all major species comprising at least 5% of total PC or PE signals were plotted. Of note, plasmalogen (ether-linked) PC and PE were not detected at levels above the 5% threshold, but this may be due to their underestimation under our assay conditions (Zemski Berry and Murphy, 2004).

To determine the statistical variations of PC and PE compositions among the muscle types, EDL muscle was selected as a "standard" muscle to compare the variations that occurred in GAS, SOL, and TA. GAS and TA had more similar PC and PE profiles to EDL, and SOL had more pronounced variations. In PC (**Figure 1A**), relatively modest variations with EDL were detected in GAS (increased PC 40:6) and TA (increased PC 36:4). SOL showed substantially more variation with EDL, with SOL having decreased PC 34:1, PC 34:2, PC 36:4, PC 38:5, and PC 38:6; and increased PC 40:6 and PC 40:8. The most pronounced variation of PC in SOL was the markedly high levels of PC 40:6, which includes FA 22:6/DHA-containing PC 18:0_22:6 as an abundant isomer in muscle cells (Valentine et al., 2018).

In PE (**Figure 1B**), GAS had high levels of PE 40:6 compared to EDL. This same variation was more pronounced in SOL, which also varied from EDL in having low levels of PE 38:5. The four most abundant PE peaks—PE 38:6, PE 40:6, PE 40:7, and PE 40:8—may all contain DHA in their fatty chain sets, suggesting PE as a class may have been rich in DHA. To determine if PE might, as a class, be relatively enriched in any of the muscles, we calculated the ratios of total PE to total PC (sum of all PE peak areas/sum of all PC peak areas). While GAS and TA had total PE/total PC ratios that were similar to the ratio in EDL, the ratio in SOL was higher (**Figure 1C**). Together these data indicate that notable variations occurred in SOL that includes elevated levels of the DHA-containing peak PC 40:6 and elevated levels of PE, which as a class may have been rich in DHA-containing peaks. Notably, these mice were raised on a standard rodent diet (CE-2 standard chow) that has appreciable levels of DHA and EPA fish oils (**Table 3**). This is also likely to influence the prominence of DHA-containing peaks in PC and PE profiles because dietary DHA intake influences the amounts of DHA-containing phospholipids in tissues (Calder, 2016). It is also important to note that plasmalogen-type PC and PE species may have been inefficiently detected in our data-set but may also contain significant amounts of DHA chains.

Metabolic Gene Expression in Skeletal Muscles of C57BL/6 Mice

Different skeletal muscle groups have different embryonic origins and acquire different physiological characteristics during development depending on their physiological roles to generate rapid bursts of motion or more sustained but less rapid motion. Accordingly, the compositions of fiber types within muscles vary in terms of fast-twitch vs. slow-twitch fibers and glycolytic vs. oxidative fibers. In mice, SOL contains a majority (>75%) of oxidative fibers, both slow-twitch (Type I) and fast-twitch (Type IIA), while TA, EDL, and GAS, contain primarily fast-twitch, glycolytic fibers (Type IIB and IIX) (Augusto et al., 2004; Talbot and Maves, 2016; Terry et al., 2018). It is possible the distinctive PC and PE features we detected in SOL may be related to the metabolic characteristics of this muscle, because high phospholipid-DHA levels and high PE levels may be associated with high oxidative metabolic capacity in muscle (Hishikawa et al., 2017; Heden et al., 2019). Thus, we measured the mRNA expression of metabolic-related genes in the muscles of the same 15-week-old C57BL/6 mice that had been used for the comparative analyses of PC and PE compositions between EDL, GAS, SOL, and TA. In comparing the expression of genes among the muscle types that are involved in the metabolic regulation of membrane compositions, we first measured the gene expressions of several troponins as markers of fast- and slow-twitch fibers (**Figures 2A,B**). EDL was again used as a "standard" muscle to determine the statistical variations. SOL was markedly enriched in mRNA for the slow-type troponins TnnC1, TnnI1, and TnnT1 (**Figure 2A**). SOL also showed moderately reduced mRNA levels of the fast-type troponins TnnC2 and TnnI2 (**Figure 2B**). In a similar cohort of 14- to 16-week-old mice, proteins levels were analyzed. Similar to the mRNA data, SOL also had high protein levels of slow-type TnnI1, while fast-type TnnI2 protein was moderately decreased in SOL compared to EDL (**Figures 2C,D**).

Our lipidomic data had shown that SOL had high levels of DHA-containing PC 40:6 and was also possibly rich in DHA-containing PE (**Figures 1A–C**). Levels of PC 40:6 and several DHA-containing PE species were previously shown to be regulated in muscle cells by 1-acyl-*sn*-glycerol-3-phosphate O-acyltransferase 3 (AGPAT3), also called LPAAT3, an enzyme that selectively incorporates DHA into phospholipids (Valentine et al., 2018). To assess whether SOL may have enhanced levels of AGPAT3 or other enzymes that may regulate PC and PE compositions, we measured the expression of four AGPAT enzymes (AGPAT1-4) and another candidate enzyme (AGPAT5) which may regulate fatty chain compositions during *de novo* synthesis of phospholipids (**Figure 2E**; West et al., 1997; Lu et al., 2005; Shindou and Shimizu, 2009; Yuki et al., 2009; Eto et al., 2014). Consistent with our hypothesis, AGPAT3 expression was highest in SOL, which also showed higher levels of AGPAT2, compared to the other muscles (**Figure 2E**). While AGPAT3 is highly selective to utilize DHA as substrate and generate DHA-containing phospholipids (Koeberle et al., 2012; Iizuka-Hishikawa et al., 2017; Shindou et al., 2017), it is unknown how enhanced levels of AGPAT2 might impact PC and PE compositions in tissues. Major physiological roles in lipid metabolism are known for AGPAT2 (Agarwal et al., 2002; Cortes et al., 2009), and its high levels in SOL might be related to the high metabolic capacity of this muscle.

We also examined mRNA levels of peroxisome proliferator-activated receptors (PPARs) and PPAR Gamma Coactivator-1α (PGC-1α), which are ligand-activated transcriptional regulators of cellular metabolism (**Figure 2F**). PPARα, PPARδ, and PGC1α are major transcriptional regulators of genes involved in oxidative metabolism, and PPARγ is a transcriptional regulator of glucose metabolism. While these genes were expressed in GAS and TA at similar levels as EDL, the levels in SOL were higher. PPARδ and PGC1a cooperatively promote oxidative metabolism and increase endurance in skeletal muscle (Fan and Evans, 2017; Phua et al., 2018). We previously reported that PPARδ and PGC1α agonists lead to enhanced levels of DHA-containing PC and PE in skeletal muscle cells through upregulation of

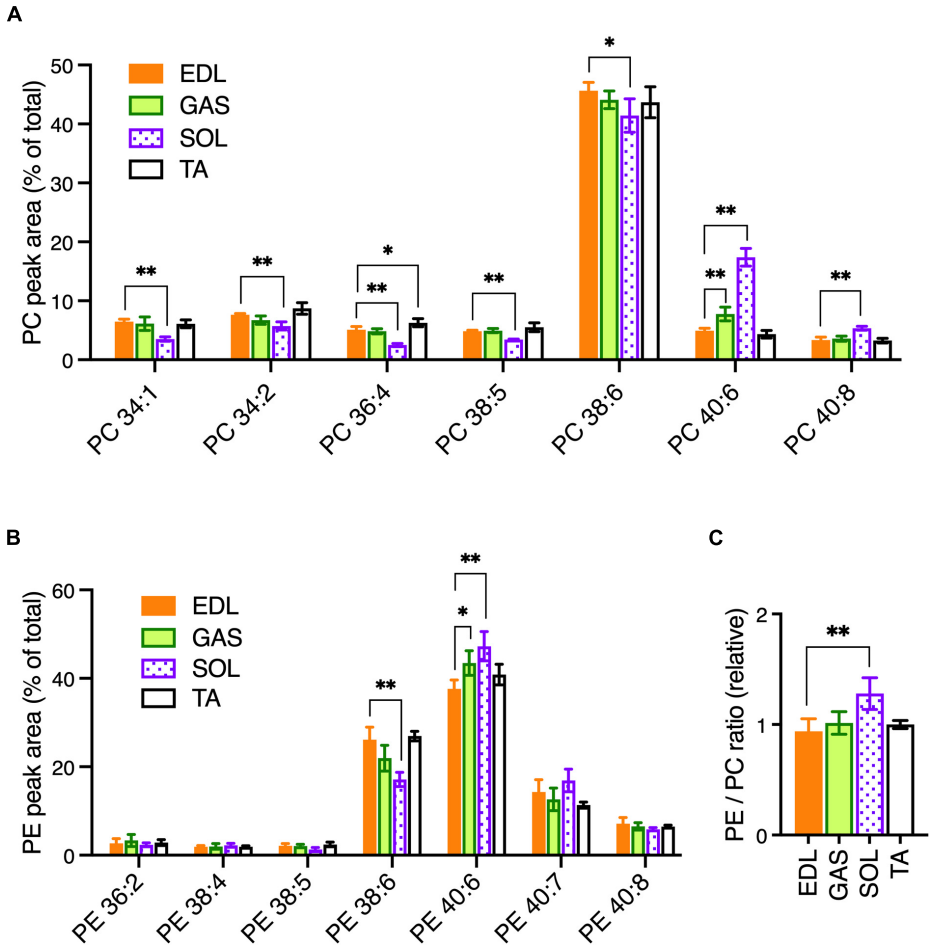

FIGURE 1 | PC and PE profiles in healthy EDL, GAS, SOL, and TA skeletal muscles of adult (15-week-old) C57BL/6 mice raised on CE-2 standard chow. PC **(A)** and PE **(B)** were measured by LC-MS/MS. EDL was selected as a standard muscle to determine the statistical variations. **(C)** Relative ratios of total detected amounts of PE to PC (ratio in EDL = 1). PC and PE peak values are expressed as the percentage of total PC or PE signals and means ± *SD* are plotted. The statistical significance of variations vs. EDL is based on Dunnett's multiple comparison tests. *$p < 0.05$, **$p < 0.01$; $n = 4$ mice/group.

AGPAT3 (Valentine et al., 2018), and it is possible that a similar PPAR pathway contributes to high levels of AGPAT3 and DHA-containing phospholipid in SOL. Overall, EDL and GAS muscles showed similar patterns of gene expression to EDL, while the patterns in SOL varied markedly (**Figures 2A–F**). Together with the lipidomic analyses (**Figures 1A–C**), these results support that the markedly different metabolic character of SOL compared to EDL, GAS, and TA is also reflected in PPAR-signaling pathways that impact fatty acid compositions of muscle cell membranes.

Phosphatidylcholine and Phosphatidylethanolamine Profiles in Skeletal Muscles of Wild-Type and *Mdx* Mice

In *mdx* mice, myofiber plasma membrane may be similarly destabilized as in DMD, and it has been suggested that similar PC alterations also occur. In order to determine the specific alterations of *mdx* mouse muscles, we measured PC and PE compositions of WT and *mdx* muscles by LC-MS/MS. All tissues used for comparative analyses of WT vs. *mdx* muscles were from B10 strain male mice, and all mice were raised on CE-2 standard chow diets, except in special cases for custom diet studies.

To assess the *mdx*-specific alterations in adult mouse muscles, PC and PE compositions were measured in EDL, GAS, and SOL of 18-week-old adult WT and *mdx* mice (**Figures 3A–C**). The patterns of muscle-type variations in PC and PE between EDL, GAS, and SOL in these tissues (**Supplementary Figures 1A–C**) were similar to those observed in the 15-week-old WT C57BL/6 tissues (**Figures 1A–C**), consistent with our observations that PC and PE compositions are relatively stable in adult mouse muscle tissues between from ages 12-weeks to at least 24-weeks, and also indicating that mouse strain has little influence in influencing the PC and PE profiles between B10-WT and C57BL/6 mice. As for the *mdx*-specific alterations that were detected in comparative analyses of the adult B10-WT and B10-*mdx* mice, EDL and GAS showed similar patterns in PC (**Figures 3A,B**; left graphs), with the *mdx*-associated PC alterations including high PC 34:1,

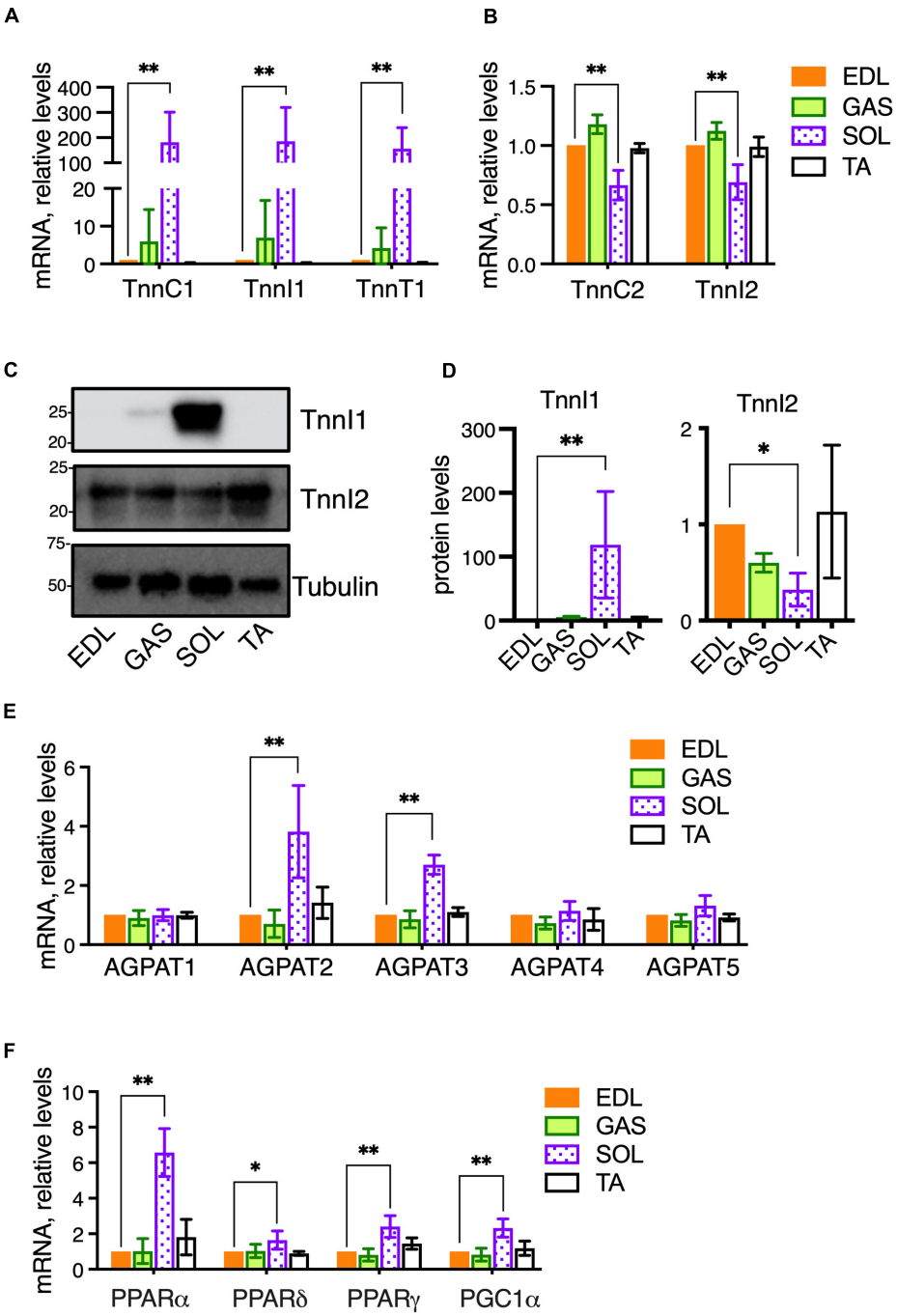

FIGURE 2 | Metabolic gene expressions in healthy skeletal muscles of adult (14–16-week-old) C57BL/6 mice raised on CE-2 standard chow. mRNA levels were measured by qPCR and protein levels (for TnnI1 and TnnI2) were detected by Western blotting. EDL was selected as a "standard" muscle to determine the statistical variations, and the plotted values reflect relative abundances compared to the levels in EDL (arbitrarily set to "1"). Compared to EDL, SOL had markedly high levels of slow-type troponins TnnC1, TnnI1, and TnnT1 **(A)** and moderately decreased fast-type troponins TnnC2 and TnnI2 **(B)**. Similar patterns in SOL were observed for the protein levels of TnnI1 (high levels) and TnnI2 (moderately decreased) **(C,D)**. mRNA levels of AGPATs **(E)** and PPARs/PGC1-alpha transcriptional regulators **(F)** were also determined. mRNA levels were normalized to 18S RNA and protein levels were normalized to Tubulin. The means ± *SD* are plotted. Statistical significance is based on Dunnett's multiple comparison tests. *$p < 0.05$, **$p < 0.01$; $n = 4$ mice/group.

high PC 34:2, high PC 36:4 high PC 38:5, and reduced PC 38:6. In SOL; however, these *mdx*-associated alterations were diminished below significance (**Figure 3C**, left graph). PE profiles were also measured (**Figures 3A–C**, right graphs), and several *mdx*-specific alterations were detected. PE 40:7 was moderately higher in *mdx* in all three muscle types, and other alterations

varied among the muscles. Overall, the PC and PE patterns were more similar in EDL and GAS but varied somewhat in SOL. Transcriptional profiling studies (Terry et al., 2018) indicated that EDL and GAS had high transcriptome similarity with TA and several other skeletal muscles (quadriceps, plantaris, and masseter), while SOL had similarity with a different cluster that included the diaphragm. Our data suggest that muscles like TA, EDL, and GAS may also cluster in terms of phospholipid profiles and *mdx*-specific alterations and indicate that muscle type sampled is one factor that affects the detection of PC alterations in dystrophic muscle.

Time Course of Alterations of Phosphatidylcholine and Phosphatidylethanolamine in *Mdx* Muscles

The muscle pathology in *mdx* mice proceeds in stages. Muscles of neonate *mdx* mice lack signs of overt muscle pathology before the initial wave of degeneration occurs at age ∼ 3-weeks (**Supplementary Figures 2A,B**; DiMario et al., 1991; Pastoret and Sebille, 1995). In *mdx* mice of ∼ 3-weeks of age, clusters of muscle fibers undergo initial rounds of necrosis and regeneration, evident in muscle tissue sections as regions populated by degenerated and small reforming fibers. Both WT and *mdx* mouse muscles grow rapidly from ages 3- to 6-weeks and are nearly fully grown by age 12-weeks. Abundant centrally located nuclei within myofibers indicate the active regeneration in adult (i.e., 6- and 12-week-old) *mdx* muscles (**Supplementary Figure 2C**).

We examined how the *mdx*-alterations in EDL, GAS, and SOL correlated with the time course of *mdx* muscle pathology. PC compositions in 2-, 6-, and 12-week-old muscles were examined in order to determine whether PC alterations detected in mature adult muscles (i.e., ages 12-weeks) also occurred before muscle disease onset (age 2-weeks) or in young adult muscle undergoing maximum growth (age 6-weeks) (**Figures 4A–C**). Similar to the *mdx*-alterations detected in 18-week-old EDL and GAS muscles (**Figure 3A**), in 12-week-old EDL and GAS (**Figures 4A,B**) *mdx*-associated high PC 34:1 and high PC 34:2 were observed, consistent with our observations that adult PC and PE profiles are fully developed and stable in WT and *mdx* mice by age 12-weeks. At age 6-weeks, high *mdx*-levels of PC 34:1 were also evident in EDL and GAS, however PC 34:2 was also transiently increased in WT muscles at age 6-weeks and additional *mdx*-associated elevations of PC 34:2 were modest (in EDL) or not detected (in GAS) at this time point. The other major *mdx*-associated alterations of PC, reduced PC 38:6, was evident in all muscles at age 6- and 12-weeks, but the alteration was diminished in SOL compared to EDL and GAS (**Figures 4A–C**). *Mdx*-alterations detected in adult muscles at ages 6- or 12-weeks were largely not present at age 2-weeks before the onset of muscle pathology (high PC 38:4 in GAS was an exception), and other minor *mdx*-associated PC alterations detected at age 2-weeks (i.e., in PC 30:0 in GAS or SOL) might reflect roles of dystrophin during muscle development (Dumont et al., 2015). PE compositions were also examined, and the adult *mdx*-associated alterations detected by age 6- or 12-weeks were not detected at age 2-weeks (**Supplementary Figure 3**).

Although PC 34:1 and PC 34:2 were similarly enhanced in 12-week-old *mdx* EDL and GAS muscles (**Figures 4A,B**), the pattern of change in WT muscles between ages 2- to 6-weeks was opposite with PC 34:1 decreasing and PC 34:2 increasing. These two abundant PC species are of great interest because they may harbor a large proportion of the FA 18:1 and FA 18:2 chains that are reportedly altered in the PC of DMD patients' muscles. Reduced PC 38:6 was also one of the most pronounced PC alterations we detected in *mdx*-muscles, and the extended time course of the dynamic change in all three species was examined in EDL and SOL. High *mdx*-levels of PC 34:1 and PC 34:2, and reduced *mdx*-levels of PC 38:6 were detected in EDL at ages 6-, 12-, and 18-weeks (**Figure 5A**). These same *mdx*-alterations were generally diminished in SOL (**Figure 5B**); however, surprisingly the time course of these alterations in SOL was also different, with all three alterations maximally detected earlier in SOL, at age 3-weeks, and then diminished or absent at later time points.

Phosphatidylcholine and Phosphatidylethanolamine Profiles in Extensor Digitorum Longus Muscles of Wild-Type and *Mdx* Mice Raised on Different Diets

While elevated levels of PC 34:1 in *mdx* muscles were consistently reported by several studies, altered levels of PC 34:2 are variably reported to occur. Dietary fats strongly influence fatty chain compositions of phospholipids in tissues (Levental et al., 2020); therefore, we examined how dietary factors may affect *mdx*-specific PC and PE alterations. In addition to CE-2 standard chow (CLEA, Japan, Inc.), we also raised mice on either of two custom diets that were formulated based on the commonly used AIN-93G rodent diet but with the sources of fats adjusted so as to be relatively high in FA 18:1 or FA 18:2. The fatty chain compositions and nutritional estimates of all three diets are shown in **Tables 3**, **4**. CE-2 standard chow differs from both custom diets in nutritional contents and also in being relatively rich in EPA and DHA compared to the custom diets; however, all diets contain at least 3% of fatty chains as FA 18:3 (n-3) and provide adequate amounts of essential fatty acids including omega-3s.

PC and PE compositions were measured in EDL muscles of adult WT and *mdx* mice raised on CE-2 standard chow (chow) (**Figure 6A**), the high-FA 18:1 custom diet (oleic) (**Figure 6B**), or the high-FA 18:2 custom diet (linoleic) (**Figure 6C**). The diets were provided to the mice from birth, starting with being fed to their nursing mothers, and tissues were collected at 12-weeks of age, as at this age the PC and PE profiles of the muscles were stable and fully matured, both in WT and *mdx* tissues. Diets profoundly affected the PC and PE compositions regardless of *mdx* status, with the most evident diet-dependent differences being observed between CE-2 standard chow and the custom diets. Some of these differences may reflect the relative lack of DHA in the custom diets, such as the large

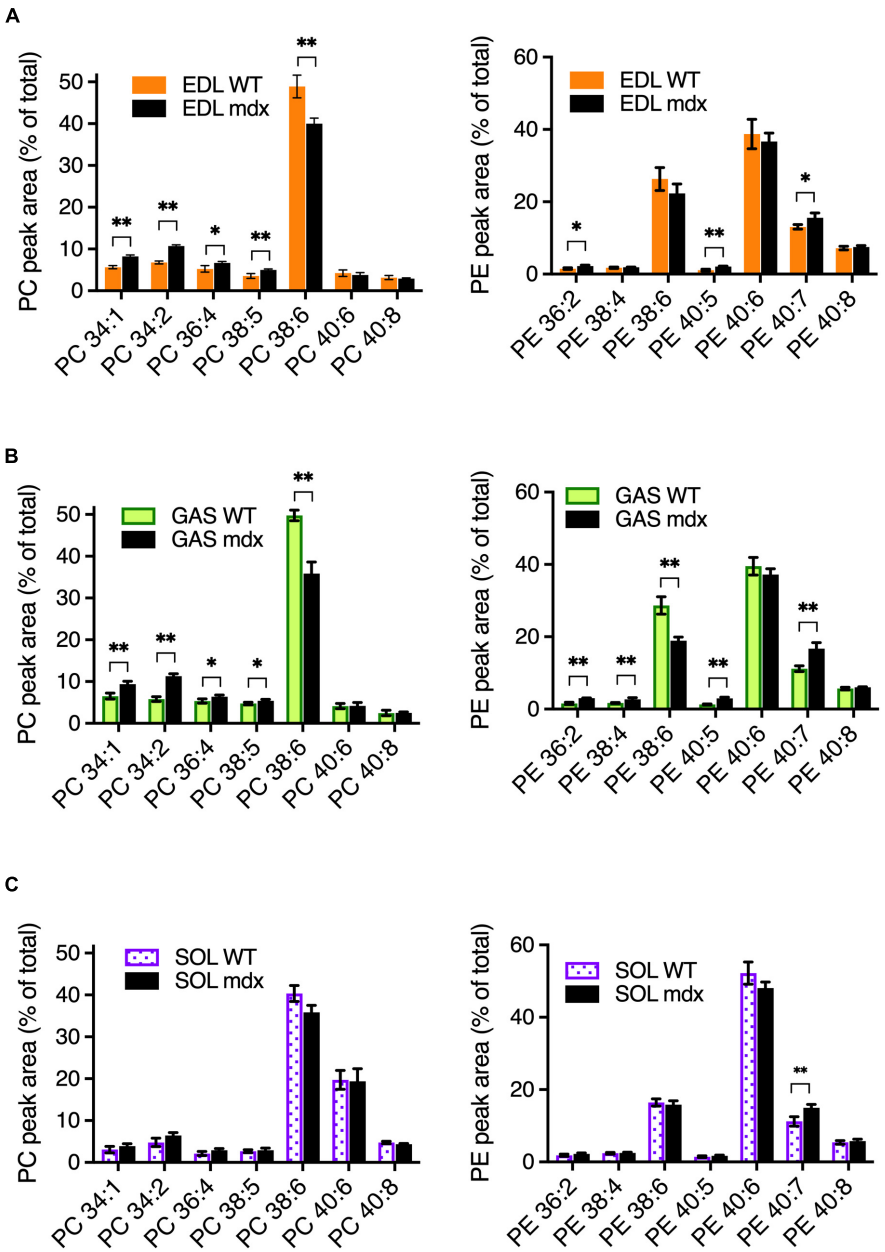

FIGURE 3 | *Mdx*-related PC and PE alterations in EDL, GAS, and SOL of adult (18-week-old) B10-WT and *-mdx* mice raised on CE-2 standard chow. EDL **(A)** and GAS **(B)** showed similar patterns of *mdx*-associated PC alterations. PC alterations were diminished in SOL **(C)**. The most prominent *mdx*-associated PC alterations in EDL and GAS were high PC 34:1, high PC 34:2, and reduced PC 38:6 levels. *Mdx*-associated alterations in PE are also shown. PC and PE were measured by LC-MS/MS. Peak values are expressed as the percentage of total PC or PE signals and means ± *SD* are plotted. Statistical significance of corresponding WT and *mdx* tissues is based on FDR-controlled multiple *t*-tests (FDR < 5%). $*p < 0.05$, $**p < 0.01$; $n = 3–5$ mice/group.

reduction in the presumed DHA-containing PC 38:6 peak and a corresponding increase in the non-DHA-containing PC 36:4 peak, which was observed in muscles of custom diet-raised mice (**Figures 6B,C**) compared to chow-raised mice (**Figure 6A**).

Several of the *mdx*-specific alterations in the major PC peaks were influenced by the diets to various extents. High-*mdx* levels of PC 34:1 were consistently observed in adult EDL regardless of the diet. In contrast, alterations of PC 34:2 were strictly diet-dependent, and high-*mdx* levels were only detected if mice were raised on CE-2 standard chow (**Figure 6A**) but not if mice were raised on either custom diet (**Figures 6B,C**). The low-*mdx* levels of PC 38:6 were also consistently observed in *mdx* muscles regardless of diet, although the overall abundance of this peak was much lower in custom diet-raised mice compared to CE-2 standard chow, suggesting the PC species

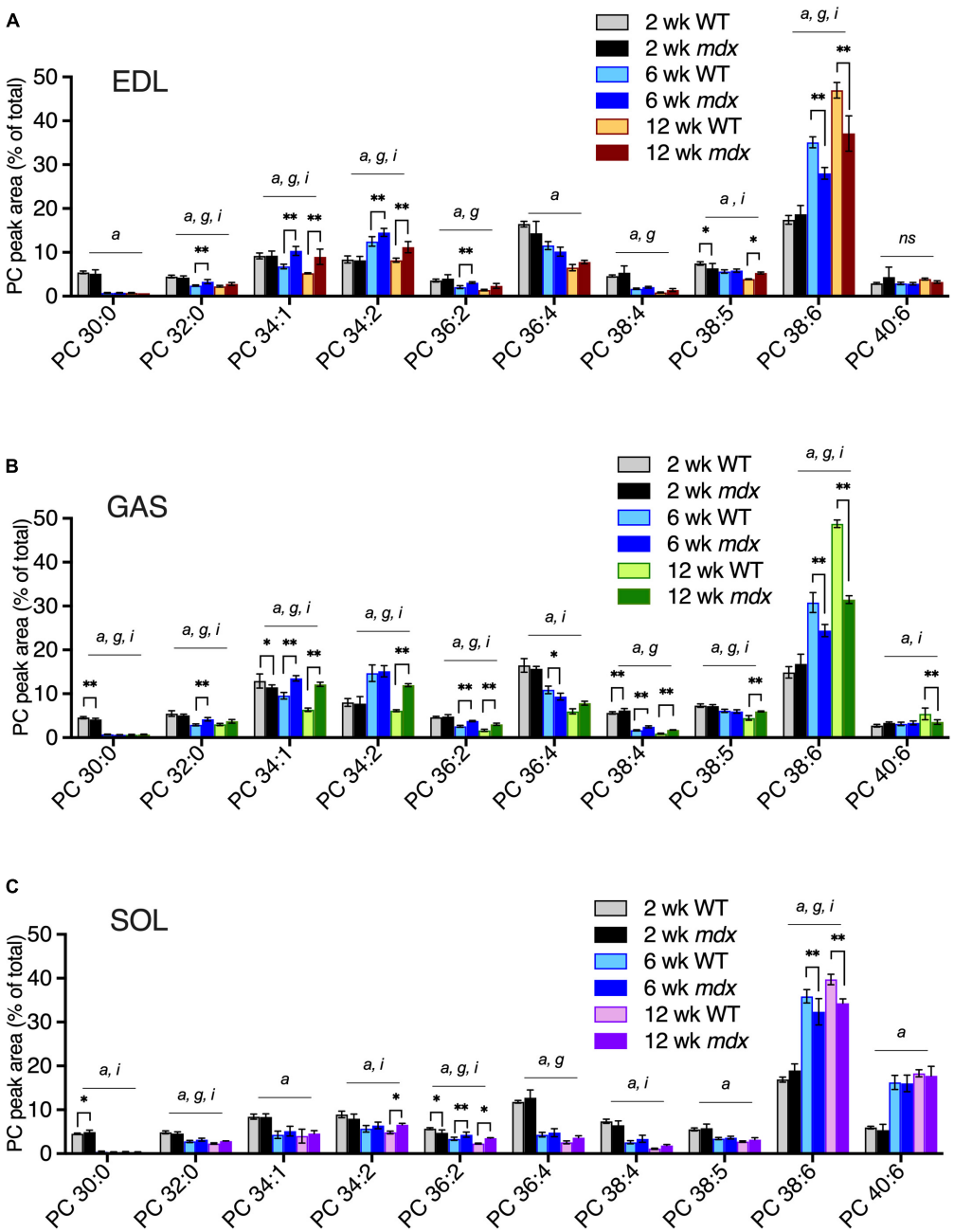

FIGURE 4 | PC alterations in EDL, GAS, and SOL of B10-WT and -*mdx* mice of various ages (2-, 6-, and 12-week-old) were raised on CE-2 standard chow. EDL **(A)** and GAS **(B)** showed similar patterns of *mdx*-associated PC alterations for increased PC 34:1 and decreased PC 38:6 at ages 6- and 12-weeks, and increased PC 34:2 at age 12-weeks, as well as at age 6-weeks in EDL. *Mdx*-associated PC alterations in SOL **(C)** were diminished or absent in several cases. PC peak values are expressed as the percentage of total signals and means ± *SD* are plotted. Significant variation ($p < 0.05$) was determined by two-way ANOVA and factor effects for each peak are indicated for age (*a*), *mdx* genotype (*g*), and interactive effects (*i*). Significant pair-wise differences between same-aged WT and *mdx* muscles were determined by Sidak's post-tests; *$p < 0.05$, **$p < 0.01$. n = 3–6 mice/group. *ns*; non-significant.

in this peak may be replaced or compensated for by other species, possibly in the PC 36:4 peak, in a diet-dependent manner. Both the PC 36:4 and PC 38:6 peaks are likely to contain mixtures of isomers including those that contain FA 18:2 in their chain sets, which will be important to investigate in future studies.

We also examined how the PC 34:1, PC 34:2, and PC 38:6 levels varied during early growth and development (ages 1–3-weeks) compared to those seen in adult EDL tissues of mice raised on the custom diets (**Supplementary Figures 4A,B**). During the first 3 weeks following birth, the pattern of changes in all three peaks was similar to those we had observed in

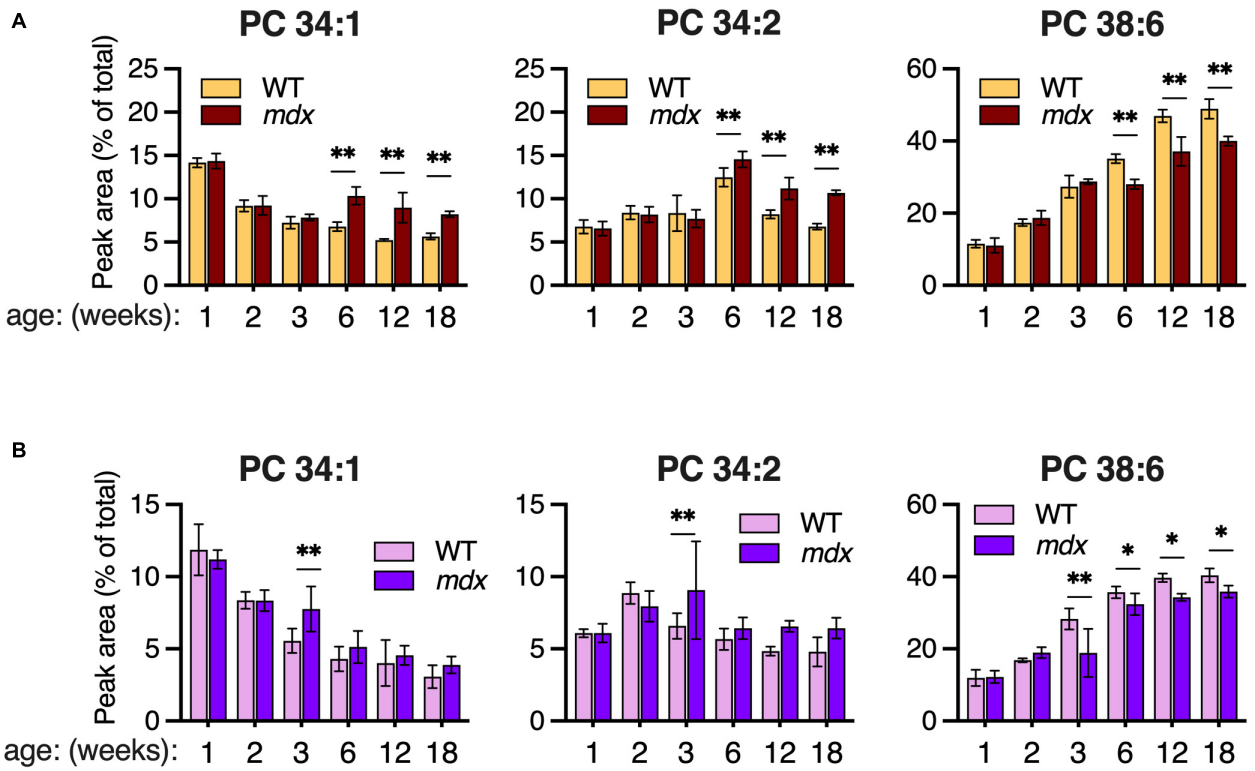

FIGURE 5 | Time course of major PC alterations in EDL and SOL of 1–18-week-old B10-WT and -*mdx* mice raised on CE-2 standard chow. PC compositions were measured by LC-MS/MS and means ± *SD* are plotted. In EDL **(A)**, high *mdx*-levels of PC 34:1 and PC 34:2 and reduced *mdx*-levels of PC 38:6 were detected at ages 6-, 12-, and 18-weeks. In SOL **(B)**, these alterations tended to be detected earlier at age 3-weeks and were diminished at later time points. Significant differences between corresponding WT and *mdx* muscles were determined by FDR-controlled multiple *t*-tests (FDR < 5%). *$p < 0.05$, **$p < 0.01$; $n = 3$–8 mice/group; includes identical data shown in **Figure 3** (18-week-old) and **Figure 4** (2-, 6-, and 12-week-old).

EDL of chow-raised mice (**Figure 5A**), with no *mdx*-specific alterations being apparent. PC 34:1 was high in neonates and decreased until age 3-weeks, while PC 34:2 and PC 38:6 tended to increase until age 3-weeks. The pattern of alterations detected at age 12-weeks of PC 34:1 (high in *mdx*) and PC 38:6 (low in *mdx*) were also qualitatively similar in all three diets (**Figures 6A–C**); however, lack of any *mdx*-specific elevation of PC 34:2 at age 12-weeks in custom-diet raised mice indicates that the high PC 34:2 levels observed in chow-raised *mdx* muscles is not only *mdx*- but also diet-dependent, possibly reflecting increased nutritional demands in the regenerating fibers and distinguishing it from the high levels of PC 34:1 that are diet-independent features of regenerating *mdx* muscles.

Metabolic Gene Alteration in Extensor Digitorum Longus Muscles of Adult *Mdx* Mice

We have shown that the mRNA expression profiles of various genes involved in metabolism in skeletal muscles of wildtype mice are markedly different in SOL when compared to the other muscles examined (EDL, GAS, and TA) (**Figures 2A–F**), which correlated with altered phosphatidylcholine and phosphatidylethanolamine compositions (**Figures 1A,B**). It was therefore critical to determine whether mRNA expression profiles of the metabolic genes are also altered in muscles of *mdx* mice and correlate with the altered lipid profile of *mdx* muscle tissue. We profiled the expression levels of fast type troponins and slow type troponins, AGPATs, and PPAR/PGC1-alpha transcriptional regulators in the EDL tissues of adult WT and *mdx* mice (chow-raised) in order to document the differences, if any, that exist in the muscles of *mdx* mice and correlate with the altered lipid profiles.

Extensor digitorum longus (EDL) muscles of 12-week-old WT and *mdx* mice were selected for the comparative analyses because the characteristic *mdx*-specific PC alterations are fully manifested by this age, and mRNA levels of the metabolic genes were measured by qPCR (**Figures 7A–D**).

Among the troponin genes analyzed, elevated levels of slow-type troponin TnnI1 were detected in the *mdx* tissues (**Figure 7A**) while fast-type troponins TnnC2 and TnnI2 were decreased in *mdx* tissues (**Figure 7B**). Among the AGPAT1-5, AGPAT1, a molecule involved in phospholipid and triglyceride synthesis, was slightly decreased in the *mdx* tissue (**Figure 7C**). Among several PPAR/PGC1α transcriptional regulators, PPARα was markedly down regulated in the *mdx* tissue (**Figure 7D**).

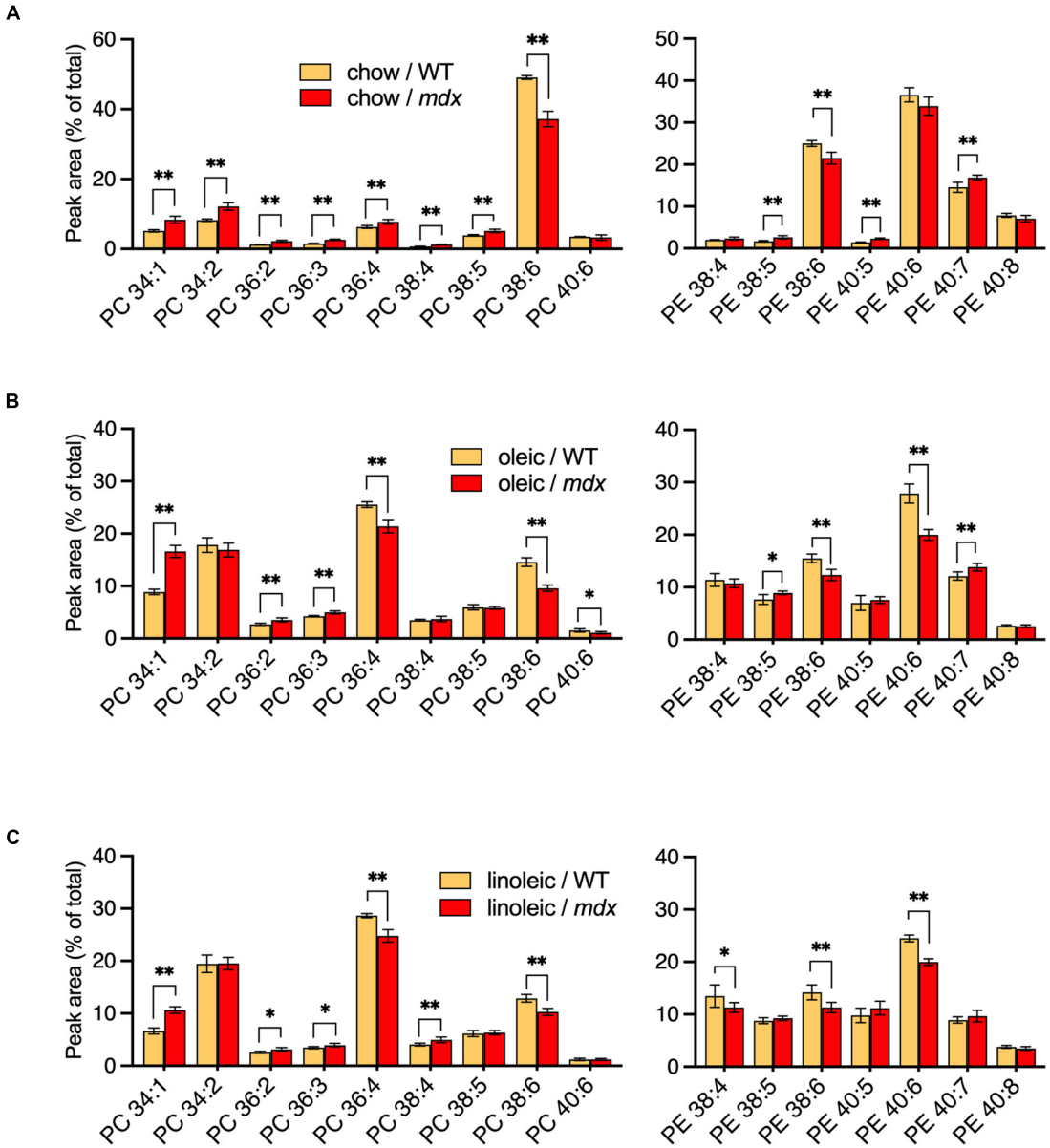

FIGURE 6 | PC and PE profiles of EDL from 12-week-old B10-WT and -*mdx* mice fed different diets from birth. Mice were raised on CE-2 standard chow (chow) **(A)**, or custom diets rich in FA 18:1 (oleic) **(B)** or FA 18:2 (linoleic) **(C)**. PC compositions were measured by LC-MS. PC 34:1 showed a similar increase in *mdx* tissue regardless of diet, but increased PC 34:2 was variably detected in *mdx* tissues, depending on the diets. PC and PE peak values are expressed as the percentage of total signals and means ± *SD* are plotted. Significance is based on FDR-controlled multiple *t*-tests (FDR < 5%). $^{*}p < 0.05$, $^{**}p < 0.01$; $n = 4$–8 mice/group.

Besides these alterations, other tendencies were noted, i.e., levels of the slow troponins TnnC1 and TnnT1 also tended to increase in *mdx* tissues, although not reaching statistical significance. Overall, these results indicated that EDL muscles of *mdx* mice do have altered metabolic gene expressions that accompany their altered lipid alterations. Some alterations such as increased slow-type and decreased fast-type troponin mRNA levels qualitatively resemble patterns seen in SOL, while other patterns differ such as in AGPATs and PPAR/PGC1α transcriptional regulators.

DISCUSSION

In DMD, myofiber membrane fragility caused by lack of dystrophin is a direct cause of the skeletal muscle pathology, and lipid alterations in DMD and the *mdx* mouse model have been long noted and are of great interest because of their possible impact on the disease course (for review see Saini-Chohan et al., 2012). Increase of FA 18:1 and decrease of FA 18:2 chains in PC of DMD patients muscles were noted in early studies (Takagi et al., 1968; Kunze et al., 1975; Pearce et al., 1981). In

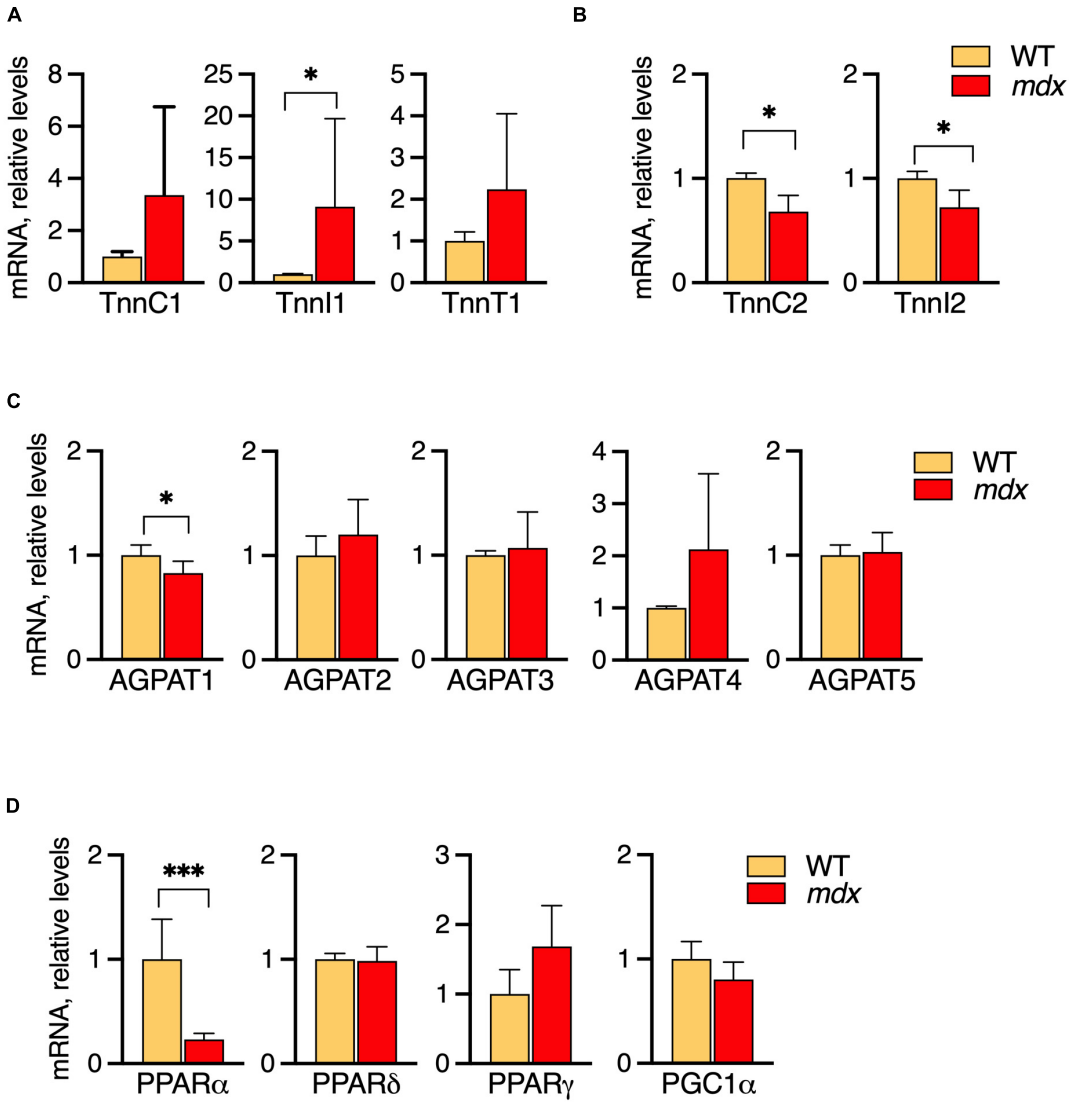

FIGURE 7 | Profiles of mRNA levels of metabolic genes in EDL of 12-week-old B10-WT and -*mdx* mice raised on CE-2 standard chow. mRNA levels were measured by qPCR and the abundances in *mdx* tissues relative to those in WT are plotted. High levels of slow-type troponin TnnI1 were observed in the *mdx* tissues **(A)** while fast-type troponins TnnC2 and TnnI2 were decreased in *mdx* tissues **(B)**. Among several AGPATs, AGPAT1 was slightly decreased in the *mdx* tissue **(C)**. Among several PPAR signaling molecules, PPARα was markedly down regulated in the mdx tissue **(D)**. The means ± *SD* are plotted. Significance is based on *t*-tests. $^{*}p < 0.05$, $^{***}p < 0.001$; $n = 4$–5 mice/group.

later studies, LC-MS/MS-based technologies were combined with coarse imaging capabilities to localize the PC alterations in tissues (Tahallah et al., 2008). PC 34:1, containing 16:0_18:1 chain sets, and PC 34:2, containing 16:0_18:2 chain sets, were detected as major PC species in muscle. Elevated PC 34:1/PC 34:2 ratios were detected in DMD muscle, with higher PC 34:1/PC 34:2 ratios detected in more affected areas both in regions of regenerating fibers as well as intercellular spaces (Tahallah et al., 2008). A more recent MS-imaging study also reported enhanced PC 34:1 as a prominent feature of DMD muscle (Dabaj et al., 2021), however, the relationship and impact of the enhanced PC 34:1 to the membrane fragility and progressive muscle wasting remains an open and pressing question.

Fatty acid (FA) 16:0, FA 18.1, and FA 18:2 were reported to constitute the majority of fatty chains in PC of normal human muscle throughout life, with FA 18:1 levels high in gestation and decreasing through development until adulthood, while FA 18:2 levels follow a reciprocal pattern of low in gestation and becoming high by adulthood (Bruce and Svennerholm, 1971). This observation suggests that PC 34:1 and PC 34:2 may be major PC species in human skeletal muscle throughout life, with PC 34:1 high in gestational and newborn muscle and decreasing through development as it is replaced by PC 34:2. In DMD muscle, replacement of FA 18:2 chains with FA 18:1 chain at high levels as reported in the early studies (Takagi et al., 1968; Kunze et al., 1975; Pearce et al., 1981) suggests that affected

DMD muscle may reaquire a high PC 34:1/low PC 34:2 aspect that is also characteristic of the fetal and early development of muscle. As PC is the most abundant phospholipid (Vance, 2015) it is possible that the relative amounts of FA 18:1 and FA 18:2 chains in PC must be appropriately regulated in order to maintain appropriate biophysical properties of lipid bilayers critical for various aspects of muscle development and function. It has been shown that artificial lipid bilayers of giant PC liposomes (∼20-micron diameter) containing only FA 18:1 chains were less flexible but withstood twice as much tension force before rupture as PC liposomes containing only FA 18:2 chains (Olbrich et al., 2000; Rawicz et al., 2000). Thus it is conceivable that control of the fatty chains in membrane phospholipids might have a similar therapeutic potential as other membrane-stabilizing strategies being pursued, most notably for synthetic block copolymers such as Poloxamer 188, to treat DMD and other conditions where membrane integrity is compromised (Houang et al., 2018). Whether and to what extent FA 18:1 and FA 18:2 abundances may influence biophysical properties of biological membranes such as the sarcolemma of dystrophic myofibers is currently unknown and will require rigorous experimental model systems to be addressed.

Enhanced PC 34:1 also occurs in the skeletal muscle of *mdx* mice, indicating they may be a useful model to elucidate the biological meaning of any therapeutic potential of the PC alterations in DMD patients' muscles. Touboul et al. (2004) used MALDI-TOF MS with course imaging capabilities to measure the PC 34:1/PC 34:2 ratios in structured (i.e., relatively healthy) vs. destructured (i.e., severely affected) areas of *mdx* mouse muscles. In this ground-breaking study, the PC 34:1/PC 34:2 ratios were higher in destructured areas of *mdx* muscle than in the relatively structured areas or healthy WT muscle. In an illuminating follow-up study (Benabdellah et al., 2009), the more destructured area of *mdx* muscles again had a higher PC 34:1/PC 34:2 ratio than in structured *mdx* muscles or WT, and a cohort of *mdx* mice was treated with a regimen of the nitric oxide donor molsidomine to improve the dystrophic phenotype of their muscles. The treatment indeed improved their muscle conditions, which was accompanied by a reversion (decrease) of the PC 34:1/PC 34:2 ratio to close to that in the healthy WT muscle. Their studies indicate that increased PC 34:1/PC 34:2 in *mdx* muscle occurs as part of the disease course, and in a reversible manner should the muscle pathology be improved. However, in other studies (Senoo et al., 2020) as well as the present study, it is clear that increased PC 34:1/PC 34:2 ratios variably manifest in affected *mdx* tissues. As PC 34:1 and PC 34:2 may harbor the bulk of the FA 18:1 and FA 18:2 chains, respectively, that are at altered levels in DMD muscles, understanding the basis for the discrepancies in reported PC 34:1/PC 34:2 ratios is critical if we are to effectively utilize the *mdx* model to elucidate the biological meaning of altered PC in DMD patients' muscles. Accordingly, we have investigated possible causes of the discrepancies focused on three likely factors to impact PC compositions—muscle-type, age, and diet.

One source of variation in the *mdx*-phospholipid patterns was the muscle type. In adult healthy C576BL/6 mice, similar PC and PE patterns were observed among EDL, GAS, and TA, but the patterns in SOL differed more from the other muscles (**Figures 1A,B**). The expression patterns of genes related to the regulation of metabolic capacity and lipid metabolism also differed markedly in SOL from the other muscles (**Figures 2A–F**). The unique PC and PE patterns and metabolic gene expressions in SOL might reflect unique metabolic characteristics of this muscle related to its high content of slow-twitch and oxidative muscle fibers (Isaeva et al., 2005). In B10-WT and -*mdx* mice, the patterns and *mdx*-associated alterations of PC and PE species were also relatively similar in EDL and GAS but differed substantially in SOL (**Figures 4A–C**). In PC, the *mdx*-associated increases of PC 34:1 and PC 34:2 detected in adult EDL and GAS appeared diminished or nearly absent in SOL.

Age of muscle was another important factor influencing *mdx*-associated PC alterations. The PC alterations detected in mature adult *mdx*-muscles (12-week-old) were generally not detected in 2-week-old muscles, before disease onset, but were generally evident at age 6-weeks, when muscle regeneration was already underway (**Figures 4A–C**). In EDL (**Figure 5A**), the time course of change in levels of PC 34:1 and PC 34:2 differed, with PC 34:1 showing a rebound pattern in *mdx* tissue after disease onset suggesting reactivation of an early developmental program, while PC 34:2 increased in both *mdx* and WT tissues between ages 3–6-weeks, a period of rapid growth, suggesting that in mature adult *mdx* muscle (i.e., 12- or 18-weeks-old) high-*mdx* levels of PC 34:2 levels might reflect high nutritional demand of regenerating fibers, and therefore vary in its manifestation depending upon the nutritional supplies of fatty chains.

The time course of PC alterations observed in SOL differed from EDL and GAS in that the magnitude of the *mdx*-associated alterations were much diminished in the adult tissues and were maximally detected earlier, at age 3-weeks (**Figure 5B**). In *mdx* mice, SOL is reported to undergo a stage of early and severe degeneration, and it will be fascinating to examine in future studies whether the patterning of lipid alterations reflects or impacts the disease susceptibility for various muscle groups to *mdx* pathology, especially in relation to early or severe degeneration reported for muscles such as SOL (early) or diaphragm (severe) compared to other muscles (Carnwath and Shotton, 1987; Stedman et al., 1991).

Diet was a major factor to affect the *mdx*-specific PC alterations and is likely the major factor to influence the variability in different reports as to whether or not PC 34:1/PC 34:2 ratios were increased in affected *mdx* muscles. We found that PC 34:1 showed a consistent pattern of upregulation in affected *mdx* muscle regardless of diet, while PC 34:2 variably showed alterations in *mdx* muscle, depending on which diet mice were raised on. *Mdx* mice raised on CE-2 standard chow, a standard laboratory mouse diet in our institutions, showed increased PC 34:2 compared to WT mice, but this alteration was completely absent in mice raised on oleic- or linoleic-rich custom diets. These diets formulations resemble that of another common laboratory diet, AIN-93G. Unlike AIN-93G and the custom diets, CE-2 standard chow contains significant levels of DHA and EPA fish oils (**Table 3**). This or another variable between the CE-2 chow and the other diets may be a primary factor to cause the diet-dependent variations of patterns of PC 34:2 in *mdx* muscle, while the variation in oleic acid and linoleic acid levels between the

two custom diets had less affect on the qualitative patterns of *mdx*-specific alterations (**Figures 6A–C**).

Although the current study highlights the PC alterations and the experimental variables that affect their detection in *mdx* muscle, it is limited in that it does not address the biological origin of the altered PC, nor how the PC alterations might affect disease onset, progression, or severity. More insight is also needed as to why *mdx*-specific PC alterations are less detectable in SOL than in EDL and GAS, and whether this is related to differences in the muscle pathologies and/or the fiber-type compositions. PC compositions vary between membranes of different organelles, and future studies must determine in which specific membranes of myofibers the PC alterations are manifested, such as plasma membranes, sarcoplasmic reticulum membranes, or mitochondrial membranes. This will also shed light on how the PC alterations might impact or reflect various pathological aspects of dystrophic muscle such as plasma membrane fragility, calcium mishandling, and mitochondrial dysfunction or deficit. Moreover, identification of the biological origin of the altered PC, including the lipid synthesizing or degrading molecules involved and impacts of nutrients, is required and will enable genetic- or pharmacological-based strategies to assess the disease impact or therapeutic potential of altered PC in dystrophic muscle.

In summary, our results indicate high PC 34:1 is a common characteristic of regenerating *mdx* muscle while alteration of PC 34:2 was variable and highly dependent on mouse diets. Other *mdx*-specific alterations in PC such as decreased PC 38:6 also occurred and might have significant biological impacts, as may additional *mdx*-associated alterations in less abundant species and other lipid classes not analyzed in our study. The present study focused on PC 34:1and PC 34:2 because these abundant PC species may be major repositories for the FA 18:1 and FA 18:2 chains in PC which are reported to be highly altered in the affected muscles of DMD patients. Further studies are required to determine the origin and biological significance of enhanced PC 34:1 and other lipid alterations in dystrophic muscle.

DATA AVAILABILITY STATEMENT

The original contributions presented in the study are included in the article/**Supplementary Material**, further inquiries can be directed to the corresponding author/s.

ETHICS STATEMENT

The animal study was reviewed and approved by the Ethics Committee for animal experiments of the National Center for Global Health and Medicine, Tokyo, Japan.

AUTHOR CONTRIBUTIONS

WV designed the study, performed the experiments, analyzed the data, and wrote the manuscript. SM performed the experiments, analyzed the data, and interpreted the results. ST, FH, YK, and NI analyzed the data. JN and NM interpreted the results. YA wrote the manuscript. TS and HS designed and wrote the manuscript. All authors reviewed and agreed to the manuscript.

FUNDING

This work was supported by the AMED-CREST 21gm0910011 (to HS). Additional support was provided from the Japan Society for the Promotion of Science 18K15074 (to NI), 18K07544 (to YA), 19K16849 (to JN), and Grants-in-Aid for Research on Nervous and Mental Disorders (28-6).

ACKNOWLEDGMENTS

We thank Keizo Waku (Teikyo University) for valuable advice and guidance. We thank Juliet Gentile (Research Diets, Inc.) for excellent support with the design of custom diets. We thank all members of the Shimizu laboratory for their advice, discussion, and support.

SUPPLEMENTARY MATERIAL

The Supplementary Material for this article can be found online at: https://www.frontiersin.org/articles/10.3389/fphys.2021.698166/full#supplementary-material

REFERENCES

Agarwal, A. K., Arioglu, E., De Almeida, S., Akkoc, N., Taylor, S. I., Bowcock, A. M., et al. (2002). AGPAT2 is mutated in congenital generalized lipodystrophy linked to chromosome 9q34. *Nat. Genet.* 31, 21–23. doi: 10.1038/ng880

Asaro, N. J., Guevara, M. A., Berendt, K., Zijlstra, R., and Shoveller, A. K. (2017). Digestibility is similar between commercial diets that provide ingredients with different perceived glycemic responses and the inaccuracy of using the modified atwater calculation to calculate metabolizable energy. *Vet. Sci.* 4:54. doi: 10.3390/vetsci4040054

Augusto, V., Padovani, C. R., and Campos, G. E. (2004). Skeletal muscle fiber types in C57BL6J mice. *Braz. J. Morphol. Sci.* 21, 89–94.

Benabdellah, F., Yu, H., Brunelle, A., Laprevote, O., and De La Porte, S. (2009). MALDI reveals membrane lipid profile reversion in MDX mice. *Neurobiol. Dis.* 36, 252–258. doi: 10.1016/j.nbd.2009.07.013

Bielohuby, M., Bodendorf, K., Brandstetter, H., Bidlingmaier, M., and Kienzle, E. (2010). Predicting metabolisable energy in commercial rat diets: physiological fuel values may be misleading. *Br. J. Nutr.* 103, 1525–1533. doi: 10.1017/S000711450999345X

Bruce, A., and Svennerholm, L. (1971). Skeletal muscle lipids. I. Changes in fatty acid composition of lecithin in man during growth. *Biochim. Biophys. Acta* 239, 393–400. doi: 10.1016/0005-2760(71)90032-4

Calder, P. C. (2016). Docosahexaenoic acid. *Ann. Nutr. Metab.* 69(Suppl 1), 7–21.

Carnwath, J. W., and Shotton, D. M. (1987). Muscular dystrophy in the mdx mouse: histopathology of the soleus and extensor digitorum longus muscles. *J. Neurol. Sci.* 80, 39–54. doi: 10.1016/0022-510x(87)90219-x

Cortes, V. A., Curtis, D. E., Sukumaran, S., Shao, X., Parameswara, V., Rashid, S., et al. (2009). Molecular mechanisms of hepatic steatosis and insulin resistance in the AGPAT2-deficient mouse model of congenital generalized lipodystrophy. *Cell Metab.* 9, 165–176. doi: 10.1016/j.cmet.2009.01.002

Coutinho, A., and Meo, T. (1978). Genetic basis for unresponsiveness to lipopolysaccharide in C57BL/10Cr mice. *Immunogenetics* 7, 17–24. doi: 10.1007/BF01843983

Dabaj, I., Ferey, J., Marguet, F., Gilard, V., Basset, C., Bahri, Y., et al. (2021). Muscle metabolic remodelling patterns in Duchenne muscular dystrophy revealed by ultra-high-resolution mass spectrometry imaging. *Sci. Rep.* 11:1906.

Derveaux, S., Vandesompele, J., and Hellemans, J. (2010). How to do successful gene expression analysis using real-time PCR. *Methods* 50, 227–230. doi: 10.1016/j.ymeth.2009.11.001

DiMario, J. X., Uzman, A., and Strohman, R. C. (1991). Fiber regeneration is not persistent in dystrophic (MDX) mouse skeletal muscle. *Dev. Biol.* 148, 314–321. doi: 10.1016/0012-1606(91)90340-9

Du, X., Poltorak, A., Silva, M., and Beutler, B. (1999). Analysis of Tlr4-mediated LPS signal transduction in macrophages by mutational modification of the receptor. *Blood Cells Mol. Dis.* 25, 328–338. doi: 10.1006/bcmd.1999.0262

Dumont, N. A., Wang, Y. X., Von Maltzahn, J., Pasut, A., Bentzinger, C. F., Brun, C. E., et al. (2015). Dystrophin expression in muscle stem cells regulates their polarity and asymmetric division. *Nat. Med.* 21, 1455–1463. doi: 10.1038/nm.3990

Eto, M., Shindou, H., and Shimizu, T. (2014). A novel lysophosphatidic acid acyltransferase enzyme (LPAAT4) with a possible role for incorporating docosahexaenoic acid into brain glycerophospholipids. *Biochem. Biophys. Res. Commun.* 443, 718–724. doi: 10.1016/j.bbrc.2013.12.043

Fan, W., and Evans, R. M. (2017). Exercise mimetics: impact on health and performance. *Cell Metab.* 25, 242–247. doi: 10.1016/j.cmet.2016.10.022

Feller, S. E., Gawrisch, K., and Mackerell, A. D. Jr. (2002). Polyunsaturated fatty acids in lipid bilayers: intrinsic and environmental contributions to their unique physical properties. *J. Am. Chem. Soc.* 124, 318–326.

Heden, T. D., Johnson, J. M., Ferrara, P. J., Eshima, H., Verkerke, A. R. P., Wentzler, E. J., et al. (2019). Mitochondrial PE potentiates respiratory enzymes to amplify skeletal muscle aerobic capacity. *Sci. Adv.* 5:eaax8352. doi: 10.1126/sciadv.aax8352

Hishikawa, D., Valentine, W. J., Iizuka-Hishikawa, Y., Shindou, H., and Shimizu, T. (2017). Metabolism and functions of docosahexaenoic acid-containing membrane glycerophospholipids. *FEBS Lett.* 591, 2730–2744. doi: 10.1002/1873-3468.12825

Hoffman, E. P., Brown, R. H. Jr., and Kunkel, L. M. (1987). Dystrophin: the protein product of the Duchenne muscular dystrophy locus. *Cell* 51, 919–928. doi: 10.1016/0092-8674(87)90579-4

Houang, E. M., Sham, Y. Y., Bates, F. S., and Metzger, J. M. (2018). Muscle membrane integrity in Duchenne muscular dystrophy: recent advances in copolymer-based muscle membrane stabilizers. *Skelet. Muscle* 8:31. doi: 10.1186/s13395-018-0177-7

Iizuka-Hishikawa, Y., Hishikawa, D., Sasaki, J., Takubo, K., Goto, M., Nagata, K., et al. (2017). Lysophosphatidic acid acyltransferase 3 tunes the membrane status of germ cells by incorporating docosahexaenoic acid during spermatogenesis. *J. Biol. Chem.* 292, 12065–12076. doi: 10.1074/jbc.M117.791277

Isaeva, E. V., Shkryl, V. M., and Shirokova, N. (2005). Mitochondrial redox state and Ca^{2+} sparks in permeabilized mammalian skeletal muscle. *J. Physiol.* 565, 855–872.

Koeberle, A., Shindou, H., Harayama, T., Yuki, K., and Shimizu, T. (2012). Polyunsaturated fatty acids are incorporated into maturating male mouse germ cells by lysophosphatidic acid acyltransferase 3. *FASEB J.* 26, 169–180. doi: 10.1096/fj.11-184879

Kunze, D., Reichmann, G., Egger, E., Olthoff, D., and Dohler, K. (1975). Fatty acid pattern of lipids in normal and dystrophic human muscle. *Eur. J. Clin. Invest.* 5, 471–475. doi: 10.1111/j.1365-2362.1975.tb00479.x

Levental, K. R., Malmberg, E., Symons, J. L., Fan, Y. Y., Chapkin, R. S., Ernst, R., et al. (2020). Lipidomic and biophysical homeostasis of mammalian membranes counteracts dietary lipid perturbations to maintain cellular fitness. *Nat. Commun.* 11:1339. doi: 10.1038/s41467-020-15203-1

Lu, B., Jiang, Y. J., Zhou, Y., Xu, F. Y., Hatch, G. M., and Choy, P. C. (2005). Cloning and characterization of murine 1-acyl-sn-glycerol 3-phosphate acyltransferases and their regulation by PPARalpha in murine heart. *Biochem. J.* 385, 469–477. doi: 10.1042/bj20041348

Menke, A., and Jockusch, H. (1991). Decreased osmotic stability of dystrophin-less muscle cells from the mdx mouse. *Nature* 349, 69–71. doi: 10.1038/349069a0

Olbrich, K., Rawicz, W., Needham, D., and Evans, E. (2000). Water permeability and mechanical strength of polyunsaturated lipid bilayers. *Biophys. J.* 79, 321–327. doi: 10.1016/S0006-3495(00)76294-1

Oosting, A., Verkade, H. J., Kegler, D., Van De Heijning, B. J., and Van Der Beek, E. M. (2015). Rapid and selective manipulation of milk fatty acid composition in mice through the maternal diet during lactation. *J. Nutr. Sci.* 4:e19. doi: 10.1017/jns.2015.13

Paran, C. W., Zou, K., Ferrara, P. J., Song, H., Turk, J., and Funai, K. (2015). Lipogenesis mitigates dysregulated sarcoplasmic reticulum calcium uptake in muscular dystrophy. *Biochim. Biophys. Acta* 1851, 1530–1538. doi: 10.1016/j.bbalip.2015.09.001

Pastoret, C., and Sebille, A. (1995). mdx mice show progressive weakness and muscle deterioration with age. *J. Neurol. Sci.* 129, 97–105. doi: 10.1016/0022-510x(94)00276-t

Pearce, P. H., Johnsen, R. D., Wysocki, S. J., and Kakulas, B. A. (1981). Muscle lipids in Duchenne muscular dystrophy. *Aust. J. Exp. Biol. Med. Sci.* 59, 77–90.

Phua, W. W. T., Wong, M. X. Y., Liao, Z., and Tan, N. S. (2018). An aPPARent functional consequence in skeletal muscle physiology via peroxisome proliferator-activated receptors. *Int. J. Mol. Sci.* 19:1425. doi: 10.3390/ijms19051425

Rawicz, W., Olbrich, K. C., Mcintosh, T., Needham, D., and Evans, E. (2000). Effect of chain length and unsaturation on elasticity of lipid bilayers. *Biophys. J.* 79, 328–339. doi: 10.1016/S0006-3495(00)76295-3

Saini-Chohan, H. K., Mitchell, R. W., Vaz, F. M., Zelinski, T., and Hatch, G. M. (2012). Delineating the role of alterations in lipid metabolism to the pathogenesis of inherited skeletal and cardiac muscle disorders: Thematic Review Series: genetics of human lipid diseases. *J. Lipid Res.* 53, 4–27. doi: 10.1194/jlr.r012120

Senoo, N., Miyoshi, N., Kobayashi, E., Morita, A., Tanihata, J., Takeda, S., et al. (2020). Glycerophospholipid profile alterations are associated with murine muscle-wasting phenotype. *Muscle Nerve* 62, 413–418. doi: 10.1002/mus.26993

Shin, J. H., Hakim, C. H., Zhang, K., and Duan, D. (2011). Genotyping mdx, mdx3cv, and mdx4cv mice by primer competition polymerase chain reaction. *Muscle Nerve* 43, 283–286. doi: 10.1002/mus.21873

Shindou, H., Koso, H., Sasaki, J., Nakanishi, H., Sagara, H., Nakagawa, K. M., et al. (2017). Docosahexaenoic acid preserves visual function by maintaining correct disc morphology in retinal photoreceptor cells. *J. Biol. Chem.* 292, 12054–12064.

Shindou, H., and Shimizu, T. (2009). Acyl-CoA:lysophospholipid acyltransferases. *J. Biol. Chem.* 284, 1–5.

Stedman, H. H., Sweeney, H. L., Shrager, J. B., Maguire, H. C., Panettieri, R. A., Petrof, B., et al. (1991). The mdx mouse diaphragm reproduces the degenerative changes of Duchenne muscular dystrophy. *Nature* 352, 536–539. doi: 10.1038/352536a0

Straub, V., Rafael, J. A., Chamberlain, J. S., and Campbell, K. P. (1997). Animal models for muscular dystrophy show different patterns of sarcolemmal disruption. *J. Cell Biol.* 139, 375–385. doi: 10.1083/jcb.139.2.375

Tahallah, N., Brunelle, A., De La Porte, S., and Laprevote, O. (2008). Lipid mapping in human dystrophic muscle by cluster-time-of-flight secondary ion mass spectrometry imaging. *J. Lipid Res.* 49, 438–454.

Takagi, A., Muto, Y., Takahashi, Y., and Nakao, K. (1968). Fatty acid composition of lecithin from muscles in human progressive muscular dystrophy. *Clin. Chim. Acta* 20, 41–42. doi: 10.1016/0009-8981(68)90382-3

Talbot, J., and Maves, L. (2016). Skeletal muscle fiber type: using insights from muscle developmental biology to dissect targets for susceptibility and resistance to muscle disease. *Wiley Interdiscip. Rev. Dev. Biol.* 5, 518–534. doi: 10.1002/wdev.230

Terry, E. E., Zhang, X., Hoffmann, C., Hughes, L. D., Lewis, S. A., Li, J., et al. (2018). Transcriptional profiling reveals extraordinary diversity among skeletal muscle tissues. *elife* 7:e34613. doi: 10.7554/eLife.34613

Touboul, D., Piednoel, H., Voisin, V., De La Porte, S., Brunelle, A., Halgand, F., et al. (2004). Changes of phospholipid composition within the dystrophic muscle by matrix-assisted laser desorption/ionization mass spectrometry and mass spectrometry imaging. *Eur. J. Mass Spectrom. (Chichester)* 10, 657–664. doi: 10.1255/ejms.671

Tuazon, M. A., and Henderson, G. C. (2012). Fatty acid profile of skeletal muscle phospholipid is altered in mdx mice and is predictive of disease markers. *Metabolism* 61, 801–811. doi: 10.1016/j.metabol.2011.10.019

Turner, P. R., Westwood, T., Regen, C. M., and Steinhardt, R. A. (1988). Increased protein degradation results from elevated free calcium levels found in muscle from mdx mice. *Nature* 335, 735–738. doi: 10.1038/335735a0

Valentine, W. J., Tokuoka, S. M., Hishikawa, D., Kita, Y., Shindou, H., and Shimizu, T. (2018). LPAAT3 incorporates docosahexaenoic acid into skeletal muscle cell membranes and is upregulated by PPARdelta activation. *J. Lipid Res.* 59, 184–194. doi: 10.1194/jlr.M077321

Vance, J. E. (2015). Phospholipid synthesis and transport in mammalian cells. *Traffic* 16, 1–18. doi: 10.1111/tra.12230

Vogel, S. N., Hansen, C. T., and Rosenstreich, D. L. (1979). Characterization of a congenitally LPS-resistant, athymic mouse strain. *J. Immunol.* 122, 619–622.

West, J., Tompkins, C. K., Balantac, N., Nudelman, E., Meengs, B., White, T., et al. (1997). Cloning and expression of two human lysophosphatidic acid acyltransferase cDNAs that enhance cytokine-induced signaling responses in cells. *DNA Cell Biol.* 16, 691–701. doi: 10.1089/dna.1997.16.691

Yuki, K., Shindou, H., Hishikawa, D., and Shimizu, T. (2009). Characterization of mouse lysophosphatidic acid acyltransferase 3: an enzyme with dual functions in the testis. *J. Lipid Res.* 50, 860–869. doi: 10.1194/jlr.m800468-jlr200

Zemski Berry, K. A., and Murphy, R. C. (2004). Electrospray ionization tandem mass spectrometry of glycerophosphoethanolamine plasmalogen phospholipids. *J. Am. Soc. Mass Spectrom.* 15, 1499–1508. doi: 10.1016/j.jasms.2004.07.009

Author Disclaimer: Department of Lipid Signaling, National Center for Global Health and Medicine is financially supported by Ono Pharmaceutical Co., Ltd. The Lipidomics Laboratory at the University of Tokyo is supported by Shimadzu Corporation.

Conflict of Interest: The authors declare that the research was conducted in the absence of any commercial or financial relationships that could be construed as a potential conflict of interest.

Publisher's Note: All claims expressed in this article are solely those of the authors and do not necessarily represent those of their affiliated organizations, or those of the publisher, the editors and the reviewers. Any product that may be evaluated in this article, or claim that may be made by its manufacturer, is not guaranteed or endorsed by the publisher.

Advantages of publishing in Frontiers

OPEN ACCESS
Articles are free to read for greatest visibility and readership

FAST PUBLICATION
Around 90 days from submission to decision

HIGH QUALITY PEER-REVIEW
Rigorous, collaborative, and constructive peer-review

TRANSPARENT PEER-REVIEW
Editors and reviewers acknowledged by name on published articles

Frontiers
Avenue du Tribunal-Fédéral 34
1005 Lausanne | Switzerland

Visit us: www.frontiersin.org
Contact us: frontiersin.org/about/contact

REPRODUCIBILITY OF RESEARCH
Support open data and methods to enhance research reproducibility

DIGITAL PUBLISHING
Articles designed for optimal readership across devices

FOLLOW US
@frontiersin

IMPACT METRICS
Advanced article metrics track visibility across digital media

EXTENSIVE PROMOTION
Marketing and promotion of impactful research

LOOP RESEARCH NETWORK
Our network increases your article's readership